Investigating the Role of Osteopontin in Cardiac Hypertrophy

Amrita Lucette Asirvatham

BSc, MSc

This thesis is submitted for the
degree of Doctor of Philosophy (Ph.D.)
in the College of Medical, Veterinary & Life Sciences at
the University of Glasgow

June 2022

Impact of COVID-19

Prior to the announcement of the in the UK lockdown and at the request of the UAE government, I took a decision to prepone my two-week annual leave to remain close with my family based in the UAE during the global pandemic. After a period of winding down, I finally halted my work in the lab on March 17th, 2020 and left the UK on March 18th 2020. However, my stay in the UAE extended beyond my original plan due to flight restrictions. I ended up staying in the UAE until the UK borders reopened in August 2020. The circumstances surrounding the global pandemic significantly affected the progress of my experimental work, detailed below:

Cell and extracellular vesicle work:

To support the analysis of my hypotheses, I conducted experiments such as transfections, cell hypertrophy assays, and Extracellular Vesicle (EV) production and isolation using H9c2 cells (prior to the lockdown), with a goal to achieve an n=3 for each experiment. However, my early departure from the country resulted in these experiments being incomplete.

Upon my return to the UK, my ability to restart the cell work was delayed because of the complete shutdown of the cell culture facilities in our lab. This further impacted my planned downstream characterisation experiments such as western blots using the isolated EVs. Generally, the experiment takes up to three months to restart cell culture and EV isolations, and at least two months to perform the necessary experiments and data collection. Thankfully, the university granted me a four-month extension on my project given the COVID-19 disruption. This additional time was sufficient to restart and complete my cell work and EV isolations, but it did not permit me to finish my planned characterisation experiments.

Animal study:

Due to circumstances surrounding the lockdown, access to the animal house was restricted leading us to put a pause on the Transverse Aortic Constriction (TAC) study. Consequently, the ease of data collection and analysis was limited since the university computers were housed with the required software (GraphPad). These

restrictions were further exacerbated due to the flight restrictions that impeded my physical access. Therefore, the data and images from the echocardiography conducted on the rats could not be collected and downloaded to analyse.

The above statement provides an explanatory account of the challenges that I faced in completing my experimental work during the five-month period, specifically in the two areas of cell and EV work, and animal study. These challenges were mainly due to the disruptions caused by the global pandemic. I evaluated these consequences and re-prioritised the conclusions of my thesis based on existing data that I gathered, leading to the completion of my thesis.

Abstract

Cardiovascular disease (CVD) remains to be the leading cause of morbidity and mortality in the developed world. Cardiac hypertrophy is an adaptive response to pressure or volume stress, mutations of sarcomeric (or other) proteins, or loss of contractile mass from prior infarction. Hypertrophic growth accompanies many forms of heart disease, including ischemic disease, hypertension, heart failure, and valvular disease. The stroke-prone spontaneously hypertensive rat (SHRSP) is an animal model of essential hypertension and is used in research of CVD together with a normotensive reference strain Wistar-Kyoto (WKY). The SHRSP animals exhibit a significant increase in the left ventricular mass index (LVMI) compared to the WKY strain and this significant phenotypic difference is apparent at 5 weeks of age, prior to the onset of hypertension in this model. Osteopontin or secreted phosphoprotein 1 (*Spp1*) plays an important role in cardiac remodeling in CVDs, including coronary heart disease and heart failure. Patients and animal models with acute and chronic CVD have increased *Spp1* expression in the heart predominantly within cardiomyocytes resulting in cardiac hypertrophy. The aim of this project was to determine that early overexpression of Spp1 leads to a susceptibility of cardiac phenotypes in the SHRSP strain.

Multiple single nucleotide polymorphisms (SNPs) exist within the *Spp1* promoter region between the SHRSP and WKY rat strains. To determine whether the overexpression of *Spp1* begins during gestational development, leading to increased levels of cardiac hypertrophy and fibrosis, we used gestational day 18 rat hearts from the SHRSP and WKY strains. We aimed to quantify and compare the expression levels of *Spp1* by conducting quantitative real-time polymerase chain reaction (qRT-PCR). We found a significant increase in *Spp1* expression during gestational development in the SHRSP strain compared to the WKY strain even before the onset of the disease. We also generated promoter constructs for the SHRSP and WKY strains and compare the transcriptional activity of segments of the *Spp1* promoter by using dual luciferase assay. When these constructs were transfected into H9c2, we observed a trend towards increased luciferase activity in the SHRSP constructs when compared to the WKY constructs. However, when this experiment was repeated using HeLa cells our results were inconsistent. Microarray analysis

was conducted on 5 weeks vs neonatal SHRSP vs WKY.SP$_{Gla}$14a strains (chromosome 14 congenic strain) to capture gene expression changes responsible for the disease phenotype. Using Ingenuity Pathway Analysis (IPA), 101 genes were identified that were differentially expressed and found in common between the SHRSP and WKY.SP$_{Gla}$14a strains. From these 101 genes, a Tox analysis was conducted to identify genes downstream that potentially contribute towards cardiac hypertrophy and are connected to *Spp1*. Desmin (*DES*), Matrix metalloproteinase-14 (*MMP14*), Cathepsin-D (*CTSD*), Solute carrier family 25 member 11 (*SLC25A11*), and Myomesin-1 (*MYOM1*) were the 5 genes identified downstream that are connected to *Spp1* and the enlargement of the heart.

Following this, we aimed to establish and characterize the minimally invasive transverse aortic constriction (TAC) pressure overload model of left ventricular hypertrophy (LVH) in the WKY, WKY.SP$_{Gla}$14a congenic strain, SHRSP *Spp1* WT, and SHRSP *Spp1*^{em1} (*Spp1* knock out) rats. We assessed the impact of TAC surgery on body weight and blood pressure, assessed differences in LVMI and assessed cardiac phenotype parameters such as relative wall thickness (RWT), stroke volume (SV) fractional shortening (FS), ejection fraction (EF) and cardiac output (CO) in the SHAM and TAC operated rats. We also aimed to examine strain differences in response to TAC-induced pressure overload in these strains. Our results showed that we were able to successfully establish the TAC model in our WKY and chromosome 14 congenic strain by showing significantly increased LVH in these strains 8 weeks post-TAC surgery. We however were unable to show an exaggerated hypertrophic response in the hearts of the SHRSP *Spp1* WT and SHRSP *Spp1*^{em1} rats with no evidence of progression to heart failure.

Finally, to investigate the functional response of *Spp1* overexpression we used the cardiac cell line H9c2 as a model in our experiments to determine cell size. H9c2 cells were transfected with *Spp1* and pcDNA control to measure any changes in cell size post-transfection. We observed a significant increase in cell size in cells transfected with *Spp1* when compared to the control. Furthermore, we aimed to assess the functional role of EVs isolated from *Spp1* transfected H9c2 and HeLa conditioned media on H9c2 cells. Over-expression of *Spp1* in H9c2 cells results in a significant increase in cell size, most likely contributing to cardiac hypertrophy in

models of cardiovascular disease. We also investigate the role of extracellular vesicles (EVs) in *Spp1* trafficking released from *Spp1* transfected H9c2 cells. EVs were isolated from H9c2 cells transfected with *Spp1* and then overlayed onto a fresh batch of H9c2 cells to observe any changes in cell size. By doing this we observed a significant increase in cell size indicating the potential role EVs play in the mediation of *Spp1* trafficking. This study also implicates the role of EVs in cardiac disease. Following this, mass spectrometry analysis was conducted on EVs isolated from transfected H9c2 cells to characterize protein content. The results showed high quantities of foetal bovine serum (FBS) proteins and cross-contamination of keratin from the surrounding environment while the samples were being prepared. This was rectified by optimizing the protocol and preparing EV samples inside a sterilized tissue culture hood. However, despite there being cross-contaminants and high quantities of FBS, we were able to identify proteins of interest that were found in common between the control-EV and *Spp1*-EV samples, desmoplakin or DSP gene and zinc transporter ZIP8 synthesized by the SLC39A8 gene.

RNA sequencing (RNAseq) was conducted on RNA isolated from control and *Spp1* transfected EVs to determine whether *Spp1* was transferred into EVs post-transfection and to identify any significantly differentially expressed protein and long non-coding RNAs that may be involved in processes affecting cell size. Initial test samples revealed *Spp1* to be ranked 8th among the genes identified in the *Spp1* transfected EV-RNA sample with a coverage of 1178 reads per kilobase per million (RPKM). The control group showed *Spp1* to be ranked 774th with a coverage of 2.84 RPKM. This indicates that *Spp1* was successfully transferred from transfected H9c2 cells into the EVs with a higher coverage compared to the control pcDNA EV sample. Further analysis using a new set of EV-RNA samples showed Spp1 expression was significantly increased, with a fold change of 5598 in the *Spp1* EV-RNA sample when compared to the control. Analysis of the two data sets suggests that *Spp1* was successfully transferred in the EVs.

In summary, the data presented in this thesis elucidate Spp1 as a key modulator for LVH and cardiac fibrosis and how early changes in gene expression initiate cardiac phenotypes in the SHRSP strain even before the onset of the disease.

Table of Contents

List of tables

List of Figures

Acknowledgments

I would first like to thank my supervisors Dr. Martin McBride and Dr. Delyth Graham for giving me an opportunity to work on this project, for their constant guidance and support in this project, even during the COVID-19 pandemic.

To Martin, thank you so much for taking the time to teach me and being patient even when I'm slow to understand. I have not been the easiest to work with, but through it all you have never failed to help me when I needed it. Your generosity, kindness and support during this project have meant a great deal to me and I would not have gotten this far without it. To Del, thank you for all your help, guidance and support during my time in the CRF. I would not have even been able to hold a rat without your training and constant reassurances.

To my lab mates, thank you for all your help during my time in the lab. To Sonia, your very presence in the lab made me feel supported, especially when performing plasmid preps. Thank you for answering my never-ending questions and always letting me know that it was going to be okay. To those I have not mentioned by name, every person has played an important role during my time in the lab, and I will always be thankful.

To my best friends, Akshaya and Terry, thank you from the bottom of my heart for all your love and support. These past couple of years have been difficult to say the least but the two of you have been amazing through it all. With 24 hour zoom calls to keep me company while I write and our many random conversations to keep me awake, you guys have brought a smile to my face and helped lift my spirits when needed. To Eliane, Esther and Femi, thank you for your prayers, constant pep talks and calls to check in and make sure I was doing okay. You guys are my family here in Glasgow and I am so grateful for your presence in my life.

Finally, to my family, especially my sister Regina and mum, you mean the world to me. What the two of you have done for me I cannot put into words. I will forever be indebted to you, and I am so thankful and grateful for your love, support, and prayers. You deserve it all.

Author’s Declaration

I declare that this thesis has been written entirely by myself and the results presented within are entirely my own work, except where otherwise stated or acknowledged. Ingenuity Pathway Analysis of microarray gene expression profile of 5 weeks vs neonatal SHRSP and WKY.SP$_{Gla}$14a was conducted by Dr. Martin McBride. No part of this thesis has been previously submitted in whole or in part for any other degree at any university. The research was carried out at the British Heart Foundation Glasgow Cardiovascular Research Centre (BHF GCRC), The College of Medical Veterinary and Life Sciences, University of Glasgow under the supervision of Dr. Martin W. McBride and Dr. Delyth Graham.

List of Publications, Conferences and Awards

Poster presentation:

Targeted resequencing using the MinION long read sequencing platform, McBride, M.W., Ellis, H., Fisher, S., Asirvatham, A. and Jones, M. (2019. The FASEB Journal, 33: 637.3-637.3.doi: 10.1096/fasebj.2019.33.1_supplement.637.3

'Over-expression of Osteopontin Implicates Exosomes in H9c2 Cell size'. 2020. Journal of Human Hypertension 34 (S1): 1–20. https://doi.org/10.1038/s41371-020-00410-6.

Awards:

Wellcome Trust Institutional Strategic Support Fund (ISSF). Nov 2019.

List of Abbreviations

CVD	Cardiovascular disease
PI3K	Phosphoinositide 3-kinase
ECM	Extracellular matrix
IGF1	Insulin-like growth factor 1
GPCR	G protein-coupled receptors
PI3K	phosphoinositide 3-kinase
Ang II	Angiotensin-II
ET-1	Endothelin-1
HSF1	Heat shock factor protein 1
MAPKs	Mitogen-activated protein kinases
PKC	Protein Kinase C
PKD	Protein Kinase D
LV	Left ventricle
LVH	Left ventricular hypertrophy
TGF-β	Transforming growth factor-β
CT-1	Cardiotrtopin-1
alpha1-AR	Alpha1-adrenergic receptors
AT1a	Angiotensin II type-1a receptor
ANP	Atrial natriuretic peptide
BNP	Brain natriuretic peptide
GATA	Gata Binding Protein
MEF2	Myocyte enhanced factor-2
NFAT	Nuclear factor of activated T-cells
SERCA	Sarco/endoplasmic reticulum
RAAS	Renin-angiotensin-aldosterone system
CaMKII	Calmodulin-dependent protein kinase II
EPC	Endothelial progenitor cells
CSC	Cardiac stem-progenitor cells
mRNA	messenger RNA
miRNA	micro-RNA
MVs	Microvesicles
MVBs	Multivesicular bodies
ARF6	ADP-ribosylation factor 6
PLD	Phospholipase D
ERK	Extracellular signal-regulated kinases
MLCK	Myosin light-chain kinase
ESCRT	Endosomal sorting complexes required for transport
VPS4	Vacuolar protein sorting-associated protein 4A
ALIX	ALG-2-interacting protein X
ILV	Intraluminal vesicles
GTP	Guanosine triphosphate
RAB	Ras-associated binding

TSG101	Tumor susceptibility gene 101
GM130	Golgi matrix protein 130
SNARE	Soluble N-ethylmaleimide attachment protein receptor
MFGE8	Milk fat globule-EGF factor 8
TIM4	T cell immunoglobulin mucin 4
RNA	Ribonucleic acid
AFM	Atomic force microscopy
DLS	Dynamic light scattering
NTA	Nanoparticle tracking analysis
TRPS	Tunable resistive pulse sensing
ELISA	Enzyme linked immune-sorbent assays
WB	Western blot
ISEV	International Society of Extracellular Vesicles
EM	Electron microscope
PCR	Polymerase chain reaction
qRT-PCR	Real-Time quantitative reverse transcription PCR
RNP	Ribonucleoprotein complexes
FBS	Foetal bovine serum
NGS	Next generation sequencing
ncRNA	Noncoding RNA
rRNA	Ribosomal RNA
snRNA	Small nuclear RNA
tRNA	Transfer RNA
lncRNA	Long non-coding RNA
HMC-1	Human mast cell-1
LDL	Low density lipoprotein
HDL	High density lipoprotein
DNA	Deoxyribonucleic acid
Spp1	Osteopontin
BN	Brown Norway rat
NHLBI	National Heart, Lung, and Blood Institute
RGPEST	Rat Expressed Sequence Tag
RGD	Rat Genome Database
RGP	Rat Genome Project
SHR	Spontaneously hypertensive rat
SHRSP	Stroke-prone spontaneously hypertensive rat
WKY	Wistar Kyoto rat
SHHF	spontaneously hypertensive heart failure prone rat
QTL	Quantitative trait loci
pQTL	physiological QTLs
eQTL	Expression quantitative trait loci
BP	Blood pressure
GWAS	Genome wide association studies
LSP1	Lymphocyte-specific protein 1

TNNT3	Troponin T protein 3
SOX6	SRY-Box Transcription Factor 6
NOS3	Nitric Oxide Synthase 3
SNP	Single nucleotide polymorphism
MTHFR-NPPB	Methylene tetrahydrofolate reductase-natriuretic peptide
NPR3	Natriuretic peptide C receptor
AGT	Angiotensinogen
LD	Linkage disequilibrium
ENCODE	Encyclopaedia of DNA Elements
nsSNP	Non-synonymous single nucleotide polymorphisms
MAS	Marker assisted selection
Hsd17b13	Hydroxy steroid dehydrogenase 17-beta 13
Znf644	Zinc finger protein
Rrad	Ras-related associated with diabetes
CM	Cardiomyocytes
kDa	Kilodaltons
cDNA	Complementary DNA
α5β1	Alpha-5 beta-1
α9β1	Alpha-9 beta-1
fOPN	Full length osteopontin
nOPN	Thrombin-cleaved osteopontin
NK	Natural killer cells
OPN	Osteopontin
MI	Myocardial infarction
WT	Wild type
KO	Knockout
LVMI	Left Ventricular Mass Index
LVDD	Left ventricular diastolic dysfunction
Runx2	Runt-related transcription factor 2
hRluc2	Renilla reniformis Luciferase
luc2	Luciferase
RWT	Relative wall thickness
SV	Stroke volume
FS	Fractional shortening
EF	Ejection fraction
CO	Cardiac output
TAC	Transverse aortic constriction
SBP	Systolic blood pressure
VPR	Volume pressure recording
M-mode	Motion-mode
PWT	Posterior wall thickness
AWT	Anterior wall thickness
EDD	End diastolic dysfunction
ESV	End systolic volume

EDV	End diastolic volume
HR	Heart rate
ANOVA	Analysis of variance
SEM	Standard error of the mean
mmHg	millimetres of mercury
cm	centimetre
nm	nanometre
Hsp	Heat shock proteins
EV	Extracellular vesicles
IL-6	Interleukin-6
TNK-α	Tumour Necrosis Factor alpha
SEC	Size exclusion chromatography
UC	Ultracentrifugation
MEM	Minimum essential media
Rpm	Revolutions per minute
PBS	Phosphate buffered saline
SDS-PAGE	Sodium dodecyl sulfate–polyacrylamide gel electrophoresis
PVDF	Polyvinylidene fluoride
TBST	Tris-Buffered Saline tween
TBS	Tris-Buffered Saline
BAM	Binary alignment matrix
ADAM10	ADAM Metallopeptidase Domain 10
RQ	Relative quantification
CT	Cycle threshold
MS	Mass spectrometry
DSP	Desmoplakin
SLC39A8	Solute carrier family 39 member 8
DES	Desmin
MMP14	Matrix metalloproteinase-14
MYOM1	*My*omesin-1
CTSD	Cathepsin-D
CTSD-p	Procathepsin-D
SLC25A11	Solute carrier family 25 member 11
ATP	Adenosine triphosphate
ER	Endoplasmic reticulum
B2M	β-2-microglobulin

Chapter 1. Introduction

1.1 Cardiovascular disease

1.1.1 Human cardiovascular disease

Cardiovascular disease (CVD) is a leading cause of global death and one of the most serious health problems worldwide (Amini, Zayeri, and Salehi 2021). In 2019, the WHO reported an estimated 17.9 million people died from CVDs, of which 32% represented global deaths. Of these, 85% of deaths were due to heart attack and stroke (WHO, 2021). CVD is referred to as a class of disease which involves the heart or blood vessels. The disease consists of stroke, hypertension, heart failure, and several other vascular and cardiac problems. In the UK, heart and circulatory diseases cause more than 160,000 deaths each year (BHF, 2021).

Cardiac hypertrophy is the heart's response to various extrinsic and intrinsic stimuli that can cause increased biomechanical stress (Frey and Olson 2003). It is a common type of remodelling process wherein individual myocytes grow in length (or width) as a method of reducing ventricular wall and septal stress, and increasing cardiac pump function resulting in a state of compensated hypertrophy (Heineke and Molkentin 2006). Although hypertrophy can eventually normalize wall tension, it can be linked with adverse outcomes and threaten patients resulting in a progression to heart failure or sudden death (Frey and Olson 2003). Cardiac hypertrophy is classified as 'physiological' when it occurs in healthy individuals after exercise or pregnancy and is not associated with cardiac damage. However, when hypertrophy results from pressure or volume overload, or after a myocardial infarction, it is referred to as 'pathological'. This can also include an adaptive or compensatory phase that can reduce wall stress and maintain cardiac output. However, these functions can change and result in a decline in ventricular function, leading to heart failure (Kehat and Molkentin 2010).

1.1.2 Pathophysiological remodelling of the heart

Physiological cardiac hypertrophy is associated with normal or enhanced cardiac function whereas, pathological cardiac hypertrophy can eventually lead to heart failure (Weeks and McMullen 2011).

Physiological hypertrophy is described with a heart having normal or enhanced contractile function combined with a normal cardiac structure and it maintains cardiac function overtime (Shimizu and Minamino 2016; Nakamura and Sadoshima 2018). Physiological hypertrophy includes hearts having preserved or increased contractile function with no interstitial or replacement fibrosis or cell death. Physiological hypertrophy is reversible and does not lead to heart failure, except for postnatal hypertrophy (Nakamura and Sadoshima 2018). This kind of hypertrophy is mainly facilitated by signalling through insulin-like growth factor-1 and growth hormone, and is transduced by phosphoinositide 3-kinase (PI3K)/Akt signalling (Dorn and Force 2005). Pathological cardiac hypertrophy includes cellular and molecular remodelling such as increase in myocyte length without affecting its proliferation, changes in the expression of proteins that are involved in excitation-contraction coupling, and changes in the metabolic state of the myocyte. These changes are accompanied by changes in the extracellular matrix (ECM) and by myocyte death caused by apoptosis or necrosis. The transition from compensated hypertrophy to dilated heart failure causes these cellular and molecular changes to increase, resulting in myocyte lengthening, ECM remodelling, chamber dilation and systolic and/or diastolic dysfunction (Kehat and Molkentin 2010).

IGF1- phosphoinositide 3-kinase [PI3K, (p110α)]-Akt pathway and Gαq signalling (downstream of G protein-coupled receptors (GPCR) activated by angiotensin-II (Ang II), endothelin-1 (ET-1) and catecholamines), respectively have been best characterised as signalling cascades responsible for facilitating physiological and pathological cardiac hypertrophy (figure 1.1). Other signalling pathways associated with physiological hypertrophy include gp130/JAK/STAT pathway, thyroid hormone signalling, and heat shock transcription factor 1 (HSF1). In contrast, pathological hypertrophy has been associated with abnormalities leading to enhanced PI3K(p110γ), mitogen activated protein kinases (MAPKs), protein kinase C (PKC) and D (PKD), and calcineurin (Bernardo et al. 2010).

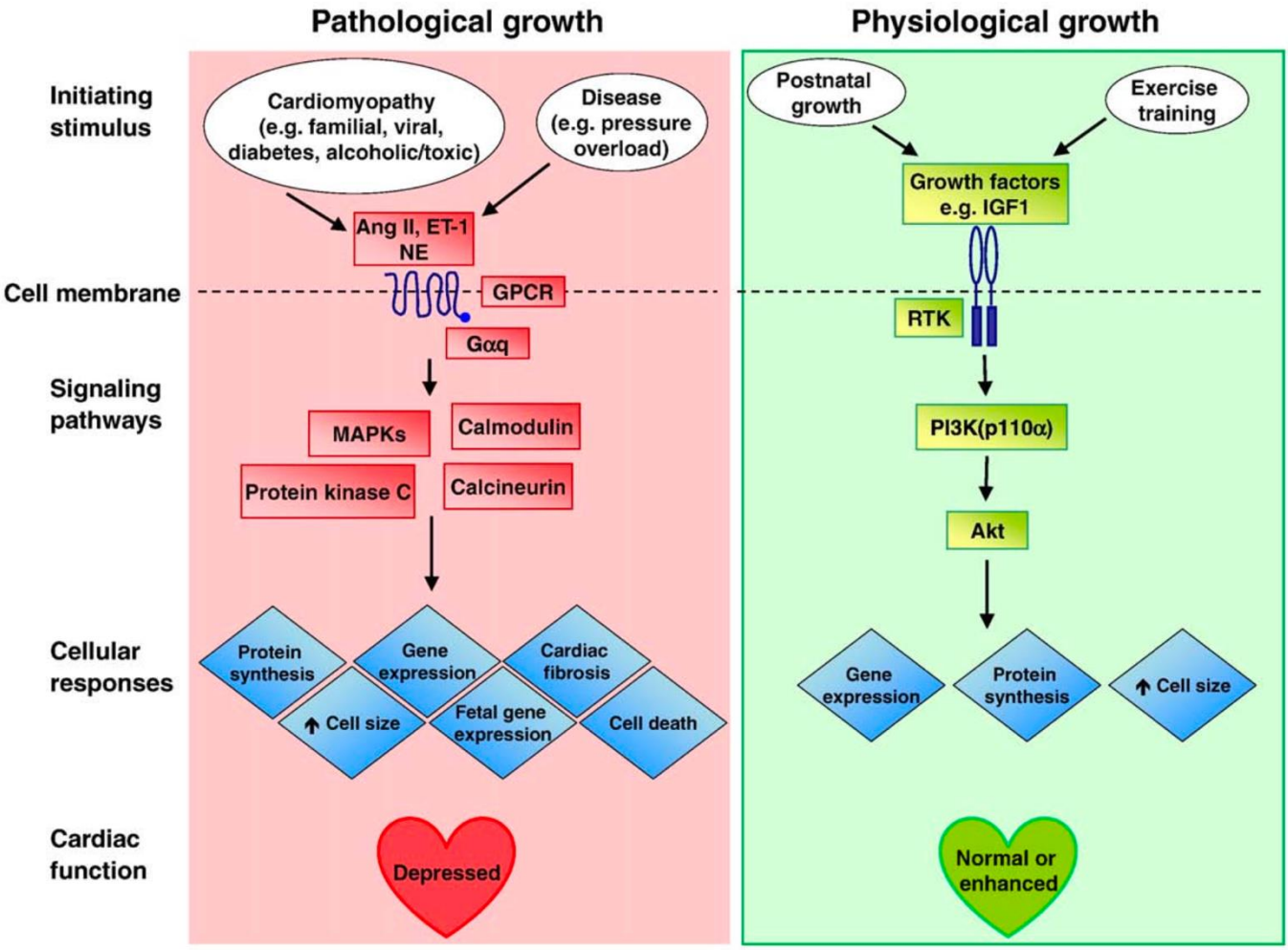

Figure 1.1: A schematic overview of pathological and physiological hypertrophy

A summary of important differences in initiating stimuli, signalling pathways, cellular responses, and cardiac function. Signalling pathways involved in facilitating pathological and physiological cardiac hypertrophy are shaded in red and green respectively (Bernardo et al. 2010).

Cardiac hypertrophy can also be classified into two unique phenotypes based on the geometry of the heart. Eccentric hypertrophy develops with volume overload and non-pathological eccentric hypertrophy shows increased ventricular volume coupled with increase in wall and septal thickness (Shimizu and Minamino 2016). Eccentric hypertrophy is associated with volume overload and is characterised by an increase in myocyte length resulting in a dilated left ventricle with thin walls (Nauta et al. 2020). Whereas, concentric hypertrophy is associated with pressure overload resulting in increased left ventricular wall thickness without or with a little increase in chamber size (Nakamura and Sadoshima 2018). Pathological eccentric hypertrophy can develop with diseases such as myocardial infarction and dilated cardiomyopathy, and can lead to ventricular dilatation with lengthening of cardiomyocytes (Shimizu and Minamino 2016). It is characterised by the organisation of contractile-protein units in series, leading to the increase of myocyte size by length and not by width. This increase in cardiomyocyte length can be more prominent in forms of cardiac dilation in which the heart increases in size through the lengthening of myocytes and the addition of sarcomeres in series, with a reduction in cell width (Kehat and Molkentin 2010). In pressure-overload concentric hypertrophy, the organisation of contractile-protein units in parallel rather than in a series results in a relative increase in myocyte width (Nakamura and Sadoshima 2018). This condition develops under pathological conditions such as hypertension or valvular disease. However in exercise settings such as wrestling, it has been known to induce non-pathological concentric hypertrophy (Shimizu and Minamino 2016).

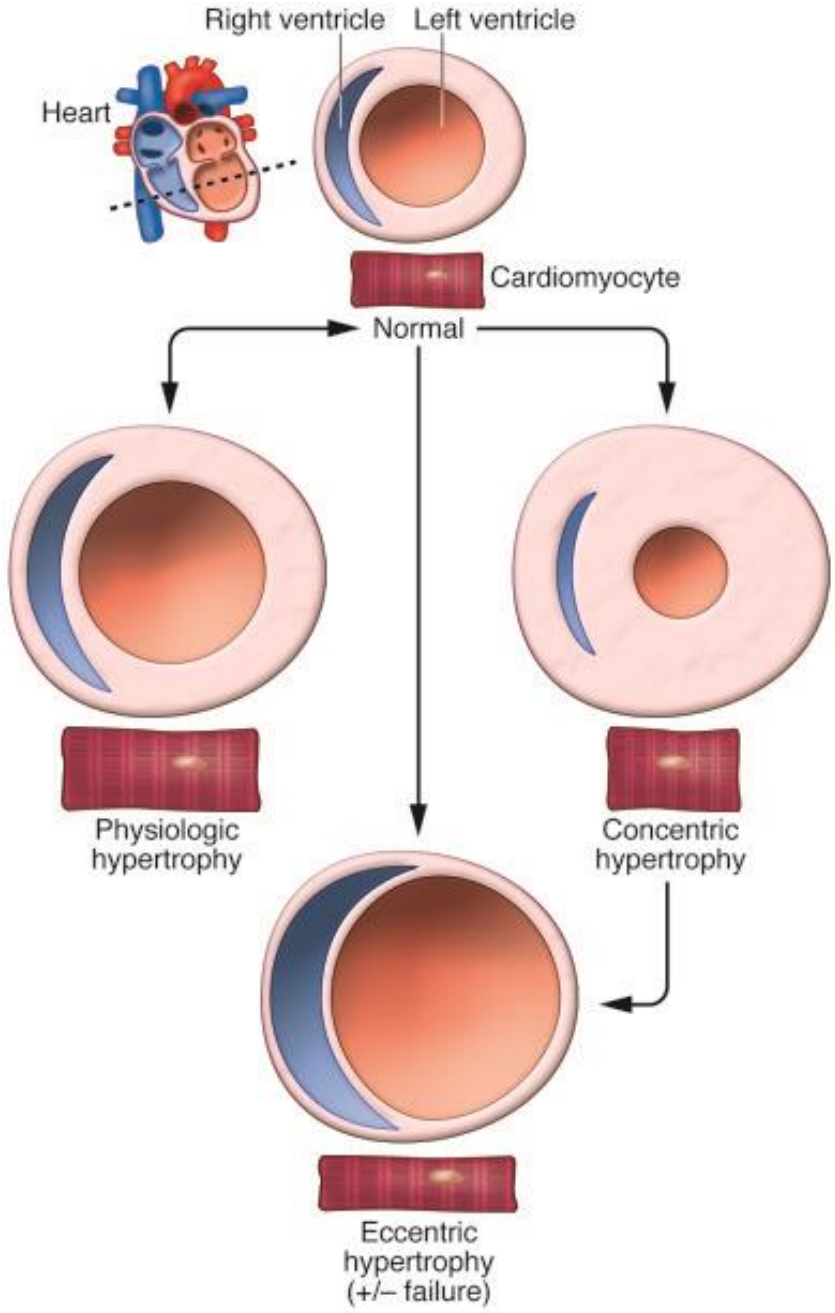

Figure 1.2: Pathophysiological remodelling of the heart

The geometric effects of cardiac cells following pathological and physiological events leading to hypertrophy. Left ventricular volume is reduced in concentric hypertrophy. Eccentric hypertrophy results in increased ventricular volume (van Berlo, Maillet, and Molkentin 2013).

1.1.3 Left Ventricular Hypertrophy (LVH)

Left ventricular hypertrophy (LVH) is when the heart is conditioned to sustained arterial hypertension by developing concentric hypertrophy (Rossi 1998). This may cause the heart to have impaired cardiac function, increased mortality from congestive heart failure and coronary artery disease (V.-E. Smith et al. 1985). Concentric hypertrophy can gradually lead to eccentric hypertrophy, and eventually to systolic heart failure if the stress is maintained. The transition from compensated hypertrophy to decompensated cardiac failure, severe fibrosis can occur in parallel with cardiomyocyte hypertrophy, cellular apoptosis and inflammatory cell infiltration (Jiang et al. 2021). LVH and remodelling are important compensatory developments that occur over time in response to wall stress or significant haemodynamic pressure and volume overload (Bornstein, Rao, and Marwaha 2020).

In pressure overload, remodelling is mainly concentric due to the addition of myocyte sarcomeres in a parallel formation. Hence, thickness of the LV wall increases in comparison to volume of the LV cavity. This results in an increase in LV mass to end-diastolic volume (M/V) ratio. However, disorders caused by volume overload are usually associated with eccentric remodelling and cause a proportional increase in mass and volume (Rosen et al. 2005). In pressure overload of the left ventricle, increase in wall thickness compensates for the increase in systolic pressure. It also maintains a constant and normal left ventricular wall stress, hence enabling the left ventricle to release a normal stroke volume against high resistance (Panidis et al. 1984).

An increase in LV wall stress is a main mechanical factor in the development of LVH. Blood pressure is the main factor for LV mass. There are however some additional haemodynamic factors that can play a role in the development and maintenance of LVH (Panidis et al. 1984). Haemodynamic overloads increase ventricular stroke work, which is the area surrounding a pressure-volume loop. In a volume overload setting, stroke work increases because volume, the horizontal axis of the pressure-volume loop, increases. The demand of overloaded states is met by the development of ventricular hypertrophy (Carabello et al. 1992). Salt intake has also been known to influence LV mass as a reduction in dietary sodium was shown to reduce LV hypertrophy (Nadruz 2015). Whereas an increase in sodium intake could

increase intravascular volume and increase LV preload. These changes to the vascular structure coupled with increased arterial stiffness can result in increased systolic blood pressure leading to the development of LVH (Kahan 2005).

Haemodynamic overload can subject cardiomyocytes to mechanical stretching, and autocrine and paracrine humoral factors including AngII, endothelin 1 (ET-1), Insulin-like growth factor 1 (IGF1), transforming growth factor-β (TGF-β) and cardiotrophin 1 (CT-1) are released. When these factors bind to receptors on cardiac cells, it in turn activates intracellular signalling pathways that lead to cell growth. Complex signalling cascades and proteins responsible for cardiac growth and hypertrophy, and extensive crosstalk have been identified (figure 1.3).

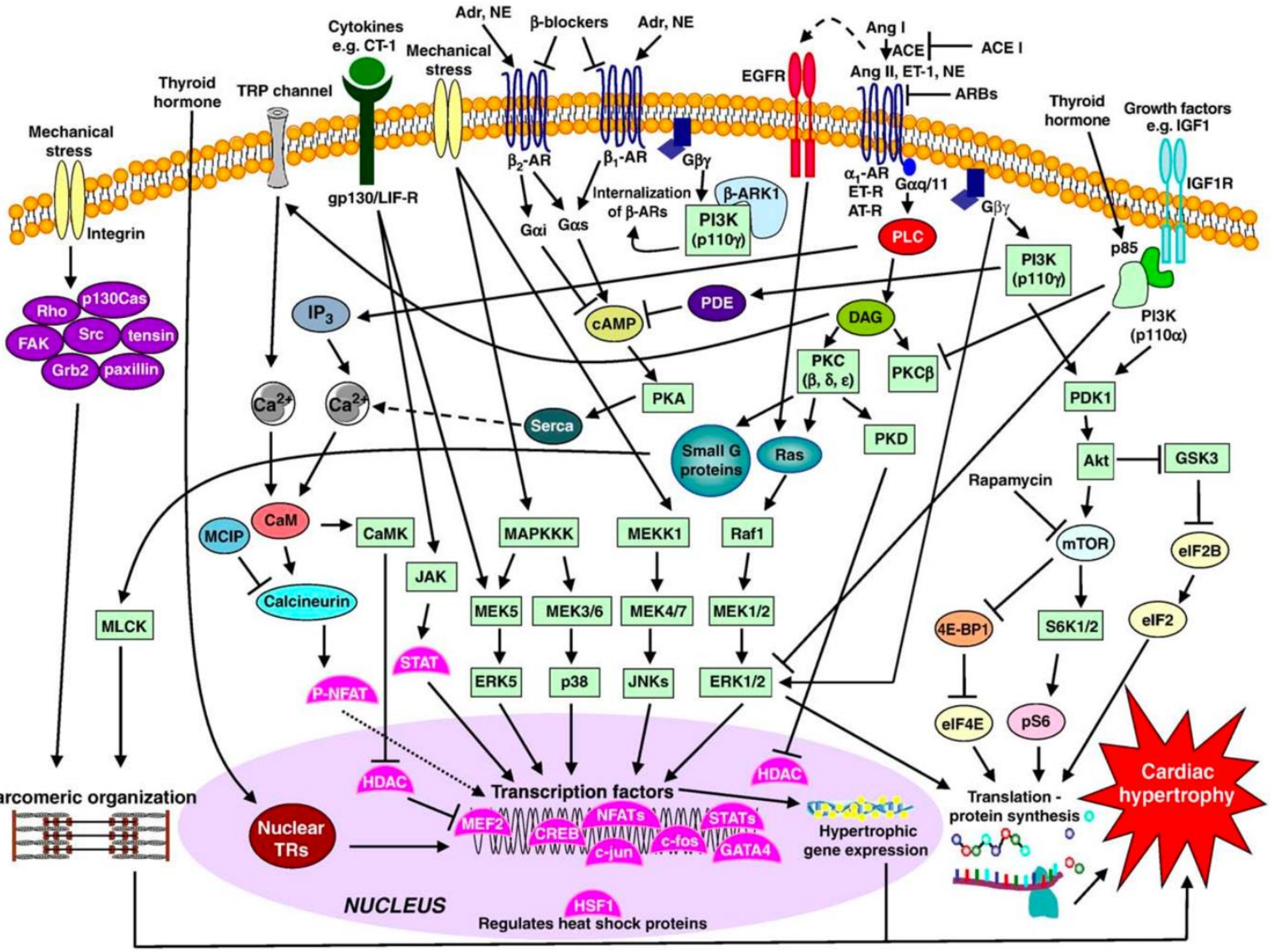

Figure 1.3: Signalling cascades and proteins responsible for cardiac growth and hypertrophy

A schematic representation of major signalling pathways that are involved in cardiac hypertrophy, showing complex and extensive crosstalk and the integration of various pathways (Bernardo et al. 2010).

In athletes, LVH can be a physiological adaptation to a rigorous exercise regime. This is typically benign and reverts when the individual reduces their amount of physical activity. It can also be a pathological condition wherein LVH is either a genetic or secondary response to LV overload. This compensatory response can eventually become maladaptive and progress towards LV dysfunction and heart failure (Lazzeroni, Rimoldi, and Camici 2016). A physiological adaptation of the heart results from an intense exercise routine and is characterised by increase LV mass (LVM), cavity dimensions and wall thickness (Pelliccia et al. 2002). Long-term training also induces a hypertrophic response called athletes' heart. This increase in myocardial mass is linked with preserved or enhanced cardiac function without cardiac fibrosis, cardiomyocyte apoptosis, or changes in foetal gene expression (Ellison et al. 2012). Additionally, the protective role exercise plays in cardiovascular disease prevention and treatment has been extensively documented (Shephard and Balady 1999).

There are certain factors that are preferentially release in response to a pathological and physiological trigger and this has been demonstrated in both human and animal studies (Bernardo et al. 2010). It has been known that IGF1 is released in postnatal development and in response to exercise training (Koziris et al. 1999; Neri Serneri et al. 2001). In professional athletes, production of cardiac IGF1 was shown to be increased when compared to the control subjects. In contrast, cardiac formation of AngII was increased in heart failure patients with hypertrophied hearts, and pressure overload is associated with increased AngII levels, catecholamines and ET-1 (Rapacciuolo et al. 2001; Serneri et al. 2001). There are also a variety of ligands that can activate Gαq-coupled receptors, such as alpha1-AR (nor-epinephrine and phenylephrine), the angiotensin II type-1a receptor (AT1a) and ET-1 receptor. These receptors have been shown to stimulate a hypertrophic response in cultured neonatal rat ventricular myocytes (Ito et al., n.d.; Simpson 1983).

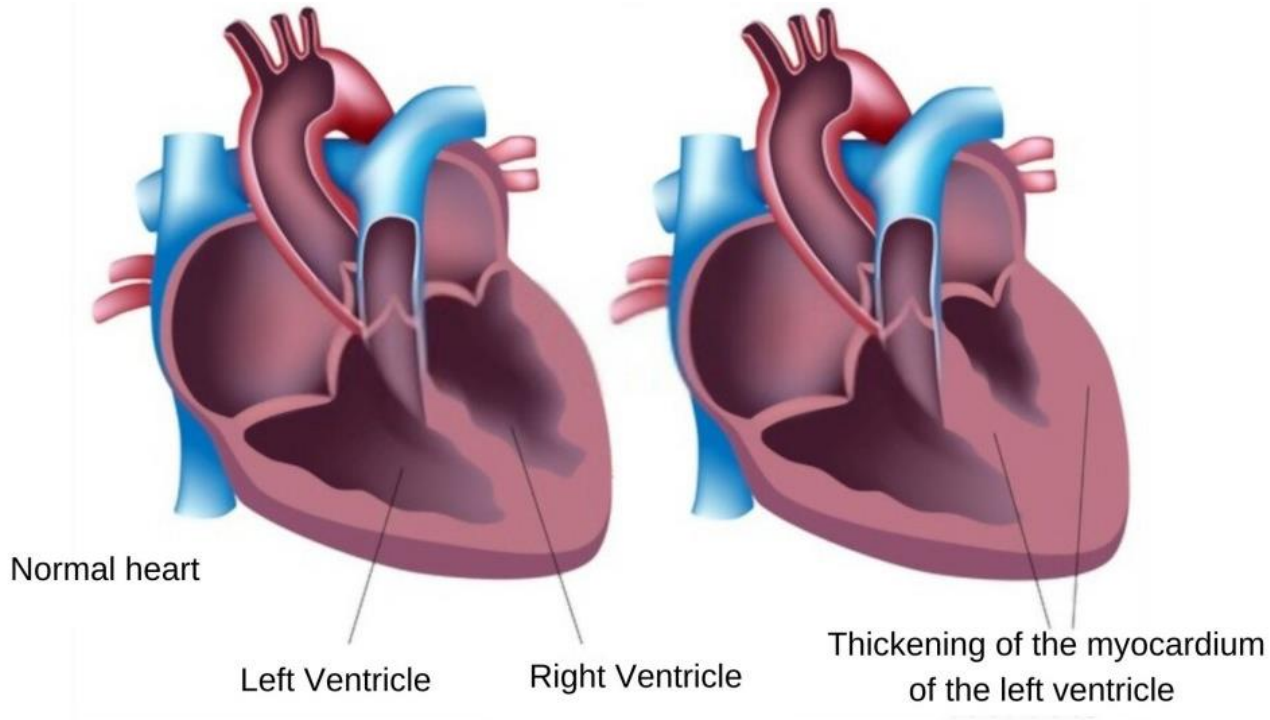

Figure 1.4: Left Ventricular Hypertrophy

The heart on the left shows a heart with normal muscle thickness. The heart on the right shows left ventricular hypertrophy, where the left side of the muscles in the heart are thicker resulting in an increase in heart size.

1.1.4 Pathological LVH

Pathological hypertrophy results from either pressure or volume overload that is induced by diseases such as hypertension and valvular disorders. It is usually associated with the loss of cardiomyocytes, fibrotic replacement, cardiac dysfunction and increased heart failure and death (Ellison et al. 2012). Initially, it is a compensatory response to increased biomechanical stress in order to maintain normal cardiovascular function (J. R. McMullen et al. 2003). Eventually, the heart can decompensate leading to ventricular dilatation, which overtime, can progress to systolic and diastolic myocardial dysfunction or heart failure (Bernardo et al. 2010).

Physiological and pathological hypertrophy are induced significantly distinct signalling pathways and they are characterised by different gene and protein expression profiles, despite them having some morphological similarities (Rosen et al. 2005). Typically, pathological hypertrophy has been related to the reactivation or upregulation of the foetal cardiomyocyte gene programme, including ANP, BNP, α-skeletal actin, and β-myosin heavy chain (Marketou, Parthenakis, and Vardas 2016).

The expression of foetal genes is known to be the foundation in the pathophysiology of pathological hypertrophy (Pandya and Smithies 2011). In a physiological hypertrophic model, recapitulation of the foetal gene programme and switch does not normally occur (Paylor et al. 2013). A complex network of transcription factors including, GATA4, GATA6, Csx/Nkx2.5,MEF2, c-jun, c-fos, c-myc, nuclear factor k B and NFAT coordinate the activation of cardiac genes in response to a hypertrophic stimuli (Frohlich, González, and Díez 2011).

Changes in gene expression patterns play an important role in influencing hypertrophic phenotype. The modifications in the expression of genes encoding several proteins occur in the myocyte. These include the sarcomere; calcium transport and binding (Na^+/Ca^{2+} exchanger, α-subunit of the Na^+K^+-ATPase, calmodulin, calcineurin, $SERCA_2$ [Ca^{2+}-ATPase], ryanodine receptors); hormone and cell signalling systems (the α1-adrenergic receptor, renin-angiotensin-aldosterone system (RAAS), natriuretic peptides, G proteins, protein kinases); and energy metabolism (Swynghedauw 1997). In situations of chronic overload, the sarcoplasmic reticulum (SR) pumps less calcium against the SR-cytoplasmic gradient because the density/cell of Ca^{2+}-ATPase is lower. Poor contractile (systolic) or filling (diastolic) of the LV could result from a diminished capacity of the hypertrophied ventricle to protect sudden changes in intracellular calcium (Arnett, de las Fuentes, and Broeckel 2004). Mutations in the sarcomeric proteins can lead to severe, monogenic forms of hypertrophy, specifically hypertrophic cardiomyopathy (Niimura, Chudley, and Sole 1998). These hereditary diseases are mostly characterised by significant LVH, decreased myocyte contractility, and ventricular arrhythmias (Roberts and Sigwart 2001). Hypertrophic cardiomyopathy results from mutations in both the thick and thin actin filaments of the sarcomere: cardiac β-myosin heavy chain, cardiac troponin I, cardiac troponin T, α tropomyosin ventricular myosin essential light chain, ventricular myosin regulatory light chain, and cardiac myosin-binding protein C. These structural proteins apply a dominant effect on LV structure and function (Robinson et al. 2007).

Efforts made in gene discovery for LVH in humans have been limited to severe forms of hypertrophy. Applying knowledge about pathways that contribute to myocardial cell growth or derangement might lead to candidate pathways whereby genes exert their influence on the left ventricle (Arnett 2000). Figure 1.5 describes genes that are likely to contribute to changes in LV mass and function.

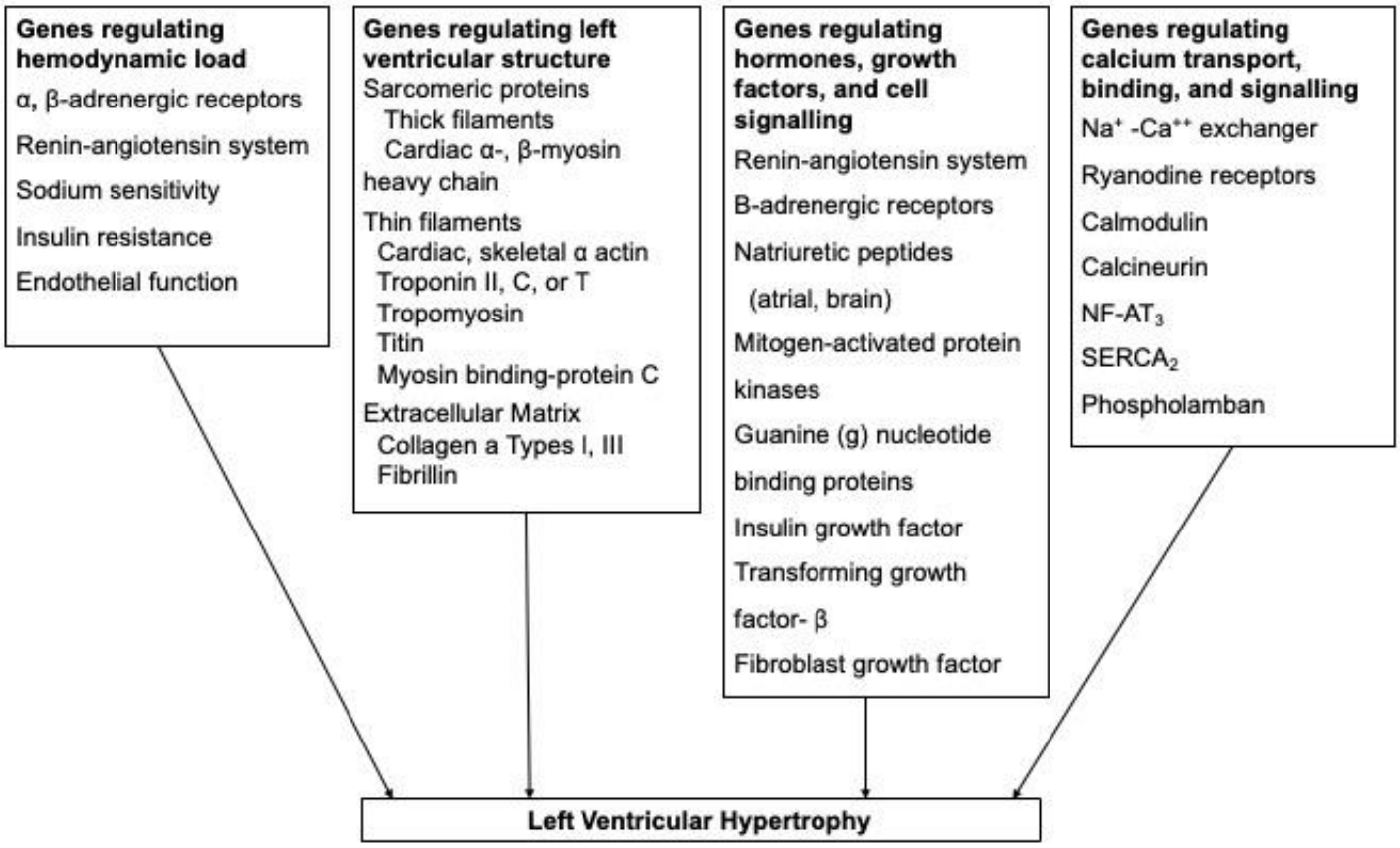

Figure 1.5: Candidate genes that contribute towards phenotypic variation in left ventricular hypertrophy, systolic and diastolic dysfunction

These genes encode for proteins regulating LV structure, hemodynamic load, calcium homeostasis, hormones, growth factors and cell signalling (Image adapted from Arnett 2000)

Systolic and diastolic blood pressure are also major determinants of afterload and myocardial function. The level of LVH increases with higher blood pressure. There is a possibility that increased diastolic and systolic wall stress due to contractile myocardial impairment can cause different neurohormonal mechanisms to activate such as adrenergic, renin-angiotensin, or other mechanisms that could lead to LV hypertrophy (Rosen et al. 2005). RAAS is activated in response to haemodynamic stress such as pressure overload (Bernardo et al. 2010). This activation can lead to an increase in angiotensin II (AngII) levels and can directly induce cardiac hypertrophy via the activation of CaMKII signalling. The CaMKII pathway is the core mechanism to promote myocardial hypertrophy and heart failure (Anderson, Brown, and Bers 2011). Studies conducted in humans and rodents have shown that during heart failure, cardiac CaMKII activity is increased. This increased function leads to cardiac hypertrophy. Whereas, when CaMKII activity is inhibited, it enhances myocardial hypertrophy and improves heart failure (Shimizu and Minamino 2016). Pharmacological agents that act on the renin-angiotensin system can regulate the activation of endothelial progenitor cells (EPC), thereby introducing a therapeutic role in LVH and its regression (Müller et al. 2009).

1.2 Animal models

Animals used for the study of cardiovascular diseases have been proven to be valuable for understanding the pathophysiology of a disease. They have also been useful in developing therapeutic interventions for a disease (Leong, Ng, and Jaarin 2015). The key limitations rise from the differences found between human and experimentally induced pathology, in both genetic regulatory mechanisms and factors that influence cardiovascular function. Experimental models and preparations used in cardiovascular research include cell and tissue-based assays or structures immersed in organ baths. In small animals, there have been several models developed with cardiovascular conditions that can result in spontaneous genetic mutations, or they can alternatively be induced by specific genomic modification. Gene transfer is one such technique that has been used as it involves the controlled induction of mutations. This results in the expression of abnormalities associated with the development of different types of cardiovascular diseases (Chorro, Such-Belenguer, and López-Merino 2009).

Animal models used for research include mice, rats, rabbits, pigs, fish (zebra fish and other fish species), birds, dogs, and primates. They have been reported as useful animals in studying and understanding diseases that afflict humans and animals (Leong, Ng, and Jaarin 2015). An ideal animal model for any cardiovascular disease in humans should have five characteristics: (1) they should be able to mimic human disease, (2) they should allow the study of chronic and stable diseases, (3) they should produce symptoms that are predictable and controllable, (4) they should satisfy economical, technical and animal welfare considerations, and (5) they should allow the measurement of all relevant cardiac, biochemical and haemodynamic parameters (Doggrell 1998). Rats and mice are the most used animal models since they share a high degree of homology to the human genome, each with 30,000 protein coding genes (Riehle and Bauersachs 2019). There are major advantages of using rodent models in research such as relative short breeding cycles and low housing costs. There have been several small animal models developed as tools to decode heart failure aetiologies and develop new strategies for the treatment of heart failure (Zaragoza et al. 2011). However, with all the benefits of using rodent models in research there is insufficient consideration being given to other criteria,

particularly whether rat models of cardiovascular disease can mimic human disease. CVDs such as hypertension and heart failure in humans usually develop slowly with a wide-range in neurohumoral adaptations in contrast to many surgical or drug-induced rat models where the onset of symptoms are acute. CVDs are uncommon in young humans but significantly increase with age whereas, most rodent models of hypertension and heart failure only use young adult rats (Doggrell 1998).

1.2.1 Rat model

Rats have been used as an important animal model in biochemical research for over 100 years. Their initial use was largely in areas of nutrition, cancer and behaviour (Gill et al. 1989). Laboratory rats originate from Rattus Norvegicus and is a leading laboratory animal. Acknowledging the importance of rats as an excellent animal model in cardiovascular research, the NIH, led by the National Heart, Lung, and Blood Institute (NHLBI) Project, and the Rat Genome Project (RGP), the Rat Expressed Sequence Tag (RGPEST) Project, and the Rat Genome Database (RGD) to develop important genomic tools and resources that will further improve the rat model systems (Jacob 1999). The Rat Genome Sequencing Consortium (RGSC) in association with other academic institutions and industry have sequenced the Brown Norway (BN) rat strain which represents a high-quality ‘draft’ covering over 90% of the genome (Rat Genome Sequencing Project Consortium 2004). The rat genome data has enhanced the efficacy of the rat models. Individual researchers now have a better understanding of the phenotypes exhibited by the rat, and they have a higher degree of confidence and precision of the rat gene content that is suitable for research (J. R. Smith et al. 2019).

Different laboratory groups have undertaken breeding efforts which have led to rat subtypes such as Wistar, Long/Evans, Sprague-Dawley, Fisher, and various others. These rats have specific features, for example, Sprague-Dawley rats continue to grow and show significant weight gain throughout their lifetime. There are many advantages to using rats as animal models for cardiovascular disease such as their body size, their large volume of blood in comparison to mice which make blood collection easier and less stressful to the animal, and low cost compared to larger animal models (Dillmann 2008).

Inbred rat strains like the spontaneously hypertensive rat (SHR) are a suitable and well-established model of hypertension because of how similar it is to humans with primary hypertension. These similarities include a genetic predisposition to high BP without specific aetiology, total increase in peripheral resistance without expansion in volume, and similar responses to drug treatment (J. G. Dickhout and Lee 1998). The use of SHR for studies related to metabolic syndrome and other aspects of CVD have also been explored. Additionally, salt sensitive rats (Dahl rats) and salt resistant rats are other excellent models for hypertension-related pathophysiological studies (J P Rapp 1982). Furthermore, rats that have a higher tendency to develop cardiac hypertrophy and heart failure have been developed such as the spontaneously hypertensive, heart failure prone (SHHF) rat. It represents a congenital model of dilated cardiomyopathy with hypertension that progresses to decompensated heart failure. This strain shows several trademark signs of the disease state in humans (Heyen et al. 2002).

Rat models of hypertension like the spontaneously hypertensive rat (SHR) have shown that a strong correlation takes place between specific gene loci and hypertension. Therefore, determinants of gene expression may provide some understanding into the molecular basis of complex traits like hypertension. With the availability of the rat genome sequence and the ability to generate congenic and consomic rat strains, it has been possible to link gene expression levels of QTLs (termed eQTLs) with physiological QTLs (pQTLs). An eQTL is a locus that can explain a fraction of the genetic variance of a gene expression phenotype (Nica and Dermitzakis 2013). eQTL mapping is a relatively recent technique used for assessing associations between transcript expression and genotype in order to identify locations within the genome ((Petretto et al. 2006). With more extensive mapping of QTLs and eQTLs, and the prospective of obtaining specific gene knockout rats, the rat will continue to be a valuable tool in cardiovascular research (Dillmann 2008). In chapter 4 of this thesis, we go into more detail about the SHRSP *Spp1*^{em1} knockout rat strain, a collaboration between our laboratory and the MCW Gene Editing Rat Resource Centre in Milwaukee, to generate this strain using CRISPRCas9 technology to knock-out *Spp1* in the SHRSP$_{Gla}$ strains.

1.2.2 Stroke-Prone Spontaneously Hypertensive (SHRSP) Rat model

In 1974, a separate colony of the stroke-prone hypertensive rats (SHRSP) was established from the SHR rats. The SHR rats developed by Okamoto and Aoki in 1963 was selectively bred for high BP without any provocative dietary or environmental stimuli (Okamoto and Aoki, 1963). The SHR and "control" stock from Wistar-Kyoto rats (WKY) were imported by the National Institutes of Health (NIH) in the United States before either strain was fully inbred and distributed to commercial suppliers. Before full inbreeding, a substrain of SHR, from an outbred WKY stock in Kyoto, Japan, was found with very high BP that was susceptible to stroke than other SHR substrains. This substrain was then selectively bred for a high incidence of stroke, the stroke-prone spontaneously hypertensive rat (designated as SHRSP) (John P. Rapp 2000). The SHRSP rat is also a unique genetic model of severe hypertension and cerebral stroke (Nabika et al. 2012). The differences in genetic and metabolic features between the SHRSP and the normotensive WKY rats can also provide insight into blood pressure regulation in human essential hypertension (Akira, Imachi, and Hashimoto 2005). The SHRSP rat was developed under the following conditions: (1) the selection began with the 24th generation SHR rats, (2) only after three generations of selection was the high stroke susceptibility fixed, and (3) the severe hypertension and stroke susceptibility was fixed simultaneously. The SHRSP strain had a higher incidence of stroke (80% vs. 10%) and severe hypertension (systolic blood pressure between 220 – 240 mmHg vs. 180 – 200 mmHg) when compared to the SHR strain (Nabika et al. 2012). As in humans, the male SHRSP rats have a higher blood pressure than females.

The SHRSP is an excellent experimental animal model of human cardiovascular disease as it exhibits spontaneous onset of hypertension between 8 – 12 weeks of age. The genetic determination of hypertension in the SHRSP rats is due to multiple gene-gene and gene-environment interactions (John P. Rapp 2000). The SHRSP rats can develop several cardiovascular complications including cardiac hypertrophy, stroke, and endothelial dysfunction due to oxidative stress. Even though increased blood pressure plays a role in end-organ damage in the SHRSP rats, there are also genetic factors that also contribute. Genome-wide linkage studies have proved successful in identifying large regions in the chromosome that contains quantitative

trait loci (QTLs) for blood pressure regulation in the SHRSP rats. Two blood pressure QTLs have been identified and mapped to chromosome 2 and have become a major focus for congenic studies in our lab and others (Clark et al. 1996; Dutil and Deng 2001; Jeffs et al. 2000). This region on chromosome 2 has common or overlapping QTLs and has been linked to several rat crosses (Delles et al. 2008). Furthermore, a QTL for sex-specific BP was identified on chromosome 3 and a QTL for LVH was detected on rat chromosome 14 (Clark et al. 1996).

The University of Glasgow British Heart Foundation, Glasgow Cardiovascular Research Centre (BHF, GCRC) maintains inbred colonies of SHRSP from Glasgow colonies and normotensive reference strain WKY rats. These strains are recognised as $SHRSP_{Gla}$ and WKY_{Gla}. Previous work in our lab has shown that the SHRSP strain also exhibits a significant increase in LVMI compared to the WKY strain and this significant phenotypic difference is apparent at 5 weeks of age, prior to the onset of hypertension in this model.

1.3 Identification of Quantitative Trait Loci

Quantitative traits are multifactorial and are influenced by many polymorphic genes and environmental factors. Hence, one or more QTLs can play a role in influencing a trait or phenotype. Phenotypic variation caused by environmental factors are also independent of genotype or through gene-environment interactions. Environmental and genetic factors play and complex role in the pathogenesis of CVD. Mutations found in single genes, such as monogenic forms of hypertension, can be observed resulting in severe phenotype. There are, however, a majority of CVDs that involve mutations found in large number of genes (Dominiczak et al. 2005). Genome wide linkage analysis has found to be successful in the past decade to localize large chromosomal regions containing known QTLs for high blood pressure, left ventricular hypertrophy and ischaemic stroke in F2 crosses that were derived from the SHRSP and normotensive WKY rats (Jeffs et al. 2000). A study conducted by Tanase et al, described a segregation study of 23 inbred normotensive and hypertensive rat strains. They estimated that 65% to 75% of strain difference in the heart weight was due to genetic factors (Tanase et al. 1982). There have been several other studies that have also conducted segregation and genetic linkage analysis using F2 progeny derived from a pair of progenitor strains that show a significant difference in adult cardiac mass (John P. Rapp 2000). These studies have analysed co-segregation in crosses between a hypertensive and normotensive strain and have identified QTLs for cardiac mass or cardiac hypertrophy in several chromosomal regions (Kato et al. 1999; Innes et al. 1998; Inomata et al. 2005).

Using GWAS to find variants associated with blood pressure has been the implemented in custom-made genotyping arrays. An example of such an array is the HumanCVD BeadChip (Illumina, San Diego, CA). It contains 49,452 SNPs and provides dense coverage of ~2000 genes considered a priori more likely to have functional effects on cardiovascular traits, including BP (Keating et al. 2008). By using this array 8 genetic associations with BP traits were identified in a meta-analysis of 26,000 individuals of European ancestry (T. Johnson et al. 2011). Three associations were found at new blood pressure loci, LSP1/TNNT3, SOX6, and NOS3 new SNP associations were found at the methylene tetrahydrofolate reductase-natriuretic peptide B and natriuretic peptide C receptor (MTHFR-NPPB and NPR3),

and previously reported associations at (ATP2B1, AGT, and HFE) were replicated. Using this array, an analysis of ambulatory blood pressure in 520 white European ancestry found a significant association at the MTHFR-NPPB locus, which based on linkage disequilibrium (LD) suggested that there was a third signal at this locus (Tomaszewski et al. 2010). Results from both studies features the use of different arrays and samples to find blood pressure genes, and show any potential to find new signals at established BP loci (Munroe, Barnes, and Caulfield 2013). This array includes SNPs that were not captured by earlier genome-wide chips, and the additional information not only led to the discovery of new BP genes but also helped in gene discovery of other cardiovascular traits (Shah, Patel, and Freedman 2018). ENCODE and pathway analysis tools were used to annotate each SNP and its close proxies for which the results are presented in Table 1.1.

Table 1.1: Summary of blood pressure loci and SNPs associated with blood pressure traits. Table adapted from (Munroe, Barnes, and Caulfield 2013)

SNP	Locus Nickname	Chr	BP Position (Build 37)	Potential Blood Pressure Candidates	Novel Drug Network, ENCODE or nsSNP Candidates
rs880315	CASZ1	1	10796866	CASZ1†	…
rs5068‡	NPPA/NPPB	1	11905974	MTHFR*†, CLCN6†, NPPA*, NPPB*	PLOD1*, AGTRAP*
rs17030613	ST7L-CAPZA1	1	113190807	SLC16A1	CAPZA1*†, ST7L†, MOV10†
rs2004776‡	AGT	1	230848702	AGT*†	…
rs16849225‡	FIGN-GRB14	2	164906820	FIGN	…
rs13082711	SLC4A7	3	27537909	SLC4A7†	EOMES*
rs9815354	ULK4	3	41912651	ULK4†, CTNNB1*	…
rs319690	MAP4	3	47927484	MAP4†, SMARCC1	CDC25A*
rs419076	MECOM	3	169100886	MECOM†	…
rs871606	CHIC2	4	54799245	PDGFRA*	…
rs16998073	FGF5	4	81184341	FGF5†	-
rs13107325	SLC39A8	4	103188709	SLC39A8†	…
rs6825911	ENPEP	4	111381638	ENPEP*†, PITX2	…
rs13139571	GUCY1A3-GUCY1B3	4	156645513	GUCY1A3*†, GUCY1B3*†	…
rs1799945	HFE	6	26091179	HFE†	SLC17A1*, HIST1H4C†, HIST1H2BB†
rs805303	BAT2-BAT5	6	31616366	DDAH2*, HSPA1L *, HSPA1A*, HSPA1B*	CSNK2B*, C6ORF25*, NEU1*, EHMT2*
rs17477177	PIK3CG	7	106411858	…	…
rs3918226	NOS3	7	150690176	ABP1*, KCNH2*, NOS3*†, ACCN3,	CDK5*, SLC4A2*
rs2898290	BLK-GATA4	8	11433909	PINX1*, GATA4*, MTMR9	CTSB*, SOX7*, NEIL2*, BLK†, LINC00208†
rs2071518	NOV	8	120435812	NOV†, ENPP2	…
rs11014166‡	CACNB2	10	18708798	CACNB2*†,	…
rs1530440	c10orf107	10	63524591	…	C10orf107†
rs932764	PLCE1	10	95895940	PLCE1†	…
rs11191548‡	CYP17A1-NT5C2	10	104846178	CYP17A1*†	NT5C2†
rs1801253‡	ADRB1	10	115805056	ADRB1*†	…
rs661348	LSP1-TNNT3	11	1905292	CTSD*	LSP1*†
rs7129220	ADM	11	10350538	ADM*†	SBF2†
rs2014408	SOX6	11	16365282	SOX6*†	…
rs381815	PLEKHA7	11	16902268	PLEKHA7†	…
rs633185	FLJ32810-TMEM133	11	11538410	PGR*, TRPC6*	ARHGAP42†
rs11222084	ADAMTS8	11	130273230	…	ADAMTS8†
rs17249754‡	ATP2B1	12	90060586	ATP2B1*†	DUSP6*
rs653178‡	SH2B3	12	112007756	ALDH2*, PTPN11*, SH2B3*†	ACAD10*, RPL6*, CUX2*
rs2384550‡	TBX3-TBX5	12	115352731	TBX5*, TBX3	…
rs1378942‡	CYP1A1-CSK	15	75077367	CYP1A1*, CYP1A2*†, CSK*†, ULK3, MPI	LMAN1L*, SCAMP2*,hsa-mir-4513†
rs2521501	FES-FURIN	15	91437388	FES*†, FURIN*†	PRC1*
rs13333226	UMOD	16	20365654	UMOD†	ACVR2A†, ORC4†
rs17608766	GOSR2	17	45013271	GOSR2†	WNT3*, NSF*, RPRML†
rs16948048	ZNF652	17	47440466	ZNF652†, NGFR	PHB*, IGF2BP1*
rs1327235	JAG1	20	10969030	JAG1	
rs6015450	GNAS-EDN3	20	57751117	GNAS*, ZNF831*†, EDN3*	

This table contains a subset of SNPs associated with blood pressure traits, listed in chromosomal order. bp indicates base pair; CEU, Utah residents with ancestry from northern and western Europe; Chr, chromosome; nsSNP, if index SNP at a locus or a SNP in high linkage disequilibrium (r2>0.8) is nonsynonymous SNP; RAF, risk allele frequency; and SNP, single-nucleotide polymorphism.

- *Genes which interact with the antihypertensive drug network.
- †Genes with putative functional LD proxy variants supported by ENCODE or Annovar nsSNP analysis.
- ‡The identity of the first SNP associated at a particular locus.
- §Risk allele frequency in E Asians.

Genome wide linkage studies was successful in identifying large chromosomal regions that contain QTL for blood pressure regulation in the SHRSP rats. After the identification of QTLs of interest, the next step is gene identification which is accomplished by genetic and physiological analysis of congenic lines that have been developed from the genetic locus. The development of a congenic strain will help confirm or refute the existence of a QTL (Jeffs et al. 2000; John P. Rapp, 1995).

1.3.1 Congenic strains

A congenic strain is constructed by transferring a chromosome segment containing a QTL of interest from a host strain and replacing it with a homologous region from a donor strain by serial backcrossing and selection. Chromosomal regions are examined at each backcross for heterozygosity by using polymorphic microsatellite markers. According to Mendelian laws, after 8 to 12 backcrosses more than 99% of the genetic background will have been replaced by the recipient strain. This process is continued until the integrity of the host strain background has been restored (Carr et al. 2002; Shao et al. 2010). If for instance, the blood pressure of the congenic strain is significantly different from the recipient strain, it can be concluded that the chromosomal segment does contains a QTL that promotes differences in blood pressure in both the donor and recipient strains (Jeffs et al. 2000). Using reciprocal congenic strains derived from a cross of SHR and WKY rat strains, WKY.SHR-Sa (WConSa) and SHR.WKY-Sa (SConSa), a QTL for blood pressure was mapped to rat chromosome 1 in F2 rats (Frantz et al. 1998).

Another method for producing congenic strains is by speed congenics, also referred to as marker-assisted selection or MAS. Using the rat genome sequence, dense maps of polymorphic markers can be used to speed-up the development of congenic rat strains, select for smaller donor-derived intervals and estimate background contamination (Armstrong, Brodnicki, and Speed 2006). The resulting offspring that contains the largest percentage of the recipient background can be selected and used for subsequent breeding all the while maintaining heterozygosity of the chromosomal segment derived from the donor (Beth Bennett, Thomas E. Johnson 1998). Speed congenic breeding protocols have been used to develop WKY and SHRSP rat congenic strains containing various segments of chromosome 2 (McBride et al. 2003). The transfer of the rat chromosome 2 segment containing the

QTL for blood pressure from WKY into the SHRSP genetic background (SP. $WKY_{Gla}2a$) decreased baseline and salt-loaded systolic blood pressure by ~20mmHg and 40mmHg respectively, in male congenic rats when compared to the parental SHRSP rat strain (Jeffs et al. 2000).

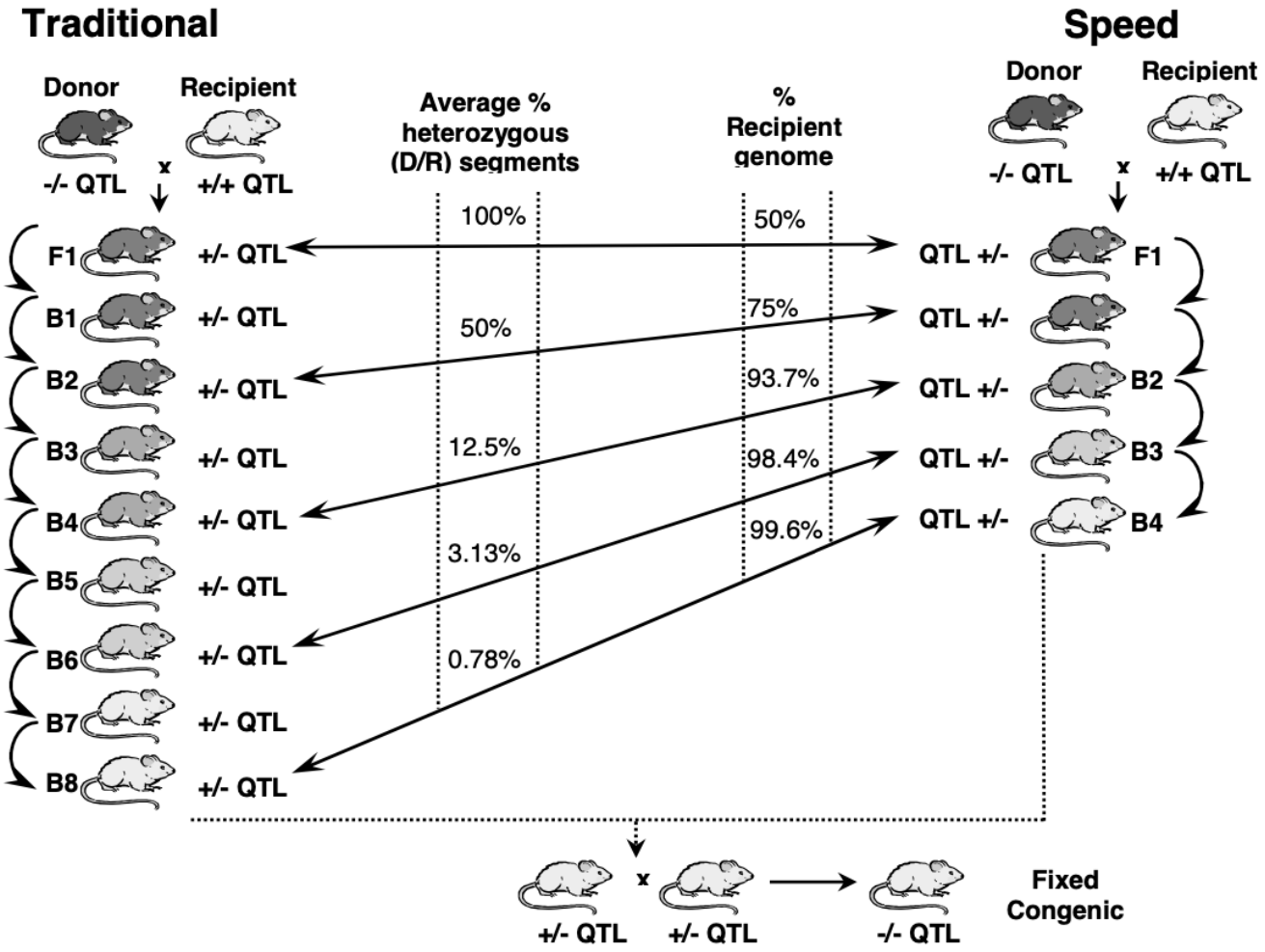

Figure 1.6: Traditional breeding vs. speed congenics

Congenic strain construction to illustrate differences between the traditional and marker-assisted speed congenic approach. The gradient from grey to white represents the increase in dilution of the donor genome in the genetic background. F1 - first filial generation, B - backcross, D – donor strain alleles, R – recipient strain alleles.

1.3.2 Generation of chromosome 14a congenic strains

The chromosome 14a congenic strain was developed to identify and confirm the QTL for LVMI since it is regarded an indicator for LVH and is a clinically important marker for CVD (Antoniucci et al. 1997). Previous work in the McBride & Graham laboratory successfully identified a QTL for left ventricular mass index (LVMI) by genome-wide linkage studies. This QTL was mapped to the $SHRSP_{Gla}$ rat on chromosome 14 and was validated by constructing congenic strains on both WKY and SHRSP genetic backgrounds; SP. WKY_{Gla}14a labelled (F) and WKY.SP_{Gla}14a labelled (D). These strains were confirmed through genotyping. Furthermore, the SP. WKY_{Gla}14a (F) rat strain showed improved cardiac parameters even though, their systolic blood pressure was similar to the SHRSP rats. The WKY_{Gla}14a (F) rat strain showed increased fibrosis and decreased LV diastolic function (Douglas et al. 2010).

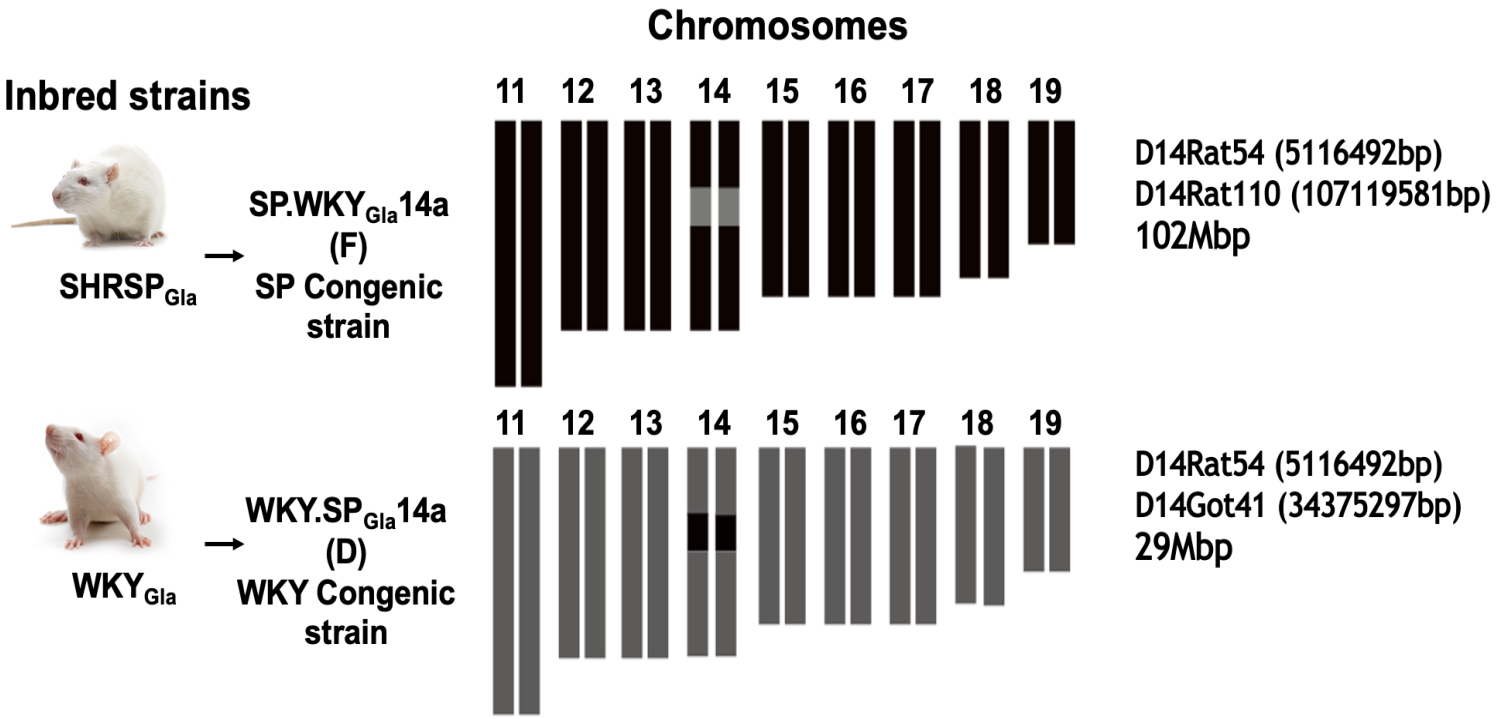

Figure 1.7: SHRSP, WKY and chromosome 14 congenic strains

Previous work within the laboratory identified a quantitative trait locus (QTL) for left ventricular mass index (LVMI) on chromosome 14, and congenic strains (SP.WKY$_{Gla}$14a & WKY.SP$_{Gla}$14a) on both the SHRSP and WKY genetic backgrounds were constructed. SNP genotyping in the SHRSP and WKY strains confirmed the microsatellite genotyping data and identified SNP's principally to a 29Mbp region (between 5-34Mbp) on chromosome 14 confirming the LVMI QTL data. The remaining region of chromosome 14 was identical by descent in the SHRSP and WKY. Congenic breeding allows the introgression of a 29Mbp section of the SHRSP onto the WKY background, and a 102Mbp section of the WKY onto the SHRSP background.

1.3.3 Phenotypic data

As mentioned previously, genome-wide linkage studies successfully identified a QTL for LVMI in the SHRSP$_{Gla}$ rat strain mapping to chromosome 14. The QTL for LVMI was confirmed by the construction of chromosome 14 congenic strains WKY.SP$_{Gla}$14a (D) and SP. WKY$_{Gla}$14a (F) on both genetic backgrounds. Echocardiography and blood pressure measurements were carried out in the parental (SHRSP and WKY) and congenic strains [SP. WKY$_{Gla}$14a labelled (F) and WKY.SP$_{Gla}$14a labelled (D)] at 5 week and 16-week time points by previous members of the McBride and Graham group. They measured LVMI and systolic blood pressure and made comparisons between the parental and congenic strains. The LVMI phenotype differences were observed between the parental strains and are apparent at 5 weeks of age, prior to the onset of hypertension.

Results showed LVMI to be significantly increased in the WKY. SP$_{Gla}$14a (D) strain at both the 5-week and 16-week time point compared to the WKY strain, and it showed LVMI to be significantly decreased in the SP. WKY$_{Gla}$14a (F) strain at both the 5-week and 16-week time point compared to the SHRSP strain (figure 1.8B).

The systolic blood pressure measurements were recorded using radiotelemetry method (between 12 – 16 weeks of age). The SHRSP and SP. WKY$_{Gla}$14a (F) strains both showed hypertensive systolic measurements and the WKY and WKY. SP$_{Gla}$14a (D) strains both showed normotensive systolic measurements. They however did observe a small but significant increase in BP in the WKY. SP$_{Gla}$14a (D) (figure 1.8C).

The combination of the parental SHRSP$_{Gla}$ and WKY$_{Gla}$ strains, the congenic WKY.SP$_{Gla}$14a (D) and SP. WKY$_{Gla}$14a (F) strains, and cardiac, neonatal microarray gene expression profiling identified Osteopontin (*Spp1*) as a positional candidate gene for LVMI. This gene was mapped to the minimal transferred congenic interval on chromosome 14. To identify gene expression changes that are responsible for the disease phenotype and to differentiate between the hypertrophy phenotype established in 5-week rats, previous members of the McBride and Graham group determined cardiac gene expression profiles from neonatal SHRSP$_{Gla}$, WKY$_{Gla}$, WKY.SP$_{Gla}$14a (D) and SP. WKY$_{Gla}$14a (F) rats (figure 1.8D). By filtering the genes

that were found significant between the parental and congenic strains, four genes were identified to be consistently differentially expressed: osteopontin (Spp1), hydroxy steroid dehydrogenase 17-beta 13 (Hsd17b13), Zinc finger protein (Znf644) and Ras-related associated with diabetes (Rrad). From these four genes only osteopontin (*Spp1*) mapped to the congenic interval and this was validated by conducting qRT-PCR which showed significantly increased expression of *Spp1* in heart tissue and in primary isolated cardiomyocytes (figure 1.8E).

In this thesis we look at how *Spp1* is an important modulator for LVH and fibrosis in the $SHRSP_{Gla}$ strain and how early changes in *Spp1* gene expression, before the onset of hypertension, initiates cardiac phenotypes in the $SHRSP_{Gla}$ strain. *Spp1* has been significantly associated with diastolic dysfunction in a Japanese population. SNPs in the human *Spp1* promoter that affect transcriptional activity have been identified and the -156insG promoter polymorphism has been linked to *Spp1* transcriptional activity by the generation of an additional Runx2 binding site (Nakayama et al. 2011). Furthermore, in chapter 3 of this thesis, we aim to characterise the functional effects of the *Spp1* promoter constructs generated to analyse and compare transcriptional activities and promoter function.

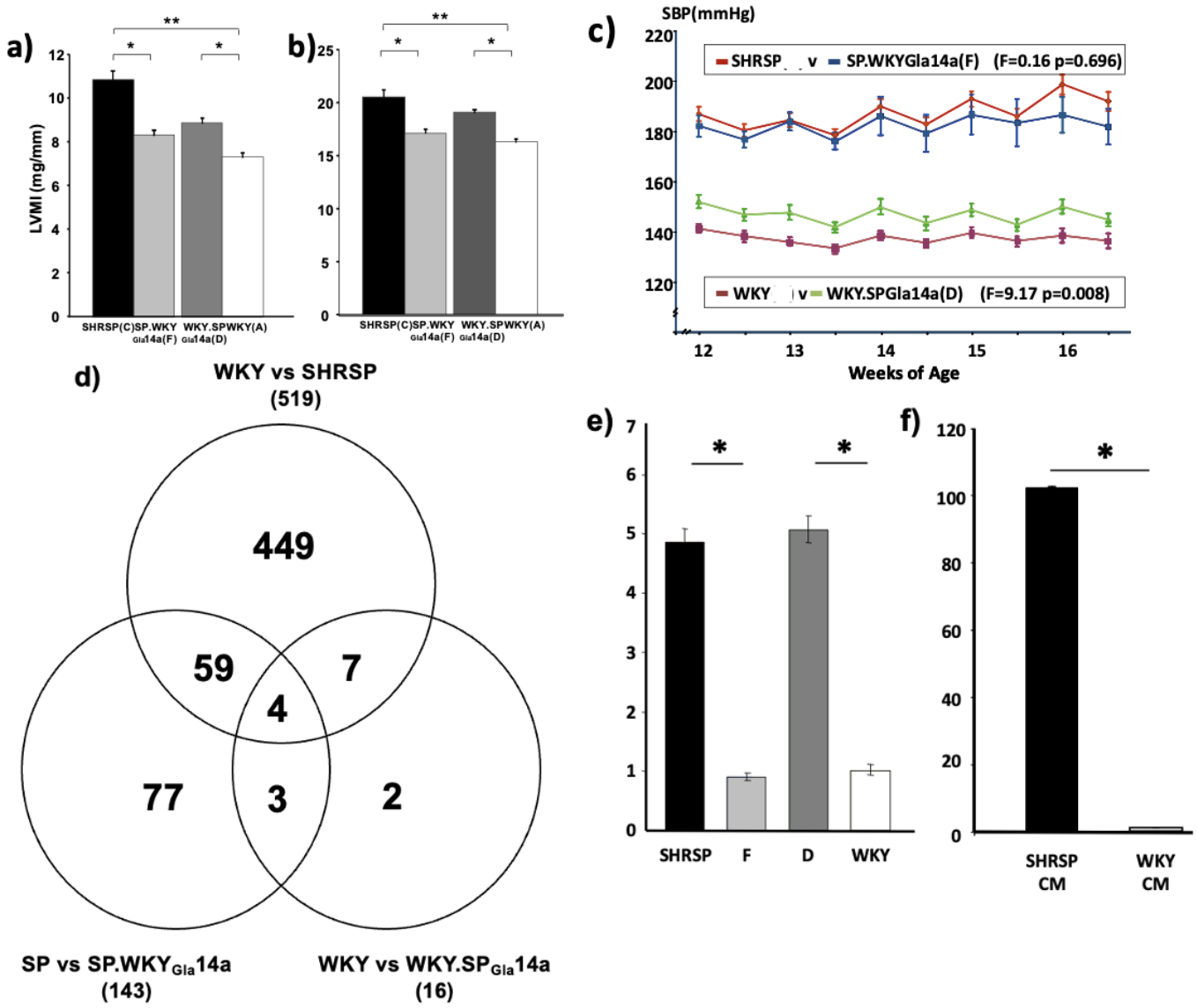

Figure 1.8: a) Graph shows significant differences in LVMI when comparing SHRSP with SP. WKY$_{Gla}$14a congenic strain, and b) WKY with WKY.SP$_{Gla}$14a congenic strain at 5-week and 16-week time points. c) Radiotelemetry blood pressure measurement. d) Microarray expression profiling results identifying four genes that were consistently differentially expressed: osteopontin (*Spp1*), hydroxy steroid dehydrogenase 17-beta 13 (*Hsd17b13*), Zinc finger protein (*Znf644*) and Ras-related associated with diabetes (*Rrad*). Osteopontin (*Spp1*) mapped to the congenic interval on chromosome 14. e) qRT-PCR confirmation of Spp1 expression in whole neonatal heart. f) Spp1 qRT-PCR data from isolated neonatal primary cardiomyocytes (CM) from SHRSP$_{Gla}$ and WKY$_{Gla}$.

1.4 Osteopontin

1.4.1 Structure of Spp1

Osteopontin, also known as secreted phosphoprotein-1 (*Spp1*) is an acidic phosphorylated acidic glycoprotein that has been associated in several physiological and pathological events, including maintenance and reconfiguration of tissue integrity during inflammatory processes, biomineralization, leukocyte recruitment and cell survival (Denhardt et al. 2001; O'Brien et al. 1994). *Spp1* is a multifunctional protein and even though it is highly expressed in bone, it is also expressed in many other cell types including macrophages, endothelial cells, smooth muscle cells and epithelial cells (O'Brien et al. 1994).

Spp1 is a negatively charged acidic hydrophilic protein that contains approximately 300 amino acid residues and is secreted into all body fluids. The *Spp1* protein is 314 amino acids long, with a predicted molecular weight of 32 kilo Daltons (kDa). *Spp1* cDNA from different mammals show a higher degree of sequence homology. Alternate splice sites are found however no functional significance have been shown (Mazzali et al. 2002). *Spp1* is a monomer ranging from 264 to 301 amino acids in length. It undergoes a wide range of post-translational modification including phosphorylation, glycosylation, and cleavage which results in molecular mass variants from 25 kDa to 75 kDa. It contains a hydrophilic sequence of 16 amino acids, characteristic of a secreted protein, a potential calcium phosphate apatite binding region of consecutive asparagine residues, a cell attachment GRGDS sequence, a thrombin cleavage site, and two glutamines whose substrates are recognised for transglutaminase-supported multimer formation (G. A. Johnson et al. 2003; O'Regan and Berman 2001).

Spp1 has an arginine-glycine-aspartic acid (RGD) cell binding sequence, a calcium binding site and two heparin binding domains. Cells may bind to *Spp1* through multiple integrin receptors including the vitronectin receptor αv (β1, β3, or β5) and various β1 and β5 integrins. Integrin binding could be RGD-dependent or RGD-independent (Mazzali et al. 2002). RGD-dependent *Spp1* receptor interactions are regulated by thrombin cleavage of *Spp1*. For example, thrombin-cleaved *Spp1* can support RGD-dependent migration of melanoma cells (L. L. Smith and Giachelli

1998). Similarly, K562 erythroleukemia cells to the RGD sequence through activated α5β1 in thrombin-cleaved *Spp1*. RGD-independent interaction with α9β1 via the SVVYGLR sequence, is located between the RGD sequence and the thrombin cleavage site (figure 1.9). This sequence becomes accessible to integrins after *Spp1* is cleaved by the protease thrombin (Denhardt et al. 2001; Yokosaki et al. 1999). Thrombin cleavage of *Spp1* can reveal additional cryptic binding sites and produce functional chemotactic fragments (O'Regan and Berman 2001). *Spp1* can also bind to various isoforms of CD44 in an RGD-independent manner (Mazzali et al. 2002).

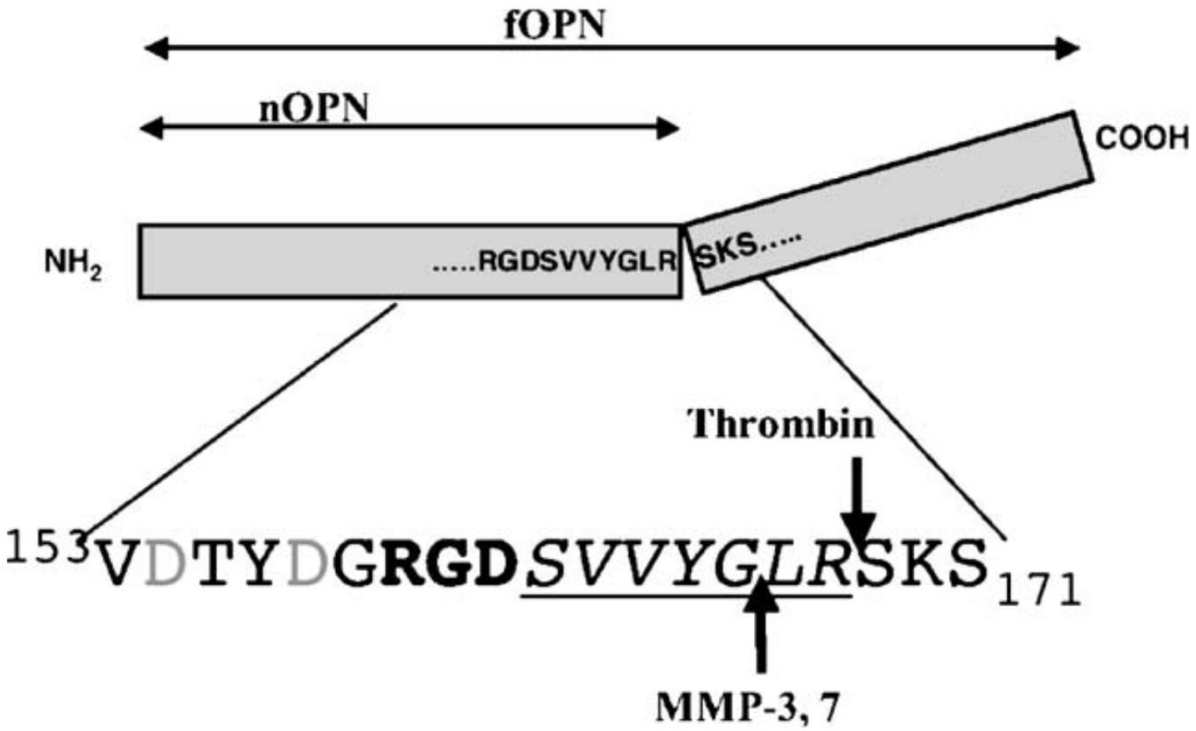

Figure 1.9: Map of the integrin-binding region of *Spp1*

N-terminal fragment of thrombin-cleaved osteopontin (nOPN), full length osteopontin (fOPN). Aspartic acid residues replaced with alanine are shown in grey. RGD sequence identified by integrins αvβ6, αvβ3, αvβ5, and α5β1 is in bold text. SVVYGLR sequence is identified by integrin α9β1 and is in underlined italics. MMP-3 and MMP-7 cleaves between Gly and Leu within the SVVYGLR. The thrombin cleavage site is designated by an arrow (Yokosaki et al. 2005).

1.4.2 Function and regulation of Spp1

Spp1 is a multifunctional protein and plays a significant role in many biological processes, including bone resorption, immune cell activation, inhibition of vascular calcification and ECM remodelling (Kazanecki, Uzwiak, and Denhardt 2007). Biological functions of *Spp1* can be influenced by post-translational modifications of *Spp1*. Additionally, proteolytic cleavage of *Spp1* by thrombin and matrix metalloproteinases (MMPs) improves its adhesion properties compared to the full-length protein. This seems to be due to increased activity of the RGD site, a possible indication of conformational change which results in a higher affinity binding (Scatena, Liaw, and Giachelli 2007). *Spp1* is also a key cytokine that is involved in immune cell recruitment and type-1 (th1) cytokine expression at inflammation sites (K. X. Wang and Denhardt 2008).

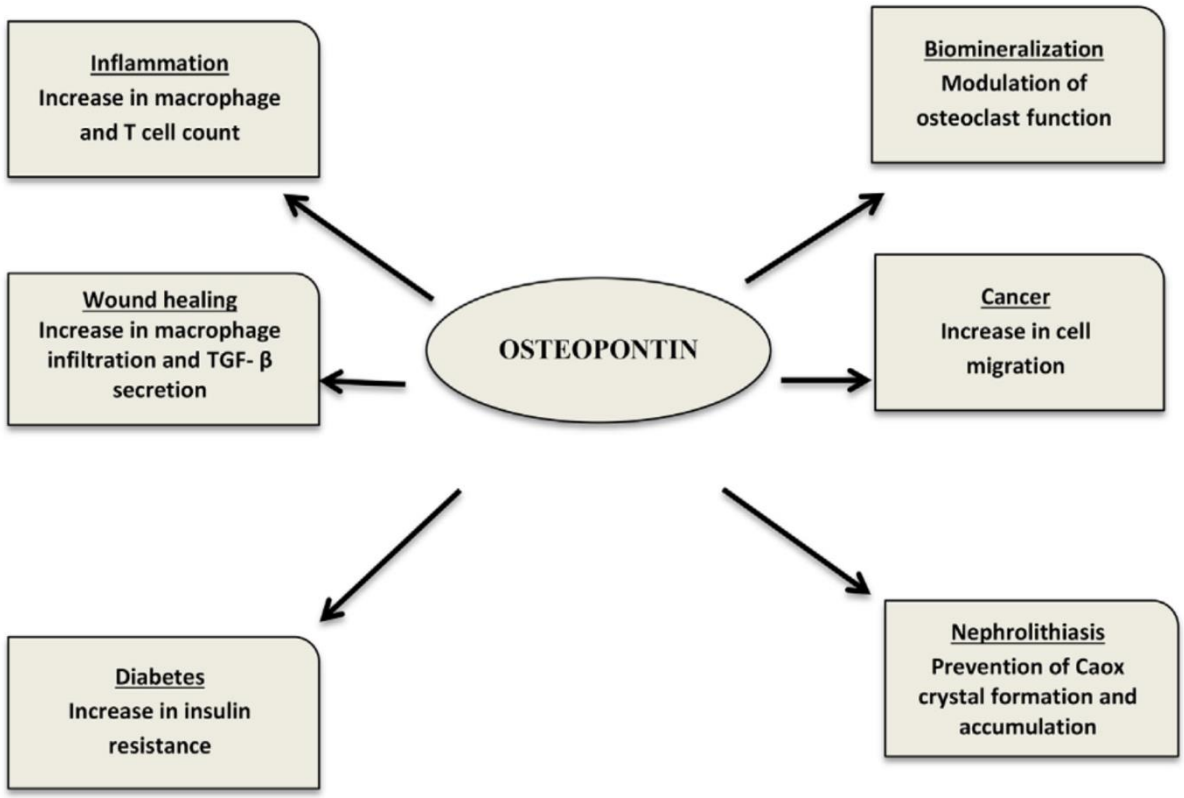

Figure 1.10: Major biological functions of *Spp1*

Osteopontin takes important roles in inflammation, biomineralization, cardiovascular diseases, cellular viability, cancer, diabetes and renal stone disease through different mechanisms (image from Icer and Gezmen-Karadag 2018).

Spp1 has multiple functional motifs which allows interactions with different cell types including smooth muscle cells, endothelial cells, and inflammatory cells, thus facilitating a wide range of biological functions. *Spp1* is inadequately conserved among species (63% human to mouse, 30% human to chicken) however, its functional domains are conserved (Lund, Giachelli, and Scatena 2009). Highly conserved sequence motifs and post-translational modifications contributes to different *Spp1* functional activities (K. X. Wang and Denhardt 2008). The highly conserved motifs include abundance of acidic residues, the RGD integrin biding domain, similar phosphorylation and glycosylation motifs, and the recognition that at least one site of controlled proteolysis (Bellahcène et al. 2008).

Spp1 has shown to play a role in the inflammatory response. It regulates the immune system at different levels as it is expressed by many different cell types including macrophages, neutrophils, dendritic cells, NK cells, and T and B lymphocytes (figure 1.11). It acts as a chemotactic molecule to help promote the migration of inflammatory cells to sites of injury and acts as an adhesive protein to retain cells at the site (Lund, Giachelli, and Scatena 2009; K. X. Wang and Denhardt 2008). *Spp1* is upregulated in response to injury and every organ such as, cardiac tissue, lung, bone, brain, kidney, liver, adipose tissue and most tumours, are checked for inflammation (Gómez-Ambrosi et al. 2007; Sodek, Batista Da Silva, and Zohar 2006).

Spp1 can also function as a cell survival factor and can protect cells from undergoing apoptosis (Mazzali et al. 2002). *Spp1* can also protect cells from apoptosis via its binding to the αvβ3 integrin of endothelial cells. This causes the activation of pro-survival transcription factor NFkB and protects the cells from undergoing apoptosis (Scatena et al. 1998). Cell types including vascular smooth muscle cells and haemopoietic cells also report following this pathway (Weintraub et al. 2000).

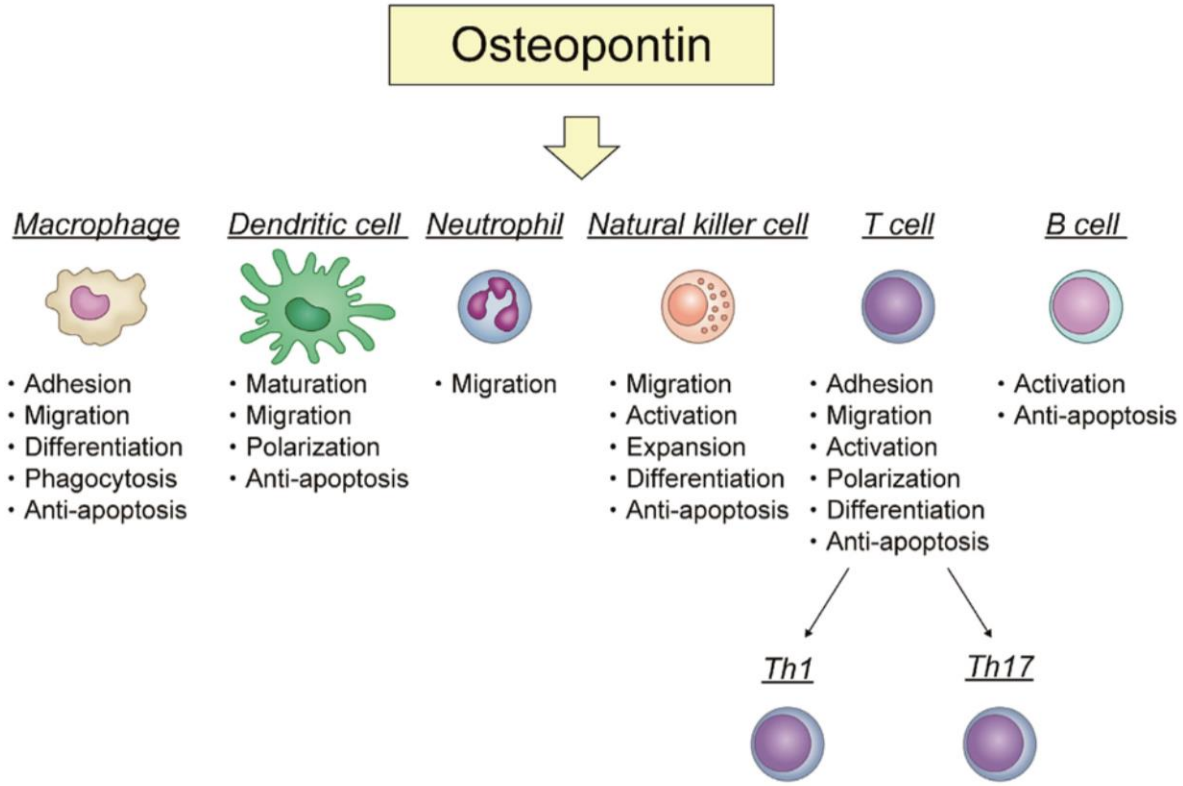

Figure 1.11: Role of *Spp1* on immune cells during inflammation and apoptosis

Spp1 is an important chemical attractant for macrophages and T cells. An increase in *Spp1* release is reported from macrophages, activated T cells, epithelial and endothelial cells as well as smooth muscle cells during inflammation process (image from Icer and Gezmen-Karadag 2018)

Spp1 is also important in tissue repair and its association with tissue fibrosis by the infiltration of macrophages and the production of TGF-β (Ophascharoensuk et al. 1999). However, recent data has suggested that *Spp1* could play a direct role in the development of tissue fibrosis, *Spp1* causes the recruitment of fibroblasts, stimulates their proliferation and regulates the secretion of MMPs by fibroblasts (G. Li et al. 2000; Mazzali et al. 2002).

Spp1 has also been shown to play an important role in cardiovascular diseases such as atherosclerosis, valvular stenosis, hypertrophy, myocardial infarction (MI) and heart failure (M. Singh et al. 2010a). Studies have shown that the development of heart failure has been associated with the expression of *Spp1* in the heart (K. Singh et al. 1999). It has been suggested that *Spp1* plays a crucial role in the development of cardiac fibrosis. The upregulation of *Spp1* mRNA expression in cardiac fibroblasts by AngII and the blockage of mitogenic effects of AngII by an anti-OPN antibody on rat cardiac fibroblasts suggests that *Spp1* is an important mediator of AngII induced cardiac fibrosis (Ashizawa et al. 1996; Collins et al. 2004; Matsui et al. 2004).

1.4.3 Expression of Spp1 and its role in the heart

The heart expresses low levels of *Spp1* under basal conditions however, its expression increases significantly under several pathological conditions (M. Singh, Dalal, and Singh 2014a). Increased expression of *Spp1* has been associated with the development of cardiac remodelling and fibrosis, cardiac hypertrophy and heart failure (Abdelaziz Mohamed et al. 2019). Cell types of the heart, such as myocytes, fibroblasts and microvascular endothelial cells express low levels of *Spp1*. AngII, glucocorticoid hormones and cytokines (interleukin-1β+ interferon-γ) increase *Spp1* expression in different cell types of the heart (M. Singh, Dalal, and Singh 2014a; M. Singh et al. 2010a) (figure 1.12).

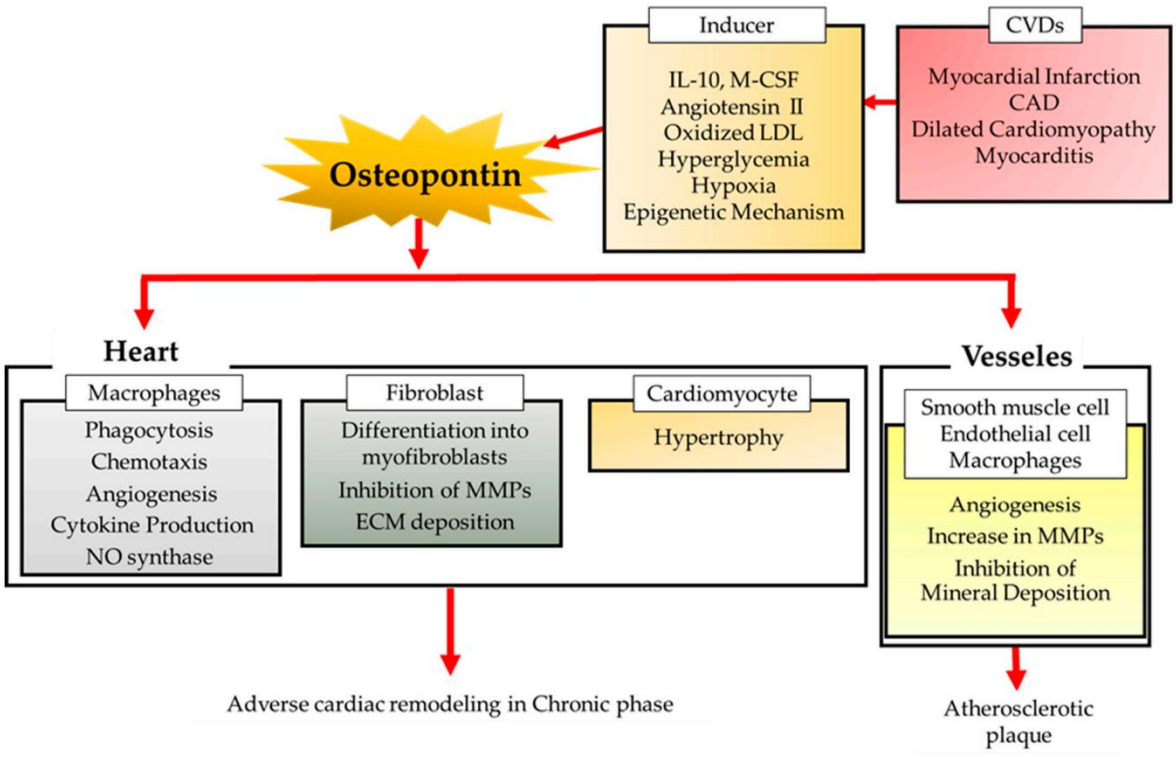

Figure 1.12: *Spp1* in cardiac remodelling

Spp1 is involved in a number of CVDs including ischemic heart diseases, hypertension, heart failure, dilated cardiomyopathy, atherosclerosis, and several cardiomyopathies, and the major source and role of *Spp1* is dependent on pathological states (Image from (Shirakawa and Sano 2021).

In many experimental animal models, including MI, ischemia perfusion injury and AngII or aldosterone-infusion, decreased *Spp1* expression was associated with significant decrease in myocyte apoptosis and improved cardiac function (M. Singh et al. 2010b; M. Singh, Dalal, and Singh 2014a). It has also been shown that increased levels of *Spp1* in rat models resulted in the development of cardiac decompensation from LVH (Frerker et al. 2012; Trueblood et al. 2001). Even though infiltrating macrophages are the main source of *Spp1* protein, under various pathological conditions and stresses cardiomyocytes and fibroblasts can also express *Spp1* (Subramanian et al. 2007; Graf et al. 1997).

The expression of *Spp1* in the heart has been shown to play a role in the remodelling of the LV and extracellular matrix. The expression of *Spp1* in the heart has been associated with the development of heart failure. In both mice and human hearts, myocardial *Spp1* expression was increased in pressure overload LVH. Serum *Spp1* could also be associated with LVH in patients suffering from essential hypertension (Graf et al. 1997; Hou et al. 2014; Xie, Singh, and Singh 2004). However, there has been other research that shows that the polymorphism of *Spp1* gene promoter has no association with LVMI, but it does with left ventricular diastolic dysfunction (LVDD) and lower LV systolic function in hypertensive patients (Nakayama et al. 2011). LV diastolic function is an early marker of cardiac target organ damage in hypertension and its early detection, before LVH, may suggest a clinical advantage for the treatment and prognosis of hypertension. High levels of *Spp1* can be an indicator of LVMI and can be indirectly associated with LV diastolic function since *Spp1* is secreted by myocytes and cardiac fibroblasts (Ashizawa et al. 1996; Yang, Wang, and Gao 2020).

Increased *Spp1* expression also plays an important role in LVH, and a recognised route through which *Spp1* can mediate this hypertrophic effect is through the activation of pro-hypertrophic kinases and pathways (Abdelaziz Mohamed et al. 2019). Cardiomyocytes are an important source of *Spp1* in LVH in both rats and humans. However, the association of LVH development and the expression of ventricular ANP, a known marker of myocyte hypertrophy, is linked to the upregulation of *Spp1* expression (Graf et al. 1997). To examine *Spp1* expression in cardiomyocytes, Graf et al. (1997) treated cultured neonatal cardiac myocytes with

AngII, Endothelin-1 (ET-1), and norepinephrine (NE). In LVH induced by overload or by myocardial infarction, cardiac expression of ET-1 has been shown to increase, and elevated plasma levels of ET-1 have also been measured in HF patients (Cody et al. 1992; Sakai et al. 1996). It is also possible that ET-1 could contribute to the increase in *Spp1* expression in LVH. These observations suggest that increased *Spp1* production occurs in cardiomyocyte hypertrophy in both *in vivo* and *in vitro* (Graf et al. 1997).

The mechanism of myocardial pathophysiology and the progression into cardiac hypertrophy has been a study of interest ever since the discovery of stem cells in the heart. These cells have the ability to differentiate into various cardiac cell lineages (Sluijter, Doevendans, and Goumans 2011). It has been documented that the adult heart contains a pool of cardiac stem-progenitor cells (CSCs) that can not only restock cardiomyocyte cells but also regenerate coronary vessels (Torella et al. 2007). In CVD, extracellular vesicles (EVs) of cardiac cells regulate the exchange of molecular signals and vectors to activate target molecules for the regulation of inflammatory factors, which can ultimately promote, which can cardiac regeneration and function (Shah, Patel, and Freedman 2018; M. Xu et al. 2019). In the cardiovascular system, EVs from different cellular origins have been identified.

1.5 Extracellular Vesicles (EVs)

Cells communicate in three different ways: direct cell-cell contact, secreted molecules like hormones, cytokines and extracellular vesicles or EVs (Petrovčíková, Vičíková, and Leksa 2018). EVs are a heterogenous family of lipid bound vesicles that originate from the endosome or plasma membrane and are secreted into the extracellular space (Abels and Breakefield 2016; Doyle and Wang 2019). Initially, they were known to be part of a disposal mechanism that releases unwanted waste or materials from cells. Further research has shown that EVs are an important mediator of intercellular communication involved in normal pathophysiological processes and developments (Frühbeis, Fröhlich, and Krämer-Albers 2012). EVs enclose packages of biomolecules that are released from the cells into the extracellular environment. These molecules include particles such as exosomes, ectosomes, microvesicles, oncosomes and apoptotic bodies (Théry et al. 2018). These particles are differentiated based on their biogenesis, pathways they are released from, their size, content and function (Zaborowski et al. 2015). The content of EVs consists of lipids, nucleic acids, and proteins, specifically associated with the plasma membrane, cytosol and those involved in lipid metabolism (Bebelman et al. 2018; Doyle and Wang 2019). EVs have been isolated from cultured cells and from body fluids such as urine, breast milk, blood plasma and cerebrospinal fluid (Petrovčíková, Vičíková, and Leksa 2018). Immune cells such as B cells, T cells, dendritic cells, macrophages, natural killer cells, mast cells, or platelets have been known to produce EVs. They are also involved in the intercellular exchange of proteins and RNA, and in the regulation of angiogenesis or immune responses. Transfer of EV content to a recipient cell makes them possible carriers of and delivery vehicles of therapeutic RNA, protein and even drugs. EVs can also stimulate specific signalling pathways and can be used as potential therapeutics (Petrovčíková, Vičíková, and Leksa 2018; Pulliero et al. 2019; Raposo and Stoorvogel 2013).

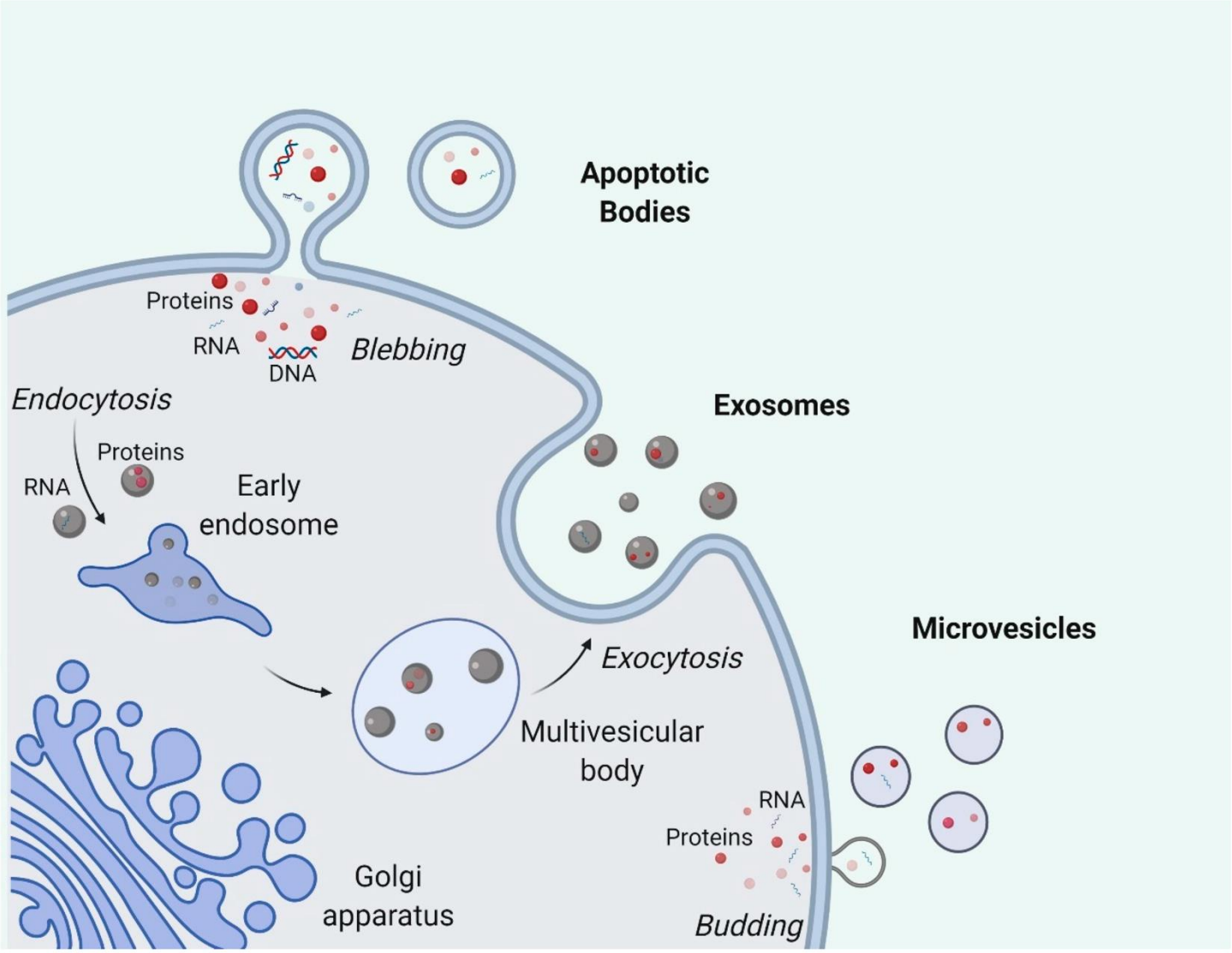

Figure 1.13: Biogenesis of EV subtypes: microvesicles (MVs), exosomes and apoptotic bodies

Microvesicles are formed by the outward shedding of the cell membrane into the extracellular space. Exosomes are intraluminal vesicles that are released when a multivesicular body fuses with the cell membrane through exocytosis. Apoptotic bodies are generated when cells undergo apoptosis (Dang et al. 2020).

1.5.1 EV biogenesis

EVs can be divided into three main types based on their origin. Microvesicles (MVs), exosomes and apoptotic bodies. MVs originate from shedding of the plasma membrane and have a size range between 50 nm to 1 um. Exosomes originate from multivesicular bodies (MVBs) and have range between 30 nm to 150 nm in size, and apoptotic bodies originate from apoptotic cells that are produced upon the activation of apoptotic paths and range between 50 nm to 2 um in size (Doyle and Wang 2019; Zaborowski et al. 2015).

MVs are released from the surface of the cell by an outward budding and the fission of the plasma membrane. They are formed by the redistribution of phospholipids, repositioning of phosphatidylserines to the outer leaflet and the contraction of cytoskeletal structures by actin-myosin system (Akers et al. 2013). ADP-ribosylation factor 6 (ARF6) begins the flow that activates phospholipase D (PLD) followed by the extracellular signal-regulated kinase (ERK) recruited to the plasma membrane. It then phosphorylates and activates the myosin light chain kinase (MLCK). The phosphorylation of the myosin light chain initiates the release of MVs (Muralidharan-Chari et al. 2009). MVs and MVBs are formed by the endosomal sorting complex required for transport (ESCRT). ESCRT contains around thirty proteins, for example: vacuolar protein sorting-associated protein 4 (VPS4), ALG-2-interacting protein X (ALIX), and many other. These proteins can be divided into four types: ESCRT-0, ESCRT-I, ESCRT-II, and ESCRT-III. The ESCRT-0 complex recognises ubiquitinated transmembrane proteins in the endosomal membrane. ESCRT-I and ESCRT-II distorts the membrane to form buds containing sorted cargos. ESCRT-III can induce the scission of vesicles (Hanson and Cashikar 2012). Non-apoptotic plasma membrane blebs are another mechanism of MV biogenesis. This mechanism is frequently observed in highly aggressive cancer cells (Bebelman et al. 2018). These blebs expand and retract at the surface of the cell and contribute to cell motility (Fackler and Grosse 2008). These blebs are also released as MVs by actin cytoskeleton rearrangements at the vesicle budding neck that results in membrane scission (Muralidharan-Chari et al. 2009).

Exosomes are produced as intraluminal vesicles (ILVs) by the inward budding of MVBs and are derived from the endosomal system. This network of ILVs can be used to degrade, recycle or exocytose proteins, lipids, and nucleic acids. Within the endosomal system or endocytic pathway, endosomes are differentiated into three compartments: early endosomes, late endosomes, and recycling endosomes. Early endosomes fuse with endocytic vesicles and fuse their content into those meant for recycling, degradation, or exocytosis. The contents intended for recycling are sorted into recycling endosomes and the remainder of the early endosomes undergo a series of transformations to develop into late endosomes (Akers et al. 2013; Abels and Breakefield 2016). Late endosomes accumulate ILVs formed by the inward budding of the endosomal membrane. During the process, cytosolic proteins, nucleic acids, and lipids are sorted into these small vesicles. These small vesicles are known as MVBs. The ESCRT machinery is the pathway of MVB biogenesis that is responsible for sorting ubiquitinated proteins into ILVs. This is first initiated by ESCRT-0, where ubiquitinated proteins are recognised and retained in the late endosomal membrane. After the primary enfolding of the limiting membrane into the MVB lumen which is activated by ESCRT-I and ESCRT-II, a spiral shaped structure is formed by ESCRT-II that tightens the budding neck and ATPase VPS4 drives membrane scission (Bebelman et al. 2018; Henne, Buchkovich, and Emr 2011). The role of the Rab family of small GTPases in vesicle trafficking and fusion with the plasma membrane indicates that these proteins (Rab7, Rab11, Rab27a/b and Rab35) affect exosome release (Stenmark 2009). Exosomes released by fusion of MVBs with the plasma membrane are enabled by Rab11 and Rab35, and this was identified when screening with dominate-negative Rab GTPase mutants (Hsu et al. 2010). Exosomes release by this mechanism are found to be rich in proteins such as flotillin and other cell specific proteins that include Wnt, PLP, and transferring receptor (TfR) (Abels and Breakefield 2016). Exosomes released by Rab27a/b are associated with the late endosomal and secretory compartments. They are also rich in late endosomal proteins such as CD63, ALIX and TSG101 (Stenmark 2009). SNARE proteins have also been involved in the membrane fusion of two organelles.

Apoptotic bodies are products of programmed cell death, also known as apoptosis. It is a genetically programmed physiological process of cell death, for example, in tissue remodelling or haematopoiesis, dysregulation leads to the development of many pathologies. Apoptosis involves many cellular signalling pathways that are triggered by various stimuli, intracellular proteolytic cascades, DNA cleavage that is followed by cytoplasmic condensation, membrane blebbing and the formation of apoptotic bodies (Kerr, Wyllie, and Currie 1972). Even though apoptotic bodies are larger in size and are characterised by the organelles present within the vesicles, smaller vesicles are released during the development of apoptotic bodies (Akers et al. 2013). Most apoptotic bodies are phagocytosed by macrophages during its normal development and this process is cleared locally. This clearance is facilitated by specific interactions between recognition receptors on the phagocytes and changes in the composition of the apoptotic cell membrane (Erwig and Henson 2008). It is also possible to observe organelles that are not present other EV types. During the development of apoptotic bodies, phosphatidylserines are translocated to the outer leaflet of the plasma membrane. Here it can be recognised by annexin V, milk fat globule-EGF factor 8 (MFGE8), or T cell immunoglobulin mucin 4 (TIM4) (Akers et al. 2013; Petrovčíková, Vičíková, and Leksa 2018).

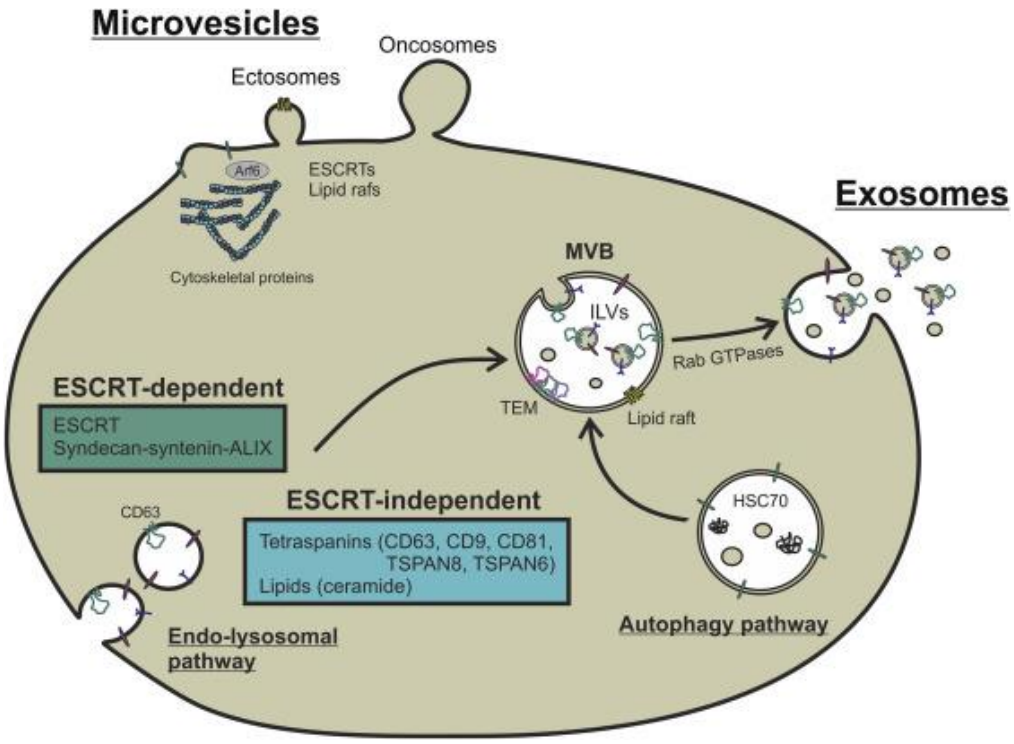

Figure 1.14: EV biogenesis pathways

Microvesicles (MVs) are shed from the plasma membrane after budding and fusion events. Exosomes can be formed through ESCRT-dependent or ESCRT-independent pathways. ESCRT complexes and syndecan-syntenin-ALIX interactions can lead endosomal cargo sorting and ILV budding into multivesicular bodies (MVBs).

1.5.2 EV characterisation

Characterisation of EVs is essential to not only determine and confirm the presence of EVs in the sample but to also attain information on the cargo and its potential implication in biological processes (Lötvall et al. 2014). Features such as size, morphology, density, concentration, and molecular content are used to characterise EVs. Characterising EV groups (MVs, exosomes and apoptotic bodies) is also essential in the analysis and interpretation of data because some composition such as RNA or protein may be found more in abundance in some groups than others. It is recommended by ISEV that each EV preparation be defined by quantitative measures of the source of EVs (such as number of secreting cells, volume of bio fluid, mass of tissue), to characterise EV preparations to the full extent to determine the abundance of EVs (total particle number, protein or lipid content), to test for the presence of components associated with EV subtypes and, to test for the presence of non-vesicular or co-isolated components (Théry et al. 2018). Another important characteristic of EVs which should be analysed is the integrity of the isolated vesicle. It is critical for EVs to maintain their integrity and efficacy after multiple cycles of freezing and thawing. Storing EVs in PBS can also lead to a major reduction in particle number due to EV adherence to storage tubes, or reduced EV integrity upon rupture during the freeze-thawing process (Görgens et al. 2022). Phosphate buffered saline (PBS) is the most used buffer for EV isolation and storage. However, buffers containing phosphate are known to exhibit pH shifts with concentration changes or upon freezing, which may lead to aggregation or loss of enzymatic activity. It can lead to a huge reduction in EV recovery within days and it has been reported that diluting EV samples in PBS can severely reduce recovery within minutes. Furthermore, phosphate precipitates in the presence of high concentrations of metal ions, such as calcium which can impact buffering capacity. HEPES buffered saline or HBS instead of PBS as a buffer during isolation has shown a significantly higher particle recovery and a lower, but not significant, protein recovery, leading to a higher particle/protein ratio. Furthermore, HBS has shown increased abundance of EV protein markers suggesting that it is preferable to use over PBS during the isolation process (Görgens et al. 2022; van de Wakker et al. 2022). This is essential to the development of a drug delivery system (Usman et al. 2018). Additionally, EVs can also be characterised to determine from which cell type they originate. This is

based on matching EV surface antigens and antigens found on the surface of its origin cell (Carnino, Lee, and Jin 2019).

There are currently many techniques that are used to characterise EVs that include electron microscopy, atomic force microscopy (AFM), dynamic light scattering (DLS), nanoparticle tracking analysis (NTA), tunable resistive pulse sensing (TRPS), flow cytometry, enzyme linked immune-sorbent assays (ELISA), and western blotting (WB) (Chiriacò et al. 2018) (Table 1.2). These methods are used to measure the physical (size, morphology, concentration) and molecular (protein content, surface marker expression) features of EVs. Due to differences in the physical properties and composition of different EV subpopulations, a combination of different techniques is needed for both qualitative and quantitative EV characterisation. The International Society of Extracellular Vesicles (ISEV) also recommends using at least two independent technologies to characterise individual EVs (Lötvall et al. 2014).

Characterisation of nucleic acids in EVs have broadened ever since the discovery of EV-mediated RNA transfer (Valadi et al. 2007). By using next generation sequencing (NGS) or microarrays, and validation using qRT-PCR and northern blotting, EV RNA content is examined. The presence of contaminant such as lipoproteins (HDL and LDL), ribonucleoprotein complexes (RNPs), and viral particles which may originate from an EV source or from foetal bovine serum (FBS) used in cell culture media or from RNA extractions can affect downstream analysis negatively. Therefore, samples are treated with proteinase, DNase, or RNase to remove any extravesicular components and reduce contaminants. However, the impact of these treatments on nucleic acids associated with the EV surface is still not known (Mateescu et al. 2017). NGS allows for single molecule RNA sequencing which is useful for assessing the overall integrity of long EV-RNA. However, due to the large quantity of starting material required for this technology, it hinders their application to analysing EV-RNA (Veziroglu and Mias 2020). Due to the small size of contaminants and poor sensitivity technologies that are available in the market, EV characterisation is still a relatively challenging method.

Table1.2: Methods for EV characterisation (Table adapted from Chiriacò et al. 2018)

Method	Information Acquired	Advantages/Limitations
Electron microscopy (EM)	EV dimension and morphology	- Direct assessment of morphology and size; small sample amount - Time consuming; size and morphology modifications due to sample preparation
Atomic force microscopy (AFM)	EV three-dimensional topography	- No sample fixation and staining; small sample amount - Size and morphology modifications due to sample dehydration on mica surface
Dynamic light scattering (DLS)	EV size distribution	- Fast, no sample preparation; sample preservation for downstream analysis - Inaccurate with polydispersed and size heterogeneous samples
Nanoparticle tracking analysis (NTA)	EV concentration and size distribution	- Fast, no sample preparation; sample preservation for downstream analysis - Inaccurate with size heterogeneous samples and particle aggregates
Flow cytometry	EV marker characterization, absolute counting	- Quantitative and qualitative (using specific antibodies) characterization of EVs - Detection limit (>100 nm, flow cytometer dependent); swarming effect (identification of multiple vesicles as a single event); detection of protein/antibody aggregates
ELISA/Western blot	EV protein quantification	- Standard immunological methods; specific characterization of EV protein markers - Time consuming; possible detection of non-EV proteins; non-specific information on EV concentration/size/distribution

1.5.3 Characterisation of RNA contents in EVs

Extracellular RNA (EV RNA) has been recognised as a prothrombotic and proinflammatory factor that is released under pathological conditions from cells by active and passive processes (Tielking et al. 2019). EV RNA is protected from ribonucleolytic digestion from within the EVs and other vehicles such as lipoproteins, or protein complexes (Arroyo et al. 2011). EVs contain various types of RNA such as noncoding RNA (ncRNA), microRNA (miRNA), fragmented and intact mRNA, ribosomal RNA (rRNA), and long non-coding RNA (lncRNA) (Turchinovich, Drapkina, and Tonevitsky 2019). There has been research conducted that show genetic exchange of miRNA or mRNA between cells by microvesicles or EV-mediated transfer (Ekström et al. 2012; Valadi et al. 2007). Circulating EVs found in the plasma mostly originate from miRNAs, and these miRNAs are known to regulate haematopoiesis and cellular differentiation (Hunter, Kyle, and Goldberg 1994). miRNAs are small non-coding RNAs 19-22 nucleotides in length, that have important roles in the post-transcriptional regulation of gene expression (Kirchner et al. 2020). miRNAs are small non-coding RNAs 19-22 nucleotides in length, that have important roles in the post-transcriptional regulation of gene expression. miRNAs act intracellularly however, a small fraction of them are found in the extracellular environment and in different biological fluids *in vivo* as well as in cell culture media *in vitro* (Albanese et al. 2021). Extracellular miRNAs are considered to be circulating biomarkers for several cancers and other diseases as cancerous cells release typical miRNA species of diagnostic value (Creemers, Tijsen, and Pinto 2012; Turchinovich et al. 2011). miRNAs within EVs have been extensively characterised. EVs released from different cell types contain miRNAs and are delivered to other target cells, where the miRNAs regulate target genes they are connected to at the post-transcriptional level (Mittelbrunn et al. 2011). miRNAs are known to be released within and protected by EVs since circulating miRNAs are extremely stable and resistant to RNases and have been identified in EV samples purified from different cell types (Hoy and Buck 2012; K. Wang et al. 2010). An analysis of the stoichiometry of miRNAs found within exosomes suggest that EVs carry low numbers of miRNA molecules that are too few to make a biologically significant difference in target cells (Chevillet et al. 2014). It is very challenging to characterise the functionality of EV-borne miRNAs in target cells as they express the same

endogenous miRNAs species. Hence, a deeper knowledge of cell-to-cell transfer of miRNAs is necessary to address this controversy (Albanese et al. 2021).

The cellular mechanisms involved in the packaging of different types of RNA into EVs and their uptake into specific target molecules are still being studied. The differences found between the EV RNA, and intracellular RNA profiles suggest that several EV-sorting mechanisms such as the stability of special RNA species resulting from the presence of RNA-binding proteins, or special RNases in EVs must be involved. Loading RNA into EVs also depends on pathological conditions or cell activation. For example, stressors such as hypoxia change the release of EVs and RNA profile in EVs released when compared to the donor cells (Fischer and Deindl 2021).

The types of RNA identified in EVs is also dependent on the EV isolation method. Subpopulations of EVs that have been isolated from metastatic tumour tissue show distinct size and morphology and differ in their RNA cargo (Crescitelli et al. 2020). The types of RNA identified in different EVs isolated from cell culture supernatant is not only dependent on the type of donor cell but also on the type of stimulation. Studies show that after culturing mast cell line HMC-1 in a normal growth medium, MVs isolated from the supernatant did not contain any rRNA but when the cells were treated with degranulating agents such as ionomycin or complement factor in serum-free medium, MVs contained high amounts of rRNA and fewer small RNAs (Crescitelli et al. 2020; Elsemüller et al. 2019). Other studies have shown that the type of RNA isolated from cell culture supernatants depend on the conditions under which the cells were cultured. For example, bovine serum contains RNA in EVs, and methods used to remove EV RNA from bovine serum by ultracentrifugation method or affinity purification have only been partly successful (Tosar et al. 2017).

There have been many studies conducted that have failed to show whether identified extracellular RNAs were associated with EVs or with RNA-protein complexes, viral particles, RNPs or lipoproteins such as LDL and HDL, that may have been isolated along with EVs (Mateescu et al. 2017). However, it has been reported that EVs isolated by using ultracentrifugation technique may become aggregated and are contaminated by non-vesicular macromolecules. In addition, the purification techniques such as high-resolution density gradient fractionation and direct

immunoaffinity capture techniques were used to accurately characterise EVs and non-vesicular materials (Jeppesen et al. 2019).

It has also been shown that DNA that is known to be present in several biological fluids were also found in EV RNA preparations and can thus affect downstream analysis of RNA (Thakur et al. 2014). rRNA might also be associated with EVs during centrifugation and this could provide an explanation as to whether the presence of rRNA in EV preparations is natural or if they are impurities or contaminants (Mateescu et al. 2017). Small RNA-sequencing has shown that EVs are associated with various fragments from coding and non-coding RNA, including rRNA, tRNA, snRNA, lncRNA and vault RNA. Currently, it is not known whether these fragments are artefacts produced during the isolation protocol or if they are formed during specific processing steps either in the cytoplasm of donor cells or inside the vesicles (van Balkom et al. 2015; Nolte-'t Hoen et al. 2012).

In chapter 5 of this thesis, we undertake RNA sequencing from EVs isolated from osteopontin (*Spp1)* transfected H9c2 cells to identify significantly differentially expression protein coding genes and lncRNAs that could potentially be responsible for affecting cell size. The identification of *Spp1* in the EV RNA samples will confirm its successful transfer and its role in mediating size increase in H9c2 cells.

Hypothesis:

Work presented in this thesis is based on the hypothesize that early overexpression of *Spp1* leads to susceptibility of cardiac phenotypes in the $SHRSP_{Gla}$ strain.

Aims:

The aims of this thesis are as follows:

Spp1 promoter analysis:

- To characterise the functional effects of the *Spp1* promoter constructs in H9c2 and HeLa cells. The successful 6 promoter constructs along with *luc2* and *hRluc2* genes will then be transfected into H9c2 cells and HeLa cells.
- Conduct luciferase assay on transfected H9c2 and HeLa cells to analyse and compare the transcriptional activities and promoter function of each segment.

Animal study – Transverse Aortic Constriction (TAC) study:

- To assess and compare differences in LVMI adjusted to body weight and tibial length in SHAM and TAC operated SHRSP *Spp1* WT and SHRSP $Spp1^{em1}$, $WKY.SP_{Gla}14a$ chr 14 congenic rat strains.
- To assess the impact of TAC surgery on body weight in SHAM and TAC operated rats.
- To assess and compare cardiac phenotype parameters such as relative wall thickness (RWT), stroke volume (SV) fractional shortening (FS), ejection fraction (EF) and cardiac output (CO).

EV isolation and characterisation of EVs:

- To transfect H9c2 cells with *Spp1* and measure the increase in cell size.
- To isolated EVs from *Spp1* transfected H9c2 cells using ultracentrifugation technique.
- To measure cell size in H9c2 cells treated with EVs isolated from *Spp1* transfected H9c2 cells.
- To characterise EVs isolated from transfected H9c2 cells by size, using Nanoparticle Tracking Analysis (NTA) to implicate EVs.

RNA sequencing (RNAseq) of EVs:

- To prepare RNA from EVs isolated from transfected H9c2 cells.
- To undertake long RNAseq from EVs isolated *Spp1* transfected H9c2 cells and compare *Spp1* transfected versus transfected controls.

Chapter 2. General Methods and Materials

2.1 General methods

2.1.1 Polymerase Chain Reaction (PCR)

All thermal cycling for standard PCRs was conducted on a MJ Research DNA Engine PTC-225 Peltier Thermal Cycler in 96-well plates purchased from ABgene. (Genetic Research Instrumentation, Essex, UK). Primers were previously designed and bought by Eurofins Genomics. The manufacturer's protocol was followed for each reaction (New England BioLabs). The PCR reaction requires several components: a heat-stable DNA polymerase enzyme such as Thermus aquaticus (Taq) polymerase, nucleotides, buffer, magnesium, primers, and the template DNA. PCR can only be carried out on DNA, so for RNA pathogens the RNA must first be transcribed into cDNA in a reverse transcriptase (RT) step. The PCR reaction is carried out in a thermal cycler containing a thermal block that can be rapidly heated and cooled down. Upon heating, double stranded DNA is denatured and split into single strands. The temperature is then reduced to allow the specific primers to anneal to the single stranded DNA. The Taq polymerase then enzymatically adds nucleotides, using the primers as template to assemble and extend a complementary strand of DNA. Each copy of DNA can serve as a template for further amplification. The cycle of heating and cooling is repeated 30 to 40 times, doubling the PCR product with every cycle. Therefore, as each copy of DNA can act as a template in the next cycle, one copy of DNA can by multiplied into billions of copies over 30 to 40 cycles.

Table 2.1: Reaction mixture

Master mix	Volume (ul)
10X thermopol reaction buffer	2.5ul
dNTPs (1mM)	0.5ul
Forward primer (5pmol/ul)	0.5ul
Reverse primer (5pmol/ul)	0.5ul
Template DNA	10ul
Taq DNA polymerase	0.125ul
dH_2O	10.875ul

Table 2.2: Temperature cycling parameters

Temperature	Time	
94℃	5 minutes	
94℃	30 seconds	**Repeat 34X**
60℃	30 seconds	
68℃	1 minutes and 30 seconds	
68℃	5 minutes	
4℃	5 minutes	
12℃	∞	

2.1.2 Agarose Gel Electrophoresis

The PCR product is visualised by gel electrophoresis; DNA is separated by size using an electric current and viewed using ethidium bromide which fluoresces under ultraviolet light. The sample PCR product is run with a DNA ladder (containing a series of DNA fragments of known base pair size). A band at the expected base-pair size comparable to the positive control indicates a positive result, provided positive and negative controls have behaved as expected. The following reaction mixes and temperature cycling programmes were dependent on the DNA fragment of interest. 1.5% UltraPure Agarose (Invitrogen, ref: 16500-500) gels were dissolved and electrophoresed in 1X Tris-Borate EDTA (TBE) buffer (Fisher Bioreagents). Gels were electrophoresed at 110V, BIO-RAD Power PAC 300 and BIO-RAD electrophoresis tanks were used, 1ng/100ml ethidium bromide (Sigma) was added to liquid agarose before pouring gels. Promega 1kb DNA ladders were used for sizing PCR products. Samples were loaded with 6X loading dye (50% glycerol, 0.05% bromophenol blue). Gels were visualised by UV transillumination on a BIORAD Fluor-S MultiImager.

2.1.3 Plasmid DNA Purification using QIAGEN Maxi Kit

Plasmid DNA was extracted from bacteria using the filter column based QIAGEN Plasmid Maxi Kit (Cat. No. / ID: 12162). Bacterial cultures were streaked and grown overnight at 37°C on ampicillin Luria agar plates. Single colonies were picked and used to inoculate a 10ml Luria broth starter culture, containing 100 µg/ml ampicillin. This was grown for approximately 8 hours at 37°C in shaking incubator. 1ml of this starter culture was then used to inoculate a 200ml 100 µg/ml ampicillin Luria broth to produce an overnight culture from which the plasmid was extracted. Bacteria was harvested by centrifugation at 6,000g for 15 minutes at 4°C in a Beckman Coulter Avanti J26XP. The culture media was poured out and the bacteria was re-suspended in 10ml buffer P1. 10ml buffer P2 was added, and the solutions were kept on ice for 5 minutes. 10ml pre-chilled buffer P3 was added to neutralise the lysate. The precipitated lysates were then centrifuged at 18,000g for 10 minutes at 4°C. The supernatant was collected and centrifuged again at the same speed for a further 15 minutes to ensure a clear suspension. QIAGEN-tip 500 was equilibrated with 10ml buffer QBT. The supernatant was applied to the QIAGEN-tip 500 and allowed to enter the resin by gravity flow. The columns were then washed twice with 30ml buffer QC. The plasmid DNA was eluted with 15ml buffer QF into polypropylene centrifuge tubes. Plasmid DNA was precipitated with 10.5ml isopropanol and centrifuged at 15,000g for 30 minutes at 4°C. The supernatant was carefully decanted, and the pellets were washed with 5ml 70% ethanol and centrifuged at 15,000g for 10 minutes at 4°C. The supernatant was carefully decanted, and the pellets were thoroughly air-dried (10-20 minutes) before re-suspending the DNA in 450ul of dH_2O.

2.1.4 RNA Extraction

RNA was extracted using the miRNeasy Mini Kit (Qiagen, UK, catalogue no: 217004). A total of 12 gestational day 18 foetal rat hearts from SHRSP and WKY rats (SHRSP = 6 & WKY = 6), each from the same litter were homogenised in 700 µL QIAzol Lysis Reagent four times for 30 s at 25 kHz using TissueLyser (QIAGEN, Haan, Germany) with stainless steel beads. Cells were lysed directly in cell-culture dishes by adding 700 µL QIAzol Lysis Reagent. The lysate was transferred to a microcentrifuge tube and vortexed for 1 min. Tissue and cell homogenates were either stored at -80ºC, or RNA extractions were immediately performed.

Homogenates were placed at room temperature for 5 min. Chloroform (140 µL) was added and tubes were shaken vigorously for 15 s. Tubes were placed for a further 2-3 min at room temperature. Samples were centrifuged at 12000 x g for 15 min at 4ºC. All subsequent centrifuges were performed at 20ºC. The upper aqueous phase containing RNA (350 µL) was transferred to a tube containing 525 µL 100% ETOH. The sample was mixed thoroughly by pipetting up and down several times, and 700 µL was pipetted into a RNeasy Mini Spin Column in a 2 mL collection tube. Samples were centrifuged at 11000 x g for 15 s and flow-through was discarded; this was repeated using the remainder of the sample. An optional on-column DNase digestion was performed, or extractions were performed as following. Buffer RWT (700 µL) was added to the RNeasy Mini Spin Column to wash the column. Samples were centrifuged at 11000 x g for 15 s, and flowthrough was discarded. Buffer RPE (500 µL) was added to the RNeasy Mini Spin Column to wash the column. Samples were centrifuged at 11000 x g for 15 s, and flow-through was discarded. Another 500 µL of Buffer RPE was added to dry the column, and samples were centrifuged at 11000 x g for 2 min. The RNeasy Mini Spin Column was placed in a new 2 mL collection tube and 40 µL of NFW was added. To elute the RNA, the samples were centrifuged at 11000 x g for 1 min. Samples were centrifuged again at 11000 x g for 1 min to collect the elute in the same collection tube. RNA was eluted in RNase free water at a final of 40ul. Samples were stored at -80ºC until used. 200 ng/ul stock dilutions were prepared and stored in -80C freezer for further downstream processing.

2.1.5 Preparation of cDNA samples

Complementary DNA (cDNA) were prepared in the absence of gene-specific-primers on a RNAzap (Sigma-Aldrich, Dorset, UK) and 70% ethanol (dH2O) cleaned bench, using filter pipette tips only to minimize contamination. Applied Biosystems TaqMan Reverse Transcription Reagents were used for cDNA synthesis using random hexamers. Reverse transcription reactions were performed in 96-well plates to allow multichannel pipettes to be used for PCR reaction set up. For each reaction, 500ng of RNA template was reverse transcribed using the following reagents detailed in table 2.3.

Table 2.3: TaqMan Reverse transcription reaction mix

For a single 20ul reaction	Volume (ul)	Heat Cycle
10X Reaction buffer	2ul	25°C – 10 minutes
$MgCl_2$ (25mM)	4.4ul	48°C – 30 minutes
dNTPs (2.5 mM each)	4ul	95°C – 5 minutes
Random Hexamers (50 uM)	1ul	4°C - 5 minutes
RNase Inhibitor (20 U/uL)	0.4ul	
MultiScribe Enzyme (50 U/uL)	0.5ul	
dH_2O	5.2ul	
RNA (200ng/ul dilution)	2.5ul	

2.1.6 Quantitative Real Time PCR (qRT-PCR) Reaction

Applied Biosystems Gene Expression Assays and Custom Gene Expression Assays were used for all qRT-PCRs in this chapter. The probe fluoresces only when bound to DNA and the amount of fluorescence detected is linearly proportional to the amount of DNA. The probes are covalently joined to the 5' end fluorescence molecule called reporter and the 3' primer end molecule called quencher. The reported molecule reports a signal as you generate more product, and the quencher molecule quenches the fluorescence signal from the reporter. During PCR amplification, the 5'-3' nucleolytic activity of the DNA polymerase cleaves the quencher from the probe, resulting in fluorescence levels proportional to the amount of PCR product present.

The gene of interest and the housekeeper, β-2-microglobulin (B2M), were amplified in duplex PCR reactions, probes for the gene of interest were tagged 'FAM" labelled fluorescent dyes, while B2M probes were labelled 'VIC' dye, they fluoresce at different wavelengths allowing them to be measure in the same reaction without any interference. Plates were amplified using a QuantStudio 12K Flex Real-Time PCR System (Thermofisher, Paisley, UK). All assays were performed with the same amount of template cDNA in each reaction of an experiment. For each reaction the following reagents and heat cycle parameters were used:

Table 2.4: qRT-PCR reaction mix

Master mix for single 5ul reaction	Volume (ul)
2X TaqMan Universal Master Mix II	2.5ul
FAM Probe (rat *Spp1*)	0.25ul
VIC Housekeeper Probe (rat *B2M*)	0.25ul
cDNA Template	1ul
dH_2O	1ul

Table 2.5: Heat cycling parameters

Temperature (°C)	Time (minutes)
25°C	10 minutes
48°C	30 minutes
95°C	5 minutes
4°C	5 minutes
12°C	∞

All samples were set up and amplified in triplicate. Fluorescence of FAM and VIC dyes was measured for all reactions during temperature cycling, data was analysed using a combination of Applied Biosystems SDS (Sequence Detection Software) and Microsoft Excel software. FAM and VIC fluorescence were analysed as separate data sets, a fluorescence threshold was identified for each data set where amplification curves were in their exponential phase. The CT or cycle threshold is the cycle number at which fluorescence is generated within a reaction that crosses the fluorescence threshold, a fluorescent signal significantly above the background fluorescence. The threshold cycle is inversely proportional to the original relative expression level of the gene of interest. Ct values for FAM and VIC data were exported from SDS as text files and converted to Excel documents for data analysis. Relative levels of gene expression were calculated by the '$\Delta\Delta$Ct method'.

The $\Delta\Delta$Ct method is a method of relative quantification which directly uses the CT value generated from a qPCR system to calculate the relative gene expression in the gene of interest and housekeeper samples, using the housekeeper as the normalizer (Rao et al. 2014).

2.2 Cell culture

2.2.1 Media Preparation and General Methods

All experiments were conducted under aseptic technique. H9c2 cells were cultured in Minimal Essential Medium (MEM) (Thermofisher, Paisley, UK), supplemented with 10% foetal-bovine serum, 1% L-glutamate, 1% sodium pyruvate and 1% penicillin-streptomycin (all Thermofisher, Paisley, UK). Cells were cultured in a Class-II Biosafety Laminar flow hood (Thermofisher, Paisley, UK) and incubated at a constant 37℃ with 5% CO_2. All cell cultures were performed using Corning Flasks of varying sizes (T25 (5ml), T75 (15ml) and T150 (25)) (Corning, Arizona AZ, USA).

Cells were cryopreserved in filter-sterilized culture media supplemented with 10% (v/v) dimethysulfoxide (DMSO) and aliquoted into 2ml cryovials, stored overnight in Mr. Frosty Freezing Container (Nalgene) in a -80℃ freezer, followed by transfer to liquid nitrogen for long-term storage. Recovery of cells from liquid nitrogen was performed by thawing the cryovials at 37℃ using a water bath. Once thawed, the contents of the cryovial are transferred into a universal tube and centrifuged at 1500, rpm for 5 minutes. The filter-sterilized culture media and 10% DMSO is then poured off and the cell pellet was re-suspended in a fresh 75 cm^2 flask with 14mls of media.

2.2.2 Cell Culture using H9c2 cells

H9c2 cells were handled under sterile conditions using Class-II Biosafety Laminar flow hood (Thermofisher, Paisley, UK). The cabinets were cleaned before and after use with Chemgene and 70% ethanol. Cells were maintained in 75 cm^2 and 150 cm^2 tissue culture flasks with vented caps (Corning) in inCusafe, 37°C, 5% carbon dioxide (CO2) incubators.

Cells were passaged regularly to prevent overcrowding in culture flasks. Passaging was performed by removing culture media and washing cells gently with 10ml sterile PBS before detaching them from the flask with 5 minutes incubation with 3mls 1X TE at 37°C. Cells were then washed with 9mls of Gibco Dulbecco's Minimum Essential Media (DMEM) 1X High Glucose without sodium pyruvate (Invitrogen 41965-039) supplemented with 10% foetal bovine serum (FBS), Penicillin (5%), Streptomycin

(5%), L-Glutamine (5%) and sodium pyruvate (5%), which inactivates the trypsin. This was then aspirated into a 30ml universal contained and centrifuged at 1,500 rpm for 5 minutes. Media/TE was poured off and the cell pellet was re-suspended in a fresh 75 cm^2 flask with 14mls of media. Cell media was refreshed every two days and cultured once the cells reached 70%-80% confluency.

2.2.3 Cell Culture using HeLa cells

HeLa cells were handled under sterile conditions using Class-II Biosafety Laminar flow hood (Thermofisher, Paisley, UK). The cabinets were cleaned before and after use with Chemgene and 70% ethanol. Cells were maintained in 75 cm^2 and 150 cm^2 tissue culture flasks with vented caps (Corning) in inCusafe, 37°C, 5% carbon dioxide (CO2) incubators.

Cells were passaged regularly to prevent overcrowding in culture flasks. Passaging was performed by removing culture media and washing cells gently with 10ml sterile PBS before detaching them from the flask with 5 minutes incubation with 3mls 1X TE at 37°C. Cells were then washed with 9mls of Gibco Dulbecco's Minimum Essential Media (DMEM) 1X High Glucose without sodium pyruvate (Invitrogen 41965-039) supplemented with 10% foetal bovine serum (FBS), Penicillin (5%), Streptomycin (5%), L-Glutamine (5%) and sodium pyruvate (5%), which inactivates the trypsin. This was then aspirated into a 30ml universal contained and centrifuged at 1,500 rpm for 5 minutes. Media/TE was poured off and the cell pellet was re-suspended in a fresh 75 cm^2 flask with 14mls of media. Cell media was refreshed every day and cultured once the cells reached 80% confluency.

2.3 Statistical Analysis

Statistical analysis was used to determine the statistical significance of experimental findings. All comparisons were made on data collected from individual assays this eliminating error from inter-assay variability. Three biological samples were taken for each condition that was analysed and then applied as three technical repeats for the assay. 2 sample t-tests were used when comparisons were made between two experimental groups. Analysis of variance (two-way ANOVA) was used when comparisons were made with more than 2 groups with an appropriate post-test. Tukey's multiple comparisons test was used as an appropriate post-test when all groups were compared. Threshold for significance was set at 0.05 in all the analyses. Errors bars are stated as standard error of the mean (SEM).

Chapter 3. Osteopontin Promoter Analysis

3.1 Introduction

Previous work conducted in the lab by members of the McBride and Graham group used a combination of $SHRSP_{Gla}$ and WKY_{Gla}, chromosome 14 congenic strains; SP. WKY_{Gla}14a (F) and WKY.SP_{Gla}14a (D) and microarray gene expression profiling to identify positional candidate genes for left ventricular mass index (LVMI) that would map to the minimal transferred congenic interval on chromosome 14. They determined cardiac gene expression profiles from neonatal $SHRSP_{Gla}$, SP. WKY_{Gla}14a (F), WKY.SP_{Gla}14a (D) and WKY_{Gla} (fig 3.1 A). By filtering and comparing genes that were significant across the parental versus congenic strains, they identified four genes that were consistently differentially expressed: Osteopontin (*Spp1*), hydroxy steroid dehydrogenase 17-beta 13 (Hsd17b13), Zinc finger protein (Znf644) and Ras-related associated with diabetes (Rrad). Only *Spp1* was mapped to the congenic interval and was validated by qRT-PCR with significant increase of *Spp1* expression in whole neonatal heart tissue and in primary neonatal cardiomyocytes [fig 3.1 (B) and (C)].

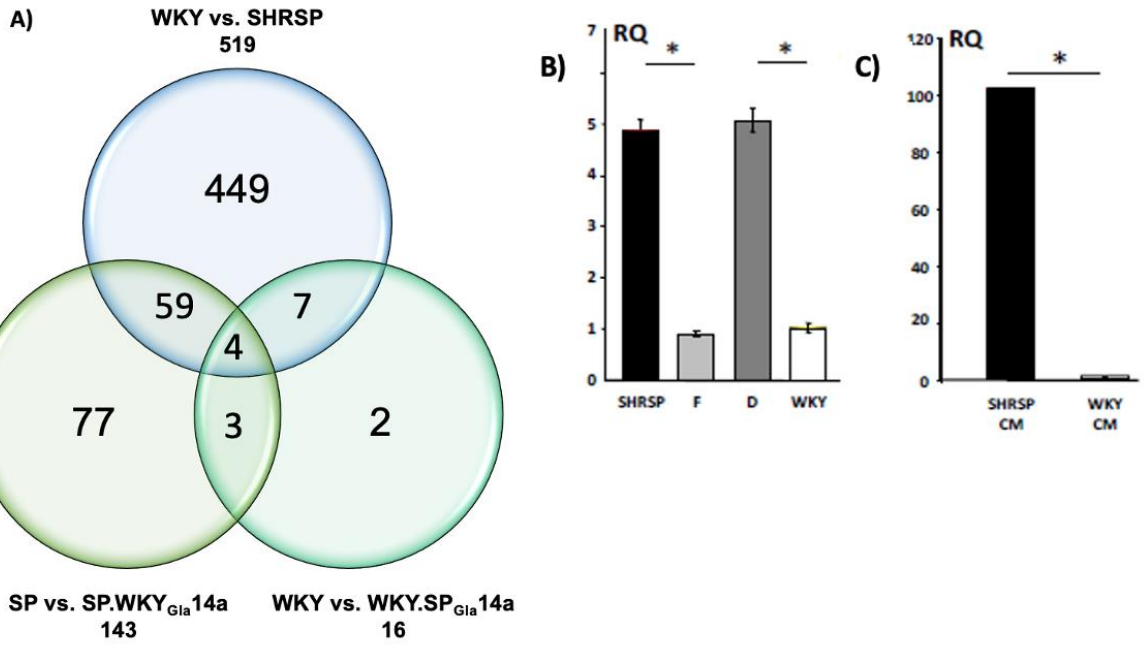

Figure 3.1: (A) Microarray expression profiling results **(B)** qRT-PCR confirmation of *Spp1* expression in whole neonatal heart. **(C)** *Spp1* qRT-PCR data from isolated primary neonatal cardiomyocytes (CM) from $SHRSP_{Gla}$ and WKY_{Gla} (Figure adapted from Crawford, W., 2011. 'Microarray analysis of chromosome 14 congenic strains in the SHRSP'. MSc. University of Glasgow).

Spp1 is a multifunctional glycophosphoprotein which was first identified in osteoblasts. However, they were also found to be expressed in other cell types including cardiomyocytes and fibroblasts. *Spp1* also plays an important role in different biological processes including, activation of immune cells as well as inhibition of extracellular matrix remodelling and vascular calcification. Furthermore, *Spp1* has been suggested to play an important role in cardiovascular diseases, such as hypertrophy, myocardial infarction (MI) and heart failure (HF) (Weber et al. 2020). Its adhesive cell and matrix properties make it a very useful candidate to contribute to vascular remodelling events as well (Ashizawa et al, 1996). *Spp1* expression is increased during both acute and chronic diseases in the heart. Cardiomyocytes appear to be the major source of *Spp1* after it had been observed that its expression was increased during cardiac hypertrophy. This expression was observed after myocardial infarction event (Renault et al, 2010).

From genetic sequencing analysis of the $SHRSP_{Gla}$ and WKY_{Gla} models, it is evident that large variations occur within the *Spp1* promoter region between the two strains. These variations consist of numerous single nucleotide polymorphisms (SNPs) as well as insertions and deletion (indels) segments. These mutations, individually or in combination with each other, may have the potential to alter the efficacy of the transcription rate of the *Spp1* gene through modifying the binding of cis-regulatory transcriptional factors (Nakayama et al, 2011). It is not known whether SNPs found within the promoter region of *Spp1* are responsible for the overexpression of this gene. If they are, the location of the SNPs is currently unknown. The responsible SNPs that are identified and the individual bases that are responsible for regulating the level of gene transcription can be changed by site-directed mutagenesis in follow-up promoter studies.

Previous work conducted in the lab by the McBride and Graham group have performed *in silico* bioinformatic analyses of the *Spp1* promoter region using the transcription element search software (TESS). This uses TRANSFAC v6.0, JASPAR 20060301, IMD v1.1, and CBIL/GibbsMat v1.1 databases (fig 3.2A & 3.2B and fig 3.3A & 3.3B). The identification of transcription factors that undergo altered binding to the *Spp1* promoter because of sequence variation will provide valuable insight into the transcriptional regulation of *Spp1*. Previously, two SNPs have been identified in

the rat promoter of *Spp1* by the McBride and Graham group that can potentially alter the efficiency of transcription factor binding. It has also been previously implicated in the cardiac transcriptional network including the *GATA* family, *Twist* and *Runx2* (R.-M. Chen, Lin, and Chou 2010; S. Singh et al. 2011).

SHRSP-*Spp1* Promoter TRANSFAC Analysis:

matrix identifier	position (strand)	core match	matrix match	sequence (always the (+)-strand is shown)	factor name
B$CRP_C	92 (-)	0.894	0.804	cattgtgaataatgACACAtaagtaa	CRP
V$HNF3B_01	115 (-)	1.000	0.969	taaatAAATAttaga	HNF-3beta
V$FOXD3_01	116 (-)	0.944	0.953	aaataAATATta	FOXD3
F$HSF_02	346 (+)	0.972	0.893	GGAATaggagagaag	HSF
I$BCD_01	604 (-)	1.000	1.000	tTAATCcc	Bcd
V$MYCMAX_02	728 (+)	1.000	0.995	gacCACGTgaca	c-Myc/Max
V$USF_Q6	729 (-)	1.000	0.976	accaCGTGAc	USF
V$NKX25_01	1134 (-)	1.000	1.000	CACTTga	Nkx2-5
V$HNF4_01	1221 (+)	0.915	0.900	atgagagTAAAGatcattt	HNF-4
V$EVI1_04	1648 (+)	0.773	0.837	ggataaaagTAGAAa	Evi-1
V$ELK1_01	1766 (+)	1.000	0.922	ccaacaGGAAGtgaca	Elk-1
V$OCT1_Q6	1878 (+)	0.909	0.931	agacatGTAAAttaa	Oct-1
V$HNF1_C	1883 (+)	0.829	0.878	tGTAAAttaatgacaac	HNF-1
V$GATA1_02	2554 (+)	1.000	0.992	ttccAGATAagggg	GATA-1
V$OCT1_Q6	2696 (-)	0.909	0.906	gggaTTTACatttta	Oct-1
V$CREL_01	2891 (-)	1.000	0.989	GGAAAatccc	c-Rel
V$PAX4_01	3298 (+)	0.979	0.830	ggcacTCAGGggttacaaaga	Pax-4
V$HNF4_01	3511 (+)	0.915	0.894	tcgtgctTAAAGggcagaa	HNF-4
I$BRCZ4_01	3537 (-)	1.000	0.975	ttttttTTATtaa	BR-C Z4
V$MYOD_01	3610 (+)	1.000	0.976	tcaCAGGTgttg	MyoD
V$PAX6_01	3950 (+)	1.000	0.898	ttgctTCACGtataattttat	Pax-6
V$CDPCR1_01	4144 (-)	1.000	0.922	aagaTCGATt	CDP CR1
V$CHOP_01	4245 (-)	1.000	0.976	gggcaTTGCAaca	CHOP-C/EBPalpha
V$HNF4_01	4576 (-)	1.000	0.909	ctgtgtgCTTTGtgcagat	HNF-4
V$EVI1_04	4935 (+)	0.763	0.830	agatacgacAAGAGt	Evi-1
I$BRCZ4_01	4993 (+)	1.000	0.975	acaATAAAgaaaa	BR-C Z4
P$SBF1_01	5133 (-)	1.000	0.964	tttTTTAAccgcaa	SBF-1

Figure 3.2 A): The figure above shows the results from the TRANSFAC analysis performed on the SHRSP-*Spp1* promoter sequence.

Matrix identifier – matrix with which the putative binding site was found.

Position (strand) – plus/minus, the strand on which the putative site was found.

Core match – the core similarity score for the matrix match. The matrix core is defined as the five consecutive most conserved nucleotides within the matrix.

Matrix match – the matrix similarity score for the matrix match. The match score can vary from 0 to 1, with 0 for the lowest similarity and 1 for the highest similarity of the match to the matrix.

Sequence – shows the matching sequence. Capital letters indicate the positions in the sequence that match with the core sequence of the matrix, while lower case letters refer to positions that match to the remaining part of the matrix.

Factor name – name of the binding factor, represented by the matrix.

shows the transcription binding factors identified in the SHRSP-*Spp1* promoter sequence along with the sequence to which they are aligned.

Figure 3.2 B): SHRSP-*Spp1* promoter TRANSFAC analysis.

The figure shows the rat SHRSP-*Spp1* promoter sequence in red text from -92 to -5133. Highlighted in blue underlined text are the transcription factors. They are represented as matrix identifier and are aligned with the promoter sequence.

WKY-*Spp1* Promoter TRANSFAC Analysis:

matrix identifier	position (strand)	core match	matrix match	sequence (always the (+)-strand is shown)	factor name
B$CRP_C	92 (-)	0.894	0.826	cattgtgaataatgACACAtaaataa	CRP
V$HNF3B_01	111 (-)	1.000	0.969	taaatAAATAttaga	HNF-3beta
V$FOXD3_01	112 (-)	0.944	0.953	aaataAATATta	FOXD3
F$HSF_02	342 (+)	0.972	0.893	GGAATaggagagaag	HSF
I$BCD_01	603 (-)	1.000	1.000	tTAATCcc	Bcd
V$MYCMAX_02	727 (+)	1.000	0.995	gacCACGTgaca	c-Myc/Max
V$USF_Q6	728 (-)	1.000	0.976	accaCGTGAc	USF
V$NKX25_01	1133 (-)	1.000	1.000	CACTTga	Nkx2-5
V$EVI1_04	1647 (+)	0.773	0.837	ggataaaagTAGAAa	Evi-1
V$ELK1_01	1765 (+)	1.000	0.922	ccaacaGGAAGtgaca	Elk-1
V$OCT1_Q6	1877 (+)	0.909	0.931	agacatGTAAAttaa	Oct-1
V$HNF1_C	1882 (+)	0.829	0.878	tGTAAAttaatgacaac	HNF-1
V$GATA1_02	2733 (+)	1.000	0.992	ttccAGATAagggg	GATA-1
V$OCT1_Q6	2875 (-)	0.909	0.906	gggaTTTACatttta	Oct-1
V$CREL_01	3070 (-)	1.000	0.989	GGAAAatccc	c-Rel
V$PAX4_01	3477 (+)	0.979	0.830	ggcacTCAGGggttacaaaga	Pax-4
V$HNF4_01	3690 (+)	0.915	0.894	tcgtgctTAAAGggcagaa	HNF-4
I$BRCZ4_01	3715 (-)	1.000	0.975	tttttTTTATtaa	BR-C Z4
V$MYOD_01	3788 (+)	1.000	0.976	tcaCAGGTgttg	MyoD

Figure 3.3 A): The figure above shows the results from the TRANSFAC analysis performed on the WKY-*Spp1* promoter sequence.

Matrix identifier – matrix with which the putative binding site was found.

Position (strand) – plus/minus, the strand on which the putative site was found.

Core match – the core similarity score for the matrix match. The matrix core is defined as the five consecutive most conserved nucleotides within the matrix.

Matrix match – the matrix similarity score for the matrix match. The match score can vary from 0 to 1, with 0 for the lowest similarity and 1 for the highest similarity of the match to the matrix.

Sequence – shows the matching sequence. Capital letters indicate the positions in the sequence that match with the core sequence of the matrix, while lower case letters refer to positions that match to the remaining part of the matrix.

Factor name – name of the binding factor, represented by the matrix.

shows the transcription binding factors identified in the SHRSP-*Spp1* promoter sequence along with the sequence to which they are aligned.

Figure 3.3 B): WKY-*Spp1* promoter TRANFAC analysis

The figure shows the rat WKY-*Spp1* promoter sequence in red text from -92 to +3788. Highlighted in blue underlined text are the transcription factors. They are represented as matrix identifier and are aligned with the promoter sequence.

In this chapter we analyse the transcriptional levels driven by different regions of the *Spp1* cis-acting promotor. Comparison between the $SHRSP_{Gla}$ and WKY_{Gla} strains transcriptional levels of these promoter fragments should provide an indication as to the region within the promoter that is responsible for the overexpression of the gene.

Table 3.1: Promoter fragment, size, and position of rat *Spp1* promotor constructs

Promoter Fragment	Size (base pairs)	Position within Rat Genome
C5289/A4090	1,163	6,660,028 - 6,658,865
10F/10R	1,289	6,664,133 - 6,662,844
11F/11R	1,964	6,662,152 - 6,660,688
10F/12R	5,214	6,664,133 - 6,658,919

Prior to the start of this study, four fragments from the rat *Spp1* promoter were identified (Table 3.1). These fragments contained multiple SNPs and indels between the two $SHRSP_{Gla}$ and WKY_{Gla} strains, as confirmed by the Rat Genome Database. The C5289/A4090 fragments was previously identified and analysed using the same methodology used in this chapter however, there were no significant changes observed between the two strains. In this chapter we will focus on the remaining three promoter fragments.

3.1.1 Hypothesis

We hypothesize that overexpression of *Spp1* begins during gestational development, leading to increased levels of cardiac hypertrophy and fibrosis.

We also hypothesize that different regions of the *Spp1* promoter, each containing multiple SNPs, will differ in their transcriptional activity levels.

3.1.2 Aim

The aims of this project are as follows:

- Quantify and compare the expression levels of *Spp1* in $SHRSP_{Gla}$ and WKY_{Gla} gestational day 18 rat hearts.
- Generate promoter constructs for SHRSP and WKY strains.
- Compare transcriptional activity of segments of *Spp1* promoter through dual luciferase reporter assay using the newly created SHRSP and WKY promoter constructs, and previously created promoter constructs as well.

3.2 Methods

3.2.1 Sub-Cloning of Promotor Fragments and pGL4.10 Luciferase Vector

Eukaryotic expression vectors were used in this chapter for the generation of promoter constructs.

Prior to sub-cloning, the *Spp1* promoter fragments were ligated within the StrataClone blunt PCR cloning vector (pSC-B-amp/kan). To successfully separate the promoter fragments from the vector, restriction digest, agarose DNA gel extraction, ligation, and transformation of resulting promoter constructs into competent cells was carried out.

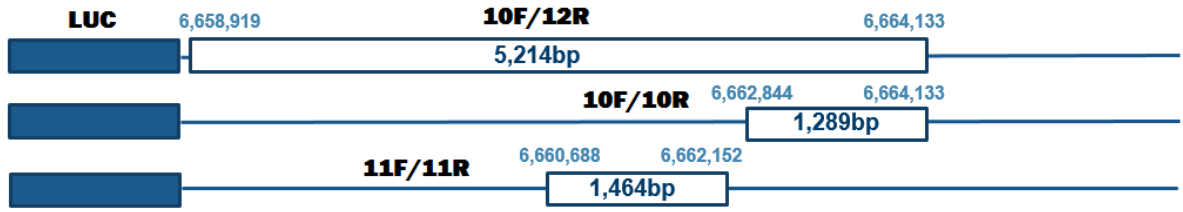

Figure 3.4: Image illustrating the 3 *Spp1* promoter fragments

SP & WKY 10F/12R – 5.2kb long, SP & WKY 10F/10R – 1.3kb long and SP & WKY 11F/11R – 1.9kb long

3.2.2 Restriction digest

Restriction enzymes Xho I and Bgl II (New England Biolabs, UK) were used in this study following the manufacturer's instructions. A 30ul reaction was incubated at 37°C for 1 hour and 30 minutes. After which the reaction mix is either kept on ice for immediate use or stored at -20°C. These restriction sites were selected as they were specific to the StrataClone blunt PCR cloning vector and the pGL4.10 luciferase vector into which the restriction fragments will be cloned.

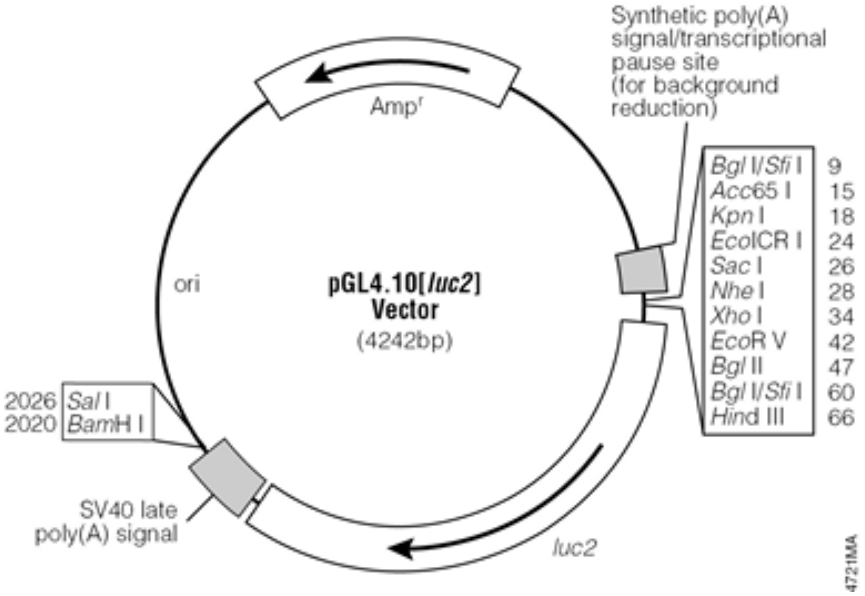

Figure 3.5: Image showing pGL4.10 luciferase vector map with restriction sites. Xho I and Bgl II were selected. [CIP2Aprom27bp-pGL4.10Luc was a gift from Jukka Westermarck (Addgene plasmid # 60876; http://n2t.net/addgene:60876; RRID: Addgene_60876)]

Table 3.2: Restriction digest master mix

Restriction digest master mix	Volume (ul)
NEB buffer 3.1	3ul
Xho I	2ul
Bgl II	2ul
Template DNA	10ul
dH_2O	13ul

3.2.3 Agarose DNA Gel Extraction

Agarose DNA gel extraction of restriction fragments following restriction digest was performed using QIAquick Gel Extraction Kit (QIAGEN catalogue no: 28704) following the manufacturer's instructions, using a bench microcentrifuge at 10,000g. Bands in agarose gels were visualised on a UV Transilluminator (UVP) and carefully excised with a scalpel blade. The bands were weighed and 3 volumes of buffer QG was added to 1 volume of gel before heating the agarose and buffer QG mixture at 50°C for 10 minutes or until the gel slice has completely dissolved. After centrifugation to adsorb the DNA to the membrane, the membrane was washed with 500ul of buffer QG followed by 750ul of buffer PE (which contains 70% (v/v) ethanol). All traces of ethanol were removed by a final centrifugation for 1 minute. DNA was eluted in 30ul of dH_2O

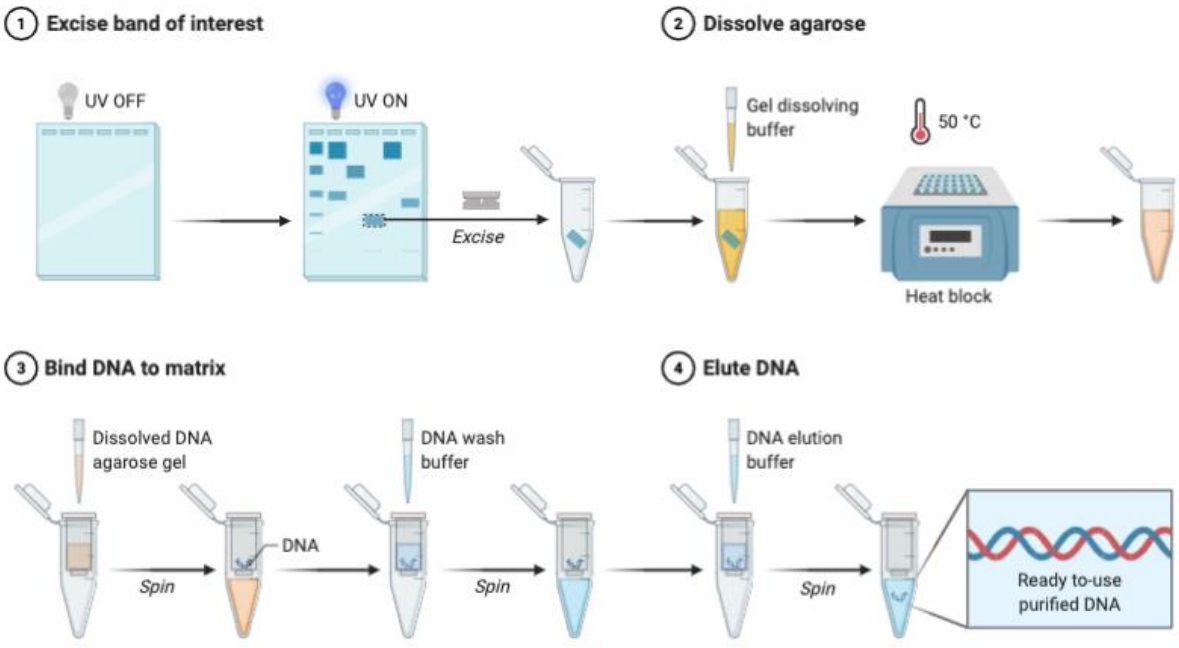

Figure 3.6: Image depicting the process of DNA gel extraction after running restriction fragments on an agarose gel. Reprinted from "DNA Gel Extraction", by BioRender.com (2021). Retrieved from https://app.biorender.com/biorender-templates

3.2.4 Ligation

Ligation of the restricted promoter fragments and pGL4.10 luciferase vector was carried out using the Quick Ligation Kit from New England Biolabs (catalogue no: M2200S). Manufacturer's protocol was followed to prepare the ligation mix. The ratio of vector: insert was 50ng: 150ng. If DNA concentrations were not high enough to meet this ratio, then the highest possible volume of insert was used. This was done without exceeding the total DNA volume. The ligation mix was incubated at room temperature (25°C) for 5 minutes and then chilled or stored at -20°C until transformed into bacterial competent cells.

Table 3.3: Ligation master mix

Ligation master mix	Volume (ul)
pGL4.10 luciferase vector (50ng)	2ul
***Spp1* promoter fragment (150ng)**	4ul
2X Quick ligation reaction buffer	10ul
Quick T4 DNA ligase	1ul
dH_2O	4ul

3.2.5 Transformation of Promotor Constructs into Competent Cells

MAX Efficiency DH5α Competent Cells from Invitrogen (catalogue no: 18258012) were used as hosts for eukaryotic expression vectors. For transformation, one tube of competent cells was gently taken out of -80°C and thawed on ice. 21ul of the ligation mixture was combined with 50ul of competent cells. The mixture was gently pipetted up and down to allow the cells and DNA to mix gently, and then incubated on ice for 30 minutes. The mixture was then heat shocked at 42°C for 30 seconds before returning to ice for a further 2 minutes. 450ul of pre-warmed SOC medium was added to the cells and they were placed in a shaking incubator (New Brunswick Scientific Inova 44) at 37°C, 250rpm, for one hour. 90mm culture plates (Sterilin) of Luria agar (Sigma) containing 100ug/ml ampicillin (Sigma) were spread and allowed to dry for 1 hour. All plasmids used in this chapter encoded ampicillin resistance for selection of transformed cells. Culture plates were placed in a 37°C incubator overnight. Plates were checked for bacterial colonies the next morning, and the DNA from the colonies was then screened for positive clones through PCR. Primers specific to the vector was used to amplify the insert region.

3.2.6 Plasmid DNA Purification using QIAGEN Maxi Kit

Plasmid DNA was extracted from bacteria using the filter column based QIAGEN Plasmid Maxi Kit (Cat. No. / ID: 12162). Bacterial cultures were streaked and grown overnight at 37°C on ampicillin Luria agar plates. Single colonies were picked and used to inoculate a 10ml Luria broth starter culture, containing 100 µg/ml ampicillin. This was grown for approximately 8 hours at 37°C in shaking incubator. 1ml of this starter culture was then used to inoculate a 200ml 100 µg/ml ampicillin Luria broth to produce an overnight culture from which the plasmid was extracted. Bacteria was harvested by centrifugation at 6,000g for 15 minutes at 4°C in a Beckman Coulter Avanti J26XP. The culture media was poured out and the bacteria was re-suspended in 10ml buffer P1. 10ml buffer P2 was added, and the solutions were kept on ice for 5 minutes. 10ml pre-chilled buffer P3 was added to neutralise the lysate. The precipitated lysates were then centrifuged at 18,000g for 10 minutes at 4°C. The supernatant was collected and centrifuged again at the same speed for a further 15 minutes to ensure a clear suspension. QIAGEN-tip 500 was equilibrated with 10ml buffer QBT. The supernatant was applied to the QIAGEN-tip 500 and allowed to

enter the resin by gravity flow. The columns were then washed twice with 30ml buffer QC. The plasmid DNA was eluted with 15ml buffer QF into polypropylene centrifuge tubes. Plasmid DNA was precipitated with 10.5ml isopropanol and centrifuged at 15,000g for 30 minutes at 4°C. The supernatant was carefully decanted, and the pellets were washed with 5ml 70% ethanol and centrifuged at 15,000g for 10 minutes at 4°C. The supernatant was carefully decanted, and the pellets were thoroughly air-dried (10-20 minutes) before re-suspending the DNA in 450ul of dH_2O.

3.2.7 Cell Counting

To ensure accurate seeding of cells in plates with a known number of cells, cells were counted using a haemocytometer (Hausser Scientific). 10ul of cell suspension was pipetted under a cover slip onto the grid of the haemocytometer. The number of cells in each 1mm square was recorded by counting the cells in each 0.25mm squares. Cells crossing the bottom or right-hand edge of any square were not counted. Dilutions of the cell suspension were made in media to seed the correct number of cells per well of the plate.

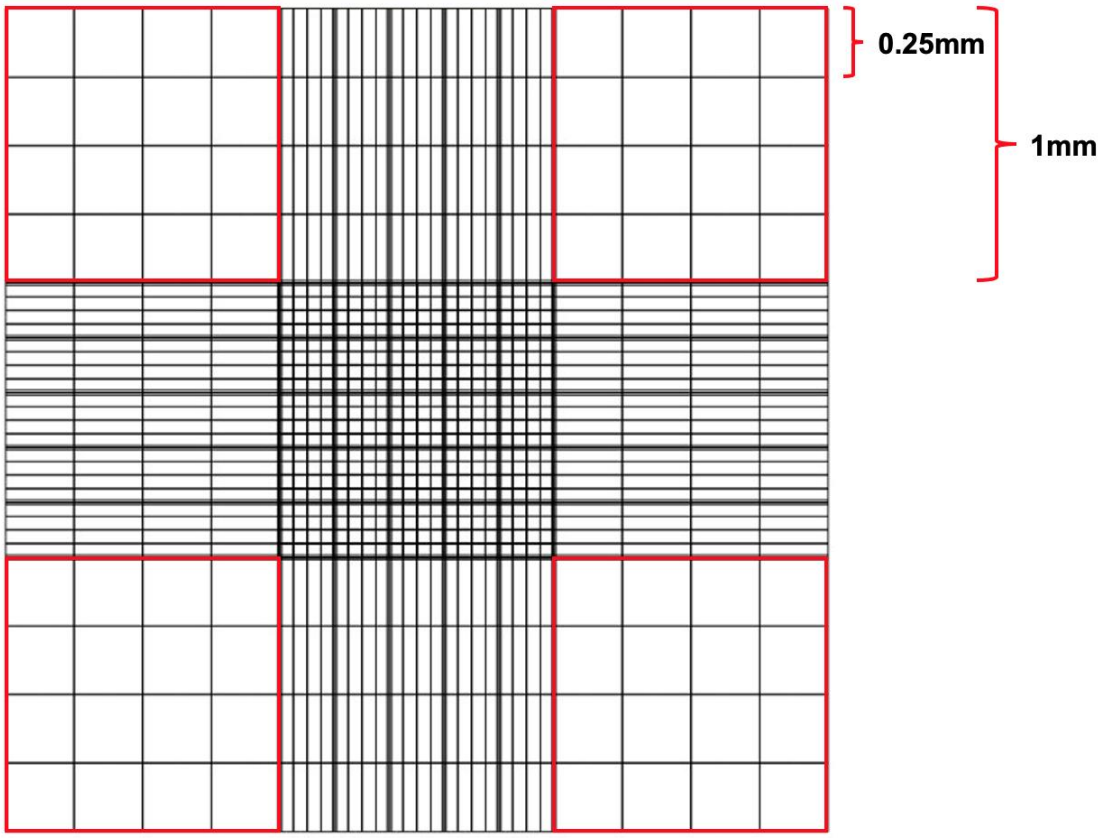

Figure 3.7: Image depicting haemocytometer grid as seen under 10X magnification

Cells found in the red boxes were counted. Any cell that was found crossing the bottom or right-hand edge of the 1mm box was not counted. The number of cells in each of the four 1mm boxes were counted. An average of the four readings were taken and multiplied by 10^4 to obtain the number of cells per ml in the sample applied to the haemocytometer.

3.2.8 Dual Luciferase Reporter Assay (DLR) using HeLa cells

The Dual-Luciferase Reporter Assay System (Promega, UK, catalogue no: E1910) was used and manufacturer's protocol was followed. The Lumat LB 9507 from Berthold Technologies has a dual injector technology and pre-programmed settings for standard luciferase assays. Luminometer tubes were used for each sample, and they were measured in duplicate to obtain average relative light unit (RLU) per sample.

Prior to conducting the luciferase assay, H9c2 cells with a seeding density of 3.4 x 10^4 per well, were seeded into a 24-well culture plate. For transfection, the constructs were transfected with the following ratio: Renilla (50ng): Promoter construct DNA (950ng). The renilla DNA acts as an internal control and enable a ratio of RLU to be used for more accurate analysis of transcription activity. The controls used in this experiment were cells only, luciferase DNA only and renilla DNA + luciferase DNA only. Each experimental condition was transfected in triplicate in order to achieve a higher level of accuracy. Transfected cells were incubated at 37°C for 48 hours before conducting the luciferase assay.

48 hours post-transfection, 100ul of 1X passive lysis buffer is added to transfected H9c2 cells. Passive lysis is performed at room temperature for 15 minutes. Lysates are then transferred to a luminometer tube. 100µl of the luciferase reagent (LARII) is first added to the sample (20µl of PBL lysate) to measure firefly luciferase activity to generate a luminescent signal lasting at least one minute. After quantifying the firefly luminescence, it is quenched by adding 100µl of Stop & Glo reagent.

3.2.9 RNA Isolation of Gestational Day 18 Rat Hearts

RNA was extracted from whole gestational day 18 rat hearts using the miRNeasy Mini Kit (Qiagen, UK, catalogue no: 217004). Six hearts from each $SHRSP_{Gla}$ and WKY_{Gla} strains were harvested from the same litter. RNA was extracted from these tissues by methods detailed under section 2.1. RNA was eluted in RNase free water at a final of 40ul. Samples were stored at -80ºC until used.

3.2.10 Preparation of cDNA samples

Complementary DNA (cDNA) samples were prepared from gestational day 18 RNA samples. Applied Biosystems TaqMan Reverse Transcription Reagents were used for cDNA synthesis using random hexamers. Reverse transcription reactions were performed in 96-well plates to allow multichannel pipettes to be used for PCR reaction set up. For each reaction, 500ng of RNA template was reverse transcribed using the following reagents:

Table 3.4: TaqMan Reverse transcription reaction mix

For a single 20ul reaction	Volume (ul)	Heat Cycle
10X Reaction buffer	2ul	25°C – 10 minutes
25mM $MgCl_2$	4.4ul	48°C – 30 minutes
2.5mM dNTPs	4ul	95°C – 5 minutes
50uM Random Hexamers	1ul	4°C - 5 minutes
20U/ul RNase Inhibitor	0.4ul	
50U/ul MultiScribe Enzyme	0.5ul	
dH_2O	5.2ul	
RNA (200ng/ul dilution)	2.5ul	

3.2.11 Quantitative Real Time PCR Reaction

Applied Biosystems Gene Expression Assays and Custom Gene Expression Assays were used for all qRT-PCRs in this chapter. The probe fluoresces only when bound to DNA and the amount of fluorescence detected is linearly proportional to the amount of DNA. The probes are covalently joined to the 5' end fluorescence molecule called reporter and the 3' primer end molecule called quencher. The reported molecule reports a signal as you generate more product, and the quencher molecule quenches the fluorescence signal from the reporter. During PCR amplification, the 5'-3' nucleolytic activity of the DNA polymerase cleaves the quencher from the probe, resulting in fluorescence levels proportional to the amount of PCR product present.

All assays were performed with the same amount of template cDNA in each reaction of an experiment. The gene of interest and B2M were amplified in duplex PCR reactions, probes for the gene of interest were tagged 'FAM" labelled fluorescent dyes, while B2M probes were labelled 'VIC' dye, they fluoresce at different wavelengths allowing them to be measure in the same reaction without any interference. Reactions were performed in 5ul volumes in 384-well plates. For each reaction the following reagents and heat cycle parameters were used:

Table 3.5: qRT-PCR reaction mix

Master mix for single 5ul reaction	Volume (ul)
2X TaqMan Universal Master Mix II	2.5ul
FAM Probe (rat *Spp1*)	0.25ul
VIC Housekeeper Probe (rat *B2M*)	0.25ul
cDNA Template	1ul
dH_2O	1ul

Table 3.6: Heat cycling parameters

Temperature (°C)	Time (minutes)	
25°C	10 minutes	
48°C	30 minutes	
95°C	5 minutes	40 cycles
4°C	5 minutes	
12°C	∞	

All samples were set up and amplified in triplicate. Fluorescence of FAM and VIC dyes was measured for all reactions during temperature cycling, data was analysed using a combination of Applied Biosystems SDS (Sequence Detection Software) and Microsoft Excel software. FAM and VIC fluorescence were analysed as separate data sets, a fluorescence threshold was identified for each data set where amplification curves were in their exponential phase. The CT or cycle threshold is the cycle number at which fluorescence is generated within a reaction that crosses the fluorescence threshold, a fluorescent signal significantly above the background fluorescence. The threshold cycle is inversely proportional to the original relative expression level of the gene of interest. Ct values for FAM and VIC data were exported from SDS as text files and converted to Excel documents for data analysis. Relative levels of gene expression were calculated by the 'ΔΔCt method'.

The ΔΔCt method is a method of relative quantification which directly uses the CT value generated from a qPCR system to calculate the relative gene expression in the gene of interest and housekeeper samples, using the housekeeper as the normalizer (Rao et al. 2014).

3.2.12 Statistical Analysis

All statistics were performed using GraphPad prism version 9 (GraphPad software, San Diego, California USA). For statistical comparisons between two groups, 2 sample t-tests were applied. Values are presented as mean ± SEM, and differences of $P \leq 0.05$ values were taken as significant.

3.3 Results

3.3.1 Quantitative Real-Time PCR (qRT-PCR) of Gestational Day 18 Rat Hearts

Quantitative real-time PCR was conducted on $SHRSP_{Gla}$ and WKY_{Gla} gestational day 18 rat hearts to quantify and compare the expression levels of *Spp1*. Samples were set up in duplicates. B2M was used as a housekeeper for normalisation. qRT-PCR results revealed that there was an increase in *Spp1* expression in the $SHRSP_{Gla}$ compared to WKY_{Gla} gestational day 18 hearts in all three experiments (fig 3.8 A: 5.9-fold increase, $p<0.0001$; fig 3.8 B: 3.3-fold increase, $p<0.0001$; fig 3.8 C: 2.9-fold increase, $p<0.00001$). Statistical analysis of the data (n=3) further confirmed a significant increase in *Spp1* expression in the SHRSP group compared to WKY (fig 3.8 A – 3.8 C).

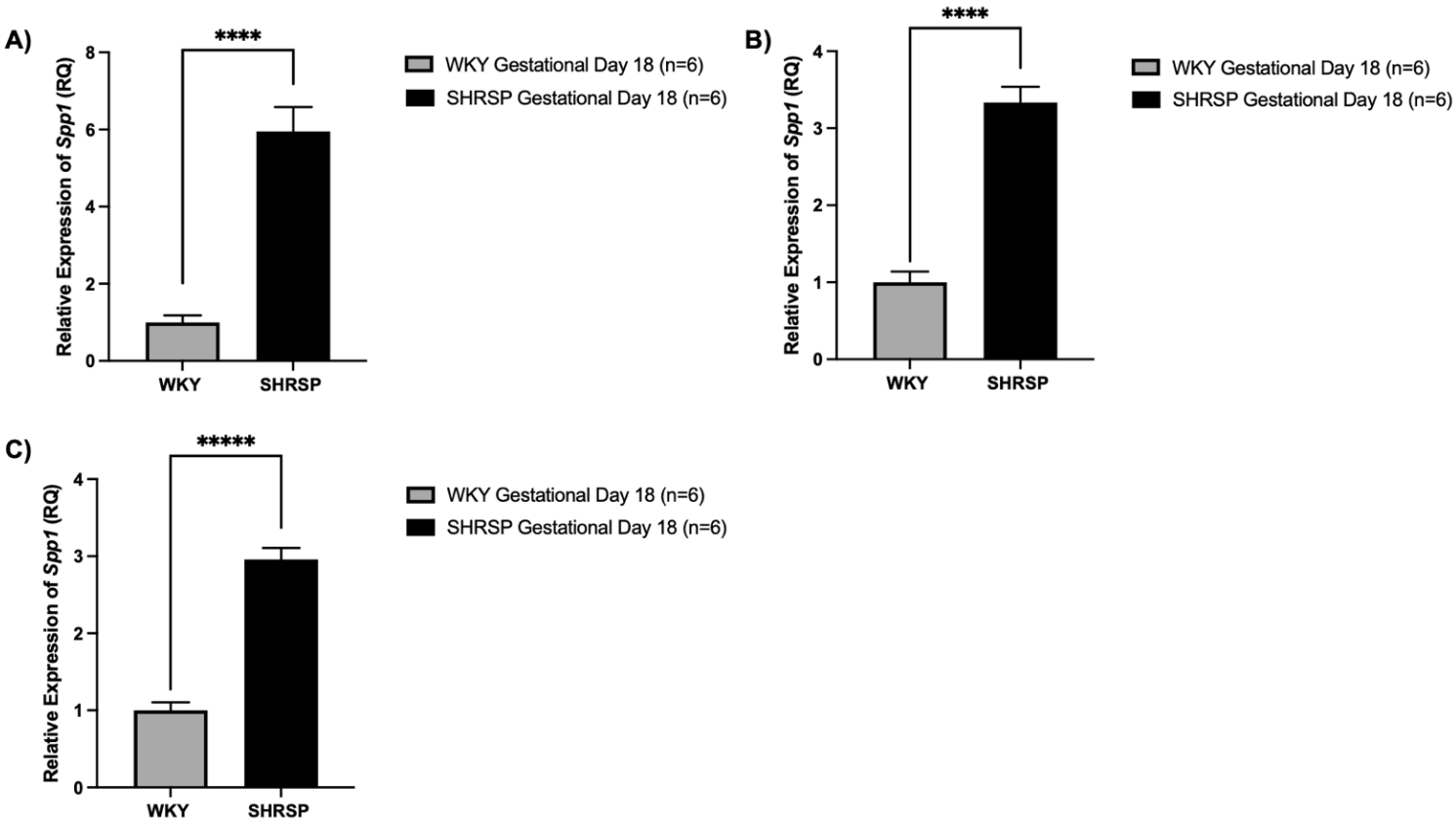

Figure 3.8: qRT-PR analysis of *Spp1* expression in SHRSP and WKY gestational day 18 rat hearts (n=6).

qRT-PCR results revealed a significant increase in *Spp1* expression in SHRSP gestational day 18 rat hearts compared to WKY gestational day 18 rat hearts. Data was analysed using student t-test. Error bars represent ±SEM.

(A) A 5.9-fold significant increase in *Spp1* expression in SHRSP gestational day 18 rat hearts compared to WKY gestational day 18 rat hearts ($p<0.0001$)

(B) A 3.3-fold significant increase in *Spp1* expression in SHRSP gestational day 18 rat hearts compared to WKY gestational day 18 rat hearts ($p<0.0001$)

(C) A 2.9-fold significant increase in *Spp1* expression in SHRSP gestational day 18 rat hearts compared to WKY gestational day 18 rat hearts ($p<0.00001$)

3.3.2 Sub-cloning of SHRSP and WKY promoter fragments into pGL4.10 vector

Using PCR and sub-cloning techniques, we were able to achieve the SP & WKY 10F/10R and SP & WKY 11F/11R promoter constructs. Previous members of the McBride and Graham group successfully sub-cloned SP & WKY 10F/10R promoter fragments into the pGL4.10 vector. Therefore, we only performed plasmid preparations to isolate the constructs from the bacterial culture and perform gel electrophoresis of these PCR products from these plasmid preparations to show the successful sub-cloning of these constructs with their expected band size 1.3kb (fig 3.9).

The SP & WKY 11F/11R promoter fragments were initially sub-cloned into the StrataClone blunt PCR cloning vector (pSC-B-amp/kan). Using restriction enzymes Xho I and Bgl II, we were able to successfully restrict the SP & WKY 11F/11R promoter fragments from the PCR cloning vector. The successful sub-cloning of SP & WKY 11F/11R promoter fragments into the pGL4.10 vector was done by conducting restriction digestion of the plasmid preparations using restriction enzymes Xho I and Bgl II. This was confirmed by gel electrophoresis with a band signal of 1.9kb for all 4 WKY plasmid preparations and 1 SP plasmid prep (fig 3.9).

However, we were unable to successfully produce the SP & WKY 10F/12R promoter constructs. This was the longest promoter fragment with a band size of 5.2kb. We were able to restrict the promoter fragments from the PCR cloning vector using restriction enzyme Xho I and Bgl II which resulted in 2 separate clear bands at the expected sizes of 4.9kb (PCR cloning vector) and 5.2kb (promoter fragments). This was confirmed as shown in figure 3.10 A. Uncut samples were also included to show a single band. However, this band cannot be sized due to plasmid supercoiling. Samples which were cut with single restriction enzymes show single bands which indicates the plasmid is in its linear form. After transforming the ligated DNA into competent cells, we conducted colony PCR to confirm the successful sub-cloning of *Spp1 &* WKY 10F/12R promoter constructs. We used primers 11F and 11R as these primers recognition sites lie within the 10F/12R promoter fragment. However, the results showed no bands at the expected 1.9kb size. We also used the four WKY

11F/11R plasmid preparations and two colony samples from WKY 11F/11R as positive controls and it shows the expected band sizes at 1.9kb (fig 3.10 B).

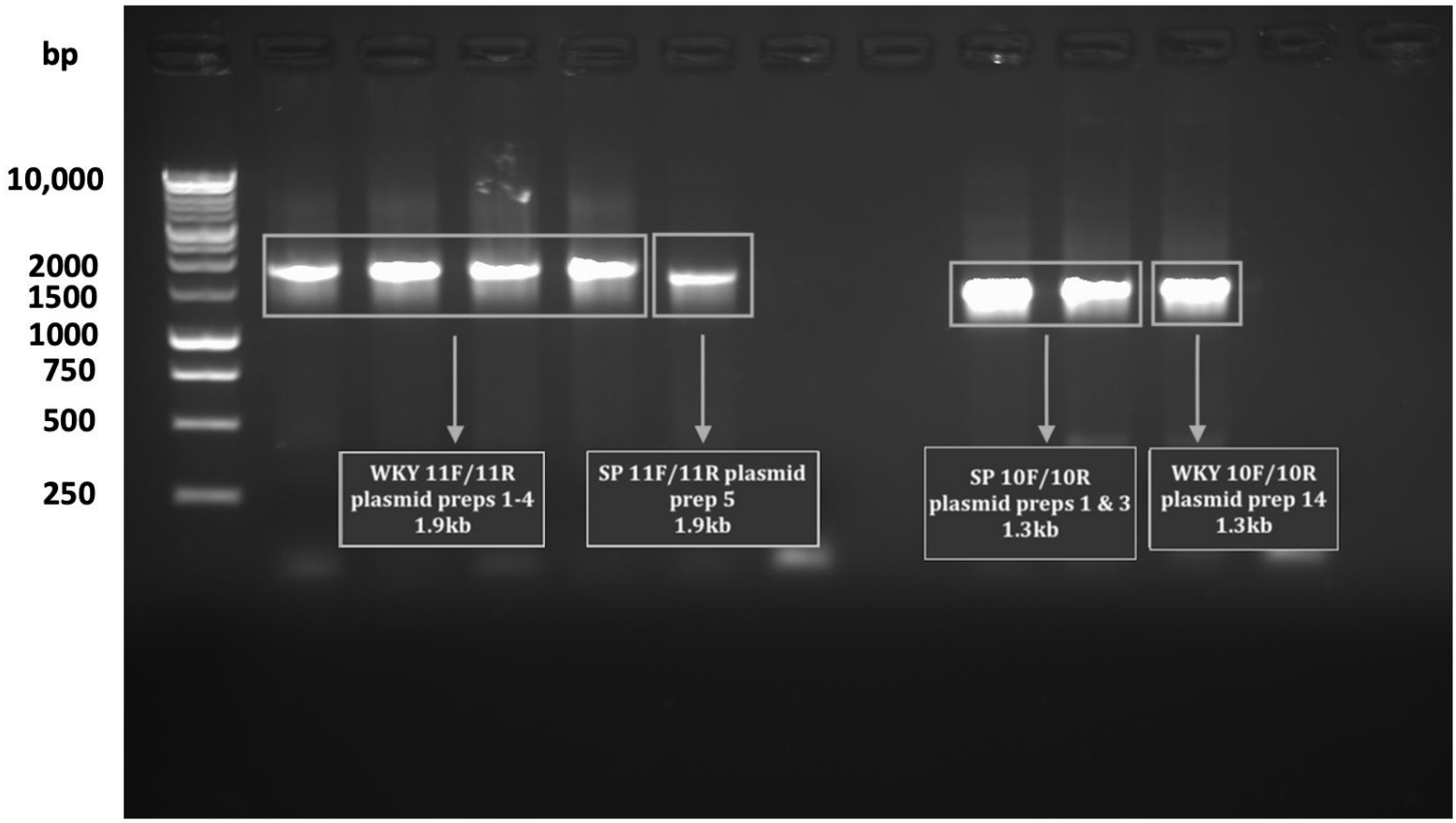

Figure 3.9: Successful cloning of SP & WKY 11F/11R and 10F/10R into PGL4.10 vector. SP&WKY 11F/11R is 1.9kb and SP & WKY 10F/10R is 1.3kb.

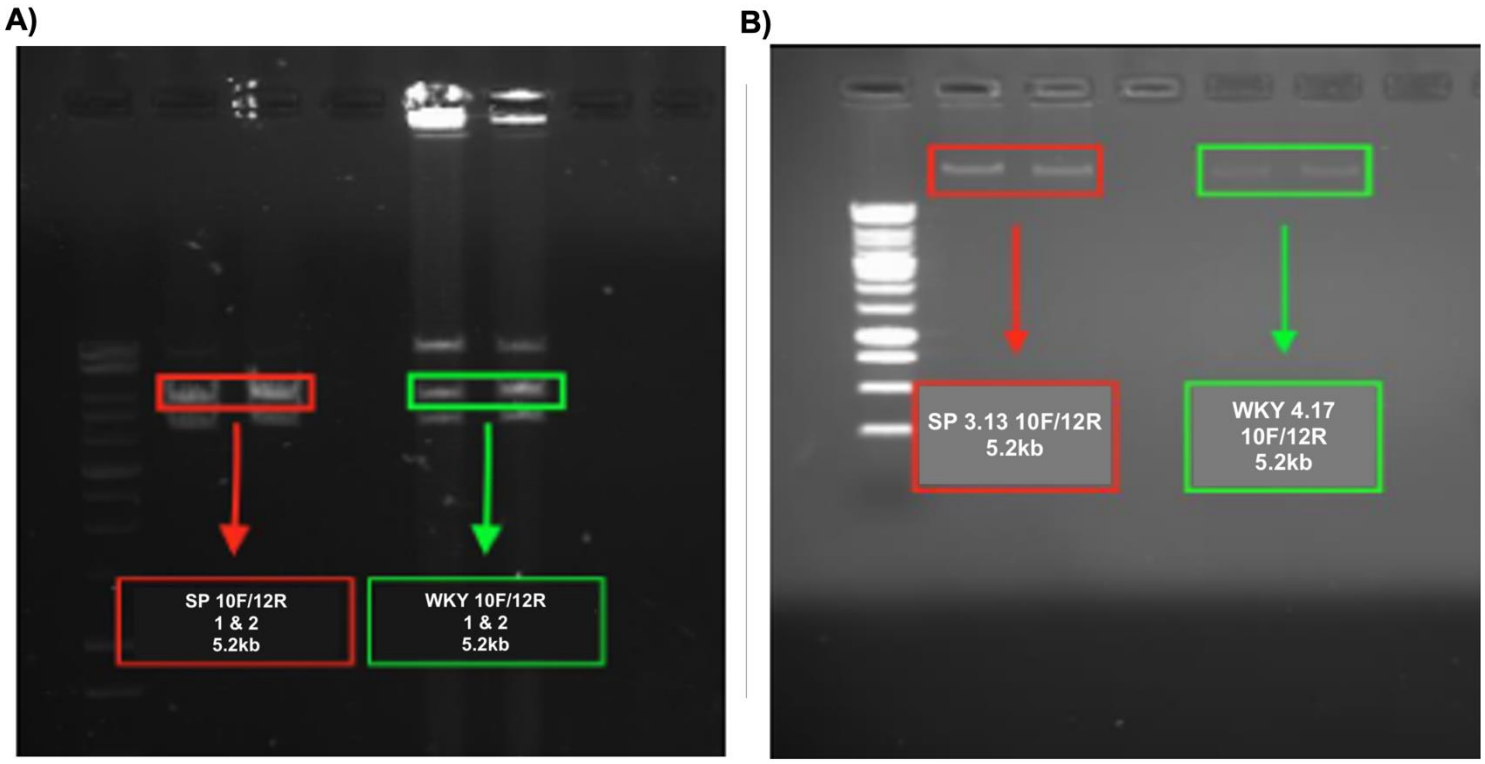

Figure 3.10: A) Shows successful restriction of SP 3.13 & WKY 4.17 10F/12R from PCR cloning vector using restriction enzymes Xho1 and Bgl2. **B)** Shows unsuccessful ligation of SP 3.13 & WKY 4.17 10F/12R with PGL4.10 vector.

3.3.3 Transcriptional activity of Spp1 promoter constructs using H9c2/HeLa cells

Using the dual luciferase reporter assay we assessed the transcriptional activity of the SHRSP and WKY promoter fragments that were sub-cloned into the pGL4.10 luciferase vector. We performed two separate experiments using two different cell lines: H9c2 cells and HeLa cells. Both cell types were transfected with the newly constructed promoter constructs; SP & WKY 10F/10R and 11F/11R. The controls used in this experiment were the luciferase reporter gene (*luc2*) pGL4.13 and the renilla luciferase gene (*hRluc*) pGL4.73.

In H9c2 cells (fig 3.11), the control conditions; renilla only and luciferase only, showed an average RLU of 486661 and 9.26991 x 10^6 respectively. Although not significant, we observed a trend to increase in luciferase activity in the SP 10F/10R and 11F/11R promoter constructs when compared to the WKY 10F/10R and 11F/11R promoter constructs. We also see that the 11F/11R region has a higher level of luciferase activity compared to the 10F/10R region for both SHRSP and WKY strains.

Table 3.7: SP & WKY 10F/10R and 11F/11R promoter constructs transfected in H9c2 cells

Promoter Constructs	RLU ratio
WKY 10F/10R	6.75 x 10^{-5}
SP 10F/10R	1.73 x 10^{-4}
WKY 11F/11R	4.53889 x 10^{-3}
SP 11F/11R	7.97622 x 10^{-3}
Renilla only	486661
Luciferase only	9.26991 x 10^6

In HeLa cells we set up an n=2 experiments (fig 3.12 & 3.13). In the first experiment (fig 3.12), the control conditions; renilla only and luciferase only, showed an average RLU of 1.86 x 10^4 and 764.946 respectively. In the promoter constructs, we observed variable levels of luciferase activity. When comparing the SP & WKY 10F/10R promoter constructs, we observed increased luciferase activity in the SP construct when compared to the WKY. In the SP & WKY 11F/11R construct, we

observed that WKY had increased luciferase activity when compared to the SP construct. Figures 3.12 & 3.13 are set up as separate experiments and represented as replicates. The experimental conditions in both experiments are the same with no changes in the set up.

Table 3.8: SP & WKY 10F/10R and 11F/11R promoter constructs transfected in HeLa cells

Promoter Constructs	RLU ratio
WKY 10F/10R	8.47×10^{-4}
SP 10F/10R	2.96075×10^{-3}
WKY 11F/11R	2.82675×10^{-3}
SP 11F/11R	2.10275×10^{-3}
Renilla only	1.86×10^{-4}
Luciferase only	764.946

In the second experiment (fig 3.13), the control conditions; renilla only and luciferase only, showed an average RLU of 3.9×10^{-4} and 6.999 respectively. In the promoter constructs, we observed variable levels of luciferase activity. In the 10F/10R promoter constructs, WKY had increased luciferase activity compared to SP. In the SP & WKY 11F/11R construct, we observed a significant increase in luciferase activity in the SP construct compared to the WKY construct.

Table 3.9: SP & WKY 10F/10R and 11F/11R promoter constructs transfected in HeLa cells

Promoter Constructs	RLU ratio
WKY 10F/10R	1.03×10^{-4}
SP 10F/10R	1.01×10^{-4}
WKY 11F/11R	7.4×10^{-5}
SP 11F/11R	2.08×10^{-4}
Renilla only	6.999
Luciferase only	3.9×10^{-4}

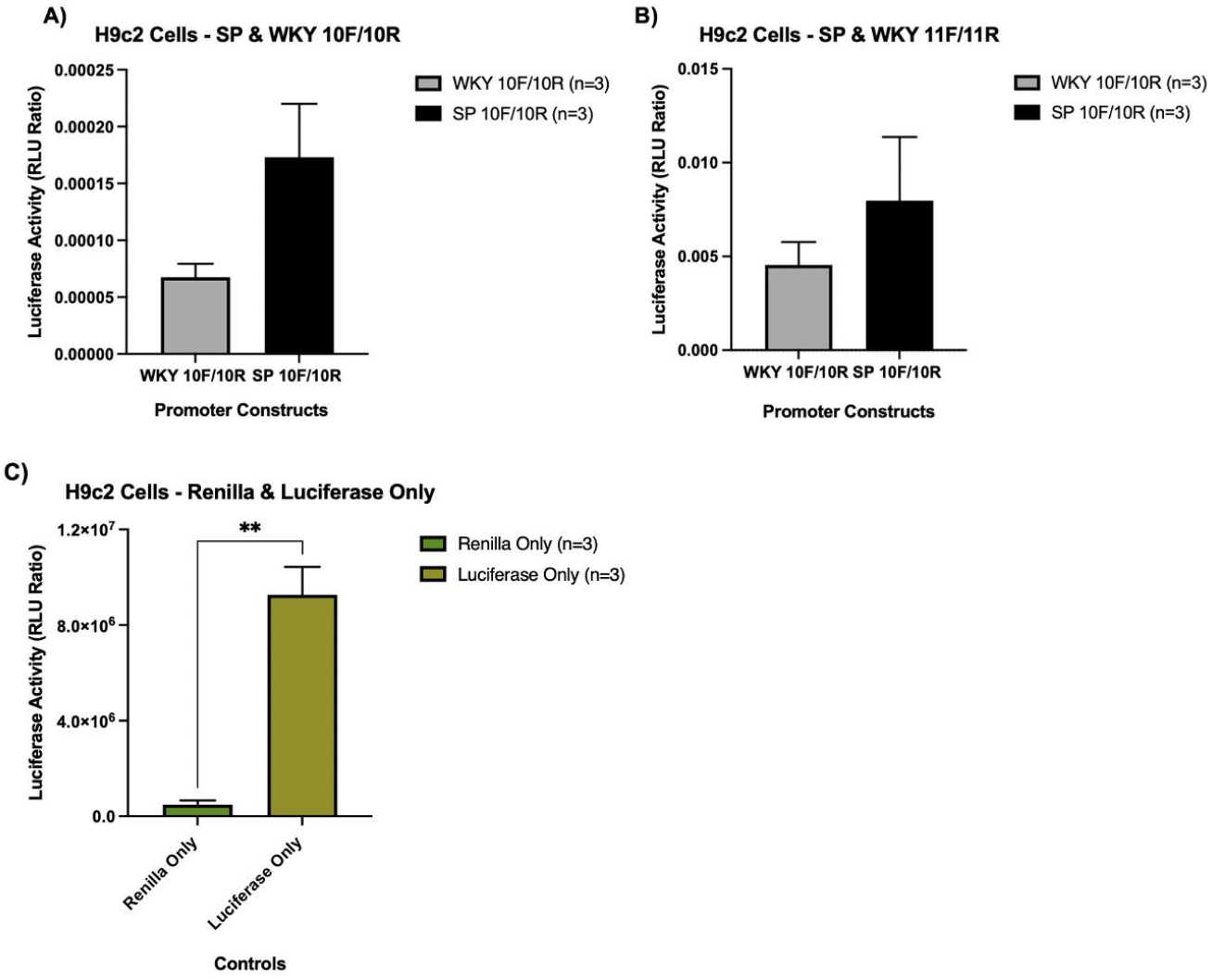

Figure 3.11: Dual Luciferase Reporter Assay results from H9c2 cells transfected with WKY_{Gla} and $SHRSP_{Gla}$ 10F/10R and 11F/11R, and Renilla & Luciferase only

The dual reporter luciferase assay was set up in 3 conditions: Renilla + WKY 10F/10R, Renilla + SP 11F/11R and Renilla & Luciferase only. We observed a significant increase in luciferase activity in the luciferase only control compared to renilla only. We also observed a trend towards increased luciferase activity in the SP 10F/10R and SP 11F/11R promoter constructs compared to WKY 10F/10R and WKY 11F/11R promoter constructs. Data was analysed using student t-test. Error bars represent ±SEM.

(A) WKY_{Gla} and $SHRSP_{Gla}$ 10F/10R promotor constructs.

(B) WKY_{Gla} and $SHRSP_{Gla}$ 11F/11R promotor constructs.

(C) Experimental controls, Renilla and Luciferase only transfections.

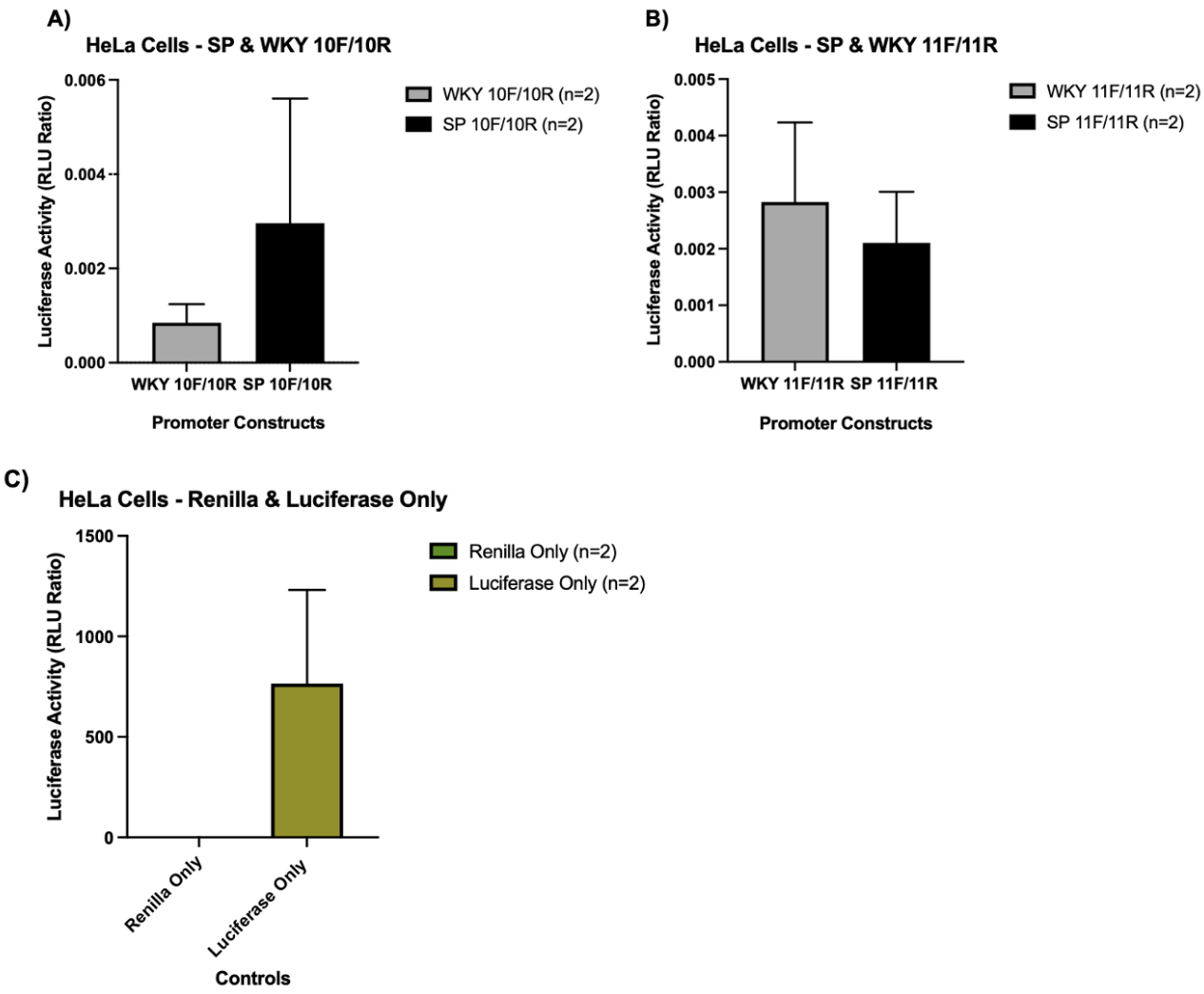

Figure 3.12: Dual Luciferase Reporter Assay results from HeLa cells transfected with WKY_{Gla} and $SHRSP_{Gla}$ 10F/10R and 11F/11R, and Renilla & Luciferase only

The dual reporter luciferase assay was set up in 3 conditions: Renilla + WKY 10F/10R, Renilla + SP 11F/11R and Renilla & Luciferase only. We observed a trend towards increased luciferase activity in the SP 10F/10R promoter construct compared to WKY 10F/10R promoter construct. In the 11F/11R promoter constructs we observed an increase in the WKY promoter constructs compared to the SP promoter construct. Data was analysed using student t-test. Error bars represent ±SEM.

(A) WKY_{Gla} and $SHRSP_{Gla}$ 10F/10R promotor constructs.

(B) WKY_{Gla} and $SHRSP_{Gla}$ 11F/11R promotor constructs.

(C) Experimental controls, Renilla and Luciferase only transfections.

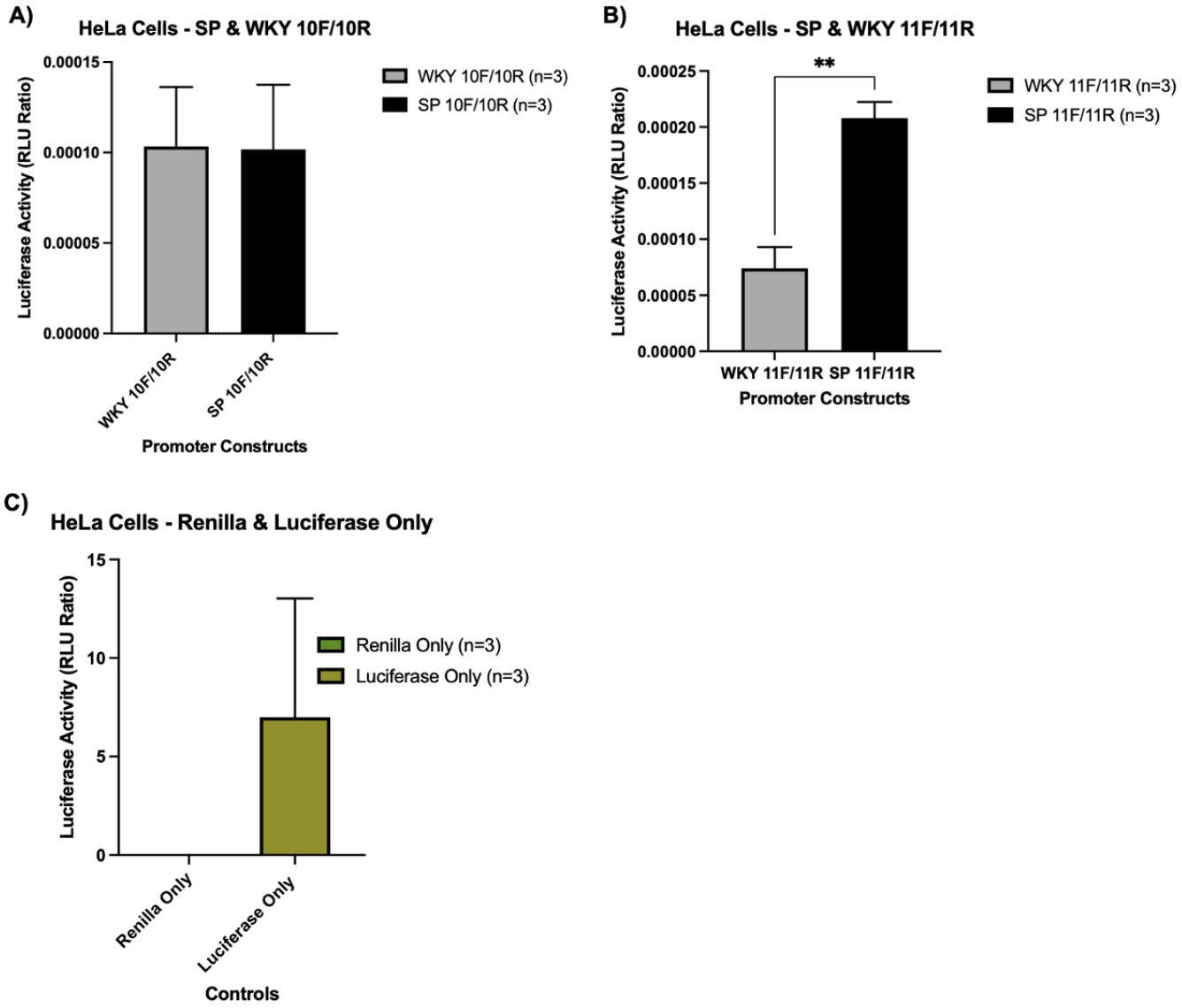

Figure 3.13: Dual Luciferase Reporter Assay results from HeLa cells transfected with WKY_{Gla} and $SHRSP_{Gla}$ 10F/10R and 11F/11R, and Renilla & Luciferase only

The dual reporter luciferase assay was set up in 3 conditions: Renilla + WKY 10F/10R, Renilla + SP 11F/11R and Renilla & Luciferase only. We observed that in the 10F/10R promoter constructs, WKY had increase luciferase activity compared to SP by 1.66667×10^{-6} RLU. In the 11F/11R promoter constructs we observed a significant increase in the SP luciferase activity compared to WKY. Data was analysed using student t-test. Error bars represent ±SEM.

(A) WKY_{Gla} and $SHRSP_{Gla}$ 10F/10R promotor constructs.

(B) WKY_{Gla} and $SHRSP_{Gla}$ 11F/11R promotor constructs.

(C) Experimental controls, Renilla and Luciferase only transfections.

3.3.4 Microarray Expression Profiling Analysis

To capture gene expression changes responsible for disease phenotype, we determined cardiac gene expression profiles from 5 weeks versus neonatal WKY, SHRSP and WKY.SP$_{Gla}$14a (D) strains.

Ingenuity Pathway Analysis (IPA) software, an advanced bioinformatics tool with a massive built-in knowledge database, was used to analyse DEG-associated canonical signalling pathways in cardiac hypertrophy by using gene expression profiles of the heart from 5-week and neonatal timepoints in the SHRSP, WKY and WKY.SP$_{Gla}$14a (D) rat strains. The Venn diagram (fig 3.14) was produced using Ingenuity Pathway Analysis (IPA) to filter and investigate differentially expressed genes between the three strains. A total of 382 differentially expressed genes were identified in the WKY strain, 361 differentially expressed genes were identified in the SHRSP strain and 223 differentially expressed genes were identified in the WKY.SP$_{Gla}$14a strains. We looked at 101 (highlighted in yellow in fig 3.14) differentially expressed genes that were found in common between the SHRSP and WKY.SP$_{Gla}$14a 5 weeks vs neonatal timepoints that potentially contribute towards cardiac hypertrophy. Further filtering was conducted based on IPA inbuilt target prediction function setting direction of *Spp1* and relevant genes (up or down regulated). IPA was used to find overlap in the restricted target list with gene expression data as well as determine connections between the predicted targets and relevant phenotypes. This list was used to further narrow down the likely targets that are relevant in our model. The use of IPA software proved invaluable in identifying pathways relevant to cardiac hypertrophy or enlargement that contained predicted targets. Eventually the list of predicted gene targets, relevant to cardiac hypertrophy, was narrowed down to 5 (*DES, MYOM1, CTSD, SLC25A11* and *MMP14)* (fig 3.15 and 3.16).

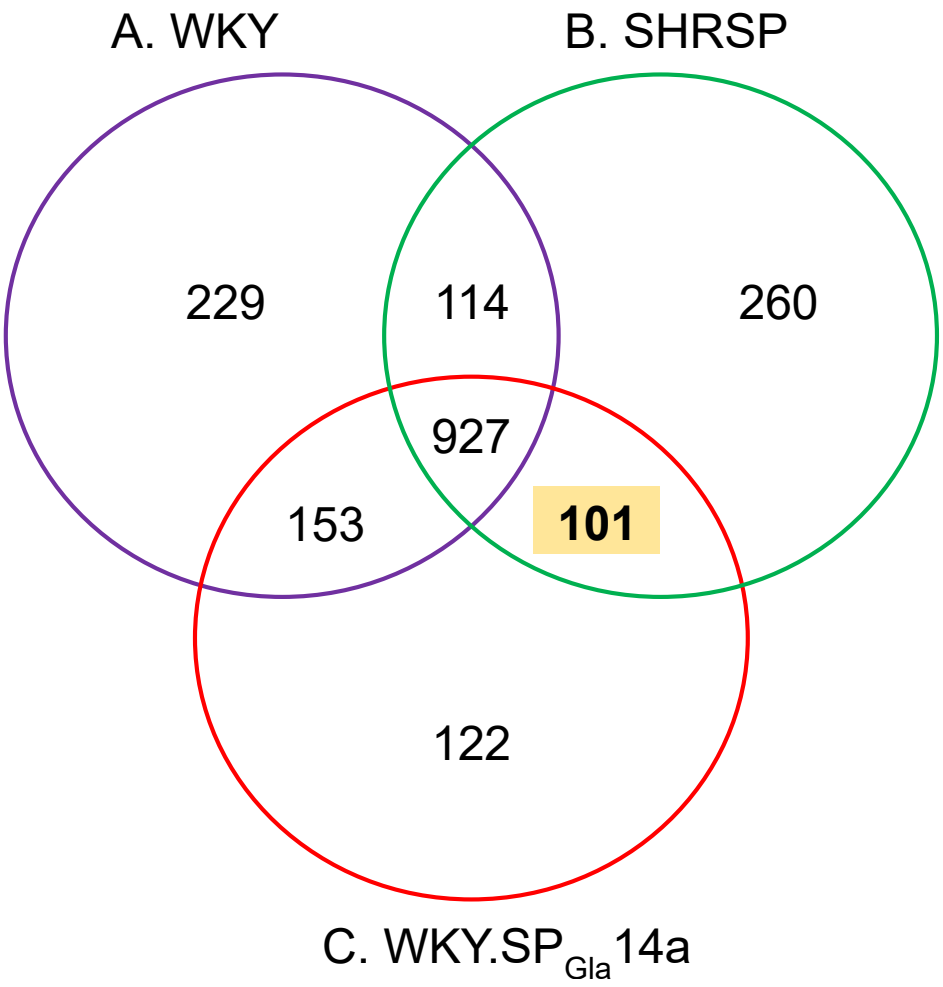

Figure 3.14: Microarray analysis of the A) WKY 5wks vs Neo, B) SHRSP 5wks vs Neo, and C) WKY.SP$_{Gla}$14a (D) 5wks vs Neo strains

The Venn diagram illustrates microarray results of gene expression profiles in the heart of rats comparing 5 weeks vs neonatal timepoints in the WKY, SHRSP and WKY.SP$_{Gla}$14a (D) strains.

Categories	Diseases or Function Annotation	p-value	Molecules	# Molecules
Cardiac Dilatation, Cardiac Enlargement	Dilated cardiomyopathy 1i	4.27E-03	↑ DES	1
Cardiac Dilatation, Cardiac Enlargement	Familial dilated cardiomyopathy	3.33E-02	↑ DES, ↑ MYOM1	2
Cardiac Dilatation, Cardiac Enlargement	Primary dilated cardiomyopathy	3.70E-02	↑ DES, ↑ MYOM1	2
Cardiac Dilatation, Cardiac Enlargement	Dilated cardiomyopathy 1s	5.00E-02	↑ DES	1
Cardiac Dilatation, Cardiac Enlargement	Dilated cardiomyopathy	5.38E-02	↑ DES, ↓ MMP14, ↑ MYOM1, ↑ SLC25A11	4
Cardiac Dilatation, Cardiac Enlargement	Idiopathic dilated cardiomyopathy	1.24E-01	↑ SLC25A11	1
Cardiac Dilatation, Cardiac Enlargement	Dominant dilated cardiomyopathy	1.50E-01	↑ DES	1
Cardiac Enlargement	Hypertrophy of heart cells	1.85E-01	↑ CTSD, ↑ MYOM1	2
Cardiac Enlargement	Enlargement of heart	2.08E-01	↑ DES, ↓ MMP14, ↑ MYOM1, ↑ SLC25A11, ↑ CTSD	5
Cardiac Enlargement	Hypertrophy of heart	3.31E-01	↑ CTSD, ↑ DES, ↑ MYOM1	3

Figure 3.15: Ingenuity Tox analysis identified genes downstream that connected to *Spp1* and are involved in the cardiac enlargement. *DES, MYOM1, CTSD* and *SLC25A11* show upregulation while *MMP14* show downregulation

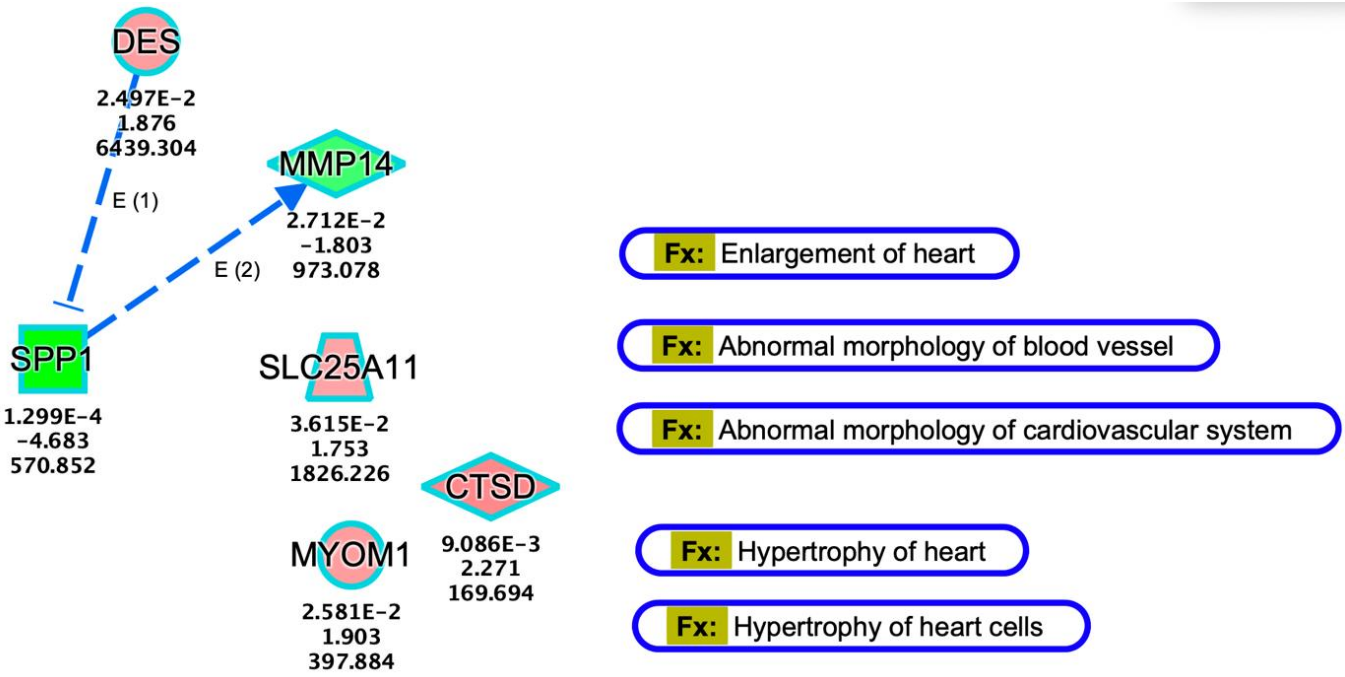

Figure 3.16: 5 genes identified downstream that are connected to *Spp1* and the enlargement of the heart. *DES, MYOM1, CTSD* and *SLC25A11* show upregulation while *MMP14* show downregulation

3.4 Discussion

In this study we aimed to quantify and compare the expression levels of *Spp1* in the $SHRSP_{Gla}$ and WKY_{Gla} gestational day 18 rat hearts and compare the transcriptional activity of segments of *Spp1* promoter through the generation of SHRSP and WKY promoter constructs. Using these constructs, we aimed to compare transcriptional activity of the segments of *Spp1* promoter through DLR.

By using a combination of targeted sequence capture and Sanger DNA capillary sequencing, two single nucleotide polymorphisms (SNPs) were identified and mapped to the $SHRSP_{Gla}$ cis-acting promoter sequence of *Spp1* by members of the McBride and Graham group. *Spp1* has been associated significantly with diastolic dysfunction in a Japanese population (Nakayama et al. 2011). SNPs found and identified in the human *Spp1* promoter have shown to affect transcriptional activity and furthermore, the -156insG promoter polymorphism has also been implicated in *Spp1* transcriptional activity by the generation of an additional Runx2 binding site (Giacopelli et al. 2004).

In this chapter we aimed to assess and compare the transcriptional activity of *Spp1* in WKY and SHRSP gestational day 18 rat hearts during cardiac development using qRT-PCR. The result from these experiments showed a significant increase in *Spp1* expression during gestational development in the SHRSP strain compared to the WKY strain even before the onset of disease. The sample size for each group was n=6, and so this gives us further confidence in these results. However, there were limitations. The samples were run in duplicate rather than triplicate due to reagent constraints and timing. The raw data also showed variations in the expression of VIC and FAM probes between duplicate samples and so triplicate samples would have been more accurate in assessing expression levels. Furthermore, the samples from each group were taken from the same litter. Future experiments could be improved by taking hearts from different litters to confirm reproducibility. The results are consistent with our hypothesis that there is significant change in expression between the WKY and SHSP gestational day 18 rat hearts. Previous work in our lab also conducted qRT-PCR on WKY_{Gla} and $SHRSP_{Gla}$ whole neonatal heart tissues and isolated primary neonatal cardiomyocytes (fig 3.1B and 3.1C). Both results showed a

significant increase in *Spp1* expression in the SHRSP strain compared to the WKY strain. Renault et al. (2010) produced a conditional transgenic mouse that specifically overexpressed *Spp1* in mouse cardiomyocytes. This overexpression led to the premature death of transgenic pups from dilated cardiomyopathy at around 12 weeks of age. However, by reducing the expression of *Spp1* prior to 11 weeks of age did not encourage premature death, but fibrosis was still found to be significantly increased suggesting there was damage to the heart (Renault et al. 2010).

Therefore, results from both whole neonatal and gestational day 18 rat hearts indicates that overexpression of *Spp1* may occur prior to the onset of disease, and consequently plays a role in the pre-disposition towards cardiac disease.

Additionally, in this chapter, we aimed to compare the transcriptional activity of various regions of the *Spp1* promoter by producing constructs with promoter regions sub-cloned into the pGL4.10 luciferase vector. The promoter fragments have previously been generated in the pGL3 basic promoterless eukaryotic expression plasmid that encodes modified firefly luciferase. Previous work in the lab successfully produced the SP & WKY 10F/10R construct in the pGL4.10 luciferase vector. During my time in the lab, we were able to produce the SP & WKY 11F/11R in the pGL4.10 luciferase vector. Using the dual luciferase reporter assay we aimed to measure the transcriptional activity of the SP & WKY 10F/10R and 11F/11R promoter constructs by transfecting them into H9c2 cells. Each promoter construct was co-transfected into H9c2 cells with plasmid encoding renilla for normalisation. The difference in luciferase activity between promoter constructs of the same size but different strain will also allow for the identification of critical SNPs in the promoter that could be responsible for differential *Spp1* expression and will aid in mapping potential transcriptional factor binding sites.

We were unable to perform this experiment using the largest promoter fragment; SP & WKY 10F/12R, as we were unsuccessful in sub-cloning it into the pGL4.10 luciferase vector. The 10F/12R promoter fragment was of importance to us because of its distance from the transcriptional start site as it could potentially influence luciferase activity (fig 3.4). Also, the combined length of the 10F/10R and 11F/11R promoter fragments falls within the length of the larger 10F/12R fragment. The distance of the 10F/10R and 11F/11R promoter fragments from the transcriptional

start site is further away and can affect promoter activity in these two fragments due to potential SNPs and transcriptional factor binding sites that could be found within the region from the transcriptional start site and the 10F/10R and 11F/11R promoter fragments. The results from this assay showed a trend towards increased luciferase activity in the SP 10F/10R and SP 11F/11R promoter constructs compared to the WKY constructs. This increased expression level within the 10F/10R region suggests a SNP driven phenomenon. However, we were unable to reach significance as this experiment was an n=1 and further repetition was required.

We then conducted this experiment using HeLa cells (n=2) to determine if using a different cell line would achieve similar results to the H9c2 cells. It is important to understand the cellular networks that regulate gene expression levels, and this is done by measuring average gene expression levels in a population of cells (Rinott, Jaimovich, and Friedman 2011). H9c2 cells are a biologically relevant cell line to use when measuring the promoter activity of *Spp1*. However, by using a different cell line, HeLa cells, allows for a comparative analysis that provides insight into the mechanisms of transcription regulation at the promoter region of the gene (Rinott, Jaimovich, and Friedman 2011). In the 10F/10R promoter construct we observed increased luciferase activity in the SP construct when compared to the WKY construct. This indicates that the SP 10F/10R construct has increased transcriptional activity when compared to WKY 10F/10R construct. However, with the 11F/11R construct we observed that the WKY construct had a trend towards increased luciferase activity compared to the SP construct. This experiment was repeated for a second time; however, we observed results that were inconsistent with our first experiment. In the 10F/10R construct, SP and WKY produced similar luciferase activity while in the 11F/11R construct, we observed a significant increase in luciferase activity in the SP construct compared to the WKY construct. The reasons behind these inconsistent and poor transfections could be due to trans-effects between promoters of the co-transfected plasmids. This interaction could potentially affect the reporter gene expression (Ávila-Flores, Arranz-Nicolás, and Mérida 2019). This can be of concern when either the control, experimental reporter vector, or both contains very strong promoter/enhancer elements. Such effects, its occurrence and magnitude will depend on the combination and activities of the genetic regulatory elements present on the co-transfected vectors, the ratio of experimental vector to

control vector transfected into the cells and the cell type transfected (Promega Technical Manual, June 2015). However, this assay needed to be repeated to assess for reproducibility and accuracy, but we were unable to do so since we were facing difficulties with culturing the H9c2 cell line due to contaminations in our tissue culture laboratory.

Using IPA, we were able to analyse the 101 differentially expressed genes that were found in common between the SHRSP and WKY.SP_{Gla}14a 5 weeks vs neonatal strains. From these 101 genes, we looked to see whether any of these genes potentially contributed towards cardiac hypertrophy and if there were connected to *Spp1*. From the 101 genes, 5 genes were isolated that were identified downstream that are connected to *Spp1* and the enlargement of the heart.

Desmin or *DES* gene is mainly expressed in muscle tissues, plays an important role in myocyte development, degeneration, and cellular function. Many *DES* mutations were found to be related with myopathies and these mutation carriers can present themselves as neurological signs, cardiologic signs, myopathy, or a combination of these (R. Chen et al. 2021; Clemen et al. 2013; Schröder and Schoser 2009).

Matrix Metalloproteinases (MMPs) are found to be activated and involved in cardiac remodeling. However, recent research has shown the induction of intracellular processes in cardiomyocytes by MMPs, either due to proteolytic processes at diverse cell surface ligands, receptors, or signalling molecules, or inside the cell, since MMPs are not only restricted to the extracellular matrix but are also active inside cardiomyocytes (Euler et al. 2021). Increased myocardial *MMP14* expression has been found in patients with LV pressure overload (Polyakova et al. 2004). In animal models of LV pressure overload, early and continuous induction of *MMP14* has also been identified (Q. Dai et al. 2008).

It has been found that Myomesin-1 or *MYOM1* is specifically expressed in the heart and skeletal muscle. It has also been that variants found in the *MYOM1* gene have been associated with restrictive cardiomyopathy, cardiac dilation, dilation cardiomyopathy (Akinrinade et al. 2015; Kostareva et al. 2016; Marston et al. 2015; Pehlivan et al. 2019; Shanks et al. 2017)*.*

Cathepsin D or *CTSD* is a ubiquitously and abundantly expressed cathepsin, synthesized in the rough endoplasmic reticulum as pre-procathepsin D. It contains a signal peptide targets the 52kD procathepsin-D (CTSD-p) to the endosomal-lysosomal pathway (Benes, Vetvicka, and Fusek 2008; Hasilik and Neufeld 1980). Through the global knockout of the *CTSD* gene, it has been shown that CTSD deficient impairs myocardial autophagy and causes restrictive cardiomyopathy in mice. Autophagic activity is found to be increased in the heart post-myocardial infarction event in the heart and this increase is associated with an upregulation of CTSD. By preventing the heart from upregulating *CTSD* during myocardial infarction, it aggravates adverse cardiac remodeling and dysfunction in mice (Wu et al. 2017). Solute Carrier Family 25 Member 11 or *SLC25A11* is a member of the mitochondrial carrier subfamily of solute carrier protein genes. Mutations in this gene have been known to result in familial hypertrophic cardiomyopathy.
With the identification of these 5 genes and its connection to *Spp1* and cardiac hypertrophy, future work should include relative gene expression changes and identification of potential pathways.

Since cardiac hypertrophy affects the relationship between adenosine triphosphate (ATP) demand and production, mitochondrial bioenergetics must keep up with the cardiac hypertrophic phenotype (Rosca, Tandler, and Hoppel 2013). Energy in the form of ATP is needed to maintain cardiac contractile and relaxation functions. With the heart being the biggest oxygen-consuming organ in the body, there is no excess capacity for ATP production versus utilization. 90% of this requirement is met by mitochondrial oxidative phosphorylation which is adjusted to the amount of energy needed. As well as providing energy for cardiac contraction and relaxation, mitochondria generates reactive oxygen species (ROS) that mediate inotropic and hypertrophic effects of sympathetic and renin-angiotensin-aldosteron systems (Andersson et al. 2011; D.-F. Dai et al. 2011). Mitochondrial oxidative capacity has been reported to either be preserved or enhanced in cardiac hypertrophy. In contrast, both human subjects and experimental models of heart failure, mitochondrial function is decreased (Doenst et al. 2010; Lindenmayer et al. 1971; Rosca et al. 2008). Study conducted by Dalal et al investigated the involvement of mitochondrial death pathway and endoplasmic reticulum (ER) stress in *Spp1*-stimulated cardiac myocyte apoptosis. Their results suggests that *Spp1*,

acting via CD44 receptors induces apoptosis in adult rat ventricular myocytes. *Spp1* stimulated apoptosis occurs via the induction of mitochondrial death pathway and ER stress. Cardiac myocyte-specific expression of *Spp1* in adult mouse heart deteriorates heart function, which is associated with increased cardiac myocyte apoptosis, mitochondrial death pathway and ER stress (Dalal et al. 2014).

In this chapter, it has been highlighted that *Spp1* expression levels are different between the $SHRSP_{Gla}$ and WKY_{Gla} rat strains at different stages of development. The trend observed between the transcriptional levels of the different promoter fragments offers an insight into an area for future development. The significant observation that *Spp1* overexpression occurs during gestational development also offers the information that overexpression is likely to have a strong genetic basis. Prior to human translation, more work will be required to isolated candidate SNPs within the osteopontin promoter and to understand how this predisposes to future disease. To this, future work would include an in depth analysis and comparison of the already identified transcription factors (fig 3.2A & 3.2B and fig 3.3A & 3.3B) and conducting TRANSFAC analysis using the newly updated mRatBN 7.2 genome assembly from the NCBI database (accession ID: JACYVU01) and aligning it to the SHR-A3 rat genome database strain (ID No. 814238) to identify any potential new critical SNPs in the promoter supporting differential *Spp1* expression or, transcription factors that undergo altered binding in the *Spp1* promoter resulting from sequence variation as it will provide insight into the transcriptional regulation of *Spp1* (de Jong et al. 2022).

Chapter 4. Analysis of left ventricular function and structure in animal models of left ventricular hypertrophy

4.1 Introduction

Transverse aortic constriction (TAC) is used to induced chronic pressure overload to study LVH and progression to cardiac failure in rodent models. In this chapter we investigate the effects of TAC on the stroke-prone spontaneously hypertensive (SHRSP *Spp1* WT) rat, SHRSP *Spp1*^{em1} rat, WKY.SP$_{Gla}$14a chromosome 14 congenic strain and the reference control strain, the Wistar Kyoto (WKY) rat. We also aim to observe any phenotypic changes that may be caused in the heart due to constriction placed on the aorta and how they differ between the four strains.

The SHRSP strain exhibits a significant increase in LVMI compared to the WKY strain. This is apparent at 5 weeks of age before the onset of hypertension. At 12 weeks of age, mature levels of blood pressure are established at approximately 180mmHg in males and 150mmHg in females in this strain. At the same age, the WKY control strain shows a BP of approximately 130mmHg in both sexes (Davidson et al. 1995). Since the SHRSP *Spp1* rats are already hypertensive, even prior to conducting the TAC surgery, we expect the surgery to have a more severe effect on their hearts in a shorter period.

The WKY.SP$_{Gla}$14a chromosome 14 congenic strain contains a QTL for LVMI introgressed from chromosome 14 of the SHRSP strain into the WKY genetic background. This congenic strain has been shown to have increased fibrosis and LV diastolic dysfunction (Douglas et al. 2010) when compared to the WKY. Using a combination of the parental SHRSP and WKY strains, chr 14 congenic strains on both SHRSP and WKY genetic backgrounds and microarray gene expression profiling, *Spp1* was identified as a candidate gene for LVMI. Previous studies conducted by the McBride and Graham group have shown the WKY.SP$_{Gla}$14a chromosome 14 congenic strain to have significantly increased LVMI at both 5-week and 16-week time points when compared to the parental WKY strain. This chr 14 congenic strain also shows a small but significantly higher BP level when compared to the WKY strain. Since the chr 14 congenic rats already show increased LVMI prior to conducting TAC, we would expect the additional cardiovascular challenges induced by TAC to induce the progression to heart failure at an earlier timepoint than the WKY strain.

The SHRSP *Spp1*^{em1}rat strain was generated on the SHRSP genetic background to help further investigate the role of *Spp1* in the LVH disease mechanism. Our laboratory in collaboration with the MCW Gene Editing Rat Resource Centre in Milwaukee generated this strain using CRISPRCas9 technology to knock-out *Spp1* in the SHRSP rat model. Hemizygous rats were bred and the *Spp1* gene knock out was confirmed in resultant pups by restriction fragment length polymorphism (RFLP), Sanger sequencing and Enzyme-linked immunosorbent assay (ELISA). The SHRSP *Spp1*^{em1} strain contains a 5bp deletion within exon 4 of the *Spp1* gene on chromosome 14. Initial studies conducted at baseline showed no significant differences in BP and cardiac phenotypes in SHRSP *Spp1* WT and SHRSP *Spp1*^{em1} strains. Hence, to determine whether knock out of *Spp1* lessens or slows down the cardiac disease process, we used TAC to enhance the cardiovascular challenge in the *Spp1* rat model. By causing a TAC-induced pressure overload, we aimed to determine any differences in the subsequent phenotypic changes between the KO and WT strains (Richards et al, 2019).

In most rodent TAC models, the constriction is typically placed between the innominate artery and the left common carotid artery. However, in this study we chose to constrict the descending aorta at a level proximal to the renal artery. This route of constriction was selected as it has previously been used successfully in rat models and is generally less severe with a longer timeframe to disease progression when compared to constricting the aortic arch (Katz et al. 2019). Therefore, this method is likely to have less welfare implication or potential for incidence of sudden death in stroke-prone rats which are hypertensive and already have established cardiac hypertrophy. This method is also less technically demanding and would ensure a consistent level of constriction in all the rats in our study. This technique can create cardiac remodeling with elevated blood pressure and LV hypertrophy but does not affect blood flow to the brain and other major organs (Katz et al. 2019). The severity of cardiac remodeling induced by TAC greatly depends on the degree and duration of the aortic constriction ((Bosch et al. 2021).

4.1.1 Hypothesis

It is hypothesized that TAC will induce cardiac hypertrophy and fibrosis in rats with a normotensive genetic background and will exaggerate cardiac disease processes leading to the progression to heart failure in rats with a hypertensive genetic background.

It is also hypothesized that the SHRSP *Spp1*^{em1} rats will exhibit decreased levels or a slower timeframe of cardiac disease progression after TAC-induced pressure overload when compared to the SHRSP *Spp1* WT rats.

4.1.2 Aim

The aims of this chapter are to:

1) Establish and characterize the minimally invasive TAC pressure overload model of LVH in the WKY, WKY.SP$_{Gla}$14a congenic (chr 14 congenic) strain, SHRSP *Spp1* WT and SHRSP *Spp1*^{em1} rats.

   a) To assess the impact of TAC surgery on body weight and blood pressure in SHAM and TAC operated rats.

   b) To assess differences in LVMI when adjusted to body weight in SHAM and TAC operated rats

   c) To assess cardiac phenotype parameters such as relative wall thickness (RWT), stroke volume (SV) fractional shortening (FS), ejection fraction (EF) and cardiac output (CO) in SHAM and TAC operated rats.

2) To examine strain differences in response to TAC-induced pressure overload.

4.2 Methods

4.2.1 Ethical Approval

In this study we used 15-week-old male SHRSP *Spp1* WT, SHRSP *Spp1*^{em1,} chr 14 congenic strains and WKY rats. At 6-weeks, pups were genotyped using tissue derived from ear notching using an ear punch. At 15-weeks, the male rats from each of the four strains were assigned to either SHAM or TAC groups. Formal randomization and blinding were not performed. All animals were included in the study analysis, and they survived the length of the study. Only males were used in this study due to time constraints and costs. Animal experiments were conducted in accordance with the UK Animals (Scientific Procedures) Act 1986. The experiments were conducted under the authority of project licenses held at the University of Glasgow (70/9021 & PP0895181 for rat breeding and maintenance, 70/8605 & PP7595276 for TAC surgery, all held by Dr Delyth Graham). Animal Research: Reporting of In Vivo Experiments (ARRIVE) guidelines were followed, and all experimental procedures were approved by the local University of Glasgow Ethics Committee.

4.2.2 Blood pressure measurements by tail cuff plethysmography

Systolic blood pressure (SBP) was measured in conscious rats one week before TAC surgery and on a weekly basis for 8 weeks post-TAC surgery using tail cuff plethysmography. Rats were placed in pre-warmed incubation boxes with heat lamps at 30°C for 15 – 20 minutes to allow dilation of arteries in the tail so that measurements of blood pressure could be made. After warming, rats were wrapped in a soft cloth to restrain them and placed on a heating mat so that only the tail was exposed. A blood pressure occlusion cuff was placed at the base of the tail followed by a piezoceramic pressure transducer cuff. The pressure transducer relies on volume pressure recording (VPR) sensor technology which measures blood pressure based on volume changes. The occlusion cuff was inflated in controlled 1mmHg steps to 250mmHg and then deflated. The point at which blood flow in the tail was occluded by the cuff was taken as a measure of systolic blood pressure. The blood pressure was recorded using equipment designed and built in-house in collaboration with the Electronics/Medical Devices Unit (NHS Greater Glasgow &

Clyde) (Evans et al. 1994). The inflation/deflation cycle was repeated 6-8 consecutive times and an average was taken for each animal to obtain mean systolic blood pressure.

4.2.3 Echocardiography

Echocardiography was performed one week before TAC surgery and every 2 weeks during the 8-week post-TAC surgery period using an Acuson Sequoia c512 ultrasound system with a linear array transducer at a frequency of 15MHz. Animals were sedated by isoflurane anaesthetic in an induction chamber (5% isofluorane in 1.5L/min O2). Rats were placed in a supine position, with a slight rotation towards their left-hand side and maintained at 2.5% isoflurane in 1.5L/min O2. Hair was removed from their chest and abdomen using an electric shaver. Ultrasound gel maintained at room temperature, was applied to the transducer and skin. The heart was imaged along the short axis and M-mode measurements were recorded for 5-6 cardiac cycles. At least 3 separate images were obtained per sitting.

Analysis of the echocardiograph images were conducted using ImageJ software. Distance between waveform peaks and troughs were measured. These measures were inputted into a formula to calculate the following: left ventricular mass (LVM), stroke volume (SV), cardiac output (CO), fractional shortening (FS) and ejection fraction (EJ).

The calculation formulae were:

- Left ventricular mass (LVM) = (ASE-cube formula with Devereux correction factor) (LVM =0.8 [1.04[(EDD + PWT + AWT)3 – EDD3]] +0.6). The value of LVM was then normalized for both body weight and tibia length. End-systolic volume (ESV) and LV end-diastolic volume (EDV) was calculated from two-dimensional images according to a modified Simpson's rule.

- Stroke volume (SV) (ml) = $EDV⁄ESV$

- Cardiac output (CO)(ml/min) = $SV \times HR$

- Fractional shortening (FS) (%) = $(EDD - ESD⁄EDD) \times 100$

- Ejection fraction (EJ) (%) = $(SV⁄EDVol) \times 100$

4.2.4 Transverse Aortic Constriction Surgical Procedure

Rats were sedated by isoflurane anaesthetic in an induction chamber (5% isofluorane in 1.5L/min O_2). After 2 – 3 minutes, fur was removed from the abdominal area using an electric shaver. The rats were placed in a supine position on a heating pad to maintain body temperature at 37°C. Anaesthesia was maintained at 2.5% isofluorane in 1.5L/min O_2 via a specially designed face mask which orients the animal in an optimal surgical position. Analgesia was administered (5mk/kg rimadyl) by subcutaneous injection. Betadine was applied to the shaved area to prevent infection at the surgical site. A sterile adhesive patch (Tegaderm, 3M, Warks) was placed over the surgical area to help prevent infection. A vertical (approx. 3cm) skin incision was made just below the rib cage to allow for the visualization of the descending aorta under a dissection microscope. Blunt dissection of the connective tissue was made to allow for clear access to the aorta and vena cava. A sterile 22-gauge needle that had previously been blunted and smoothed using emery paper to avoid snagging and damage to any internal organs was used when making the constriction. Using 2-0 mersilk suture, the descending aorta was constricted by placing the suture around the aorta and tying a knot (Figure 4.1). The blunted 22-gauge needle was used to control the tightness of the suture by laying the needle alongside the aorta while tying the knot. Following the constriction, the needle was removed and the mersilk tie left in place. The skin was then sutured, and the animal was allowed to recover in a heated incubation chamber until fully conscious. Sham operated animals were subjected to the same procedure with the exception of the constriction around the descending aorta, whereby the 2-0 mersilk was passed around the descending aorta and then removed. Animals were transferred to their home cages and housed alone for the 8 weeks post-surgery period. Animals were allowed 1 week of recovery to regain pre-op body weights before the continuation of phenotypic measurements.

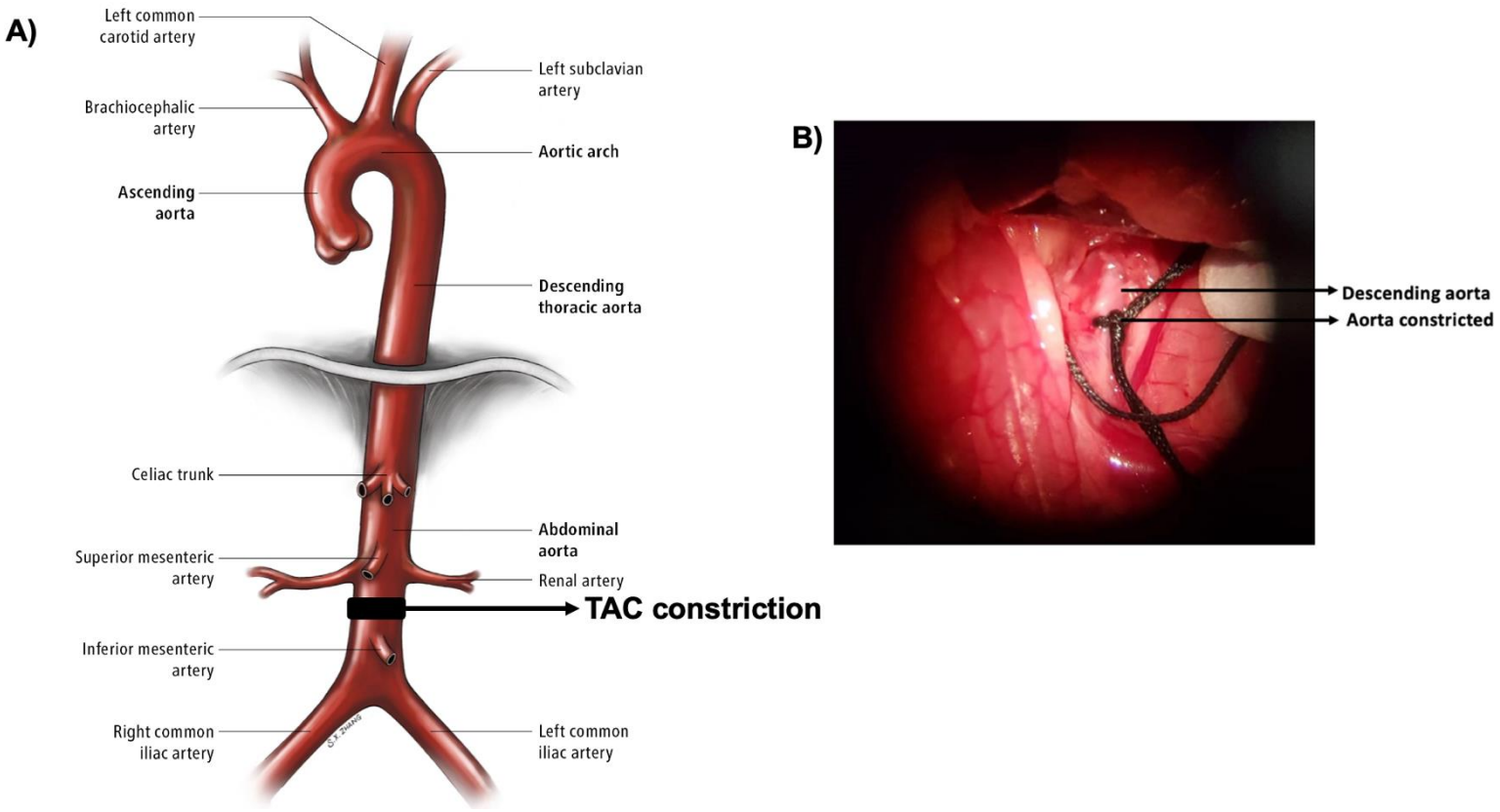

Figure 4.1: Transverse Aortic Constriction model used to induce left ventricular hypertrophy by constriction aorta proximal to renal artery. A) Image illustrating the location where the aorta was constricted in the rat's part of our study. B) Image captured during TAC surgery showing the descending aorta and the location where the constriction was placed.

4.2.5 Sacrifice Procedure

At the end of the 8-week experimental period, rats were anaesthetized and euthanized by exsanguination under sustained anaesthetic of 5% isoflurane in 1.5L/min O_2. Exsanguination was performed by making a midline incision and opening the thoracic cavity by blunt dissection of the diaphragm and cutting along either side of the rib cage. Once the heart was exposed a blood sample was collected by cardiac puncture (using a 23-gauge needle) prior to severing the thoracic aorta and removing the heart. Tissues harvested were thoracic aorta, heart, left kidney, right kidney, lungs, liver, brain and tibia bone.

4.2.6 Tissue Preparation

Blood samples from cardiac puncture were collected into VACUETTE® heparin lined tubes (Greiner Bio-One, Stonehouse, UK) and kept on ice until centrifugation at 3000rpm for 15 minutes at 4°C. Plasma was separated from the red blood cell layer and stored at -80°C for further experiments. Tissues harvested were either snap frozen in liquid nitrogen and stored at -80°C for RNA extraction and protein assays or fixed for histological assessment in a 10% formalin solution overnight at room temperature. Fixed tissues were then transferred into 70% ethanol. At the time of sacrifice both body weight and tibial length were recorded.

4.2.7 Statistical Analysis

All statistics were performed using GraphPad prism version 9.2.0 (GraphPad software, San Diego, California USA). Statistical comparison between the different groups was established using two-way analysis of variance (ANOVA) followed by Šidák's and Tukey's post-hoc multiple comparisons test post-hoc analysis. Values are presented as mean ± SEM, and differences of $p \leq 0.05$ values were taken as significant.

4.3 Results

4.3.1 Influence of TAC surgery on blood pressure

Blood pressure was measured weekly to evaluate the effect of TAC surgery in each of the rat strains (Fig 4.2). The average systolic blood pressure in the SHRSP *Spp1* WT and SHRSP *Spp1*^{em1} rat strains (SHRSP *Spp1* WT SHAM: 195.32 ±9.68mmHg & SHRSP *Spp1* WT TAC: 195.53 ± 8.00mmHg and SHRSP *Spp1*^{em1} SHAM: 193.63 ± 9.48mmHg & SHRSP *Spp1*^{em1} TAC: 196.12 ± 9.88mmHg) was significantly higher than the WKY and chr 14 congenic strains (WKY SHAM: 157.92 ± 6.30mmHg & WKY TAC: 163.26 ± 8.08 and chr 14 congenic D SHAM: 157.73 ± 5.48mmHg & chr 14 congenic D TAC: 153.14 ± 6.88mmHg). The TAC surgery had no impact on blood pressure in any of the strains overall. However, in the WKY TAC group a trend towards higher BP was observed at the week 3 time point post-TAC surgery when compared to the SHAM group. A trend towards a decrease in BP in the SHRSP *Spp1* WT TAC group is observed 2-weeks post-surgery when compared to the SHAM group.

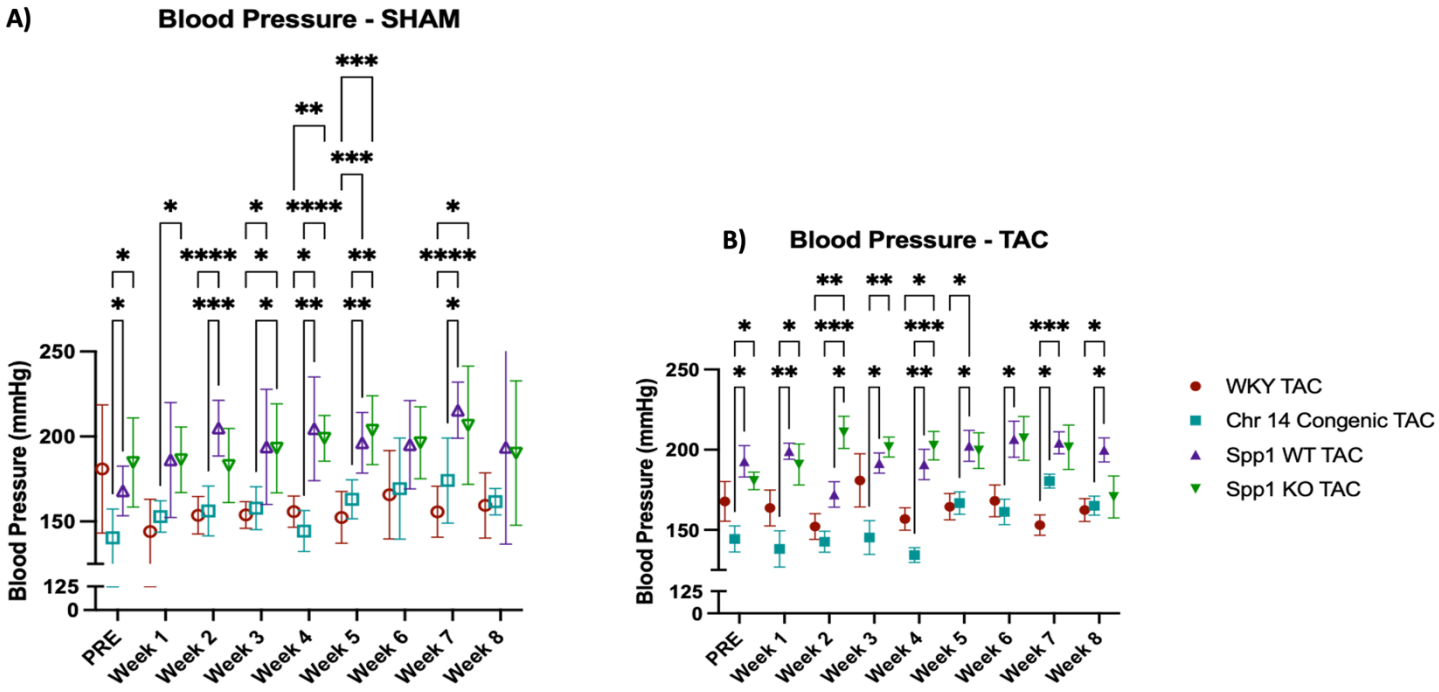

Figure 4.2: Average systolic blood pressure (mmHg) pre- and post-surgery. WKY (SHAM n = 8, TAC n = 8), WKY.SP$_{GLA}$14a (chr 14 congenic) (SHAM n = 8, TAC n = 8), SHRSP *Spp1* WT (SHAM n = 8, TAC n = 8) and SHRSP *Spp1*^{em1} (SHAM n= 7, TAC n = 7) rat strains.

A) Average systolic blood pressure of rats that received SHAM surgery over the 8-week study period. B) Average systolic blood pressure of rats that received TAC surgery over the 8-week study period.

Data was analysed using two-way ANOVA followed by Tukey's post-hoc multiple comparisons test. Data is represented as mean ± SEM and significance as * p<0.05, ** p<0.005, *** p<0.0005, **** p<0.00005

4.3.2 Influence of TAC surgery on body weight

Body weights of the rats were measured at every echo session for the duration of study and a comparison was made between SHAM and TAC operated rats (Fig 4.3). All the rats gained weight consistently as the study progressed (Fig 4.3 A and 4.3 B). Significant strain differences were observed based on body weight. The WKY and chr 14 congenic strains are heavier when compared to the SHRSP *Spp1* WT and SHRSP *Spp1*^{em1} strains pre-TAC surgery, and this pattern is maintained throughout the course of the study. However, no significant changes were observed in their body weights due to TAC. This indicates that TAC surgery had no overall effect on body weight.

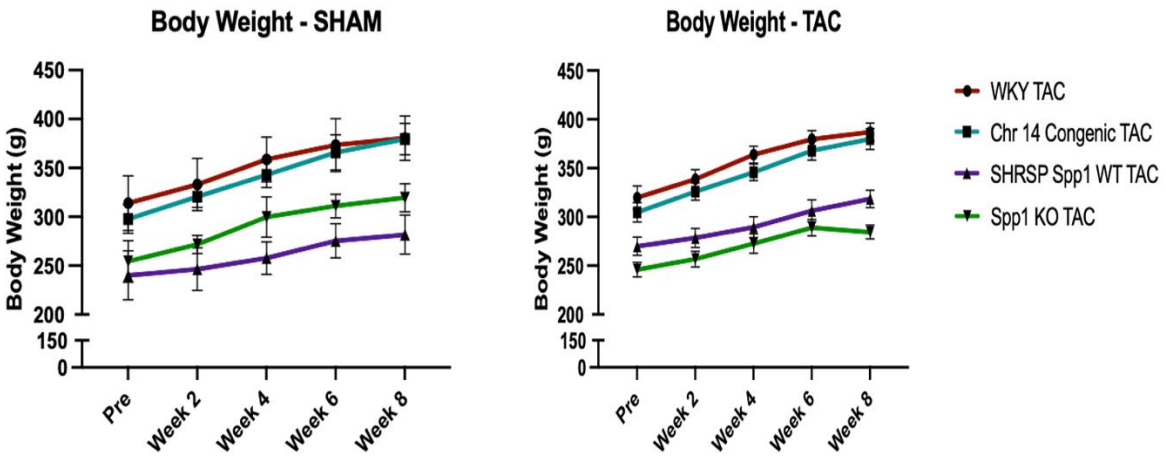

Figure 4.3: Body weights of SHAM and TAC rats' pre- and post-surgery. TAC surgery does not influence body weight

WKY (SHAM n = 8, TAC n = 8), WKY.SP$_{GLA}$14a (chr 14 congenic) (SHAM n = 8, TAC n = 8), SHRSP *Spp1* WT (SHAM n = 8, TAC n = 8) and SHRSP *Spp1*^{em1} (SHAM n= 7, TAC n = 7) rat strains.

A) Average body weights of rats that received SHAM surgery over the 8-week study period. **B)** Average body weights of rats that received TAC surgery over the 8-week study period.

Data was analysed using two-way ANOVA followed by Šidák's post-hoc multiple comparisons test. Data is represented as mean ± SEM.

4.3.3 Influence of TAC surgery on Left Ventricular Mass

Using echocardiographic assessment of the left ventricle and correcting them to their respective body weights we were able to assess LVMI. This measurement allowed assessment of the mass of the LV in comparison to the size of the rat at their final echo (week 8) (fig 4.4 A).

The echo data showed that there was a trend for an increased LVMI ratio in the TAC rats when compared to the SHAM-operated rats, however no significant changes were observed in any of the groups.

At the end of the 8-week study, the rats were culled, and their tissues harvested to conduct post-mortem analysis. Using the tissue weights and correcting them to their respective body weights, we were able to determine the LVMI for each of the strains (fig 4.4 B).

The sacrifice data showed that there were significant increases in LVMI ratio in the TAC rats when compared to the SHAM-operated rats in the WKY ($p < 0.05$) and chr 14 congenic ($p < 0.001$) group. This indicates that the TAC surgery induced a hypertrophic response in the heart in the WKY and chr 14 congenic TAC groups. However, in the SHRSP *Spp1* WT and SHRSP *Spp1*^{em1} SHAM and TAC operated rats no differences in LVMI were observed. This may indicate that the hearts of the hypertensive rats were already hypertrophied, and TAC surgery could not push their LVMI any further.

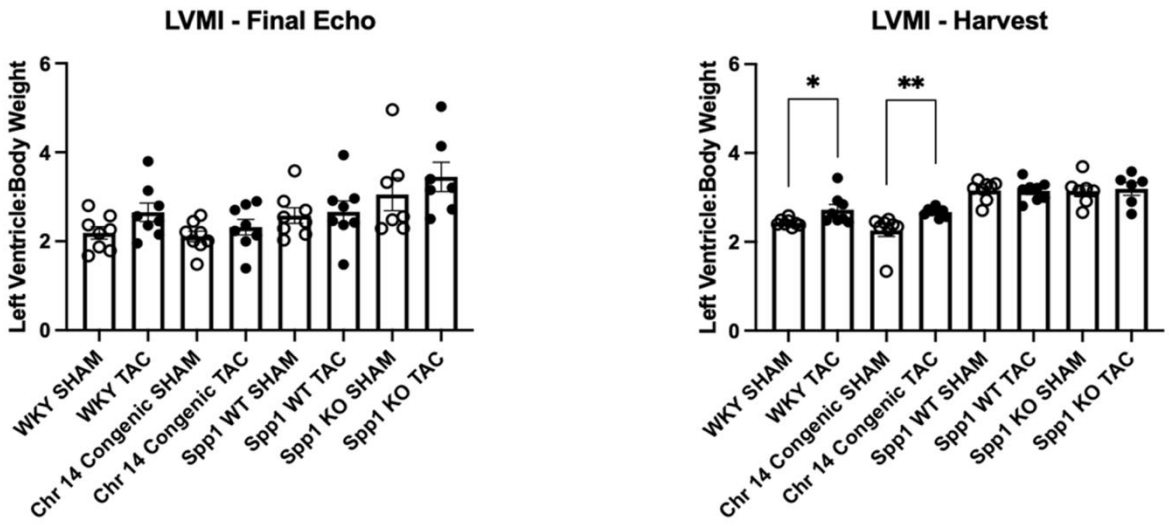

Figure 4.4: Left ventricular mass index (LVMI) following TAC surgery

WKY (SHAM n = 8, TAC n = 8), WKY.SP_{GLA}14a (chr 14 congenic) (SHAM n = 8, TAC n = 8), SHRSP *Spp1* WT (SHAM n = 8, TAC n = 8) and SHRSP *Spp1*^{em1} (SHAM n= 7, TAC n = 7) rat strains.

A) Analysis of LVMI following TAC surgery at final echo **B)** Analysis of LVMI following TAC surgery post-mortem. There was an increased LVMI ratio in the rats that received the TAC surgery when compared to the SHAM-operated rats with significant changes in the WKY ($p < 0.05$) and chr 14 congenic ($p < 0.001$) groups. Data was analysed using two-way ANOVA followed by Tukey's post-hoc multiple comparisons test. Data is represented as mean ± SEM, and significance as * $p<0.05$, ** $p<0.005$

4.3.4 Influence of TAC surgery on echocardiographic parameters

Using echocardiography, we were able to determine and analyse the following parameters: relative wall thickness, stroke volume, fractional shortening, ejection fraction and cardiac output.

4.3.4.1 Relative Wall Thickness (RWT)

In the WKY strain (fig 4.5 A), RWT in the SHAM group remains unchanged from pre-op to the end of the study. In the TAC group we see a trend towards an increase in RWT at 8 weeks post-surgery (WKY TAC: Pre; 0.42 ± 0.02 and week 8; 0.49 ± 0.04). In the chr 14 congenic strain (fig 4.5 B), we see no overall TAC effect on RWT as the levels remain unchanged in both the SHAM and TAC rats throughout the course of the study. We also observe similar patterns in both the SHRSP *Spp1* WT and SHRSP *Spp1*^{em1} strains (fig 4.5 C and D) where TAC surgery has had no overall effect on RWT for both SHAM and TAC rats.

Two-way ANOVA revealed several significant strain differences for RWT within SHAM and TAC groups (fig 4.5 E and F). SHRSP *Spp1* WT SHAM rats showed significantly greater RWT at pre-op ($p < 0.001$), Week 2 ($p < 0.0001$), Week 4 ($p < 0.05$), Week 6 ($p < 0.001$) and Week 8 ($p < 0.001$) when compared to WKY SHAM rats. In the TAC group, SHRSP *Spp1* WT rats showed significantly increased RWT at Week 2 ($p < 0.0001$) and Week 4 ($p < 0.05$) when compared to the WKY rats. Furthermore, SHRSP *Spp1* WT TAC rats showed significantly increased RWT at Week 2 ($p < 0.05$) and Week 6 ($p < 0.05$) when compared to the chr 14 congenic rats.

When comparing SHAM rats from the WKY and chr 14 congenic strains we observed that the chr 14 congenic rats showed a trend towards larger RWT than the WKY rats throughout the course of the study. However, after TAC surgery this trend was no longer evident.

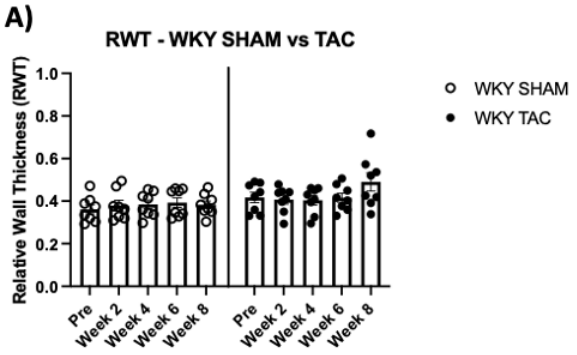
A)
RWT - WKY SHAM vs TAC
Relative Wall Thickness (RWT)
1.0
0.8
0.6
0.4
0.2
0.0
Pre
Week 2
Week 4
Week 6
Week 8
WKY SHAM
WKY TAC

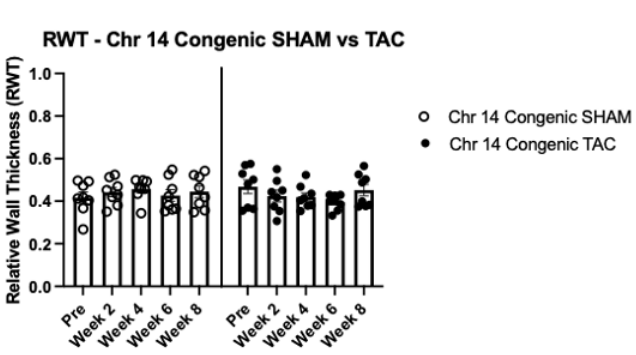
B)
RWT - Chr 14 Congenic SHAM vs TAC
Relative Wall Thickness (RWT)
1.0
0.8
0.6
0.4
0.2
0.0
Pre
Week 2
Week 4
Week 6
Week 8
Chr 14 Congenic SHAM
Chr 14 Congenic TAC

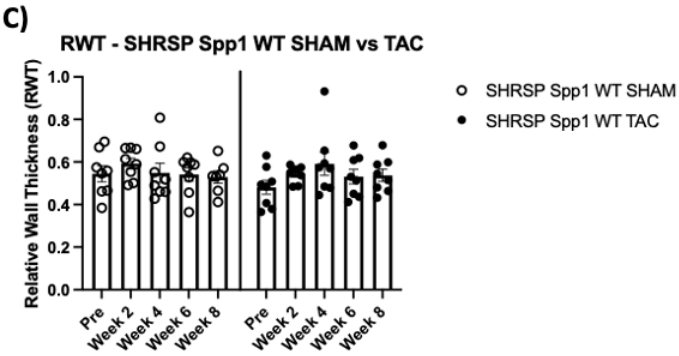
C)
RWT - SHRSP Spp1 WT SHAM vs TAC
Relative Wall Thickness (RWT)
1.0
0.8
0.6
0.4
0.2
0.0
Pre
Week 2
Week 4
Week 6
Week 8
SHRSP Spp1 WT SHAM
SHRSP Spp1 WT TAC

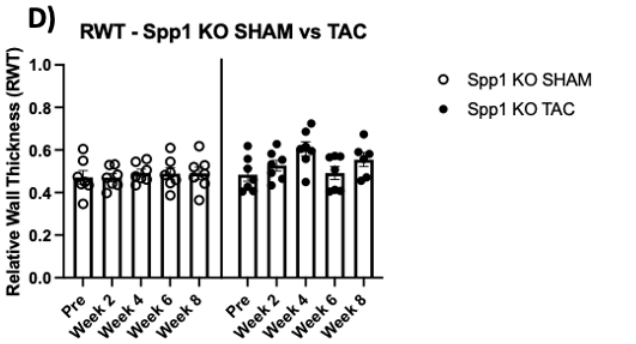
D)
RWT - Spp1 KO SHAM vs TAC
Relative Wall Thickness (RWT)
1.0
0.8
0.6
0.4
0.2
0.0
Pre
Week 2
Week 4
Week 6
Week 8
Spp1 KO SHAM
Spp1 KO TAC

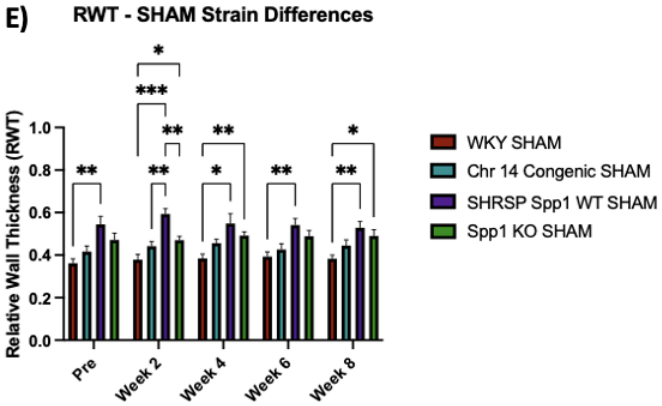
E)
RWT - SHAM Strain Differences
Relative Wall Thickness (RWT)
1.0
0.8
0.6
0.4
0.2
0.0
Pre
Week 2
Week 4
Week 6
Week 8
WKY SHAM
Chr 14 Congenic SHAM
SHRSP Spp1 WT SHAM
Spp1 KO SHAM

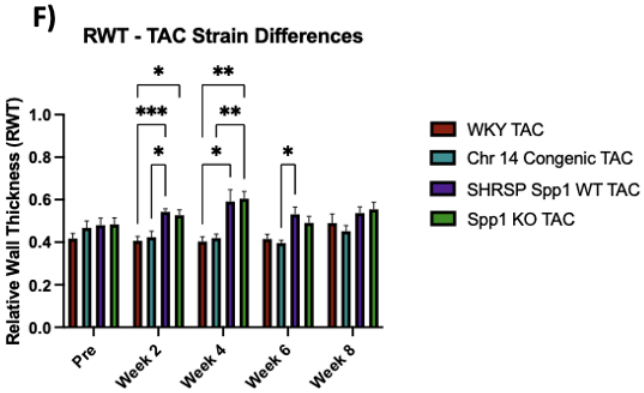
F)
RWT - TAC Strain Differences
Relative Wall Thickness (RWT)
1.0
0.8
0.6
0.4
0.2
0.0
Pre
Week 2
Week 4
Week 6
Week 8
WKY TAC
Chr 14 Congenic TAC
SHRSP Spp1 WT TAC
Spp1 KO TAC

Figure 4.5: Relative wall thickness (RWT) in rats that received SHAM or TAC surgery over the 8-week study period

WKY (SHAM n = 8, TAC n = 8), WKY.SP_{Gla}14a (chr 14 congenic) (SHAM n = 8, TAC n = 8), SHRSP *Spp1* WT (SHAM n = 8, TAC n = 8) and SHRSP *Spp1*^{em1} (SHAM n= 7, TAC n = 7) rat strains.

A), B), C) and D) Comparison of RWT in WKY, WKY.SP_{GLA}14a (chr 14 congenic), SHRSP *Spp1* WT rats and SHRSP *Spp1*^{em1} rats that received SHAM and TAC surgery. **E)** Showing strain differences of rats that received SHAM surgery over the 8-week study period including pre-op. **F)** Showing strain differences of rats that received TAC surgery over the 8-week study period including pre-op.

Data was analysed using two-way ANOVA followed by Tukey's post-hoc multiple comparisons test. Data is represented as mean ± SEM, and significance as * $p<0.05$, ** $p<0.005$, *** $p<0.0005$

4.3.4.2 Stroke Volume (SV)

In general, there were no consistent changes across time or as a result of TAC for stroke volume in each of the 4 rat strains (Fig 4.6 A, B, C, D). However, there was a significant increase in SV at week 6 in chromosome 14 congenic TAC rats compared to SHAM ($p<0.05$), and a significant decrease in SV at week 4 in *Spp1*^{em1} TAC rats compared to SHAM ($p<0.05$).

Two-way ANOVA revealed several significant strain differences for SV within SHAM and TAC groups (fig 4.6 E and F). WKY SHAM rats demonstrate significantly higher SV when compared to the chr 14 congenic SHAM rats at pre-op ($p <0.05$), Week 2 ($p <0.001$), Week 4 ($p < 0.05$) and Week 6 ($p <0.05$). WKY SHAM rats also had a significantly higher SV when compared to the SHRSP *Spp1* WT SHAM at pre-op ($p <0.0001$), Week 2 ($p <0.0001$), Week 4 ($p <0.05$) and Week 6 ($p < 0.05$) and when compared to SHRSP *Spp1*^{em1} SHAM at Week 2 ($p <0.001$). Across all timepoints it is observed that the SHRSP *Spp1*^{em1} SHAM rats maintained a higher SV when compared to the SHRSP *Spp1* WT SHAM rats with a significantly higher SV at Week 8 ($p <0.05$)

The distinct patterns observed for SV between strains in the SHAM group are not so evident after TAC surgery. For example, unlike SHAM, no significant difference was observed for SV between SHRSP *Spp1* WT rats and SHRSP *Spp1*^{em1} rats at Week 8 in the TAC group (Fig 4.6F). Moreover, the significantly lower SV observed in chr 14 congenic rats compared to WKY under SHAM conditions was not evident under TAC conditions. However, SV in the SHRSP *Spp1*^{em1} TAC group, remained significantly lower than WKY at Week 2 ($p<0.05$) and at Week 4 ($p<0.001$), and also when compared to the chr 14 congenic TAC group ($p<0.001$). .

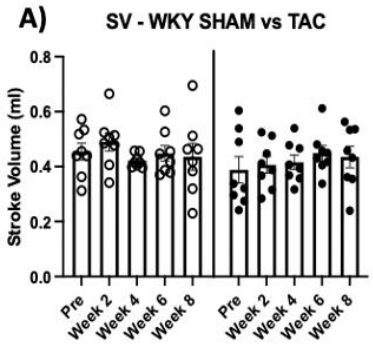
A)
SV - WKY SHAM vs TAC
Stroke Volume (ml)
0.0
0.2
0.4
0.6
0.8
Pre
Week 2
Week 4
Week 6
Week 8
WKY SHAM
WKY TAC

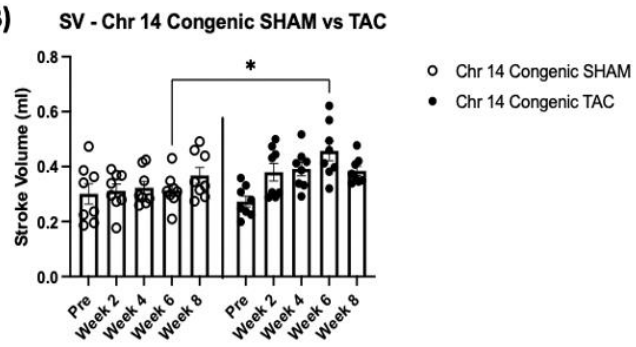
B)
SV - Chr 14 Congenic SHAM vs TAC
Stroke Volume (ml)
0.0
0.2
0.4
0.6
0.8
*
Pre
Week 2
Week 4
Week 6
Week 8
Chr 14 Congenic SHAM
Chr 14 Congenic TAC

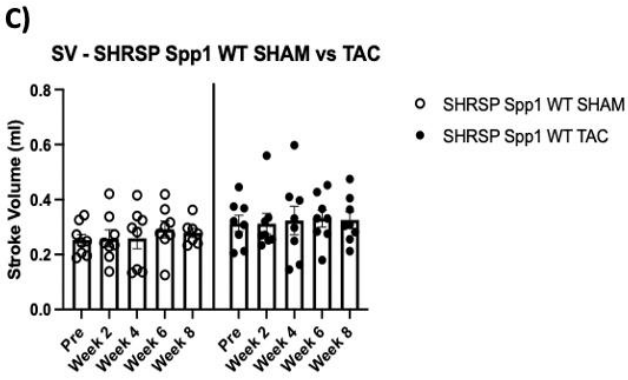
C)
SV - SHRSP Spp1 WT SHAM vs TAC
Stroke Volume (ml)
0.0
0.2
0.4
0.6
0.8
Pre
Week 2
Week 4
Week 6
Week 8
SHRSP Spp1 WT SHAM
SHRSP Spp1 WT TAC

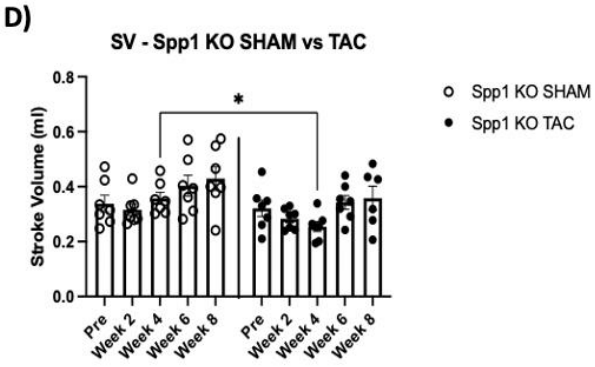
D)
SV - Spp1 KO SHAM vs TAC
Stroke Volume (ml)
0.0
0.2
0.4
0.6
0.8
*
Pre
Week 2
Week 4
Week 6
Week 8
Spp1 KO SHAM
Spp1 KO TAC

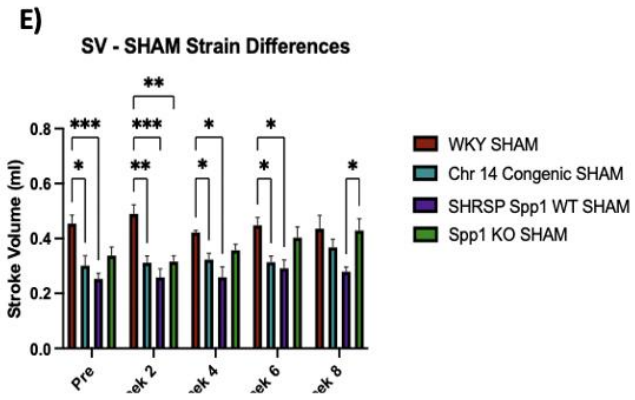
E)
SV - SHAM Strain Differences
Stroke Volume (ml)
0.0
0.2
0.4
0.6
0.8
*
**
***
Pre
WKY SHAM
Chr 14 Congenic SHAM
SHRSP Spp1 WT SHAM
Spp1 KO SHAM

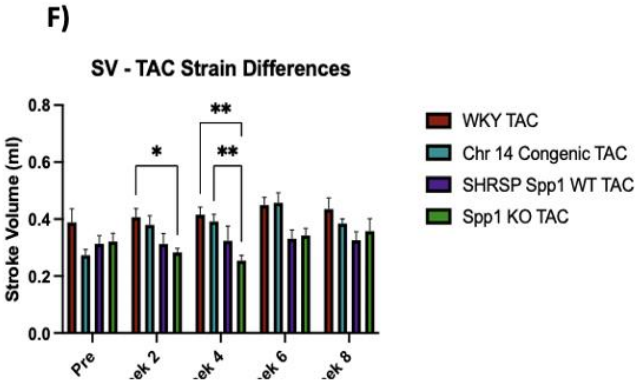
F)
SV - TAC Strain Differences
Stroke Volume (ml)
0.0
0.2
0.4
0.6
0.8
*
**
Pre
WKY TAC
Chr 14 Congenic TAC
SHRSP Spp1 WT TAC
Spp1 KO TAC

Figure 4.6: Stroke volume (SV) in rats that received SHAM or TAC surgery over the 8-week study period including pre-op

WKY (SHAM n = 8, TAC n = 8), WKY.SP_{GLA}14a (chr 14 congenic) (SHAM n = 8, TAC n = 8), SHRSP *Spp1* WT (SHAM n = 8, TAC n = 8) and SHRSP *Spp1*^{em1} (SHAM n= 7, TAC n = 7) rat strains.

A), B), C) and D) Comparison of SV in WKY, WKY.SP_{GLA}14a (chr 14 congenic), SHRSP *Spp1* WT rats and SHRSP *Spp1*^{em1} rats that received SHAM and TAC surgery.

E) Showing strain differences of rats that received SHAM surgery over the 8-week study period including pre-op. **F)** Showing strain differences of rats that received TAC surgery over the 8-week study period including pre-op.

Data was analysed using two-way ANOVA followed by Tukey's post-hoc multiple comparisons test. Data is represented as mean ± SEM, and significance as* $p<0.05$, ** $p<0.005$, *** $p<0.0005$

4.3.4.3 Cardiac Output (CO)

Significantly higher CO was observed in chr 14 congenic TAC rats ($p < 0.05$) at week 6 when compared to SHAM rats (fig 4.9 B). Conversly, (fig 4.7 D), significantly lower CO was observed at week 4 ($p < 0.05$) in SHRSP *Spp1*^{em1} TAC rats when compared with SHAM rats.

When examining strain effects for CO within the SHAM group (fig 4.7 E) by two-way ANOVA, it can be seen that WKY rats have significantly higher CO when compared to chr 14 congenic rats at pre-op ($p < 0.05$), week 2 ($p < 0.001$), week 4 ($p < 0.001$) and week 6 ($p < 0.001$). Significantly higher CO is also observed when comparing WKY rats to SHRSP *Spp1* WT rats at pre ($p < 0.0001$), week 2 ($p < 0.001$), week 4 ($p < 0.05$) and week 6 ($p < 0.001$). However, apart from week 2, there is no significant difference in CO between WKY and SHRSP *Spp1*^{em1} rats under SHAM conditions. This pattern is similar to that observed for SV.

In the TAC group (fig 4.7 F), this pattern is lost, and significantly lower CO is observed in SHRSP *Spp1*^{em1} rats when compared to WKY at week 2 ($p < 0.05$) and week 4 ($p < 0.001$).

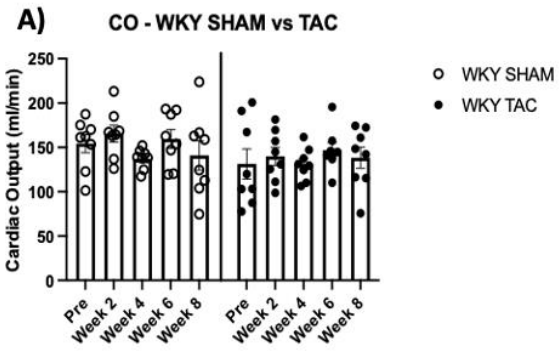
A)
CO - WKY SHAM vs TAC
Cardiac Output (ml/min)
250
200
150
100
50
0
Pre
Week 2
Week 4
Week 6
Week 8
WKY SHAM
WKY TAC

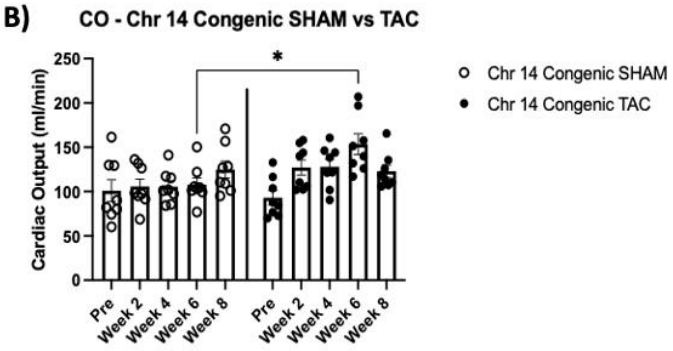
B)
CO - Chr 14 Congenic SHAM vs TAC
Cardiac Output (ml/min)
*
Chr 14 Congenic SHAM
Chr 14 Congenic TAC

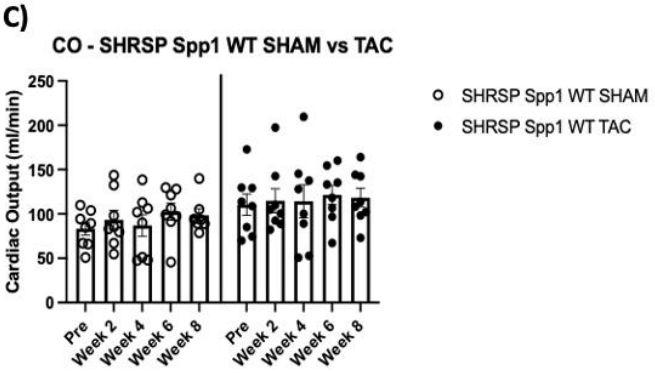
C)
CO - SHRSP Spp1 WT SHAM vs TAC
Cardiac Output (ml/min)
SHRSP Spp1 WT SHAM
SHRSP Spp1 WT TAC

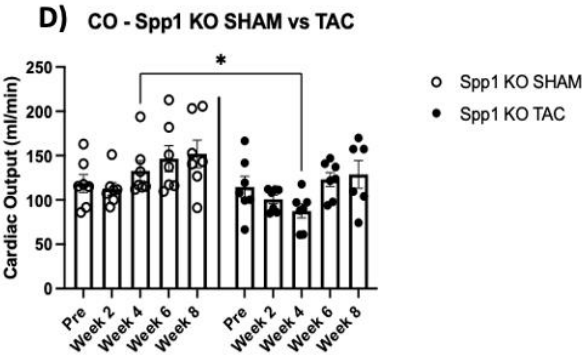
D)
CO - Spp1 KO SHAM vs TAC
Cardiac Output (ml/min)
*
Spp1 KO SHAM
Spp1 KO TAC

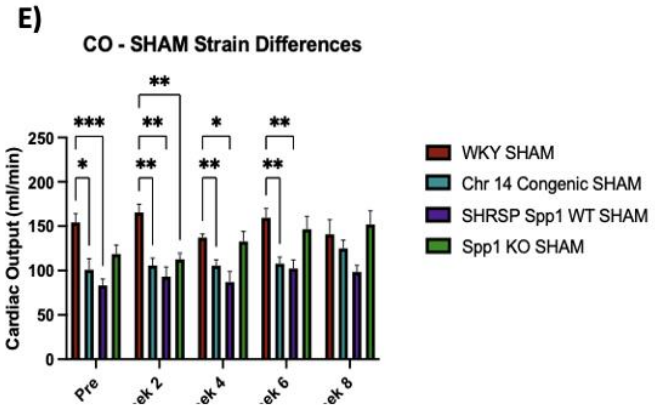
E)
CO - SHAM Strain Differences
Cardiac Output (ml/min)
WKY SHAM
Chr 14 Congenic SHAM
SHRSP Spp1 WT SHAM
Spp1 KO SHAM

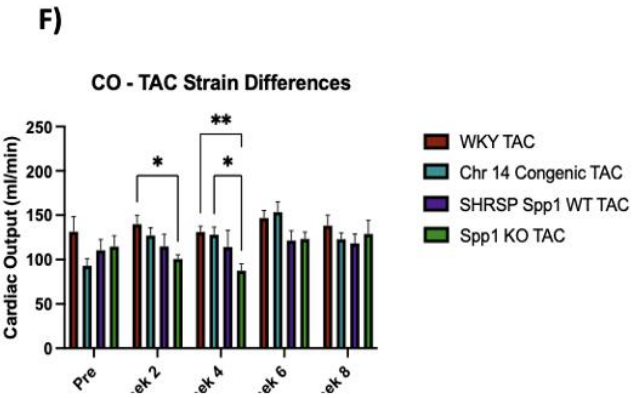
F)
CO - TAC Strain Differences
Cardiac Output (ml/min)
WKY TAC
Chr 14 Congenic TAC
SHRSP Spp1 WT TAC
Spp1 KO TAC

Figure 4.7: Cardiac output (CO) in rats that received SHAM or TAC surgery over the 8-week study period including pre-op

WKY (SHAM n = 8, TAC n = 8), WKY.SP_{GLA}14a (chr 14 congenic) (SHAM n = 8, TAC n = 8), SHRSP *Spp1* WT (SHAM n = 8, TAC n = 8) and SHRSP *Spp1*^{em1} (SHAM n= 7, TAC n = 7) rat strains.

A), B), C) and D) Comparison of CO in WKY, WKY.SP_{GLA}14a (chr 14 congenic), SHRSP *Spp1* WT rats and SHRSP *Spp1*^{em1} rats that received SHAM and TAC surgery.

E) Showing strain differences of rats that received SHAM surgery over the 8-week study period including pre-op. **F)** Showing strain differences of rats that received TAC surgery over the 8-week study period including pre-op.

Data was analysed using two-way ANOVA followed by Tukey's post-hoc multiple comparisons test. Data is represented as mean ± SEM, and significance as * $p<0.05$, ** $p<0.005$, *** $p<0.0005$

4.3.4.4 Fractional Shortening (FS)

Fig 4.8 A, B, C. D show that TAC surgery has no overall effect on FS across time in any of the strains. However, when examining strain effects within SHAM and TAC groups, a general trend towards lower FS was observed in WKY and chr 14 congenic rats when compared to SHRSP *Spp1* WT and SHRSP *Spp1*^{em1} rats. Two-way ANOVA revealed several significant strain differences (fig 4.8 E and F). Chr 14 congenic rats have significantly lower FS when compared to SHRSP *Spp1* WT rats at week 2 ($p < 0.0001$) and week 4 ($p < 0.00001$) in the SHAM and TAC groups respectively. Similarly, WKY SHAM rats at week 2 ($p < 0.05$) and WKY TAC rats at week 4 ($p < 0.001$) have a significantly lower FS when compared to SHRSP *Spp1* WT rats . A significantly lower FS was also observed in chr 14 congenic TAC rats at week 4 ($p < 0.001$) when compared to SHRSP *Spp1*^{em1} TAC rats.

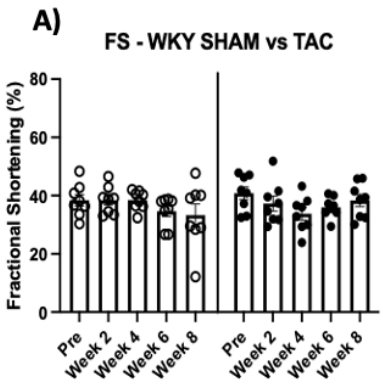
A)
FS - WKY SHAM vs TAC
Fractional Shortening (%)
0
20
40
60
80
Pre
Week 2
Week 4
Week 6
Week 8
WKY SHAM
WKY TAC

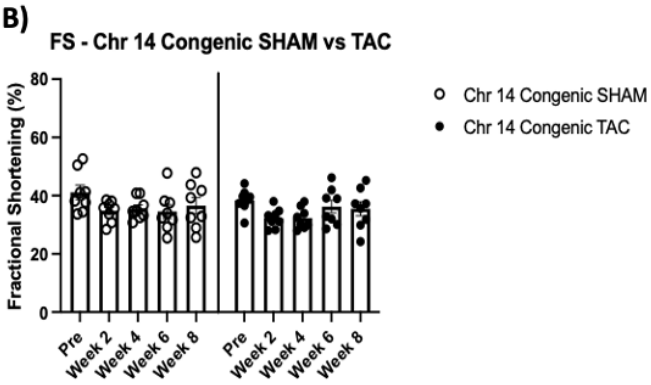
B)
FS - Chr 14 Congenic SHAM vs TAC
Fractional Shortening (%)
0
20
40
60
80
Pre
Week 2
Week 4
Week 6
Week 8
Chr 14 Congenic SHAM
Chr 14 Congenic TAC

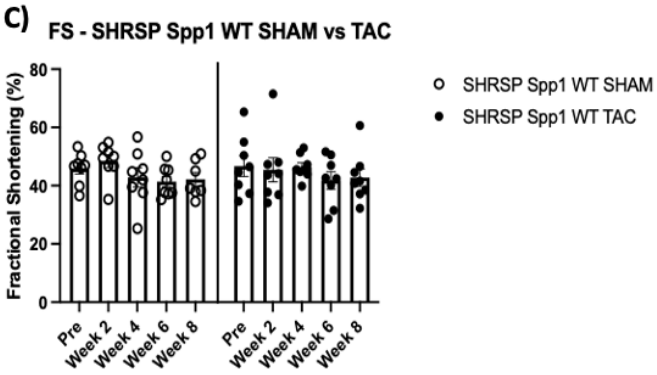
C)
FS - SHRSP Spp1 WT SHAM vs TAC
Fractional Shortening (%)
0
20
40
60
80
Pre
Week 2
Week 4
Week 6
Week 8
SHRSP Spp1 WT SHAM
SHRSP Spp1 WT TAC

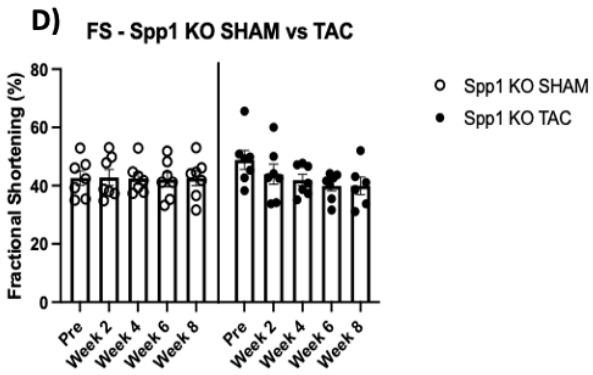
D)
FS - Spp1 KO SHAM vs TAC
Fractional Shortening (%)
0
20
40
60
80
Pre
Week 2
Week 4
Week 6
Week 8
Spp1 KO SHAM
Spp1 KO TAC

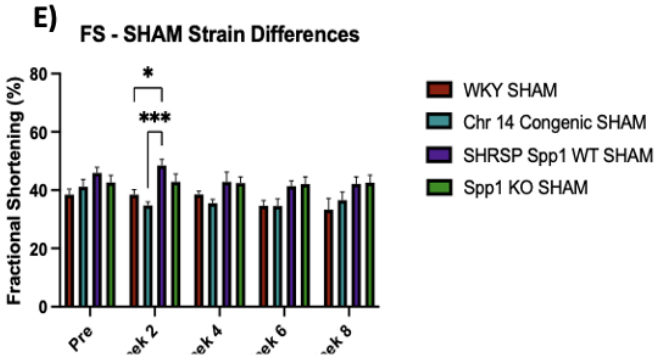
E)
FS - SHAM Strain Differences
Fractional Shortening (%)
0
20
40
60
80
*
***
Pre
WKY SHAM
Chr 14 Congenic SHAM
SHRSP Spp1 WT SHAM
Spp1 KO SHAM

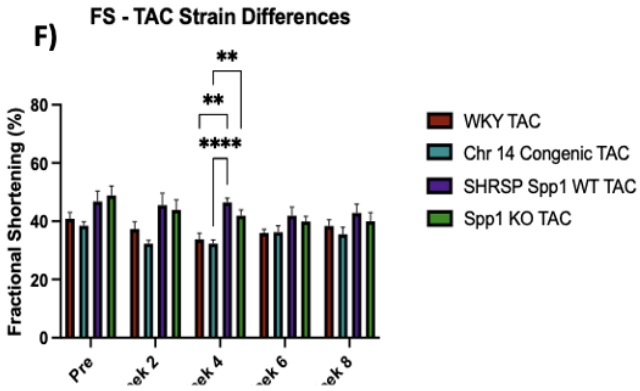
F)
FS - TAC Strain Differences
Fractional Shortening (%)
0
20
40
60
80
**
**
****
Pre
WKY TAC
Chr 14 Congenic TAC
SHRSP Spp1 WT TAC
Spp1 KO TAC

Figure 4.8: Fractional shortening (FS) in rats that received SHAM or TAC surgery over the 8-week study period including pre-op

WKY (SHAM n = 8, TAC n = 8), WKY.SP_{GLA}14a (chr 14 congenic) (SHAM n = 8, TAC n = 8), SHRSP *Spp1* WT (SHAM n = 8, TAC n = 8) and SHRSP SHRSP *Spp1*^{em1} (SHAM n= 7, TAC n = 7) rat strains.

A), B), C) and D) Comparison of FS in WKY, WKY.SP_{GLA}14a (chr 14 congenic), SHRSP *Spp1* WT rats and SHRSP *Spp1*^{em1} rats that received SHAM and TAC surgery.

E) Showing strain differences of rats that received SHAM surgery over the 8-week study period including pre-op. **F)** Showing strain differences of rats that received TAC surgery over the 8-week study period including pre-op.

Data was analysed using two-way ANOVA followed by Tukey's post-hoc multiple comparisons test. Data is represented as mean ± SEM, and significance as * $p<0.05$, ** $p<0.005$, *** $p<0.0005$, **** $p<0.00005$

4.3.4.5 Ejection Fraction (EF)

Fig 4.9 A, B, C, D show that TAC surgery had no significant effect on EF across time when compared to SHAM in any of the rat strains. Two-way ANOVA revealed several significant differences when examining strain effects between SHAM and TAC rats (fig 4.9 E and F). In the SHAM group (fig 4.9 E), chr 14 congenic rats show significantly reduced EF compared to SHRSP *Spp1* WT and SHRSP *Spp1*^{em1} rats at week 2 ($p < 0.0001$) and week 4 ($p < 0.05$) respectively. In addition, a significantly lower EF ($p < 0.05$) was observed in WKY rats compared to SHRSP *Spp1* WT rats at week 2.

In the TAC group (fig 4.9 F), a significantly lower EF in the congenic rats was observed when compared with SHRSP *Spp1*^{em1} rats at pre-op ($p < 0.05$), week 2 ($p < 0.05$) and week 4 ($p < 0.001$). A significantly lower EF in chr 14 congenic rats was observed when compared to SHRSP *Spp1* WT rats at week 2 ($p < 0.001$) and week 4 ($p < 0.00001$). In addition, a significantly lower EF in WKY rats was observed when compared with SHRSP *Spp1* WT rats at week 4 ($p < 0.001$).

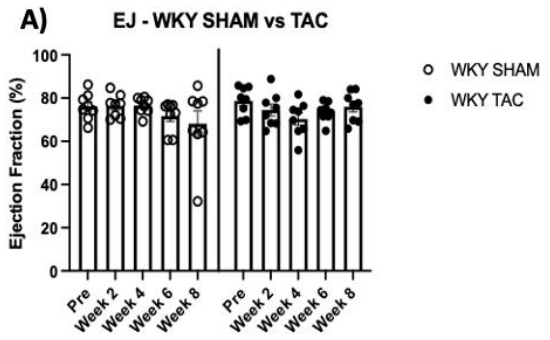
A)
EJ - WKY SHAM vs TAC
Ejection Fraction (%)
WKY SHAM
WKY TAC
Pre
Week 2
Week 4
Week 6
Week 8

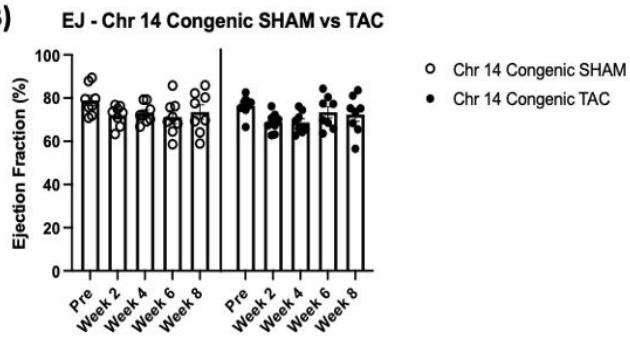
B)
EJ - Chr 14 Congenic SHAM vs TAC
Ejection Fraction (%)
Chr 14 Congenic SHAM
Chr 14 Congenic TAC
Pre
Week 2
Week 4
Week 6
Week 8

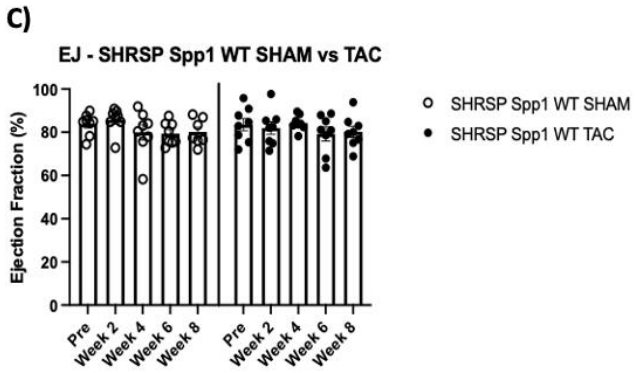
C)
EJ - SHRSP Spp1 WT SHAM vs TAC
Ejection Fraction (%)
SHRSP Spp1 WT SHAM
SHRSP Spp1 WT TAC
Pre
Week 2
Week 4
Week 6
Week 8

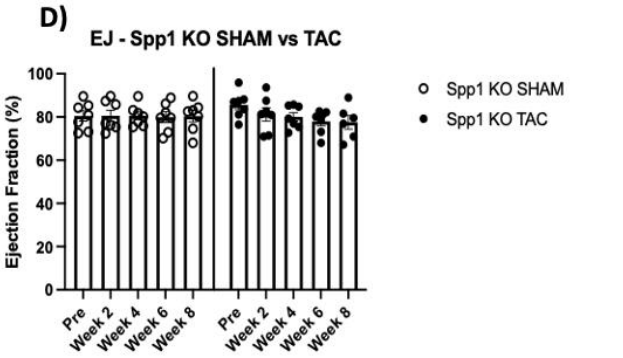
D)
EJ - Spp1 KO SHAM vs TAC
Ejection Fraction (%)
Spp1 KO SHAM
Spp1 KO TAC
Pre
Week 2
Week 4
Week 6
Week 8

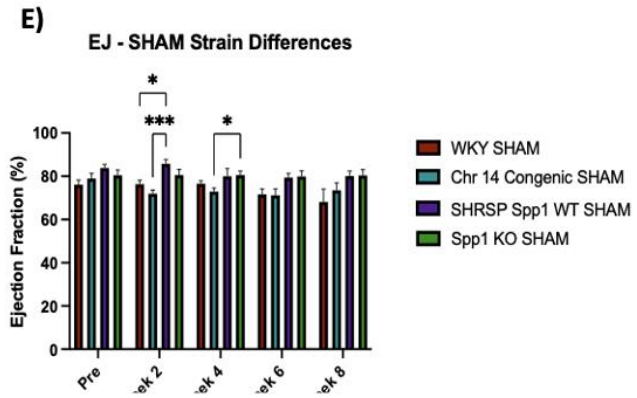
E)
EJ - SHAM Strain Differences
Ejection Fraction (%)
WKY SHAM
Chr 14 Congenic SHAM
SHRSP Spp1 WT SHAM
Spp1 KO SHAM
*
***
*
Pre

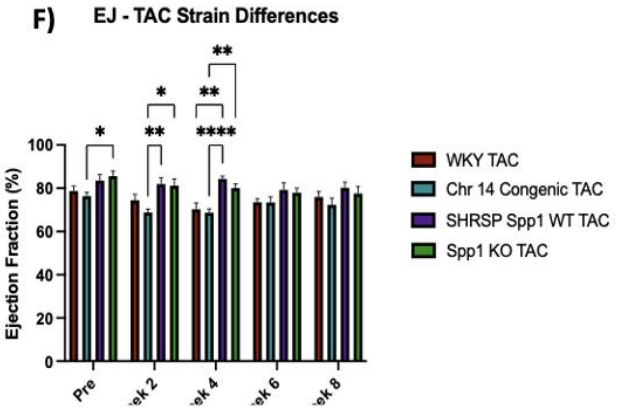
F)
EJ - TAC Strain Differences
Ejection Fraction (%)
WKY TAC
Chr 14 Congenic TAC
SHRSP Spp1 WT TAC
Spp1 KO TAC
*
**
*
**
****
**
Pre

Figure 4.9: Average ejection fraction (EF) in rats that received SHAM or TAC surgery over the 8-week study period including pre-op

WKY (SHAM n = 8, TAC n = 8), WKY.SP_{GLA}14a (chr 14 congenic) (SHAM n = 8, TAC n = 8), SHRSP *Spp1* WT (SHAM n = 8, TAC n = 8) and SHRSP *Spp1*^{em1} (SHAM n= 7, TAC n = 7) rat strains.

A), B), C) and D) Comparison of EF in WKY, WKY.SP_{GLA}14a (chr 14 congenic), SHRSP *Spp1* WT rats and SHRSP *Spp1*^{em1} rats that received SHAM and TAC surgery.

E) Showing strain differences of rats that received SHAM surgery over the 8-week study period including pre-op. **F)** Showing strain differences of rats that received TAC surgery over the 8-week study period including pre-op.

Data was analysed using two-way ANOVA followed by Tukey's post-hoc multiple comparisons test. Data is represented as mean ± SEM, and significance as * p<0.05, ** p<0.005, *** p<0.0005, **** p<0.00005

4.3.5 Influence of TAC surgery on other tissues post-mortem

In addition to the left ventricle of the heart we also examined the whole heart mass and other organs of the body to determine whether TAC surgery influenced them (fig 4.10). The weights of the organs were normalized to the body weights of the rats at the time of sacrifice. We observed significant increases in whole heart: BWT ratio in the TAC-operated WKY ($p < 0.05$) and chr 14 congenic ($p < 0.0001$) rats when compared to the SHAM (fig 4.10 A). We observed no changes in heart: BWT ratio in the SHRSP *Spp1* WT and SHRSP *Spp1*^{em1} TAC-operated rats when compared to SHAM.

No differences were observed in the Lung: BWT ratio in WKY, SHRSP *Spp1*^{em1} or WT however, we did observe a significant increase ($p < 0.05$) in lung: BWT ratio in the chr 14 congenic TAC rats when compared to the SHAM rats (SHAM – 4.03 and TAC – 4.22) (fig 4.11 B). We did not observe any differences in the kidney: BWT and Liver: BWT ratios between SHAM and TAC operated rats at the point of sacrifice (fig 4.10 C and D). This indicates that TAC surgery only influenced the heart and LV.

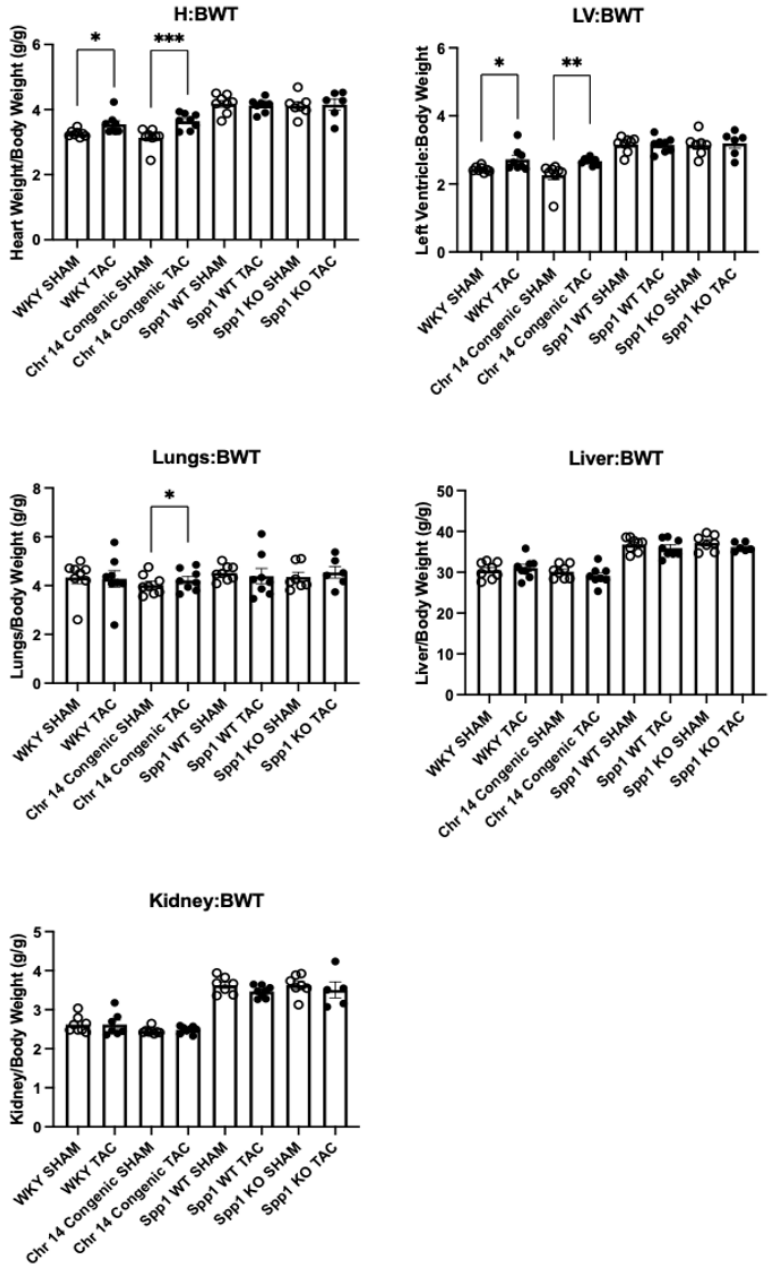

Figure 4.10: Impact of TAC surgery on other tissues.

Significant increases were observed in the WKY ($p < 0.05$) and chr 14 congenic ($p < 0.0001$) TAC rats in the H: BWT ratio. We observed a significant increase in lung: BWT ratio in chr 14 congenic ($p < 0.05$) TAC rats when compared to SHAM rats. No significant differences were observed between SHAM and TAC rats at the point of sacrifice in the Kidney: BWT and Liver: BWT ratios. Data was analysed using two-way ANOVA followed by Šidák's post-hoc multiple comparisons test. Data is represented as mean ± SEM, and significance as * $p<0.05$, ** $p<0.005$, *** $p<0.0005$

4.4 Discussion

The aim of this study was to challenge the cardiovascular system in our unique rat models (SHRSP *Spp1* WT, SHRSP *Spp1*^{em1}, WKY.SP$_{Gla}$14a, and WKY) in order to investigate the role of the *Spp1* gene in cardiac disease development. We carried out TAC in our rat models to induce LVH and assessed the impact on the cardiovascular system over an 8 week post-surgery period by measuring blood pressure, echocardiography and weights of tissues harvested from the animals at sacrifice. LVM is an important predictor of cardiovascular morbidity and mortality, and an abnormal increase in LVM or LVH is a strong predictor of CVD events. LVH is already established in SHRSP rats at the age range utilised in this study. However, these rats have been reported to have well compensated LVH whereby the contractile state and stiffness of the myocardium remain within normal limits (Korkmaz-Icöz et al. 2021), hence the requirement for the additional challenge by TAC in this study.

For many years, suture-based aortic constriction (TAC) has been used as the preferred method for increasing LV afterload and cardiac failure in rodents (Melleby et al. 2018). The biggest advantage of using a TAC model is having the ability to quantify the pressure gradient across the aortic stricture which allows for stratification of LV hypertrophy. With the sudden onset of hypertension attained with TAC, an approximate 50% increase in LV mass within 2 weeks can be observed making this model an excellent choice to examine the use of pharmacological or molecular interventions that may limit hypertrophy (Patten and Hall-Porter 2009). In recent years, several improved rat and mouse TAC models with minimal invasiveness and low mortality have been developed by research groups like Deschepper, C. F. et al. (2004), Almeida, A. C. (2010) and Hu, P. et al (2003). These improvements have made the TAC model more effective and accurate. Animals that have been subjected to TAC go through cardiac hypertrophy, fibrosis, limited amount of inflammation and eventually the development of cardiac dilation and heart failure (Deng et al. 2021). The severity of adverse cardiac remodeling induced by TAC is correlated to and relies on the degree of constriction and the duration of the constriction around the aorta (Bosch et al. 2021). The minimally invasive TAC technique, which avoids thoracotomy and artificial ventilation, is cost-effective and

carries very low operative and post-operative mortalities and it is highly efficient in inducing LVH. It simplifies the procedure and reduces the strain put on the animal and thus makes it the method of choice for the induction of LVH (Tavakoli et al. 2017). Several studies have conducted TAC on various experimental rodent models of heart disease however, our study is the first to use TAC in a stroke-prone model. In order to reduce the risk of sudden death due to stroke in our stroke-prone model, we chose to constrict the descending aorta, which is considered a less severe method of constriction, with follow-up over a relatively short post-surgery period.

A study conducted by Deng et al. (2021) used a range of needle gauges i.e., 25-, 26- and 27-gauge needles to induce distinct cardiac phenotypes in C57BL/6N mice during TAC surgery. Their results showed that all the mice subjected to TAC surgery developed significant hypertrophy. It also showed that mice subjected to 26-gauge TAC showed characteristics of HF which suggests that they transitioned from LVH to an early phase of cardiac dysfunction and HF. A study conducted by Ruppert et al. (2017) showed similar results when constricting the abdominal aorta in male Sprague-Dawley rats using a 22-gauge needle. Their results showed LVH at 3 weeks and myocardial fibrosis at 12 weeks.

In this study, we used a 22-gauge needle and 2/0 mersilk suture to establish the constriction around the aorta. Once the rats reached the end of the 8-week period, they were culled, and their tissues harvested for post-mortem analysis. Our results showed a significant increase in H: BWT and LVMI ratios in the chr 14 congenic and WKY rats from the TAC group when compared with SHAM. This confirms the TAC procedure was successful in achieving hypertrophic response in the hearts due to pressure overload. However, we did not observe any changes in H:BWT or LVMI ratios in the SHRSP *Spp1* WT and SHRSP *Spp1*^{em1} rats between TAC and SHAM groups. This suggests that rats with a hypertensive genetic background are already hypertrophied prior to conducting TAC surgery and constricting their aortas could not push them any further. A study conducted by Ding et al. (2020) has shown that the time point of the development of myocardial fibrosis (leading to heart failure and death) in rats was related to the size of the needle. Using a 7-gauge needle to constrict the abdominal aorta takes 4 weeks to develop myocardial fibrosis with a mortality rate of 18.8%, while using a 21-gauge needle took only 2 weeks. Perhaps

by using a smaller diameter needle, we could have induced a more severe impact in a shorter period in the SHRSP strain. However, by using a smaller diameter needle there is a risk for developing stroke in our rats.

(Korkmaz-Icöz et al. 2021) LVMI ratios estimated by echocardiography at week 8 of the study (immediately before tissue harvest) failed to confirm the significant TAC-induced changes observed in the WKY and chr14 congenic strains measured at sacrifice. However, variability in this echocardiography dataset was large and this may have masked any real differences.

It should be noted, that in previous (unpublished) work conducted by the McBride and Graham group, the chr14 congenic strain demonstrated a significantly increased LVMI when compared to the WKY strain at both 5-weeks of age and 16-weeks of age. However, no significant differences in LVMI were observed between chr14 congenic rats and WKY rats in the current study. This discrepancy may be explained by the different age at which LVMI was measured in this study i.e. 24 weeks of age at sacrifice rather than 5- or 16-weeks of age.

Relative wall thickness (RWT) is another echocardiography parameter used to assess LV geometry and remodeling patterns to determine cardiac hypertrophy changes due to TAC. It is also a marker for adverse events in patients with LV dysfunction. Even though analysis of the echocardiography data failed to show a significant effect of TAC on RWT, we did observe distinct strain difference patterns within the TAC and SHAM groups which were maintained throughout the course of the study. Generally, in the SHAM group, SHRSP *Spp1* WT rats showed the highest RWT, followed by SHRSP *Spp1*^{em1} and chr 14 congenic rats, with the WKY strain always showing the lowest RWT. However, this pattern is disrupted in the TAC group. At week 8 post-TAC surgery, a trend towards increased RWT is observed in chr14 congenic rats when compared to earlier post-surgery timepoints. This may suggest that if we extended the study beyond 8 weeks, we may observe a more exaggerated hypertrophic response. In WKY TAC rats, we observed a significant increase in LVMI and a trend towards increased RWT when compared to WKY SHAM rats. This would indicate that TAC successfully induced a hypertrophic response. Similar responses were observed in TAC studies conducted by Hao Chen et al. (2013) and Yalçin et al. (2019) where mice showed an increase in RWT two-

weeks post TAC surgery. This provides evidence that TAC was successful in inducing a hypertrophic response in the heart.

Other echocardiographic parameters such as SV, CO, FS and EF were assessed to evaluate LV function and performance. In all four strains, both SV and CO showed no significant changes across time between the SHAM and TAC groups. This indicates that the rats were able to maintain normal cardiac performance after TAC, and in the WKY rat this was despite undergoing structural alterations in the heart (Weinheimer et al. 2015). Chr 14 congenic SHAM rats exhibited consistently lower SV and CO when compared to the WKY SHAM strain, despite being generated on the normotensive WKY genetic background. This would indicate that the function of the heart in the chr 14 congenic rats are compromised even before TAC is conducted. However, this difference in SV and CO changes post-TAC surgery whereby chr14 congenic and WKY rats display similar levels. Conversely, SHRSP *Spp1*^{em1} SHAM rats show consistently higher SV and CO when compared to SHRSP *Spp1* WT SHAM rats, despite being generated on the same hypertensive genetic background. Moreover, SV and CO levels in the SHRSP *Spp1*^{em1} SHAM rats are similar to WKY SHAM rats indicating that the SHRSP *Spp1*^{em1} rats have better cardiac function when compared to the SHRSP *Spp1* WT rats. These patterns are lost however, post-TAC surgery, since all the strains exhibit similar SV and CO levels. The decrease in SV and CO in SHRSP *Spp1*^{em1} rats during early/mid timepoints after TAC is indicative of reduced cardiac function in this strain. These results are similar to a TAC study conducted by Richards et al. (2019) where a decrease in SV was observed in mice that underwent TAC surgery.

No changes were observed in FS and EF in all four strains and across all time points in both SHAM and TAC groups. This also indicates that none of the rats are progressing to heart failure, and although WKY rats that have undergone TAC show elevated LVMI at 8-weeks post-surgery, they are still in a state of compensatory hypertrophy. In a 12-week long TAC study conducted by Ruppert et al. (2017), it was shown that male Sprague-Dawley TAC rats demonstrated decompensated cardiac function after week 9 of the study and this became more pronounced at the end of the study at week 12. They also observed significantly enhanced myocardial fibrosis in the TAC group at week 12. If this study was extended from an 8-week post-TAC

period to 12-weeks, it could potentially give more time for development of cardiac hypertrophy and fibrosis leading into heart failure (Doggrell 1998).

(Gs et al. 2014) At sacrifice, in addition to the heart and left ventricle, we weighed liver, kidney and lungs and normalised these organs to the body weight of the rat. We observed that the chr 14 congenic TAC rats showed a significant increase in lung: BWT when compared to the SHAM rats indicating a potential influence due to TAC. Research conducted by Chen et al. (2012) has also shown that TAC conducted on C57B6J HF-mice showed significant LV hypertrophy with a significant increase in lung: BWT ratio and this increase in lung weight is a reliable marker for LV dysfunction. It has been reported that increase in lung weight is often associated with pulmonary edema. However, Chen et al, (2012) showed that this increase was not due to pulmonary edema, but it was a result of pulmonary remodeling, lung fibrosis, myofibroblast proliferation, and leukocyte infiltration. The observed increase in lung: BWT ratio in the chr14 congenic TAC rats should be followed up in future studies by examining pulmonary remodeling and evidence of inflammation.

Blood pressure data revealed that under SHAM conditions there was a clear separation of BP phenotype between the strains on the hypertensive and normotensive genetic backgrounds, with SHRSP *Spp1* WT and SHRSP *Spp1*^{em1} rats demonstrating significantly higher blood pressure than chr 14 congenic and WKY rats. BP levels displayed by the chr14 congenic and WKY rats can be mildly hypertension. However, while measuring the BPs of the WKY and chr 14 congenic strains, they showed high sensitivity to the tail-cuff method and were unable to settle and remain calm during the procedure. These unwanted behavioral responses may have contributed to the elevated BP and variability found in our dataset. After TAC, we observed a trend towards higher BP levels and greater variability in the WKY strain. However, analysis of data from the other strains indicates that TAC did not have a significant effect on BP. In a study carried out by Jung et al. (2020), TAC was conducted on male Sprague-Dawley rats at 11-weeks of age and their SBP was measured and recorded for a period of 5-weeks. Their study showed that with an ascending aorta constriction, a SBP increase of approximately 40mmHg was observed. Research also conducted by Ding et al. (2020) has shown that constricting the aorta in rats via the abdomen, for a period of 12 weeks using a 22-gauge needle,

causes a gradual increase in BP with a small range in fluctuations. In contrast to an ascending aortic constriction, constriction of the transverse aorta avoids excessive overload on the LV because it is positioned proximal to the innominate artery, thus allowing a lower resistance outlet (Rockman et al. 1991). The tail-cuff is a non-invasive technique that is more affordable and efficient, but it does require handling, warming, and restraining the animals which can lead to stress. This is a major limitation of the technique. Using pre-implanted telemetry probes allows for continuous measurement of unrestrained animals in their home environment. This technique removes the stress factor that is associated with human interaction or restraint. Even though telemetry is a direct measurement of central blood pressure and is considered the 'gold standard' technique, it requires the animal to undergo major surgery for the implantation of the telemetry probes, which in our study would be another stress factor on the animal besides the TAC surgery. Another reason why we chose the tail-cuff technique is because of the high costs of telemetry probes (Drüeke and Devuyst 2019; Wilde et al. 2017). So even though we used an appropriate method to constrict the aorta in our TAC model, we did not see any significant changes in BP. This could be due to the location of the constriction. Perhaps, extending the length of the study from 8-weeks to 12-weeks would allow significant changes in BP to be observed.

In conclusion, we have successfully established the TAC model in our WKY and chr14 congenic strains, by demonstrating significantly increased left ventricular hypertrophy 8-weeks post-TAC surgery. Although we failed to show an exaggerated hypertrophic response in the hearts of SHRSP *Spp1* WT and SHRSP *Spp1*^{em1} rats with no evidence of progression to heart failure, this may be due to the relatively short timeframe of the study and the SHRSPs ability to compensate for excessively high blood pressure. (Averill et al. 1976; McAdams et al. 2010)

Under SHAM conditions, the SHRSP *Spp1*^{em1} rat shows a pattern of consistently lower RWT and consistently higher SV and CO across all time points but shows no difference in LVMI, EF or FS when compared to SHRSP *Spp1* WT. However, despite this 'healthier' cardiac phenotype, this did not translate into protection against TAC since after TAC surgery, these distinct cardiac function patterns were lost. These

results provide preliminary evidence that the *Spp1 gene* has a detrimental impact on cardiac function in the SHRSP rat.

Chapter 5. Cell sizing assay in H9c2 cells using osteopontin (Spp1)

5.1 Introduction

Cardiomyocyte cell cultures usually taken from rat neonatal hearts have been widely used to investigate cellular and molecular changes that trigger a hypertrophic response. These changes include an increase in cell size, accumulation and reorganisation of contractile proteins and the upregulation of a hypertrophy-specific set of genes. A small number of established cardiomyocyte cell lines have provided useful alternatives as a major disadvantage of these studies is the need for large numbers of animals. The H9c2 cell line originally derived from embryonic rat ventricular tissue is important as cardiac hypertrophy resulting from hypertension mainly occurs in the ventricular muscle of the heart. These cells have many similarities to primary cardiomyocytes, including hypertrophy-associated traits when stimulated with hypertrophic agents *in vitro* (Watkins, Borthwick, and Arthur 2011).

In this chapter we overexpress *Spp1* in H9c2 cells by transfection and measure cell size. *Spp1* is synthesized by cardiac myocytes, microvascular endothelial cells, and fibroblasts. It has also been known to mediate diverse biological functions such as cell adhesion, migration and signalling. The heart expresses *Spp1* at low levels under basal conditions however, under several pathophysiological states *Spp1* expression increases significantly (Xie, Singh, and Singh 2004).

EVs are known to have an important role in intercellular communication of proximal and distal cells including cardiac cells and have been involved in the regulation of cardiomyocyte hypertrophy, apoptosis, cardiac fibrosis and angiogenesis (Waldenström and Ronquist 2014). EVs derived from cardiomyocytes have been found to contain a large variety of biomolecules, including RNA and protein, and this composition is influenced by the origin, microenvironment, and pathophysiologic state of the cell (H. Yu and Wang 2019). An important feature of these EVs is that they are enriched with heat shock proteins (Hsp) like Hsp20, Hsp60, and Hsp70, which play an important role in cardiomyocyte growth and survival (Gupta and Knowlton 2007). Furthermore, these EVs are known to carry inflammatory factors such as IL-6 and TNK-α, responsible for cardiac remodelling (X. Yu et al. 2012). EVs have also emerged as an alternative source for biomarker discovery in various disease including CVD (Boulanger et al. 2017; Sluijter, Doevendans, and Goumans

2011). Exosomes are the smallest EVs having a diameter ranging from 30nm to 100nm. They are generated inside MVBs and released into the extracellular space by the endosomal sorting complex required for transport (ESCRT) (Figure 5.1). Exosome-mediated signalling has been implicated in the progression of various CVDs such as MI, ischemia-reperfusion (IR) injury and coronary artery disease (Jadli et al. 2021).

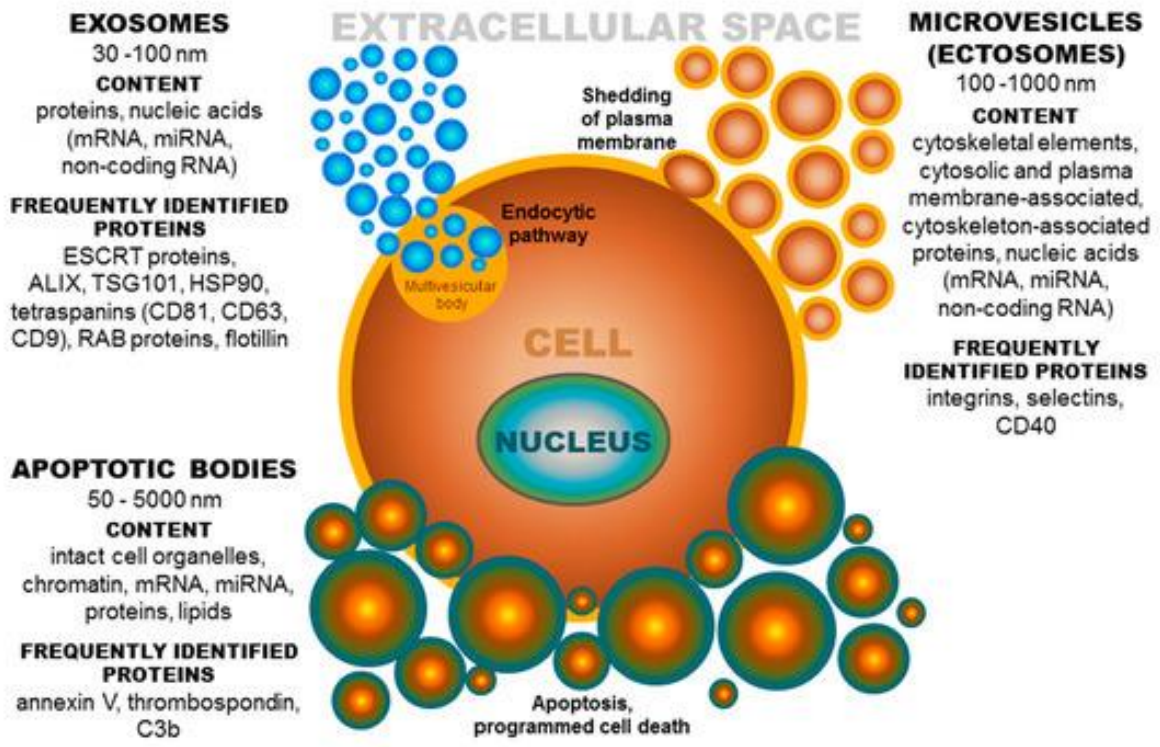

Figure 5.1: Extracellular vesicles: their origin, size and cargo

EVs represent a population of different groups of vesicles classified according to their biogenesis and release pathway, evidently overlapping in some cases. Individual membrane vesicle categories differ, not only in origin, size, and morphology, but also in content. ESCRT—endosomal sorting complex required for transport; ALIX-protein regulating cellular mechanisms, including endocytic membrane trafficking and cell adhesion; TSG101—tumour susceptibility gene 101 protein; HSP—heat shock protein, CD—cluster of differentiation; RAB- proteins included in regulation of endocytosis and secretory processes, C3b—complement (Image from Jankovičová et al. 2020)

5.1.1 Standard methods for EV isolation

EVs are released from host cells into the extracellular space and have also been found in many bodily fluids such as urine, blood, sputum, saliva, breast milk, and more. However, due to the similarities between the three main groups of EVs, their small size, and the complexity of the material they are surrounded by, it can be difficult to isolate and characterise each type of EV (Carnino, Lee, and Jin 2019).

EVs were originally isolated using ultracentrifugation-based methods, and while this method remains the gold standard, there have been other methods developed to address the challenges associated with ultracentrifugation (Zhang et al. 2018). Alternate methods have been developed based on size, immunoaffinity capture, and EV precipitation. However, even these methods do not exclusively isolate small EVs and can result in a mixture of large and small EVs, and other components from the extracellular space (Zaborowski et al. 2015). This is due to the overlap in physiochemical and biochemical properties between the different types of EVs and the heterogeneity among small EVs (Z. J. Smith et al. 2015). The challenge remains to develop isolation techniques that can differentiate between different types of EVs in the extracellular matrix and to do it rapidly, efficiently, and reproducibly (Furi, Momen-Heravi, and Szabo 2017). Furthermore, the use of multiple isolation methods is considered to further enrich exosomal content. However, this can lead to increased cost, time and technical training (P. Li et al. 2017).

There are various important considerations to consider when conducting experiments involving EVs. With progression in the field, several popular EV isolation techniques have emerged (Table 5.1), however EV yield, integrity, biodistribution, clearance and breakdown are all affected when choosing an isolation method (Lener et al. 2015). Ultracentrifugation is one of the simplest, widely available, and cost-effective techniques used for EV isolation. However, it does promote vesicle clumping and may cause soluble factors and ECM-rich protein aggregates to pellet along with the EVs (Linares et al. 2015). EV recovery using this technique is typically variable (10-80%), and is able to concentrate a sample ~8-fold (Coumans et al. 2017). Other methods include density gradient isolation where ultracentrifugation is combined with sucrose or ioxidanol gradients resulting in fractions enriched in EVs

based on mass density and can achieve EV recovery in the range of 5-50% (Cantin et al. 2008).

Size exclusion chromatography (SEC) can be conducted using a single column, can remove 99% of soluble plasma proteins, and does not induce EV aggregation. However, it is prone to co-isolate viruses, protein aggregates and very large proteins (Baranyai et al. 2015; R. Xu et al. 2016). EV recovery rate using this technique is typically between 30-90% (Welton et al. 2015).

Ultrafiltration technique can yield an EV recovery rate of 80% with an ability to concentrate from soluble component EVs, up to 250x. This technique is currently unmatched (Blaser and Aikawa 2018).

Immunoaffinity capture assays using immobilized monoclonal antibodies can be used to isolate specific subpopulations of EVs (Tauro et al. 2012). In this assay non-EV proteins can be recovered however caution must be taken towards cross-reactivity and non-specific binding (Juncker et al. 2014).

Commercially available precipitation kits have become very popular due to the simplistic protocol and ease of use. These kits influence the volume-excluding properties of polyethylene glycol polymers to reduce EV solubility (Ingham 1984). With these kits, a recovery rate of ~90% and concentration of 50x can be expected (Kim et al. 2015). However, users must be careful when attempting to quantify precipitation-isolated EVs by using nanoparticle tracking analysis, as polymer components from the precipitation buffer appear to detect false-positive EV particles frequently (Blaser and Aikawa 2018).

Table 5.1: Methods of EV isolation (Blaser and Aikawa 2018)

Isolation Method	Working Principle	Volume Reduction (fold)	EV Recovery (%)	Notes
Ultracentrifugation (UC)	Size separation: large EVs collect earlier & at lower g forces	8	10-80	Cost-effective; causes vesicle clumping; pellets soluble factors & ECM along with EVs
Density Gradient Centrifugation	Separation by density in sucrose/iodixanol gradients	1	5-50	Non-isosmotic sucrose concentrations cause leaching of EV cargoes
Size Exclusion Chromatography (SEC)	Column-based size separation	0.2	30-90	Effective separation of plasma proteins; prone to co-isolation of large proteins/aggregates
Ultrafiltration	Pressure-mediated by size/solubility	250	80	EV deformation possible; co-isolation of EV-particle aggregates
Immunoaffinity capture assay	Immobilized antibodies against EV-specific ligands	5	N/A	Cross-reactivity & non-specific binding: recovery of non-EV proteins
Precipitation	PEG polymers exclude water volume	50	90	Inexpensive; concerns re: compatibility with NTA

In this chapter we used ultracentrifugation to isolate EVs from *Spp1* transfected H9c2 cells and to investigate the potential role it plays in the packaging of *Spp1* into EVs. Recent studies have identified multiple sorting systems that actively load molecules into EVs, specifically the endosomal sorting complex required for transport (ESCRT) which is an important transporter for transferring proteins into EVs (Busatto et al. 2021; Shengyang Fu et al. 2020). EVs contain different proteins, lipids and nucleic acids and their composition is cell type dependent to some extent and can also be influenced by various cellular conditions or treatments. There are several studies that have also described the protein, lipid, and RNA content of EVs, however very little is known about how the cargo is sorted into these vesicles (Hessvik & Llorente, 2018).

There have been many studies conducted that show different types of RNA, including mRNA, miRNA and lncRNA, to be encapsulate within EVs. They can be transferred from parent to donor cell and interfere with gene expression in the latter (Turchinovich et al, 2019). Studies have shown that different EV isolation techniques can result in differences in biophysical or molecular properties of EVs, including size, density, and content of surface proteins. These methods cannot recover pure material and only allows for enrichment of certain subpopulations of EVs in a sample. Consequently, the characterisation of EV specific RNA cargo remains highly challenging and depends on the purification method. The accuracy of the analysis of EV-associated transcriptome is dependent on an RNA quantification method, including a DNA library preparation for deep sequencing. In this study, EV RNA samples were sent to Glasgow Polyomics where they used the Bioanalyser and NextSeq platform to prepare, analyse and sequence the libraries. Using these library preps, we intended to identify any significantly differentially expressed protein and long non-coding RNAs that could potentially be responsible for affecting H9c2 cell size post-transfection with *Spp1*. Identification of *Spp1* in the EV RNA samples will confirm the successful transfer of *Spp1* in EVs post-transfection which mediates cell size increase in H9c2 cells.

5.1.2 Hypothesis

It is hypothesized that overexpression of osteopontin (*Spp1*) can cause an increase in H9c2 cell size. We also hypothesize that *Spp1* trafficking is mediated by small extracellular vesicles (sEVs), released from transfected H9c2 cells.

5.1.3 Aim

The aims of this chapter are to:

- To overexpress Spp1 in H9c2 cells measure their size 48 hours post-transfection.
- To isolate extracellular vesicles from transfected H9c2 cells using ultracentrifugation technique.
- Conduct a mass spectrometry to characterise protein content in EVs isolated from pcDNA (control) and Spp1 transfected H9c2 cells.
- To characterise EVs using nanoparticle tracking analysis (NTA) and western blot analysis techniques.
- To extract RNA from EVs isolated from pcDNA (control) and Spp1 transfected H9c2 cells.
- To send EV-RNA samples to Glasgow Polyomics for RNA sequencing to identify significantly differentially expressed protein and long non-coding RNAs that may be involved in processes affecting cell size.

5.2 Methods

5.2.1 Cell Culture using H9c2 Cells

H9c2 cells are cultured in Gibco Dulbecco's Minimum Essential Media (MEM) 1X without L-Glutamine (Invitrogen 21090-022) supplemented with 50ml of 10% foetal bovine serum, 5ml L-Glutamine, 5ml sodium pyruvate and 5ml of penicillin/streptomycin (50 units/ml penicillin and 50 units/ml streptomycin). Cell culture media was changed every two days and sub-cultured once they reached 70 to 80% confluency. Cells between passages 4 – 19 were used for our experiments. A detailed methodology on how these cells were cultured is described under section 2.2.

5.2.2 Extracellular Vesicle Isolation using Ultracentrifugation Technique

Table 5.2: Table showing timeline of extracellular vesicle isolation using ultracentrifugation technique

Day 1	**Seed Cells** • H9c2 cells have a seeding density of 1 x 10^4 cells/dish • HeLa cells have a seeding density of 2.2 x 10^6 cells/dish • Plates are placed in the incubator at 37C for 24 hours
Day 2	**Transfection** • Cells are transfected with 20ug of DNA (pcDNA & *Spp1*) • Along with DNA, cells are also transfected with 6ul of xfect polymer (Xfect™ Transfection Reagent, PT5003-2). For every 1ug of DNA, 0.3ul of polymer is added • Cells are then placed in the incubator for 4 hours • After 4 hours, media in the plates are changed to EV-free media • Plates are kept in the incubator for 48 hours
Day 3	**Incubation** • Observe cells to make sure they are growing well and not infected
Day 4	**Media collection** • Collect media from all the plates and put into 30ml universal tubes • Centrifuge media at 2000g for 20 minutes at 4C • After centrifugation, filter media using 0.2um syringe filters (1 per ~15ml syringe) • Store filtered media in 4C
Day 5	**Ultracentrifugation** • Transfer media from falcon tubes to polyallomer tubes (each tube can hold ~17ml of media) • Ensure tubes are filled to the top. If not top up with PBS • Place polyallomer tubes into ultracentrifuge rotor tubes and tighten lid • Place ultracentrifuge rotor tubes in rotor corresponding to number on the lid • Centrifugation setting – 25400rpm for 90 minutes at 4C • After spin, remove supernatant carefully with a stripette and discard • Repeat spins 3 times with PBS • After final spin, resuspend pellet in 100ul of PBS and place in 1.5ml eppendorf tube • Store tubes at -80C

5.2.3 Mass spectrometry

Samples from previous EV isolation experiments were sent for mass spectrometry analysis to Glasgow Polyomics. A total of six preps (pcDNA1 & *Spp1*-1, pcDNA2 & *Spp1*-2 and pcDNA3 & *Spp1*-3), each with a total volume of 20ul and with concentrations ranging between 35ug/ml to 68ug/ml.

Using Mascot search engine (v2.6.2, Matrix Science) protein identifications were assigned to cross-examine protein sequences in the NCBIprot, using the taxonomy for Rattus and Swissprot databases. A mass tolerance of 10ppm for the precursor and 0.3 Da MS/MS was used for peptide matching.

5.2.4 Nanoparticle Tracking Analysis

NTA analysis is a unique technology that utilizes the properties of both light scattering and Brownian motion to obtain the size distribution and concentration measurement of particles in a liquid suspension. A laser beam is passed through the chamber containing the sample, and the particles in suspension scatter in the beam of light. These particles can be visualized via a 20X magnification microscope onto which a camera is mounted. The camera operates at 30 frames per second (fps), capturing a video file of the particles moving under Brownian motion. The software tracks the particles individually using the Stokes-Einstein equation which calculates their hydrodynamic diameters.

The Malvern Panalytical NanoSight LM10 instrument allows for rapid and accurate analysis of the size distribution and concentration of all types of nanoparticles from 20nm to 1000nm in diameter, depending on the instrument configuration and sample type. EV samples were diluted in 1ml PBS to achieve an optimal concentration for NanoSight analysis as per manufacturers guidelines. If the sample was too concentrated this affected the NanoSight ability to produce accurate results. From this, the particle concentration of the original sample was calculated. The diluted sample was then injected into the sample chamber of the Nanosight LM10 unit (Nanosight Ltd, Amesbury, UK) while holding the chamber vertically to ensure no air bubbles were present. The 430nm laser was then switched on and visual parameters were optimized as per manufacturer's guidelines. Five 30-second videos were

recorded for each sample and analyzed by the Nanoparticle Tracking Analysis (NTA) 2.2 software. After each sample analysis the chamber is dismantled, cleaned thoroughly with 70% ethanol and dried before the insertion of the next sample.

5.2.5 Western Blot Analysis

Gel Electrophoresis:

Western blot analysis is the most widely used scientific technique of protein analysis of a tissue homogenate or extract. The process involves gel electrophoresis to separate proteins according to their molecular weight. The proteins are then transferred to a membrane and detected using targeted antibodies. Gel Electrophoresis Sodium dodecyl sulphate - polyacrylamide gel electrophoresis (SDS-PAGE) was conducted using the Bolt™ Bis-Tris, 4% – 12% 10-well mini protein gel (Fisher-Scientific, UK) to separate proteins. These gels have a maximum loading capacity of 60ul. SDS in the sample buffer denatures multimeric proteins and polypeptide chains so that all proteins have similar charge:mass ratios. This allows the migration of proteins to be determined by size. The addition of an electrical field causes migration of the smaller proteins faster down the gel, thus proteins are separated according to molecular weight. In the far left of the gel, 7ul of Amersham™ ECL™ Rainbow™ Marker - Full range (Sigma Aldrich, UK) was loaded to allow for determination of protein sizes. EV samples were diluted 4:1 with NuPAGE™ LDS Sample Buffer (4X) and heated for 5 minutes at 95°C. 60ul samples were then loaded into the wells of the gel. Gels were run at 200 volts for 60 minutes or until separation of the protein ladder and the bromophenol blue dye had run off the gel.

Protein Transfer to Membrane:

Thermo Scientific™ PVDF Transfer Membrane, Catalogue No: 88520 (Thermofisher Scientific, UK) western blot transfer membrane was used for the transfer of proteins from the western blot gel. The PVDF membrane and blotting paper were activated via pre-soaking in 50ml 1X transfer buffer containing 100% methanol.

1X transfer buffer – 1 Litre

- Glycine = 14.4g
- Tris base = 3.03g
- Methanol = 200ml
- Distilled water = 800ml

The gels are carefully removed from the module after its run and placed onto the activated transfer paper. They are then sandwiched in between the blotting paper and loaded onto the transfer tank. The transfer module is placed in the tank and the remaining of the 1L transfer buffer is poured into the tank making sure all air bubbles are removed. The gel was then set to transfer at 25 volts for 60 minutes.

Membrane Blocking and Protein Detection:

To reduce non-specific binding of proteins once transfer is complete, the PVDF membrane was blocked for 1 hour at room temperature in 1: 1 of TBST ((1X TBS and 0.1% Tween™ 20 Surfact-Amps™ Detergent Solution (Thermofisher, UK)) and SEA BLOCK blocking buffer (Thermofisher, UK). The membrane was then washed 3 times for 10 minutes in TBST: SEA BLOCK. The membrane was then incubated overnight with a primary antibody according to manufacturer's specifications. The next morning the membrane was washed as previously described. Since the secondary antibody reacts with light, the membrane was incubated with it in a foil covered container to create a dark environment and incubated for 1 hour. The membrane was then washed with TBST: SEA BLOCK as previously described. After 1 hour, we did a final wash with TBST: SEA BLOCK as previously described. The membrane was then placed in PBS to be ready for imaging using the Li-COR Odyssey® CLx Imaging System.

5.2.6 Cell Culture using HeLa Cells

HeLa cells are cultured in Gibco Dulbecco's Minimum Essential Media (MEM) 1X without L-Glutamine (Invitrogen 21090-022) supplemented with 50ml of 10% foetal bovine serum, 5ml L-Glutamine, 5ml sodium pyruvate and 5ml of penicillin/streptomycin (50 units/ml penicillin and 50 units/ml streptomycin). Cell culture media was changed every two days and cells sub-cultured once they reached 70 to 80% confluency. A detailed methodology on how these cells were cultured is described under section 2.2.

5.2.7 RNA Extraction from Extracellular Vesicles

RNA was extracted from EVs isolated transfected H9c2 cells using miRNeasy mini kit from Qiagen (catalogue. no. 217004). EV samples were taken out of -80C freezer and left to thaw on wet ice. Once samples were thawed, 700ul of QIAzol lysis reagent was added to the sample and homogenized and disrupted by shaking vigorously. Homogenates were then incubated at room temperature (15C -25C) for 5 minutes. After 5 minutes, samples were shaken vigorously after adding 140ul of chloroform and then incubated at room temperature for 2 – 3 minutes. After incubation homogenates were centrifuged for 15 minutes at 12,000xg at 4C. Transfer the upper aqueous phase to a new collection and avoid transferring the interphase. Add 525ul of 100% ethanol and mix thoroughly by pipetting. Then pipet up to 700ul of the sample including any precipitate into a RNeasy mini column in a 2ml collection tube. Close the lid and centrifuge at ≥8000 x g for 15 seconds at room temperature. Discard the flow through and repeat with the rest of the sample. The add 700ul of buffer RWT to the RNeasy mini column, centrifuge for 15 seconds at ≥8000 x g and discard the flow through. Add 500ul of buffer RPE to the RNeasy mini column and centrifuge for 2 minutes at ≥8000 x g. Place the RNeasy mini column into a new 2ml collection tube and centrifuge again at full speed for 1 minute to further dry the membrane. Transfer RNeasy mini column to a new 1.5ml collection tube and pipet 30ul of RNase-free water onto the RNeasy mini column membrane. Close the lid and centrifuge for 1 minute at ≥8000 x g to elute. Repeat by using eluate from previous step and pipet onto the RNeasy mini column membrane and let it sit for 1 minute. Then centrifuge for 1 minute at ≥8000 x g to elute. Store samples in -80C freezer for long term storage.

5.2.8 RNA Sequencing of Extracellular Vesicle RNA

Glasgow Polyomics facility performed all library preparations but did not process samples prior to library preparations. Sequencing libraries were prepared from total RNA using the Illumina TruSeq Stranded mRNA Sample Preparation Kit. Libraries were sequenced in 75 base, paired end mode on the Illumina NextSeq 500 platform. Raw sequence reads were trimmed for contaminating sequence adapters and poor-quality bases using the program FastP. Bases with an average Phred score lower than 15 were trimmed. Reads that were trimmed to less than 54 bases were discarded. The quality of the reads was checked using the Fastqc program before and after trimming. The sequenced reads were checked for other species contamination using the Fastq-Screen program, which selects a sample of the reads and aligns them to a selection of reference genomes that are routinely sequenced at Glasgow Polyomics. The quality trimmed reads were aligned to the reference genome using the program Hisat2[4] and the transcript abundance estiamted using Stringtie. Upon analysis by Glasgow Polyomics staff, raw data was generated in the form of FASTQ files containing unaligned reads for each sample, aligned reads in the form of BAM files, normalised and raw expression estimates for gene/transcripts, and gene/transcript lists showing statistical measures of differential expression for each requested comparison of the two groups: plasmid control and *Spp1* transfected. The reads were aligned to Rattus Norvegicus genome assembly Rnor_6.0 (Ensembl GCF_000001895.5). We aimed to identify protein coding and long non-coding RNAs, transported in H9c2 EVs transfected with *Spp1* and plasmid controls, that may underlie biological processes affecting cell size.

5.2.9 Statistical Analysis

All statistics were performed using GraphPad prism version 9 (GraphPad software, San Diego, California USA). The significance threshold for all analysis was set at 0.05. For statistical comparisons between two groups, unpaired t-tests were applied.

5.3 Results

5.3.1 Transfection of *Spp1* into H9c2 cells

To observe the phenotypic effects of overexpression of *Spp1*, we transfected H9c2 cells with pcDNA eukaryotic expression vector with *Spp1* cDNA derived from the SHRSP, a pcDNA control plasmid with no insert. Post-transfection we fixed and imaged the cells using EVOS XL Core Cell Imaging Systems and measured the length of the cells using ImageJ (fig 5.2 A – B). In each group we measured a total of 300 cells and took an average of their mean lengths. Visually we were able to see a difference between the two groups. Cells in the *Spp1* transfected group were enlarged compared to the control cells. Statistical analysis of the data showed a significant increase in length of the cells in the *Spp1* group when compared to the control (fig 5.2 C – E). Figures 5.2 C - E are set up as separate experiments and represented as replicates. The same experimental conditions have been maintained in these experiments.

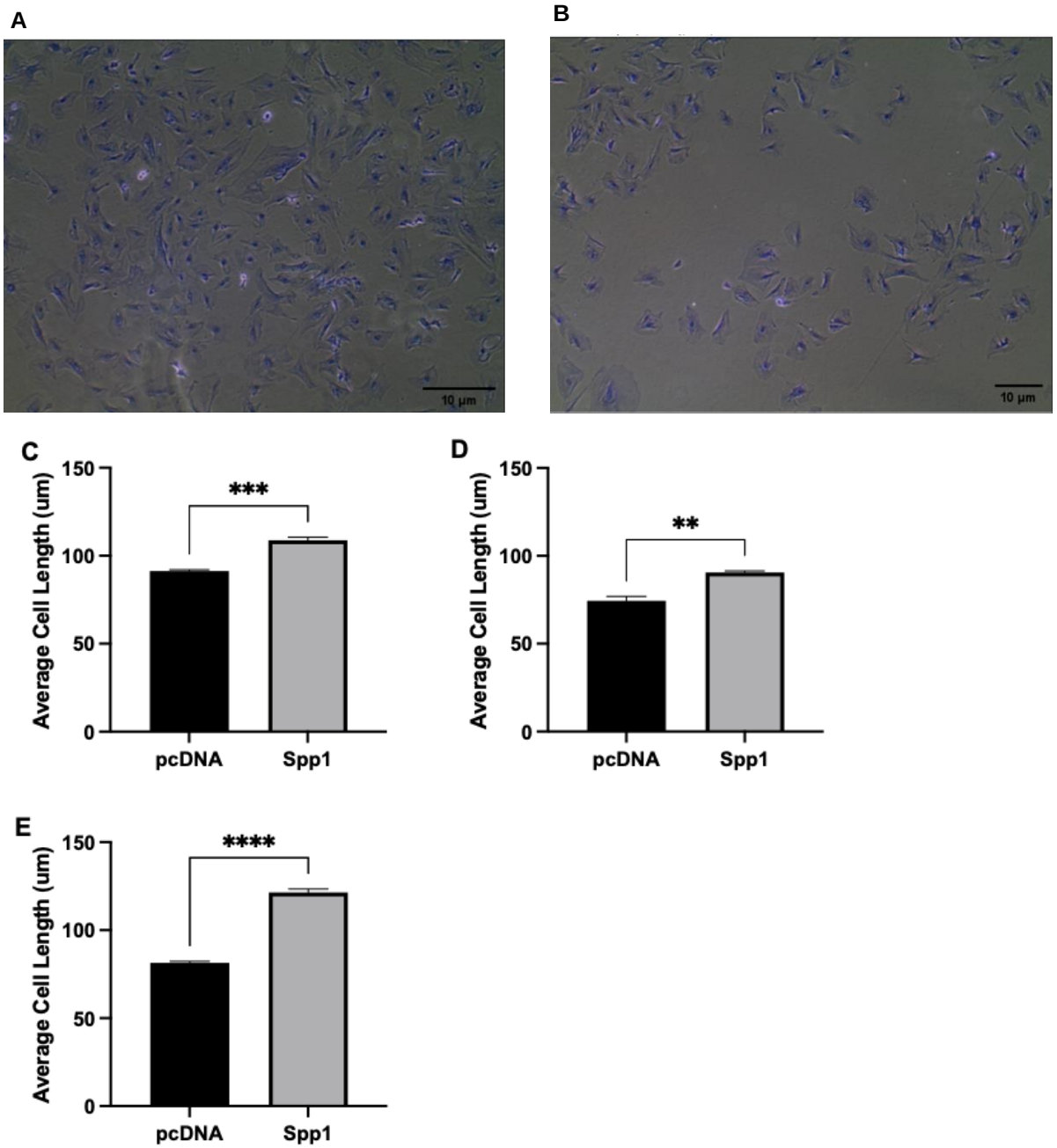

Figure 5.2: Cell sizing assay by transfection of *Spp1* and pcDNA in H9c2 cells

The effect of pcDNA and *Spp1* on the average cell length of H9c2 cells. We observed a significant increase in cell length in *Spp1* group when compared to the control after cells were incubated with pcDNA and *Spp1* for 48 hours. Data was analysed using student t-test. Error bars represent ±SEM from 3 separate experiments.

- **A) – B)** Images of cells taken post-transfection with pcDNA and *Spp1* under 10X magnification using EVOX XL Core Cell Imaging Systems
- **C)** pcDNA = 68.68 ± 1.82 and *Spp1* = 107.24 ± 0.87 (***p = ≤0.0005)
- **D)** pcDNA = 68.27 ± 2.82 and *Spp1* = 116.58 ± 6.69 (**p = ≤0.005)
- **E)** pcDNA = 62.93 ± 3 .77 and *Spp1* = 113.26 ± 8.14 (**p = ≤0.005)

5.3.2 Mass spectrometry of isolated EVs from transfected H9c2 cells

We conducted mass spectrometry analysis on EVs isolated from H9c2 cells transfected with pcDNA & Spp1. High quantities of fetal bovine serum (FBS) proteins masked our results despite using EV-free FBS. Along with cross-contamination from the FBS we also had contamination from surrounding environment like keratin (skin and hair) while preparing the samples.

Using the NCBIprot database with the taxonomy Rattus, and the Swissprot database, a list of proteins was identified (refer to table 5.4 in appendix). Out of the many different proteins identified in pcDNA (1-3) and Spp1 (1-3), we were able to categorize the proteins found common between the two databases and between each condition.

We were also able to categorize proteins that were found unique between the n's of each group (n=3), pcDNA and Spp1. These proteins were also identified using the NCBIprot and Swissprot database (refer to table 5.4 in appendix).

5.3.3 Characterisation of EVs by Nanoparticle Tracking Analysis (NTA)

To confirm the presence of EVs in our control and Spp1 EV preps, we used the NanoSight tracking analysis (NTA) equipment. EVs were isolated from H9c2 conditioned media using ultracentrifugation technique and then resuspended in 100ul of PBS. All experiments were conducted using a 1:100 dilution with distilled water. The EVs had a spherical shape (fig 5.3 A) with mean sizes of 80nm to 150nm (fig 5.3 B – 5 E). We also observed high particle concentrations with an average of 2.49 $x10^9$ particles/ml for the EVs isolated from control conditioned media and 6.19 x 10^8 particles/ml for EVs isolated from Spp1 conditioned media. Therefore, we could confirm that our EV preps for both control and Spp1 contained EVs as their size distribution is characteristic of them. Figures 5.3 B - E are set up as separate experiments and represented as replicates. The same experimental conditions have been maintained in these experiments.

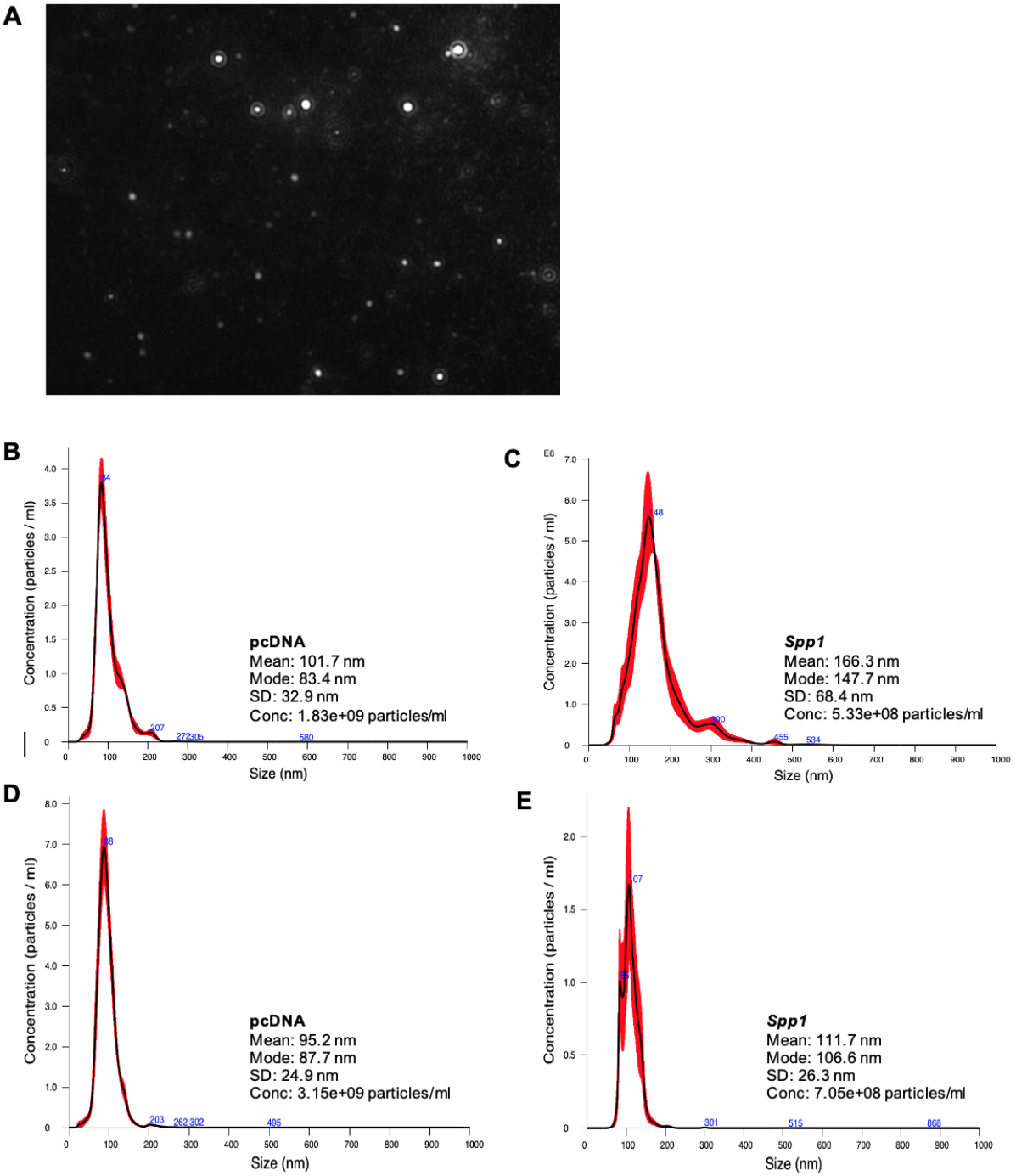

Figure 5.3: Size distribution analysis of EVs isolated from H9c2 cells transfected with pcDNA and *Spp1* using ultracentrifugation

A) Nanosight still image of moving particles from EV samples.

B) – E) Graphical representation of NTA results showing size distribution of EVs isolated from transfected H9c2 cells. EVs were isolated by ultracentrifugation technique at 25400rpm. The calculated size distribution is depicted as mean size (black line) with standard errors (red shaded area).

5.3.4 Characterisation of EVs by Western Blot technique using EV specific markers

Western blot technique was used to characterise the EVs that were isolated from H9c2 cells that were transfected with control and *Spp1*. To further confirm the presence of EVs in our samples using EV specific markers such as ADAM10, TSG101, Annexin XI, CD63 and CD81 (table 5.3). However, we were only able to detect a signal from TSG101. We used TSG101 rabbit polyclonal antibody (1:200 dilution) followed by donkey anti-rabbit antibody (1:15000 dilution) as the secondary antibody. The particle concentration of control and *Spp1* EVs loaded in the gel were $3.15x10^9$ particles/ml and $1.96x10^9$ particles/ml respectively. Faint bands were detected in the un-transfected control and both control and *Spp1* EV preps at 52kDa indicating the presence of EVs in our samples (fig 5.4). We also used cell lysates as positive controls and detected bands for all 3 samples.

Table 5.3: Table of common EV proteins used to detect the presence of EVs in the sample isolated from H9c2 conditioned media

TSG101 detected while ADAM10, Annexin XI, CD63 and CD81 not detected.

EV Marker	Marker detected?
ADAM10 (1:200)	No
TSG101 (1:200)	**Yes**
Annexin XI (1:500)	No
CD63 (1:1000)	No
CD81 1:1000)	No

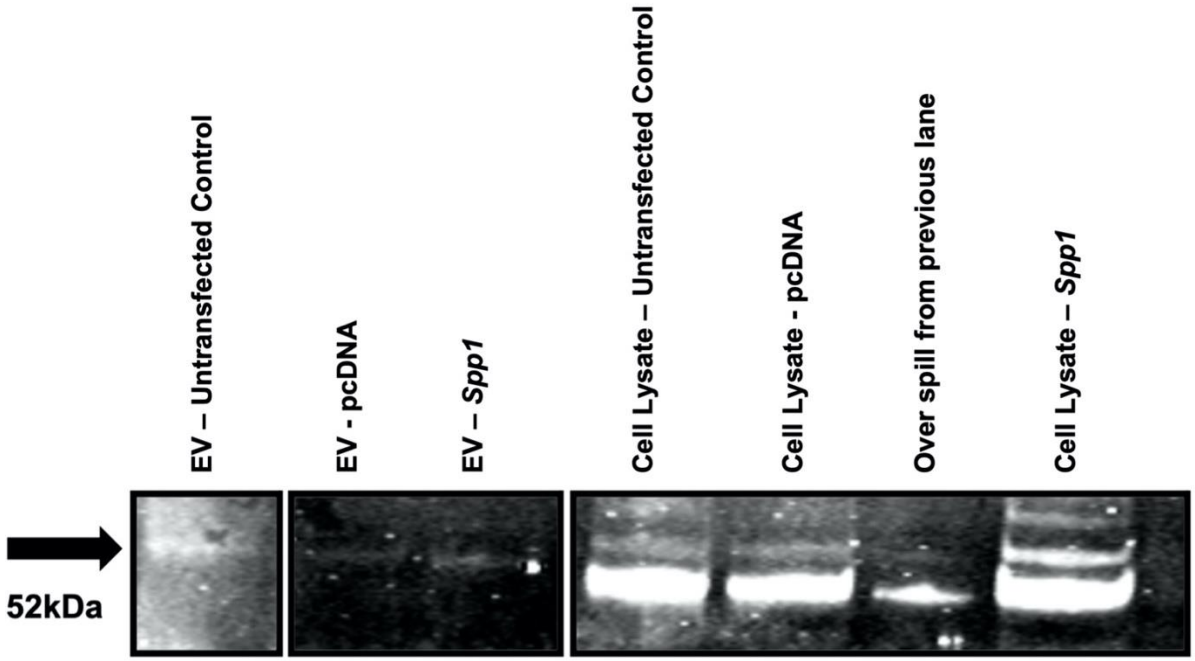

Figure 5.4: Western blot for EV and cell lysate preps from H9c2 cells transfected with pcDNA and *Spp1*

H9c2 cells were incubated with pcDNA and *Spp1* for 48 hours. EVs were then isolated using ultracentrifugation technique, the cells were lysed using RIPA buffer, and analysed by western blotting using an EV specific marker, TSG101 (1:200 dilution), followed by donkey anti-rabbit secondary antibody (1:15000 dilution). Light bands appear at 52kDa in all three EV preps after incubating with EV specific marker, TSG101, indicating the presence of EVs.

5.3.5 Overlay of EVs isolated from Spp1 transfected H9c2 cells

To determine whether *Spp1* was being packaged into EVs post-transfection, we conducted EV isolations using ultracentrifugation technique. Untreated H9c2 cells were cultured in 10cm petri dishes with a seeding density of 1 x 10^4 cells/dish. After 48 hours, 100ul of total EV sample that was previously isolated from 10cm petri dishes (10cm petri dish x3/condition) from control and *Spp1* transfected H9c2 cells was placed onto the untreated cells for another 48 hours to observe any changes to their size. Cells were fixed and imaged using EVOS XL Core Cell Imaging Systems. We measured a total of 300 cells per group using ImageJ and took an average of their mean lengths. From the images that we collected; we were able to see that the cells in the *Spp1* group appeared larger in size compared to the cells in the control group (fig 5.5 A – 4 B). Statistical analysis of the data from our first experiment (fig 5.5 C) showed that the mean length of the *Spp1* cells were significantly higher than the control cells. In our second experiment, even though we observed an increase in the mean length of the cells in the *Spp1* group, the results did not reach statistical significance, p = 0.054 (fig 5.5 D). Figures 5.5 C - D are set up as separate experiments and represented as replicates. The same experimental conditions have been maintained in these experiments.

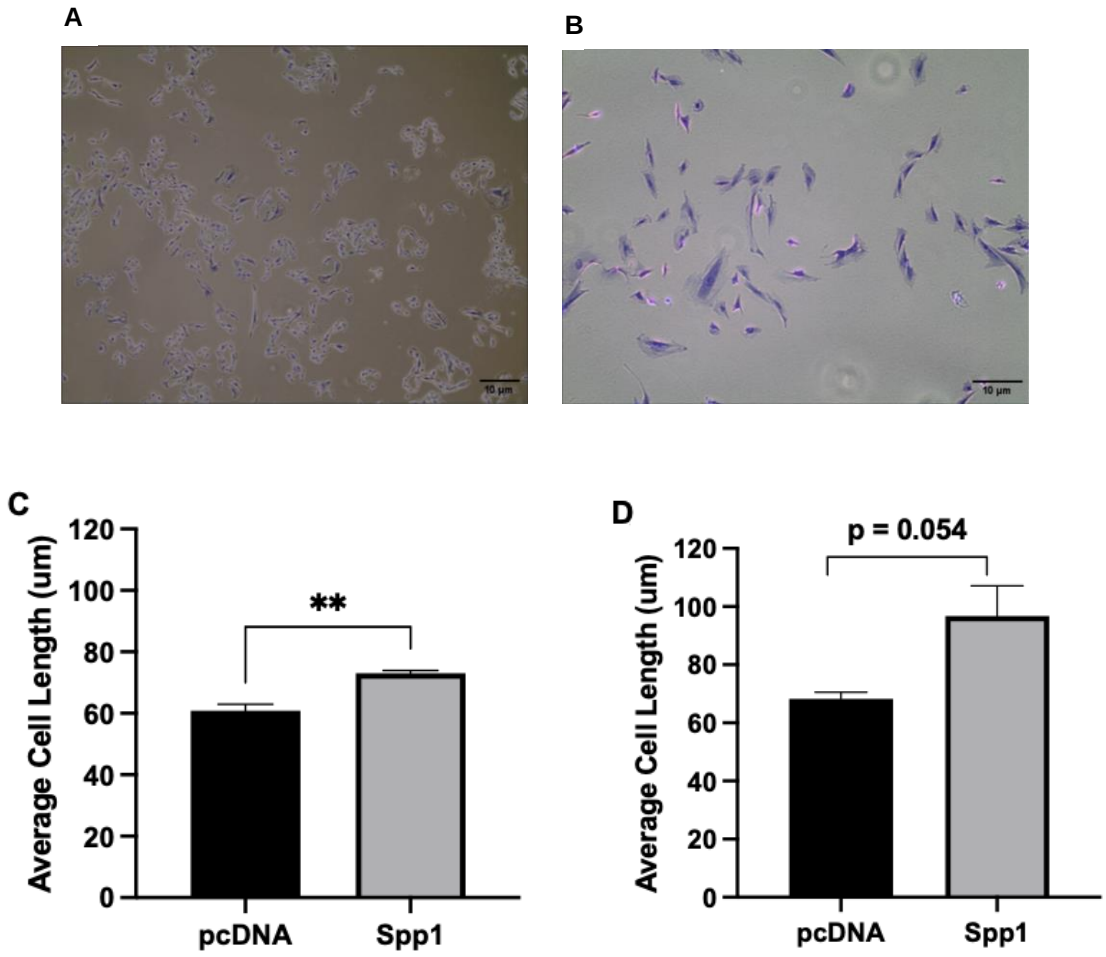

Figure 5.5: H9c2 cells treated with EVs isolated from transfected H9c2 cells
The effect of pcDNA and *Spp1* EVs on the average cell length of H9c2 cells. We observed a significant increase in cell length in the *Spp1* group when compared to the control after cells were incubated with pcDNA and *Spp1* EVs for 48 hours. Data was analysed using student t-test. Error bars represent ±SEM from 2 separate experiments.

A) – B) Images of cells taken post-transfection under 10X magnification using EVOX XL Core Cell Imaging Systems

C) pcDNA = 60.82±2.11 and *Spp1* = 73.09±0.85 (**p = ≤0.005)

D) pcDNA = 68.15±2.28 and *Spp1* = 96.77±10.37 (p = 0.054)

5.3.6 Overlay of EVs isolated from Spp1 transfected HeLa cells

We then used a different cell line, HeLa cells, to determine whether EVs isolated from different tissues showed a similar increase in cell size to EVs isolated from H9c2 cells when they are transfected with *Spp1*. We transfected HeLa cells with control and *Spp1*, and after 48 hours we isolated the EVs using ultracentrifugation technique. We then placed the HeLa EVs on untreated H9c2 cells to observe changes to their size. Cells were fixed and imaged using EVOS XL Core Cell Imaging Systems. We measured a total of 300 cells per group using ImageJ and took an average of their mean lengths. From the images that were collected we observed that the cells in the *Spp1* group appeared enlarged when compared to the cells in the control group (fig 5.6 A - B). Statistical analysis of the data (n=3) further confirmed a significant increase of cell length in the *Spp1* group compared to the control group when treated with EVs isolated from transfected HeLa cells (fig 5.6 C – E). Figures 5.6 C - E are set up as separate experiments and represented as replicates. The same experimental conditions have been maintained in these experiments.

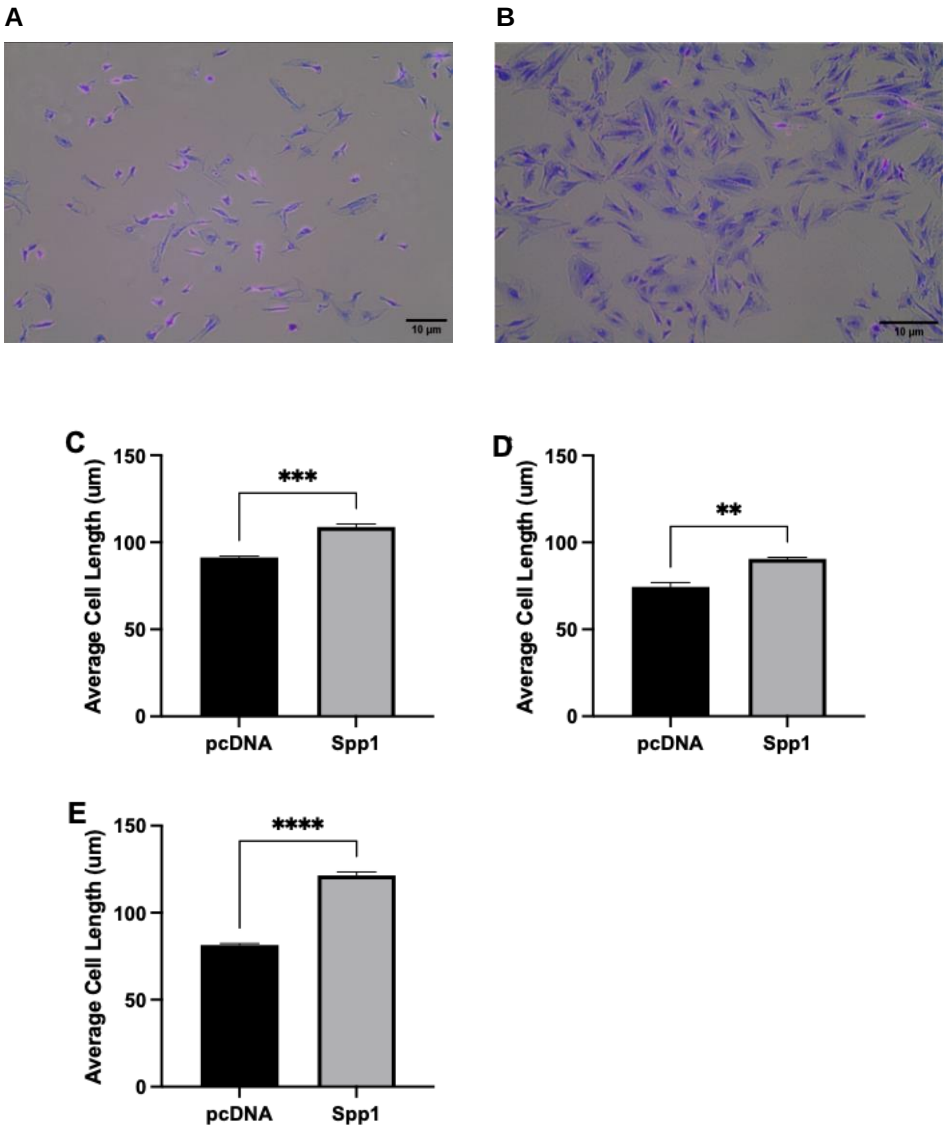

Figure 5.6: H9c2 cells treated with EVs isolated from transfected HeLa cells

EVs were isolated from HeLa cells that were transfected with pcDNA and *Spp1* plasmid. Those EVs were then placed on untreated H9c2 cells to observe the effect on the average cell length of H9c2 cells. We observed a significant increase in cell length in the *Spp1* group when compared to the control after cells were incubated with EVs for 48 hours. Data was analysed using student t-test. Error bars represent ±SEM from 3 separate experiments.

A) – B) Images of cells taken post-transfection under 10X magnification using EVOX XL Core Cell Imaging Systems

C) pcDNA = 91.25±0.87 & *Spp1* = 108.80±1.76 (***p = ≤0.0005)

D) pcDNA = 74.44±2.51 & *Spp1* = 90.52±0.94 (**p = ≤0.005)

E) pcDNA = 81.39±0.92 & *Spp1* = 121.41±1.98 (****p = ≤0.00005)

5.3.7 Quantitative Real-Time PCR (qRT-PCR) of EVs Isolated from transfected H9c2 cells

To determine *Spp1* expression in EVs isolated from pcDNA and *Spp1* transfected H9c2 cells, qRT-PCR was performed. RNA was extracted from these EVs using QIAgen miRNeasy Mini Kit. B2M was used as a housekeeper for normalisation however, B2M is not expressed in the EVs and the assumption that it will show uniform expression in both the control and experimental group could not be made. As the RQ value could not be calculated, the mean CT value for *Spp1* expression in each group was plotted. The lower the CT value, the higher the gene expression. Mean CT values for EVs isolated from pcDNA and *Spp1* transfected H9c2 cells (n=1) were 31.55±0.32 and 26.08±0.07 respectively. The results suggest a significant overexpression of *Spp1* in the EVs isolated from *Spp1* transfected cells ($p<0.001$) (figure 5.7).

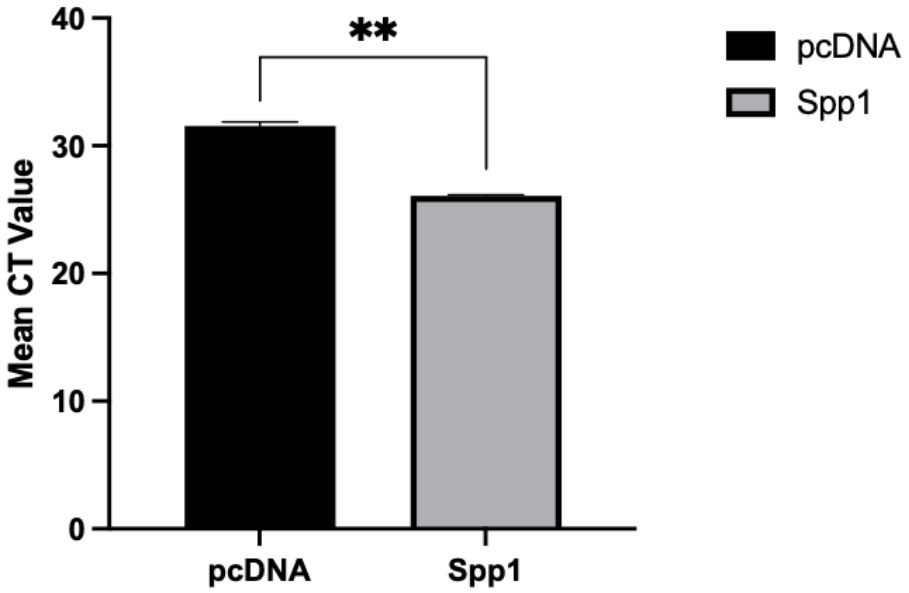

Figure 5.7: *Spp1* expression in transfected EVs isolated from H9c2 cells

Mean CT value for *Spp1* expression in pcDNA and *Spp1* transfected EVs, n=1, pcDNA = 31.55±0.32 & *Spp1* = 26.08±0.07 (**p = ≤0.001)

5.3.8 Analysis of Spp1 expression in EV RNA samples

We extracted RNA from EVs isolated from control and Spp1 transfected H9c2 cells. These RNA samples were sent to Glasgow Polyomics for RNA sequencing to help identify significantly differentially expressed protein and long non-coding RNAs that may be involved in processes affecting cell size. Data from the initial control and Spp1 test samples (n=1 per group) revealed Spp1 ranked 8th out of the 1000 genes identified in the Spp1 transfected EV sample with a high coverage of 1178 RPKM when compared to the control where Spp1 ranked 744th with a coverage of 2.84 RPKM (fig 5.8 A and 5.8 B).

We then submitted an n=3 (control and Spp1) EV RNA samples to Glasgow Polyomics for further analysis. These results showed that Spp1 expression was significantly increased in the Spp1 experimental group with a fold change of 5598 when compared to the control group (fig 5.8 C). However, in the control group we can only observe an n=2 and this was probably due to very low concentration levels found in the third sample or sample preparation failure.

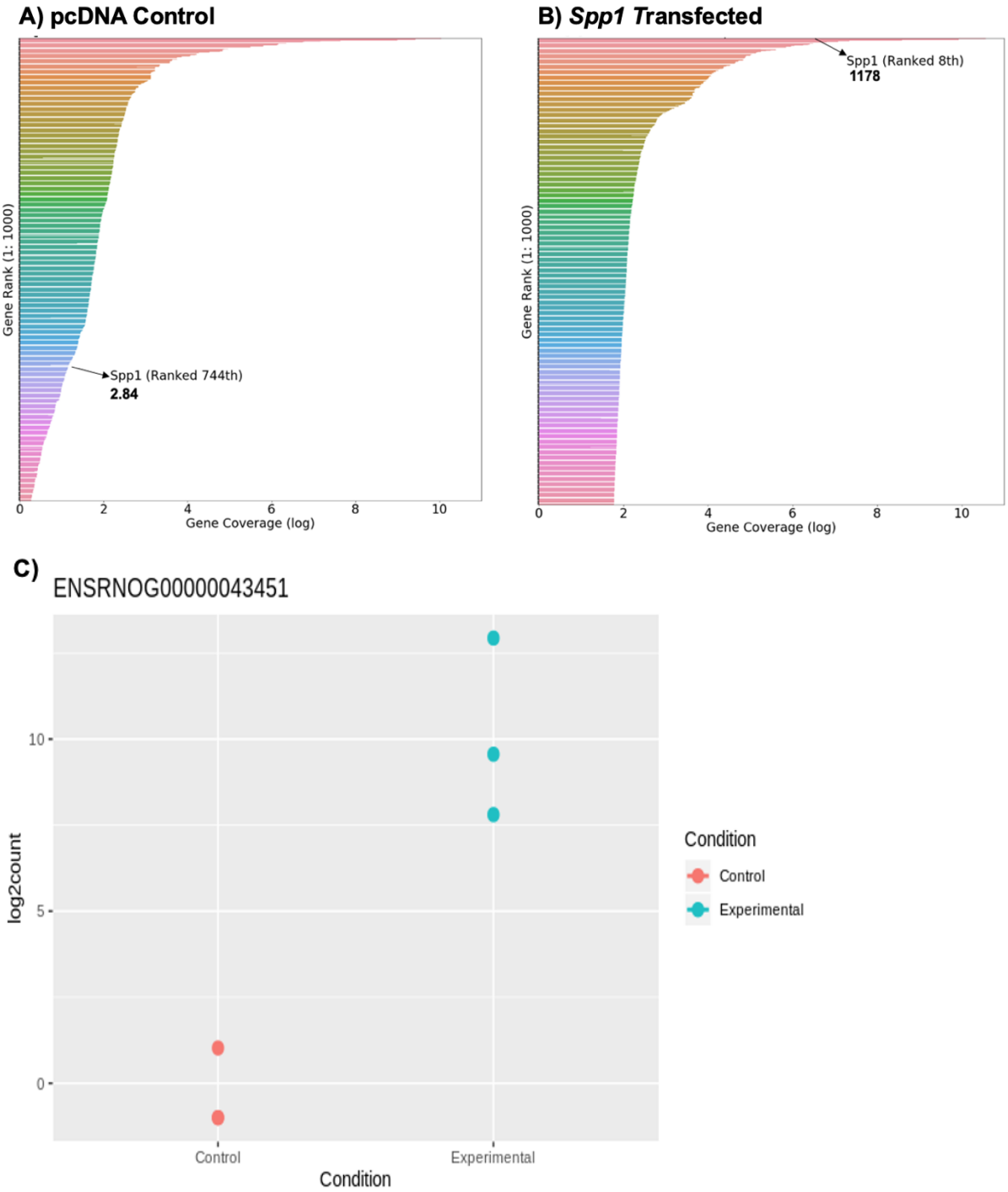

Figure 5.8: RNAseq of EVs isolated from transfected H9c2 cells

A) and B): Swarm plot representing genes identified in control and experimental RNA test samples isolated from EV samples (n=1). Genes ranked from 1 to 1000, on a log scale, based on coverage with *Spp1* showing the highest coverage in experimental sample. **C)** Graph showing expression levels of *Spp1* in control and experimental RNA samples isolated from EV samples (n=3) with *Spp1* showing higher expression in the experimental group. padj < 9.03×10^{-10}, fold change – 5598.

5.4 Discussion

The experiments performed in this chapter investigates the functional response of *Spp1* overexpression in the H9c2 cell model. We also investigate the role of EVs and how the overexpression of *Spp1* promotes an increase in cell size via EV signaling. Cardiac cell line H9c2 was used as a model in our experiments to study this overexpression as it has been long established as an excellent *in vitro* model of hypertrophic cell growth.

We observed that when H9c2 cells are overexpressed with *Spp1* by transfection, we see a significant increase in their size when compared to cells transfected with control. To further investigate whether *Spp1* trafficking is facilitated by EVs released from transfected H9c2 cells, we isolated EVs from H9c2 conditioned media using the ultracentrifugation technique. Our results showed that when we overlayed untreated H9c2 cells with EVs isolated from *Spp1* conditioned media, we observed a significant increase in their size. Since our previous experiment determined that *Spp1* can produce a significant increase in cell size when transfected in H9c2 cells, we can conclude that post-transfection *Spp1* is trafficked into EVs and then released from the cells as cargo into the media. This communication and transfer of material mediated by EVs can cause the surrounding cells to behave in the same manner as the donor cells and carry out similar functions (Lotvall & Valadi, 2007). However, the process that drives EV cargo selection and its release into target cells is yet to be fully understood.

Studies conducted by (López et al. 2013; Xie, Singh, and Singh 2004) have found that patients suffering from cardiac hypertrophy and heart failure showed increased *Spp1* expression. In an adult heart, *Spp1* is expressed at low levels under basal conditions, however its expression increases significantly under a variety of pathophysiological conditions (Dalal et al, 2014). In an unstressed rat heart, cardiomyocytes have also been shown to express *Spp1* at basal levels. However, upon the onset of cardiac hypertrophy, *Spp1* levels have shown to be elevated suggesting that it plays a role as an effector for extracellular signaling promoting myocyte growth (Mohamed et al, 2019). These findings suggest that *Spp1* acts as a mediator of cardiac hypertrophy and heart failure.

EVs have been a topic of interest as it has been shown to play a novel role in intercellular communication via transfer of their biological content which consists of proteins, lipids and nucleic acids, between cells (Willms et al. 2016).

To help characterize the EVs isolated from H9c2 conditioned media we used the nanoparticle tracking analysis (NTA) equipment to implicate EVs. NTA is a technique widely used for the characterization of particle size distribution of EVs. It tracks the Brownian motion of individual particles, allowing size determination of a single EV and a population of EVs using the Stokes-Einstein equation (Thane et al, 2019). Through analyzing large number of vesicles based on their motion and knowing the analyzed sample volume, NTA allows for an estimation of particle concentration (Vestad et al, 2017).

From our results we can see that the ultracentrifugation technique produced an average of 2.49 $x10^9$ particles/ml from control conditioned media and 6.19 x 10^8 particles/ml from *Spp1* conditioned media. The mean size of particles ranged from 80nm to 150nm in size. This is within the expected size range of EVs (Doyle and Wang 2019). We can therefore conclude that we successfully isolated EVs from H9c2 conditioned media, and this is consistent with particles visually observed on the NTA equipment. Our NTA analysis also showed the presence of some larger particles in our sample, although they were smaller in number. These larger particles could be microvesicles, proteins or apoptotic bodies. A potential limitation to address in this experiment is the unequal number of EVs released from both control and *Spp1* transfected H9c2 cells. We have observed that the number of EVs (particles/ml) isolated from the *Spp1* condition is lower when compared to the control. Over expression of *Spp1* has been associated with increased myocyte apoptosis in the heart (Dalal et al. 2014; M. Singh, Dalal, and Singh 2014b). This indicates that when *Spp1* is overexpressed in H9c2 cells, it could cause cell death in our experimental set. This could lead to a decrease in number of cells post-transfection that results in a decrease in the number of EVs released. However, further research needs to be done to confirm.

Even though there is a growing interest in the role of EVs, the inconsistencies found in the various isolation protocols have created an obstacle to advance in this field (X. Li et al. 2019). The ultracentrifugation method has remained the preferred or gold

standard technique to determine homogeneity and state of aggregation of macromolecular or nanoparticle solutions (Ohlendieck and Harding 2018). The many advantages of using this method includes its cost as it is relatively cheap, the ability to use large volume samples that can result in highly enriched EV fractions. The larger vesicles will pellet first in a lower speed spin at 10,000 xg, and then an EV-free supernatant which is formed after a high-speed spin at 100,000 xg (Coughlan et al. 2020). However, this method comes with its flaws. It results in low isolation efficiency, sample loss and potential damage due to multiple high speed spins, low exosome recovery and purity, and it is a time-consuming and cumbersome operation (J. Chen et al. 2022; Coughlan et al. 2020). So other methods have been developed to help tackle these problems. These methods were developed based on isolation by size, immunoaffinity capture, and precipitation of EVs. However, these methods fail to singularly isolate a sub-type of EVs and usually result in a complex mixture of EVs and other components of the extracellular space (Doyle et al, 2019). We used the ultracentrifugation technique because it was a protocol previously established by our lab group, due to its low processing cost, the ability to work with large volumes of conditioned media and in turn isolating large volumes of EVs at once, and the absence of additional chemicals needed for this technique. To further confirm the successful isolation of EVs from H9c2 conditioned media, we sought to identify the presence of known exosomal specific markers in our samples.

Mass spectrometry (MS) has been frequently utilized to characterize EVs due to its specificity and sensitivity. It also has the potential to identify and characterize molecular composition of these vesicles and provides far greater information that any other EV characterisation methods. The main advantage of MS is its high confidence identification of EV components such as proteins, lipids or metabolites at high resolution with mass analysis (Jalaludin, Lubman, and Kim 2021; Pocsfalvi et al. 2016).

We conducted mass spectrometry analysis on EV samples isolated from H9c2 cells transfected with control and *Spp1* to characterize their protein content. Results showed high quantities of FBS proteins as well as cross-contamination of keratin from the surrounding environment while preparing the samples. This was rectified and the protocol was optimized by now preparing EV samples inside a sterilized

tissue culture hood. This will hopefully reduce environmental contaminants in our samples. There are several studies using EV-free serum obtained by ultracentrifugation to remove bovine serum EV and avoid changes in cell biology. FBS centrifugation for 18 hours has been shown to remove 95% of RNA-containing FBS EVs (Rosa-Fernandes et al. 2017). Even though we did follow this protocol during transfection and EV isolation, we did find a lot of contaminants due to the presence of FBS proteins. Despite the presence of these FBS contaminants, we were able to find proteins of interest that were common between the experimental *Spp1* samples.

Desmoplakin or *DSP* is a gene that encodes a protein, which anchors intermediate filaments to desmosomal plaques. Mutations in this gene can cause many cardiomyopathies and keratodermas (ncbi.nlm.nih.gov, 2019). Desmoplakin is an important component in maintaining the structural integrity of desmosome structures in cardiac muscle. Desmosome is a structure by which two adjacent cells are attached by forming protein plaques in the cell membrane linked by filaments (Kam et al, 2018)

Zinc Transporter ZIP8 is a protein synthesized by the gene *SLC39A8*. Its function is to act as a manganese and zinc influx transporter and it plays a role in manganese reabsorption in the proximal tubule of the kidney and in manganese uptake into the brain (Uniprot.org, 2019). It is also expressed in many tissues including the lung, liver, pancreas and heart. Highest expression is observed in the pancreas. Further analysis needs to be done by using IPA to identify whether these proteins are involved in the *Spp1* pathway.

Apart from using MS, we also used western blot technique to characterise EVs using EV specific proteins. The process by which cargo is sorted into EVs requires specific proteins that are associated with the endosomal sorting complex required for transport (ESCRT), such as members of the tetraspanin family (CD9, CD63 and CD81), ALG-2-interacting protein X (ALIX), tumour susceptibility gene 101 protein (TSG101) and many more. Therefore, these are the commonly used markers for the identification of EVs (Abhange et al. 2021)

Using ADAM10, Annexin XI, CD63 and C81 we were unable to detect any signal from our samples. This could be due to not loading enough EVs in the gel for the markers to detect a signal since we loaded the EV sample in the gel by volume rather than using particle concentration. Hence using the NTA data we collected from the EV samples, we calculated the particle concentration/ml of each of our EV samples. We then loaded in the wells, control and *Spp1* EVs with a particle concentration of 3.15×10^9 particles/ml and 1.96×10^9 particles/ml respectively and used exosomal marker TSG101. By doing this we were able to detect a signal at 52kDa in both control and *Spp1* EV samples and the untransfected EV control. We also loaded transfected control, *Spp1* and untransfected cell lysates as positive controls and were able to detect strong signals at 52kDa. We can thus conclude that our isolation protocol successfully isolated EVs from H9c2 conditioned media by using EV markers.

Western blotting technique is one of the commonly used methods for the analysis of EVs due to its ease of use, accessibility, and its ability to detect EV surface and internal proteins. However, a key drawback of this method is that its specificity and reproducibility are limited by the quality of antibody used.

We also would like to understand the uptake and release of *Spp1* by EVs released from H9c2 cells post-transfection. From previous EV-treated cell assays we know that *Spp1* is being trafficked by EVs however, the process by which this occurs is still unknown. There is currently no consensus regarding the pathway EVs follow to deliver content in the cytosol of target cells (Matthieu et al, 2019). A direct entry into the cytoplasm happens either by the fusion of EVs to the plasma membrane of target cells or endocytosis which appears to be the most common form of entry into target cells (Abels & Breakefield, 2016). If EVs do enter by endocytosis, then their cargo must be released by the same degradative pathway as endosomes mature into lysosome. Or they are released by the MVB plasma membrane fusion pathway (Abels & Breakefield, 2016).

When comparing the transfection and EV-treated cell assay results we observed that the average cell length is lower in cells that were treated with EVs isolated from *Spp1* conditioned media when compared to direct *Spp1* transfection. This size difference in EV-treated cells could be due to a loss in EV yield when using

ultracentrifugation to isolate EVs (Brennan et al, 2020). Some have theorized that EVs could be phagocytosed by target cells (Feng et al, 2010). Other considerations include selective uptake of vesicles by target cells based on their surface receptors. There are also further unanswered questions on how genetic material such as RNA is released and localized to the cytoplasm or nuclear compartments where they are functional upon uptake of vesicles into target cells (Lee et al, 2012).

We then repeated the experiment to determine whether EVs originating from different cell types can play a role in intercellular communication. We transfected HeLa cells, an immortal cell line derived from cervical cancer cells, with *Spp1* and then isolated EVs from the conditioned media. Our aim was to overlay H9c2 cells with HeLa-derived EVs to see if we observed a similar increase in cell size as we did with H9c2-derived EVs. The results of our experiment showed that when we did overlay untreated H9c2 cells with HeLa-derived EVs isolated from *Spp1* conditioned media, we observed a significant increase in their size. This suggests that *Spp1* is trafficked into EVs and then expressed when released at the target cell. This also shows that EVs originating from different cell types do have the ability to communicate with each other (Lotvall & Valadi, 2007). A review conducted by Liu et al (2018) stated that tumour derived EVs containing proteins, mRNAs and miRNA can be transferred between different cell types and to distant locations within a cell to influence the biological activities of tumors such as proliferation, invasion and metastasis, and stimulation of angiogenesis. Even though the experimental set up in the H9c2 and HeLa EV-treated assays remained the same (figures 5.5 and 5.6), the number of EVs (particles concentration/ml) added in both the conditions were not calculated. Instead, 100ul of EVs suspended in PBS of unknown concentration was added to each condition in the assay. Future works would include calculating the exact particle concentration/ml of each EV sample prior to its use in the assay.

The release and uptake of EVs can in fact induce changes to the target cells (Meldolesi, 2018). By using an EV-mediated communication pathway, EVs can synchronise surrounding cells to be in the same physiological state as its originating cell and can carry out similar functions in its cellular environment (Lotvall & Valadi, 2007). Having a deeper understanding of EV trafficking, targeting and uptake will

help answer important questions related to the function and importance of genetic material encapsulated and transferred by such vesicles (Lee et al, 2012).

Apart from DNA, proteins and lipid molecules, EVs also carry within themselves a wide range of RNA sequences that represent many biotypes of RNA. However, with the small size and heterogeneity of EVs along with an overall low concentration of RNA in EVs, it has created many complications when it comes to the characterisation of RNA cargo within the EVs (O'Brien et al. 2020). Early studies reported that EVs contains mRNAs and mature miRNA sequences, as well as ncRNAs, with a peak size of 200 nucleotides, extending out to 5Kb or more. By using RNA sequencing methods, the presence of various types of RNAs can be detected within the subpopulations of EVs that have been isolated from biological fluids and cell conditioned media (Turchinovich et al, 2019).

In the final part of this study, we sent RNA samples (EV-RNA) that were extracted from EVs isolated from H9c2 cells transfected with pcDNA (control) and *Spp1*. These samples were sent to Glasgow Polyomics to determine whether *Spp1* was transferred into EVs post-transfection, and to identify differentially expressed protein and long non-coding RNAs. From the initial test samples that were sent for analysis, the staff at Glasgow Polyomics measured the coverage in our samples and compared them to the libraries that were prepared using the Bioanalyser. Results from those initial samples revealed *Spp1* to be ranked 8th among the genes that were identified in the *Spp1* transfected EV-RNA sample with a coverage of 1178 RPKM when compared to the control group where *Spp1* was ranked 774th with a coverage of 2.84 RPKM. This indicates that *Spp1* was successfully transferred from the transfected H9c2 cells into the EVs with a much higher coverage found in the *Spp1* EV sample when compared to the pcDNA EV sample. A study conducted by Van Balkom et al. (2015) showed that coverage can appear to be more fragmented in EV samples whereas in cells read lengths were longer, showing more than 6070bp reads which resulted in a longer average read length in cells when compared to EVs. They concluded that fragments from long coding and non-coding RNAs can be seen at low levels in both cells and EVs. It was also found that among other RNA subtypes, lncRNA fragments was found to have a higher percentage in EVs when compared to cells (Van Balkom et al. 2015). Following the initial set of

samples, we submitted pcDNA control and *Spp1* EV RNA samples to Glasgow Polyomics for further analysis and it revealed that *Spp1* expression was significantly increased, with a fold change of 5598, in *Spp1* sample group compared to the control. There is strong evidence in the literature that RNA cargo of EVs can alter recipient cell gene expression and function (O'Brien et al. 1994) and this increased expression further confirms that *Spp1* was successfully transferred into the EVs post-transfection, thus mediating H9c2 cell size.

The differences in EV RNA cargo content are due to cell type-specific RNA expression differences, different EV and RNA isolation methods, and the use of different NGS library preparation protocols and sequencing platforms (Turchinovich, Drapkina, and Tonevitsky 2019). Comparing expression levels across different samples and experiments is difficult and requires complication normalization methods however, these are still under active development. In the case of exosomal transcriptomes it is even more complex as it is very different compared to cellular transcriptomes (Jenjaroenpun et al. 2013). However, RNAseq does provides the most comprehensive characterisation of exosomal transcriptomes, and it can be used in functional modelling studies or in the discovery of biomarkers (Prendergast et al. 2018).

5.5 Appendix

Table 5.4: Proteins identified in EV samples from NCBIprot and Swissprot databases

Condition	Proteins Identified – NCBIprot Database
pcDNA1 (n=3)	**Q6IMF3.1** - RecName: Full=Keratin, type II cytoskeletal 1; AltName: Full=Cytokeratin-1; Short=CK-1; AltName: Full=Keratin-1; Short=K1; AltName: Full=Type-II keratin Kb1
Spp1 (n=3)	**NONE**
pcDNA1 (02/02/18) **Spp1 (02/02/18)**	**NP_775443.1** - hemiferrin, transferrin-like protein [Rattus norvegicus] **NP_599153.2** - serum albumin precursor [Rattus norvegicus] **P02773.1** - RecName: Full=Alpha-fetoprotein; AltName: Full=Alpha-1-fetoprotein; AltName: Full=Alpha-fetoglobulin; Flags: Precursor **EDM04518.1** - rCG34955 [Rattus norvegicus]
pcDNA (27/02/18) **Spp1 (02/02/18)**	**Q6P6Q2.1** - RecName: Full=Keratin, type II cytoskeletal 5; AltName: Full=Cytokeratin-5; Short=CK-5; AltName: Full=Keratin-5; Short=K5; AltName: Full=Type-II keratin Kb5
pcDNA1 (02/02/18) **Spp1 (02/02/18)** **pcDNA1 (13/02/18)**	**Q6IMF3.1** - RecName: Full=Keratin, type II cytoskeletal 1; AltName: Full=Cytokeratin-1; Short=CK-1; AltName: Full=Keratin-1; Short=K1; AltName: Full=Type-II keratin Kb1

Condition	Proteins Identified – Swissprot Database
pcDNA1 (n=3)	**P02769** - Serum albumin OS=Bos taurus OX=9913 GN=ALB PE=1 SV=4 **P12763 -** Alpha-2-HS-glycoprotein OS=Bos taurus OX=9913 GN=AHSG PE=1 SV=2 **A5A6M6 -** Keratin, type II cytoskeletal 1 OS=Pan troglodytes OX=9598 GN=KRT1 PE=2 SV=1 **P15636 -** Protease 1 OS=Achromobacter lyticus OX=224 PE=1 SV=1 **P00761 -** Trypsin OS=Sus scrofa OX=9823 PE=1 SV=1 **P11679 -** Keratin, type II cytoskeletal 8 OS=Mus musculus OX=10090 GN=Krt8 PE=1 SV=4 **P35527 -** Keratin, type I cytoskeletal 9 OS=Homo sapiens OX=9606 GN=KRT9 PE=1 SV=3 **Q6EIZ0 -** Keratin, type I cytoskeletal 10 OS=Canis lupus familiaris OX=9615 GN=KRT10 PE=2 SV=1
Spp1 (n=3)	**P35527 -** Keratin, type I cytoskeletal 9 OS=Homo sapiens OX=9606 GN=KRT9 PE=1 SV=3 **P00761 -** Trypsin OS=Sus scrofa OX=9823 PE=1 SV=1
pcDNA1 (02/02/18) **Spp1 (02/02/18)**	**Q29443 -** Serotransferrin OS=Bos taurus OX=9913 GN=TF PE=2 SV=1 **P34955 -** Alpha-1-antiproteinase OS=Bos taurus OX=9913 GN=SERPINA1 PE=1 SV=1 **P12725 -** Alpha-1-antiproteinase OS=Ovis aries OX=9940 PE=1 SV=1 **P49064 -** Serum albumin OS=Felis catus OX=9685 GN=ALB PE=1 SV=1 **P49822 -** Serum albumin OS=Canis lupus familiaris OX=9615 GN=ALB PE=1 SV=3 **P07724 -** Serum albumin OS=Mus musculus OX=10090 GN=Alb PE=1 SV=3 **P35908 -** Keratin, type II cytoskeletal 2 epidermal OS=Homo sapiens OX=9606 GN=KRT2 PE=1 SV=2 **Q7SIH1 -** Alpha-2-macroglobulin OS=Bos taurus OX=9913 GN=A2M PE=1 SV=2
pcDNA (27/02/18) **Spp1 (02/02/18)**	**A5A6M8** - Keratin, type II cytoskeletal 5 OS=Pan troglodytes OX=9598 GN=KRT5 PE=2 SV=1 **P49065** - Serum albumin OS=Oryctolagus cuniculus OX=9986 GN=ALB PE=1 SV=2

Condition	Proteins Identified – NCBIprot Database
pcDNA1 (02/02/18)	**NP_001008825.1** - keratin, type II cytoskeletal cochleal [Rattus norvegicus] **NP_036767.1** - anionic trypsin-1 precursor [Rattus norvegicus] **AAA40784.1** - ATP synthase alpha subunit precursor (EC 3.6.1.3), partial [Rattus norvegicus] **EDL26405.1** - mCG15232, isoform CRA_f [Mus musculus] **EDM04013.1** - rCG34636, isoform CRA_b [Rattus norvegicus] **XP_002725326.3** - PREDICTED: histone H3.1 [Rattus norvegicus] **AGX25484.1** - Toll like receptor 4, partial [Rattus tanezumi]
Spp1 (02/02/18)	**NP_001008808.1** - keratin, type II cytoskeletal 73 [Rattus norvegicus] **XP_017452928.**1 - PREDICTED: keratin, type I cytoskeletal 10 isoform X3 [Rattus norvegicus] **XP_001065013.1** - PREDICTED: keratin, type II cytoskeletal 6A-like isoform X3 [Rattus norvegicus] **AAB21182.1** - Immunoglobulin light chain [Rattus sp.] **NP_001008751.1** - keratin, type I cytoskeletal 14 [Rattus norvegicus] **NP_001008899.1** - keratin, type II cytoskeletal 2 epidermal [Rattus norvegicus] **EDM06018.1** - keratin complex 1, acidic, gene 19, isoform CRA_b [Rattus norvegicus] **P24090.2** - RecName: Full=Alpha-2-HS-glycoprotein; AltName: Full=59 kDa bone sialic acid-containing protein; Short=BSP; AltName: Full=Fetuin-A; AltName: Full=Glycoprotein PP63; Flags: Precursor **AAI00088.1** - LOC498793 protein, partial [Rattus norvegicus] **NP_001091.1** - actin, alpha skeletal muscle [Homo sapiens] **XP_017443206.1** - PREDICTED : desmoplakin isoform X2 [Rattus norvegicus] **NP_001011952.1** - zinc transporter ZIP8 precursor [Rattus norvegicus] **EDL86887.1** - Keratin 82, *Krt82*, Rat
Spp1 (13/02/18)	**NO SIGNIFICANT HITS**
pcDNA1 (27/02/18)	**P02770.2** - RecName: Full=Serum albumin; Flags: Precursor
Spp1 (27/02/18)	**NO SIGNIFICANT HITS**

Conditions	Proteins Identified - Swissprot Database
pcDNA1 (02/02/18)	P00762 - Anionic trypsin-1 OS=Rattus norvegicus OX=10116 GN=Prss1 PE=1 SV=1 O46375 - Transthyretin OS=Bos taurus OX=9913 GN=TTR PE=1 SV=1 Q29S21 - Keratin, type II cytoskeletal 7 OS=Bos taurus OX=9913 GN=KRT7 PE=2 SV=1 Q9MYN8 - Transthyretin OS=Erinaceus europaeus OX=9365 GN=TTR PE=2 SV=1 C0Q783 - UPF0227 protein YcfP OS=Salzincmonella paratyphi C (strain RKS4594) OX=476213 GN=ycfP PE=3 SV=1 A5A6H5 - ATP synthase subunit alpha, mitochondrial OS=Pan troglodytes OX=9598 GN=ATP5F1A PE=2 SV=1 O93532 - Keratin, type II cytoskeletal cochleal OS=Gallus gallus OX=9031 PE=2 SV=1 Q19AZ8 - Prothrombin OS=Sus scrofa OX=9823 GN=F2 PE=2 SV=1 Q3SZR3 - Alpha-1-acid glycoprotein OS=Bos taurus OX=9913 GN=ORM1 PE=2 SV=1 P16972 - Ferredoxin-2, chloroplastic OS=Arabidopsis thaliana OX=3702 GN=FD2 PE=1 SV=1 D0VX09 - Hemoglobin subunit alpha OS=Pteropus giganteus OX=143291 GN=HBA PE=1 SV=1 Q5R440 - Calnexin OS=Pongo abelii OX=9601 GN=CANX PE=2 SV=2 Q183G0 - Serine hydroxymethyltransferase OS=Peptoclostridium difficile (strain 630) OX=272563 GN=glyA PE=3 SV=1 P90519 - Elongation factor 1-alpha OS=Cryptosporidium parvum OX=5807 PE=2 SV=1
pcDNA1 (13/02/18)	P13664 - Major surface antigen p30 OS=Toxoplasma gondii OX=5811 PE=1 SV=1
Spp1 (02/02/18)	P13645 - Keratin, type I cytoskeletal 10 OS=Homo sapiens OX=9606 GN=KRT10 PE=1 SV=6 P04264 - Keratin, type II cytoskeletal 1 OS=Homo sapiens OX=9606 GN=KRT1 PE=1 SV=6 P01876 - Immunoglobulin heavy constant alpha 1 OS=Homo sapiens OX=9606 GN=IGHA1 PE=1 SV=2

Conditions	Proteins Identified - Swissprot Database
	Q7Z794 - Keratin, type II cytoskeletal 1b OS=Homo sapiens OX=9606 GN=KRT77 PE=2 SV=3 P0DOX7 - Immunoglobulin kappa light chain OS=Homo sapiens OX=9606 PE=1 SV=1 P02533 - Keratin, type I cytoskeletal 14 OS=Homo sapiens OX=9606 GN=KRT14 PE=1 SV=4 Q6B411 - Lysozyme C, milk isozyme OS=Bos taurus OX=9913 PE=2 SV=1 P02538 - Keratin, type II cytoskeletal 6A OS=Homo sapiens OX=9606 GN=KRT6A PE=1 SV=3 C1IIX1 - Lysozyme C OS=Fenneropenaeus merguiensis OX=71412 PE=2 SV=1 Q9NZT1 - Calmodulin-like protein 5 OS=Homo sapiens OX=9606 GN=CALML5 PE=1 SV=2 Q9UGM3 - Deleted in malignant brain tumors 1 protein OS=Homo sapiens OX=9606 GN=DMBT1 PE=1 SV=2 Q2KJF1 - Alpha-1B-glycoprotein OS=Bos taurus OX=9913 GN=A1BG PE=1 SV=1 Q3SY84 - Keratin, type II cytoskeletal 71 OS=Homo sapiens OX=9606 GN=KRT71 PE=1 SV=3 O93429 - Serotransferrin OS=Paralichthys olivaceus OX=8255 GN=tf PE=2 SV=1 Q8CGX0 - Insulin-like growth factor 2 mRNA-binding protein 1 OS=Rattus norvegicus OX=10116 GN=Igf2bp1 PE=1 SV=1 P19001 - Keratin, type I cytoskeletal 19 OS=Mus musculus OX=10090 GN=Krt19 PE=1 SV=1 P19823 - Inter-alpha-trypsin inhibitor heavy chain H2 OS=Homo sapiens OX=9606 GN=ITIH2 PE=1 SV=2 P15924 - Desmoplakin OS=Homo sapiens OX=9606 GN=DSP PE=1 SV=3 P01044 - Kininogen-1 OS=Bos taurus OX=9913 GN=KNG1 PE=1 SV=1 P28800 - Alpha-2-antiplasmin OS=Bos taurus OX=9913 GN=SERPINF2 PE=1 SV=2 A9INS9 - UDP-3-O-acylglucosamine N-acetyltransferase OS=Bordetella petrii (strain ATCC BAA-461 / DSM 12804 / CCUG 43448) OX=340100 GN=lpxD PE=3 SV=1
Spp1 (27/02/18)	Q9ZU46 - Receptor protein kinase-like protein ZAR1 OS=Arabidopsis thaliana OX=3702 GN=ZAR1 PE=1 SV=1

Chapter 6. General Discussion

In this thesis, we conducted a range of experiments to identify *Spp1* as a key modulator of LVH and fibrosis. With a combination of $SHRSP_{Gla}$, WKY_{Gla} and the chromosome 14 congenic strains and microarray gene expression profiling, positional candidate genes for LVMI that map to the minimal transferred congenic interval on chromosome 14. *Spp1* was identified as it mapped to the congenic interval. To determine that overexpression of *Spp1* in the early development of $SHRSP_{Gla}$ increase its susceptibility to cardiac hypertrophy and fibrosis, *Spp1* expression levels were quantified and compared in gestational day 18 rat hearts from $SHRSP_{Gla}$, and WKY_{Gla} rat hearts, *Spp1*. With the generation of *Spp1* promoter constructs from both $SHRSP_{Gla}$, and WKY_{Gla} strains, we also compared transcriptional activity of these constructs. We then established and characterised the minimally invasive TAC pressure overload model of LVH in the WKY, WKY.SP_{Gla}14a congenic (chr 14 congenic) strain, SHRSP *Spp1* WT and SHRSP *Spp1*^{em1} rats to challenge the cardiovascular system in these rat models and investigate the role of *Spp1* in cardiac disease development. After which, we aimed to fully characterise effect of *Spp1* overexpression in the H9c2 cell model, and the trafficking of *Spp1* mediated by EVs produced from these cells transfected with *Spp1*.

In chapter 3 of this thesis, we investigated the overexpression of *Spp1* in the early development of $SHRSP_{Gla}$ leading to increased levels of cardiac hypertrophy and fibrosis. At 5 weeks of age there is small but significant increase in the size of the heart of the $SHRSP_{Gla}$ compared to WKY_{Gla} prior to onset of hypertension, while at 16 weeks SHRSP exhibits established LVH as well as adult BP which is significantly higher in the SHRSP. The significant increase in LVMI is observed before the onset of hypertension thus indicating that blood pressure is independent development of LVH. By using chromosome 14 congenic strains and gene profiling, a QTL for LVMI was identified on chromosome 14 and *Spp1* was identified as a positional candidate gene. qRT-PCR on gestational day 18 rat hearts from the $SHRSP_{Gla}$ strain showed significant increase in *Spp1* expression even before the onset of disease when compared to the WKY_{Gla} strains and these results were consistent with our hypothesis and aligned with the results from previous work conducted in the lab WKY_{Gla} and $SHRSP_{Gla}$ whole neonatal heart tissues and isolated primary neonatal cardiomyocytes.

To identify genes that were downstream and were connected to *Spp1* and the enlargement of the heart we also analysed the differentially expressed genes found common between 5 weeks vs neonatal SHRSP and WKY.SP_{Gla}14a strains. Out of the 101 genes that were found, *DES, MMP14, MYOM1, CTSD* and *SLC25A11* were identified downstream of *Spp1* and were connected to cardiac enlargement or hypertrophy.

To identify genes that were downstream to *Spp1* and the enlargement of the heart we also analysed the differentially expressed genes found common between 5 weeks vs neonatal SHRSP and WKY.SP_{Gla}14a strains. Out of the 101 genes that were found, *DES, MMP14, MYOM1, CTSD* and *SLC25A11* were identified downstream of *Spp1* and were connected to cardiac enlargement or hypertrophy. Unfortunately, we were unable to perform any further analysis on this preliminary data. Future work could include conducting an in-depth analysis using IPA to analyze pathways relevant of *Spp1* and the five genes connected to the cardiac hypertrophy phenotype. By analyzing the differentially regulated genes and comparing them at the different time points between the two strains could identify and implicate any relevant cardiovascular pathways (Yu, Gu, and Yi 2016).

We also conducted promoter studies to evaluate the potential functional effects of the SNPs in the upstream region of *Spp1*. Dual luciferase assay was conducted to compare transcriptional activities using the generated segments of the *Spp1* promoter from the $SHRSP_{Gla}$ and WKY_{Gla} strains and co-transfecting them into H9c2 cells. By observing changes in the constructs, we can determine that we have successfully captured genetic changes with the promoter constructs and compare these changes between the two strains. Distance of the promoter fragments from the luciferase gene is also key. If the fragments are further away it could result in low transcriptional activity. It could cause an imbalance between signal and noise resulting in poor luciferase activity (De Bleser et al. 2007).Therefore, the largest promoter fragment of size 5.2kb was very important for us to generate. Its distance from the transcriptional start site and its potential to influence luciferase activity was closer when compared to the others. However, we were unsuccessful in generating this construct. Future work in this area would be to successfully generate the larger

promoter construct. This construct could help identify potential genetic changes and determine whether there is a SNP driven phenomenon.

In chapter 4 of this thesis, we investigated the TAC effect on the stroke-prone spontaneously hypertensive (SHRSP *Spp1* WT) rats, SHRSP *Spp1*^{em1} rat, WKY.SP$_{Gla}$14a chromosome 14 congenic strain and the reference control strain, the Wistar Kyoto (WKY) rat. We aimed to observe and analyse phenotypic changes that result in the heart due to the constriction placed on the aorta and how these changes differed between the four strains. There are several studies that have shown TAC being conducted on various rodent models of heart disease (Bosch et al. 2021; Kleiner et al. 2021; Nakao et al. 2022; Richards et al. 2019) however, our study is the first to use TAC in a stroke-prone model. At the end of our 8-week long study, we successfully established the TAC model in our WKY and chromsome 14 congenic strains by demonstrating a significant increase in LVH 8-weeks post-TAC surgery. Our sacrifice data also showed significant increases in LVMI ratio in the WKY and chromosome 14 congenic TAC rats indicating that a hypertrophic response in the heart was induced due to TAC surgery. However, we were unable to show any amplified hypertrophic response and any progression to heart failure in the hearts of the SHRSP *Spp1* WT rats, SHRSP *Spp1*^{em1} rats. The sacrifice data also showed no differences in LVMI indicating that the hearts were already hypertrophied and the surgery could not push their LVMI any further. This could also be due to short timeframe of the study and the ability of the SHRSP strain to compensate for increased high BP. It has been reported that TAC for a duration of 8 weeks can induce heart failure in C57BL/6NTac mice (Garcia-Menendez et al. 2013). In our study we chose 8 weeks due to welfare concerns as we were using stroke prone animals and were unaware of when they would go into heart failure due to the constriction placed in the aorta. However, as we did not observe this progression to heart failure, future work in this area could include extending the length of study to 12 weeks as the rats were well compensated.

In chapter 5 of this thesis, we investigated what functional response will the overexpression of *Spp1* cause in the H9c2 cell model. The H9c2 cardiac cell line was used as a model in our experiments to study the overexpression of *Spp1*. The H9c2 cell line derived from embryonic rat ventricle serves as a suitable cellular

model of cardiac hypertrophy (Kimes and Brandt 1976). Watkins et al have also shown that these cells are a suitable model for in vitro studies on cardiac hypertrophy and for molecular studies in heart development and disease (Watkins, Borthwick, and Arthur 2011). Using this cell model, we were able to confirm a significant increase in cell size when *Spp1* is transfected into H9c2 cells when compared to the transfected control group. To further understand the how overexpression of *Spp1* promotes an increase in cell size, we investigated the role of EVs and how *Spp1* trafficking is mediated throught he production of EVs from *Spp1* transfected H9c2 cells. EVs have been proposed as a novel mode of intercellular communication for both long and short range signalling events (Dickhout and Koenen 2018; Hafiane and Daskalopoulou 2018). In this chapter we used the ultracentrifugation method to isolate EVs. Even with the successful isolation of EVs from our transfected H9c2 cells, this technique, while being cost-effective, has its flaws which includes vesicle clumping, its long duration, potential EV damage, low reproducibilty and limitede samples that can be processed (Konoshenko et al. 2018). Future work could include using a combination of EV isolation and separation methods to yield EVs with the best quality since diverse origin, complex nature and heterogeneity of EVs require sophisticated isolation approaches (Gandham et al. 2020; Liangsupree, Multia, and Riekkola 2021).

During the formation of EVs, they can maintain surface molecules from their parent cells, as well as selected cytosolic content such as proteins, lipids and RNA (Fleury, Martinez, and Le Lay 2014). Our results showed that when EVs isolated *Spp1* conditioned media are overlayed onto an untreated batch of H9c2 cells, a significant increase in their size occurs. From this we can also conclude that *Spp1* is trafficked into EVs and are released from cells as cargo into the media. The amount and content of EVs released from cells can vary under different pathophysiological conditions. However, in our study we have observed that the amount of EVs released from *Spp1* transfected conditions are much lower in number (particles/ml) when compared to the control condition. Studies have shown that *Spp1* over expression has resulted in cardiomyocyte loss. This loss could result in a decrease in the number of EVs released (Shirakawa and Sano 2021). Future work could include investigating the relationship between *Spp1* and cell death as this can impact downstream experiments using EVs released from this condition.

Mass spectrometry analysis of EVs isolated from *Spp1* transfected H9c2 cells resulted in high quantities of FBS proteins as well as cross contamination of keratin from the surrounding environment when the samples were being prepared. This was rectified by preparing EV samples inside the sterilized laminary flow hood. However, even with the FBS contaminants, with preliminary analysis we were able to identify in common between the *Spp1* experimental and control samples desmoplakin (*DSP*) and Zinc Transporter ZIP8 protein, synthesized by the gene *SLC39A8*. *DSP* is essential for normal myocardial development and the maintenance of its structural functions (Yuan et al. 2021). *SLC39A8* has also been revealed as a potential new regulator of ventricular myocardial development (Lin et al. 2018). Future work would include using IPA to investigate these genes further and identify whether they are involved in the *Spp1* pathway and contribute towards the development of cardiac hypertrophy.

And lastly, RNAseq analysis was undertaken to assess protein and lncRNA content within the EVs. RNA was extracted from EVs isolated from *Spp1* transfected H9c2 cells and control. Coverage analysis from the the first set of samples revealed *Spp1* to be ranked 8th among the genes that were identified in the *Spp1* transfected EV-RNA samples with a coverage of 1178 RPKM, whereas the control ranked *Spp1* at 774th with a coverage of 2.84 RPKM. Thus indicating that *Spp1* was sucessfully transferred from transfected H9c2 cells into the EVs with a higher coverage found in the *Spp1* EV sample comapred to the pcDNA EV sample. Following this, further *Spp1* EV-RNA and control samples were submitted for further analysis and this revealed *Spp1* to be significantly increased with a fold change of 5598 in the *Spp1* EV-RNA sample when compared to the control. This further confirms that *Spp1* was successfully transferred into the EVs post-transfection, thus mediating cell size. Future work in this area would include a detailed analysis of the RNAseq data to assess RNA content within the EVs and to use IPA to generate plausible regulatory networks from this datasets that could provide valuable insights into the identification of biological networks and processes linked to hypertrophy.

EVs have also been identified as a readily accessible source of biomarkers. They have gained significant interest as potential therapeutic tools in cardiovascular and regenerative medicine due to their pro-angiogenic and cardioprotective properties,

and the opportunities to deliver specific agents to target cells of the cardiovascular system (Chong et al. 2019; Fleury, Martinez, and Le Lay 2014). EVs are circulated in a stable condition in all kinds of body fluids. EV-associated proteins and RNAs have been reported as tumour biomarkers for diagnosing cancer or monitoring cancer progression (Urabe et al. 2020). Studies have shown the importance of *Spp1* in cardiovascular pathogenesis. The effects of *Spp1* are disease-specific and consists of both positive and negative effects. Hence, *Spp1* can also be used as a useful biomarker for predicting the risk of CVDs. However, *Spp1* itself cannot be targeted treatments. Instead, the process by which *Spp1* is produced and release in specific disease conditions should be the target of therapy (Shirakawa and Sano 2021)

In conclusion, the work presented in this thesis demonstrates the important role *Spp1* plays in LVH and fibrosis in cardiovascular diseases. Even though our data is significant, a need for further research and experiments still remains which will be conducted in future work. It will also help explain the pathophysiology of CVD development in our animal models leading to the potential development of new therapeutic tools to treat or prevent cardiac hypertrophy.

References

ABCTB Investigators, EMBRACE, GEMO Study Collaborators, HEBON, kConFab/AOCS Investigators, NBSC Collaborators, Roger L Milne, et al. 2017. 'Identification of Ten Variants Associated with Risk of Estrogen-Receptor-Negative Breast Cancer'. *Nature Genetics* 49 (12): 1767–78. https://doi.org/10.1038/ng.3785.

Abdelaziz Mohamed, Iman, Alain-Pierre Gadeau, Anwarul Hasan, Nabeel Abdulrahman, and Fatima Mraiche. 2019. 'Osteopontin: A Promising Therapeutic Target in Cardiac Fibrosis'. *Cells* 8 (12): 1558. https://doi.org/10.3390/cells8121558.

Abels, Erik R., and Xandra O. Breakefield. 2016. 'Introduction to Extracellular Vesicles: Biogenesis, RNA Cargo Selection, Content, Release, and Uptake'. *Cellular and Molecular Neurobiology* 36 (3): 301–12. https://doi.org/10.1007/s10571-016-0366-z.

Abhange, Komal, Amy Makler, Yi Wen, Natasha Ramnauth, Wenjun Mao, Waseem Asghar, and Yuan Wan. 2021. 'Small Extracellular Vesicles in Cancer'. *Bioactive Materials* 6 (11): 3705–43. https://doi.org/10.1016/j.bioactmat.2021.03.015.

'Abstracts from the 2020 Annual Scientific Meeting of the British and Irish Hypertension Society (BIHS)'. 2020. *Journal of Human Hypertension* 34 (S1): 1–20. https://doi.org/10.1038/s41371-020-00410-6.

Ailawadi, Shaina, Xiaohong Wang, Haitao Gu, and Guo-Chang Fan. 2015. 'Pathologic Function and Therapeutic Potential of Exosomes in Cardiovascular Disease'. *Biochimica et Biophysica Acta (BBA) - Molecular Basis of Disease* 1852 (1): 1–11. https://doi.org/10.1016/j.bbadis.2014.10.008.

Akers, Johnny C., David Gonda, Ryan Kim, Bob S. Carter, and Clark C. Chen. 2013. 'Biogenesis of Extracellular Vesicles (EV): Exosomes, Microvesicles, Retrovirus-like Vesicles, and Apoptotic Bodies'. *Journal of Neuro-Oncology* 113 (1): 1–11. https://doi.org/10.1007/s11060-013-1084-8.

Akinrinade, Oyediran, Laura Ollila, Sanna Vattulainen, Jonna Tallila, Massimiliano Gentile, Pertteli Salmenperä, Hannele Koillinen, et al. 2015. 'Genetics and Genotype–Phenotype Correlations in Finnish Patients with Dilated Cardiomyopathy'. *European Heart Journal* 36 (34): 2327–37. https://doi.org/10.1093/eurheartj/ehv253.

Akira, Kazuki, Misako Imachi, and Takao Hashimoto. 2005. 'Investigations into Biochemical Changes of Genetic Hypertensive Rats Using 1H Nuclear Magnetic Resonance-Based Metabonomics'. *Hypertension Research* 28 (5): 425–30. https://doi.org/10.1291/hypres.28.425.

Albanese, Manuel, Yen-Fu Adam Chen, Corinna Hüls, Kathrin Gärtner, Takanobu Tagawa, Ernesto Mejias-Perez, Oliver T. Keppler, et al. 2021. 'MicroRNAs Are Minor Constituents of Extracellular Vesicles That Are Rarely Delivered to Target Cells'. Edited by Lin He. *PLOS Genetics* 17 (12): e1009951. https://doi.org/10.1371/journal.pgen.1009951.

Amabile, Nicolas, Susan Cheng, Jean Marie Renard, Martin G. Larson, Anahita Ghorbani, Elizabeth McCabe, Gabriel Griffin, et al. 2014. 'Association of Circulating Endothelial Microparticles with Cardiometabolic Risk Factors in the Framingham Heart Study'. *European Heart Journal* 35 (42): 2972–79. https://doi.org/10.1093/eurheartj/ehu153.

Amini, Maedeh, Farid Zayeri, and Masoud Salehi. 2021. 'Trend Analysis of Cardiovascular Disease Mortality, Incidence, and Mortality-to-Incidence Ratio: Results from Global Burden of Disease Study 2017'. *BMC Public Health* 21 (1): 401. https://doi.org/10.1186/s12889-021-10429-0.

Anderson, Mark E., Joan Heller Brown, and Donald M. Bers. 2011. 'CaMKII in Myocardial Hypertrophy and Heart Failure'. *Journal of Molecular and Cellular Cardiology* 51 (4): 468–73. https://doi.org/10.1016/j.yjmcc.2011.01.012.

Andersson, Daniel C., Jérémy Fauconnier, Takashi Yamada, Alain Lacampagne, Shi-Jin Zhang, Abram Katz, and Håkan Westerblad. 2011. 'Mitochondrial Production of Reactive Oxygen Species Contributes to the β-Adrenergic Stimulation of Mouse Cardiomycytes: ROS Increase Cardiomyocyte Ca $^{2+}$ and Contraction'. *The Journal of Physiology* 589 (7): 1791–1801. https://doi.org/10.1113/jphysiol.2010.202838.

Antoniucci, D, F Seccareccia, A Menotti, E V Dovellini, P L Prati, F Rovelli, and P F Fazzini. 1997. 'Prevalence and Correlates of Echocardiographic Determined Left Ventricular Hypertrophy in 2318 Asymptomatic Middle-Aged Men: The ECCIS Project. Epidemiolgia e Clinica Della Cardiopatia Ischemica Silente' 27 (4): 363–69.

Armstrong, Nicola J., Thomas C. Brodnicki, and Terence P. Speed. 2006. 'Mind the Gap: Analysis of Marker-Assisted Breeding Strategies for Inbred Mouse Strains'. *Mammalian Genome* 17 (4): 273–87. https://doi.org/10.1007/s00335-005-0123-y.

Arnett, Donna K. 2000. 'Genetic Contributions to Left Ventricular Hypertrophy'. *Current Hypertension Reports* 2 (1): 50–55. https://doi.org/10.1007/s11906-000-0058-3.

Arnett, Donna K., Lisa de las Fuentes, and Ulrich Broeckel. 2004. 'Genes for Left Ventricular Hypertrophy'. *Current Hypertension Reports* 6 (1): 36–41. https://doi.org/10.1007/s11906-004-0009-5.

Arraud, N., C. Gounou, R. Linares, and A. R. Brisson. 2015. 'A Simple Flow Cytometry Method Improves the Detection of Phosphatidylserine-exposing Extracellular Vesicles'. *Journal of Thrombosis and Haemostasis* 13 (2): 237–47. https://doi.org/10.1111/jth.12767.

Arroyo, J. D., J. R. Chevillet, E. M. Kroh, I. K. Ruf, C. C. Pritchard, D. F. Gibson, P. S. Mitchell, et al. 2011. 'Argonaute2 Complexes Carry a Population of Circulating MicroRNAs Independent of Vesicles in Human Plasma'. *Proceedings of the National Academy of Sciences* 108 (12): 5003–8. https://doi.org/10.1073/pnas.1019055108.

Ashcroft, B. A., J. de Sonneville, Y. Yuana, S. Osanto, R. Bertina, M. E. Kuil, and T. H. Oosterkamp. 2012. 'Determination of the Size Distribution of Blood Microparticles Directly in Plasma Using Atomic Force Microscopy and Microfluidics'. *Biomedical Microdevices* 14 (4): 641–49. https://doi.org/10.1007/s10544-012-9642-y.

Ashizawa, N, K Graf, Y S Do, T Nunohiro, C M Giachelli, W P Meehan, T L Tuan, and W A Hsueh. 1996. 'Osteopontin Is Produced by Rat Cardiac Fibroblasts and Mediates A(II)-Induced DNA Synthesis and Collagen Gel Contraction.' *Journal of Clinical Investigation* 98 (10): 2218–27. https://doi.org/10.1172/JCI119031.

Aung, Nay, Jose D. Vargas, Chaojie Yang, Claudia P. Cabrera, Helen R. Warren, Kenneth Fung, Evan Tzanis, et al. 2019. 'Genome-Wide Analysis of Left Ventricular Image-Derived Phenotypes Identifies Fourteen Loci Associated With Cardiac Morphogenesis and Heart Failure Development'. *Circulation* 140 (16): 1318–30. https://doi.org/10.1161/CIRCULATIONAHA.119.041161.

Averill, D B, C M Ferrario, R C Tarazi, S Sen, and R Bajbus. 1976. 'Cardiac Performance in Rats with Renal Hypertension.' *Circulation Research* 38 (4): 280–88. https://doi.org/10.1161/01.RES.38.4.280.

Ávila-Flores, Antonia, Javier Arranz-Nicolás, and Isabel Mérida. 2019. 'Transcriptional Activity of FOXO Transcription Factors Measured by Luciferase Assays'. In *FOXO Transcription Factors*, edited by Wolfgang Link, 1890:91–102. Methods in Molecular Biology. New York, NY: Springer New York. https://doi.org/10.1007/978-1-4939-8900-3_8.

Baietti, Maria Francesca, Zhe Zhang, Eva Mortier, Aurélie Melchior, Gisèle Degeest, Annelies Geeraerts, Ylva Ivarsson, et al. 2012. 'Syndecan–Syntenin–ALIX Regulates the Biogenesis of Exosomes'. *Nature Cell Biology* 14 (7): 677–85. https://doi.org/10.1038/ncb2502.

Balkom, Bas W. M. van, Almut S. Eisele, D. Michiel Pegtel, Sander Bervoets, and Marianne C. Verhaar. 2015. 'Quantitative and Qualitative Analysis of Small RNAs in Human Endothelial Cells and Exosomes Provides Insights into Localized RNA Processing, Degradation and Sorting'. *Journal of Extracellular Vesicles* 4 (1): 26760. https://doi.org/10.3402/jev.v4.26760.

Bang, Claudia, Sandor Batkai, Seema Dangwal, Shashi Kumar Gupta, Ariana Foinquinos, Angelika Holzmann, Annette Just, et al. 2014. 'Cardiac Fibroblast–Derived MicroRNA Passenger Strand-Enriched Exosomes Mediate Cardiomyocyte Hypertrophy'. *Journal of Clinical Investigation* 124 (5): 2136–46. https://doi.org/10.1172/JCI70577.

Baranyai, Tamás, Kata Herczeg, Zsófia Onódi, István Voszka, Károly Módos, Nikolett Marton, György Nagy, et al. 2015. 'Isolation of Exosomes from Blood Plasma: Qualitative and Quantitative Comparison of Ultracentrifugation and Size Exclusion Chromatography Methods'. Edited by Marco Rito-Palomares. *PLOS ONE* 10 (12): e0145686. https://doi.org/10.1371/journal.pone.0145686.

Barger, Philip M., Jon M. Brandt, Teresa C. Leone, Carla J. Weinheimer, and Daniel P. Kelly. 2000. 'Deactivation of Peroxisome Proliferator–Activated Receptor-α during Cardiac Hypertrophic Growth'. *Journal of Clinical Investigation* 105 (12): 1723–30. https://doi.org/10.1172/JCI9056.

Barile, L., V. Lionetti, E. Cervio, M. Matteucci, M. Gherghiceanu, L. M. Popescu, T. Torre, F. Siclari, T. Moccetti, and G. Vassalli. 2014. 'Extracellular Vesicles from Human Cardiac Progenitor Cells Inhibit Cardiomyocyte Apoptosis and Improve Cardiac Function after Myocardial Infarction'. *Cardiovascular Research* 103 (4): 530–41. https://doi.org/10.1093/cvr/cvu167.

Barve, Ruteja A., C. Charles Gu, Wei Yang, Jian Chu, Victor G. Dávila-Román, and Lisa de las Fuentes. 2016. 'Genetic Association of Left Ventricular Mass Assessed by M-Mode and Two-Dimensional Echocardiography'. *Journal of Hypertension* 34 (1): 88–96. https://doi.org/10.1097/HJH.0000000000000765.

Bebelman, Maarten P., Martine J. Smit, D. Michiel Pegtel, and S. Rubina Baglio. 2018. 'Biogenesis and Function of Extracellular Vesicles in Cancer'. *Pharmacology & Therapeutics* 188 (August): 1–11. https://doi.org/10.1016/j.pharmthera.2018.02.013.

Bellahcène, Akeila, Vincent Castronovo, Kalu U. E. Ogbureke, Larry W. Fisher, and Neal S. Fedarko. 2008. 'Small Integrin-Binding Ligand N-Linked Glycoproteins

(SIBLINGs): Multifunctional Proteins in Cancer'. *Nature Reviews Cancer* 8 (3): 212–26. https://doi.org/10.1038/nrc2345.

Benedikter, Birke J., Freek G. Bouwman, Tanja Vajen, Alexandra C. A. Heinzmann, Gert Grauls, Edwin C. Mariman, Emiel F. M. Wouters, et al. 2017. 'Ultrafiltration Combined with Size Exclusion Chromatography Efficiently Isolates Extracellular Vesicles from Cell Culture Media for Compositional and Functional Studies'. *Scientific Reports* 7 (1): 15297. https://doi.org/10.1038/s41598-017-15717-7.

Benes, Petr, Vaclav Vetvicka, and Martin Fusek. 2008. 'Cathepsin D—Many Functions of One Aspartic Protease'. *Critical Reviews in Oncology/Hematology* 68 (1): 12–28. https://doi.org/10.1016/j.critrevonc.2008.02.008.

Berlo, Jop H. van, Marjorie Maillet, and Jeffery D. Molkentin. 2013. 'Signaling Effectors Underlying Pathologic Growth and Remodeling of the Heart'. *Journal of Clinical Investigation* 123 (1): 37–45. https://doi.org/10.1172/JCI62839.

Bernardo, Bianca C., Kate L. Weeks, Lynette Pretorius, and Julie R. McMullen. 2010. 'Molecular Distinction between Physiological and Pathological Cardiac Hypertrophy: Experimental Findings and Therapeutic Strategies'. *Pharmacology & Therapeutics* 128 (1): 191–227. https://doi.org/10.1016/j.pharmthera.2010.04.005.

Beth Bennett, Thomas E. Johnson, Beth. 1998. 'Development of Congenics for Hypnotic Sensitivity to Ethanol by QTL-Marker-Assisted Counter Selection'. *Mammalian Genome* 9 (12): 969–74. https://doi.org/10.1007/s003359900908.

Biton, Yitschak, Ilan Goldenberg, Valentina Kutyifa, Jayson R. Baman, Scott Solomon, Arthur J. Moss, Barbara Szepietowska, et al. 2016. 'Relative Wall Thickness and the Risk for Ventricular Tachyarrhythmias in Patients With Left Ventricular Dysfunction'. *Journal of the American College of Cardiology* 67 (3): 303–12. https://doi.org/10.1016/j.jacc.2015.10.076.

Blaser, Mark C., and Elena Aikawa. 2018. 'Roles and Regulation of Extracellular Vesicles in Cardiovascular Mineral Metabolism'. *Frontiers in Cardiovascular Medicine* 5 (December): 187. https://doi.org/10.3389/fcvm.2018.00187.

Bobrie, Angélique, Sophie Krumeich, Fabien Reyal, Chiara Recchi, Luis F. Moita, Miguel C. Seabra, Matias Ostrowski, and Clotilde Théry. 2012. 'Rab27a Supports Exosome-Dependent and -Independent Mechanisms That Modify the Tumor Microenvironment and Can Promote Tumor Progression'. *Cancer Research* 72 (19): 4920–30. https://doi.org/10.1158/0008-5472.CAN-12-0925.

Bornstein, Abraham B, Suman S Rao, and Komal Marwaha. 2021. 'Left Ventricular Hypertrophy (LVH)', March, 17.

Bosch, Lena, Judith J. de Haan, Marissa Bastemeijer, Jennifer van der Burg, Erik van der Worp, Marian Wesseling, Margarida Viola, et al. 2021. 'The Transverse Aortic Constriction Heart Failure Animal Model: A Systematic Review and Meta-Analysis'. *Heart Failure Reviews* 26 (6): 1515–24. https://doi.org/10.1007/s10741-020-09960-w.

Boulanger, Chantal M., Xavier Loyer, Pierre-Emmanuel Rautou, and Nicolas Amabile. 2017. 'Extracellular Vesicles in Coronary Artery Disease'. *Nature Reviews Cardiology* 14 (5): 259–72. https://doi.org/10.1038/nrcardio.2017.7.

Brennan, K., K. Martin, S. P. FitzGerald, J. O'Sullivan, Y. Wu, A. Blanco, C. Richardson, and M. M. Mc Gee. 2020. 'A Comparison of Methods for the Isolation and Separation of Extracellular Vesicles from Protein and Lipid Particles in Human Serum'. *Scientific Reports* 10 (1): 1039. https://doi.org/10.1038/s41598-020-57497-7.

Bruemmer, Dennis, Alan R. Collins, Grace Noh, Wei Wang, Mary Territo, Sarah Arias-Magallona, Michael C. Fishbein, et al. 2003. 'Angiotensin II–Accelerated Atherosclerosis and Aneurysm Formation Is Attenuated in Osteopontin-Deficient Mice'. *Journal of Clinical Investigation* 112 (9): 1318–31. https://doi.org/10.1172/JCI200318141.

Brumback, Lyndia C., Richard Kronmal, Susan R. Heckbert, Hanyu Ni, W. Gregory Hundley, João A. Lima, and David A. Bluemke. 2010. 'Body Size Adjustments for Left Ventricular Mass by Cardiovascular Magnetic Resonance and Their Impact on Left Ventricular Hypertrophy Classification'. *The International Journal of Cardiovascular Imaging* 26 (4): 459–68. https://doi.org/10.1007/s10554-010-9584-5.

Bujak, Marcin, Hyuk Jung Kweon, Khaled Chatila, Na Li, George Taffet, and Nikolaos G Frangogiannis. 2008. 'Aging-Related Defects Are Associated With Adverse Cardiac Remodeling in a Mouse Model of Reperfused Myocardial Infarction' 51 (14): 9.

Buniello, Annalisa, Jacqueline A L MacArthur, Maria Cerezo, Laura W Harris, James Hayhurst, Cinzia Malangone, Aoife McMahon, et al. 2019. 'The NHGRI-EBI GWAS Catalog of Published Genome-Wide Association Studies, Targeted Arrays and Summary Statistics 2019'. *Nucleic Acids Research* 47 (D1): D1005–12. https://doi.org/10.1093/nar/gky1120.

Busatto, Sara, Dalila Iannotta, Sierra A. Walker, Luisa Di Marzio, and Joy Wolfram. 2021. 'A Simple and Quick Method for Loading Proteins in Extracellular Vesicles'. *Pharmaceuticals* 14 (4): 356. https://doi.org/10.3390/ph14040356.

Cambotti, L. J., F. E. Cole, A. A. Gerall, E. D. Frohlich, and A. A. MacPhee. 1984. 'Neonatal Gonadal Hormones and Blood Pressure in the Spontaneously Hypertensive Rat'. *American Journal of Physiology-Endocrinology and Metabolism* 247 (2): E258–64. https://doi.org/10.1152/ajpendo.1984.247.2.E258.

Cano-Gamez, Eddie, and Gosia Trynka. 2020. 'From GWAS to Function: Using Functional Genomics to Identify the Mechanisms Underlying Complex Diseases'. *Frontiers in Genetics* 11 (May): 424. https://doi.org/10.3389/fgene.2020.00424.

Cantin, Réjean, Juliette Diou, Dave Bélanger, Alexandre M. Tremblay, and Caroline Gilbert. 2008. 'Discrimination between Exosomes and HIV-1: Purification of Both Vesicles from Cell-Free Supernatants'. *Journal of Immunological Methods* 338 (1–2): 21–30. https://doi.org/10.1016/j.jim.2008.07.007.

Carabello, B. A., M. R. Zile, R. Tanaka, and G. Cooper. 1992. 'Left Ventricular Hypertrophy Due to Volume Overload versus Pressure Overload'. *American Journal of Physiology-Heart and Circulatory Physiology* 263 (4): H1137–44. https://doi.org/10.1152/ajpheart.1992.263.4.H1137.

'Cardiovascular Diseases (CVDs)'. 2021. In *Cardiovascular Diseases (CVDs)*. World Health Organization. https://www.who.int/news-room/fact-sheets/detail/cardiovascular-diseases-(cvds).

Cardon, Lon R., and John I. Bell. 2001. 'Association Study Designs for Complex Diseases'. *Nature Reviews Genetics* 2 (2): 91–99. https://doi.org/10.1038/35052543.

Carnino, Jonathan M., Heedoo Lee, and Yang Jin. 2019. 'Isolation and Characterization of Extracellular Vesicles from Broncho-Alveolar Lavage Fluid: A Review and Comparison of Different Methods'. *Respiratory Research* 20 (1): 240. https://doi.org/10.1186/s12931-019-1210-z.

Carr, F.J., C.D. Negrin, J.S. Clark, D Graham, M.W. Mcbride, N.W. Anderson, and A.F. Dominiczak. 2002. 'Chromosome 2 Reciprocal Congenic Strains to Evaluate the Effect of the Genetic Background on Blood Pressure'. *Scottish Medical Journal* 47 (1): 7–9. https://doi.org/10.1177/003693300204700104.

Chen, Jiaci, Peilong Li, Taiyi Zhang, Zhipeng Xu, Xiaowen Huang, Ruiming Wang, and Lutao Du. 2022. 'Review on Strategies and Technologies for Exosome Isolation and

Purification'. *Frontiers in Bioengineering and Biotechnology* 9 (January): 811971. https://doi.org/10.3389/fbioe.2021.811971.

Chen, Ru, Zhihua Qiu, Jing Wang, Yanyi Yao, Kai Huang, and Feng Zhu. 2021. 'DES Mutation Associated with Cardiac Hypertrophy and Alternating Bundle Branch Block'. *HeartRhythm Case Reports* 7 (1): 16–20. https://doi.org/10.1016/j.hrcr.2020.10.003.

Chen, Ruei-Ming, Yi-Ling Lin, and Chih-Wei Chou. 2010. 'GATA-3 Transduces Survival Signals in Osteoblasts through Upregulation of Bcl-XL Gene Expression'. *Journal of Bone and Mineral Research* 25 (10): 2193–2204. https://doi.org/10.1002/jbmr.121.

Chen, Yingjie, Haipeng Guo, Dachun Xu, Xin Xu, Huan Wang, Xinli Hu, Zhongbing Lu, et al. 2012. 'Left Ventricular Failure Produces Profound Lung Remodeling and Pulmonary Hypertension in Mice: Heart Failure Causes Severe Lung Disease'. *Hypertension* 59 (6): 1170–78. https://doi.org/10.1161/HYPERTENSIONAHA.111.186072.

Chevillet, J. R., Q. Kang, I. K. Ruf, H. A. Briggs, L. N. Vojtech, S. M. Hughes, H. H. Cheng, et al. 2014. 'Quantitative and Stoichiometric Analysis of the MicroRNA Content of Exosomes'. *Proceedings of the National Academy of Sciences* 111 (41): 14888–93. https://doi.org/10.1073/pnas.1408301111.

Chintalgattu, Vishnu, Di Ai, Robert R. Langley, Jianhu Zhang, James A. Bankson, Tiffany L. Shih, Anilkumar K. Reddy, et al. 2010. 'Cardiomyocyte PDGFR-β Signaling Is an Essential Component of the Mouse Cardiac Response to Load-Induced Stress'. *Journal of Clinical Investigation* 120 (2): 472–84. https://doi.org/10.1172/JCI39434.

Chiriacò, Maria, Monica Bianco, Annamaria Nigro, Elisabetta Primiceri, Francesco Ferrara, Alessandro Romano, Angelo Quattrini, Roberto Furlan, Valentina Arima, and Giuseppe Maruccio. 2018. 'Lab-on-Chip for Exosomes and Microvesicles Detection and Characterization'. *Sensors* 18 (10): 3175. https://doi.org/10.3390/s18103175.

Chong, Suet Yen, Choon Keong Lee, Chenyuan Huang, Yi Hsuan Ou, Christopher J. Charles, Arthur Mark Richards, Yub Raj Neupane, et al. 2019. 'Extracellular Vesicles in Cardiovascular Diseases: Alternative Biomarker Sources, Therapeutic Agents, and Drug Delivery Carriers'. *International Journal of Molecular Sciences* 20 (13): 3272. https://doi.org/10.3390/ijms20133272.

Chorro, Francisco J., Luis Such-Belenguer, and Vicente López-Merino. 2009. 'Modelos Animales de Enfermedad Cardiovascular'. *Revista Española de Cardiología* 62 (1): 69–84. https://doi.org/10.1016/S0300-8932(09)70023-5.

Clark, James S., Baxter Jeffs, Anne O. Davidson, Wai Kwong Lee, Niall H. Anderson, Marie-Therese Bihoreau, M. Julia Brosnan, et al. 1996. 'Quantitative Trait Loci in Genetically Hypertensive Rats: Possible Sex Specificity'. *Hypertension* 28 (5): 898–906. https://doi.org/10.1161/01.HYP.28.5.898.

Clayton, Aled, Jacquelyn Court, Hossein Navabi, Malcolm Adams, Malcolm D Mason, Jan A Hobot, Geoff R Newman, and Bharat Jasani. 2001. 'Analysis of Antigen Presenting Cell Derived Exosomes, Based on Immuno-Magnetic Isolation and Flow Cytometry'. *Journal of Immunological Methods* 247 (1–2): 163–74. https://doi.org/10.1016/S0022-1759(00)00321-5.

Clemen, Christoph S., Harald Herrmann, Sergei V. Strelkov, and Rolf Schröder. 2013. 'Desminopathies: Pathology and Mechanisms'. *Acta Neuropathologica* 125 (1): 47–75. https://doi.org/10.1007/s00401-012-1057-6.

Cody, R J, G J Haas, P F Binkley, Q Capers, and R Kelley. 1992. 'Plasma Endothelin Correlates with the Extent of Pulmonary Hypertension in Patients with Chronic Congestive Heart Failure.' *Circulation* 85 (2): 504–9. https://doi.org/10.1161/01.CIR.85.2.504.

Collins, Alan R, Janet Schnee, Wei Wang, Sarah Kim, Michael C Fishbein, Dennis Bruemmer, Ronald E Law, Susanne Nicholas, Robert S Ross, and Willa A Hsueh. 2004. 'Osteopontin Modulates Angiotensin II- Induced Fibrosis in the Intact Murine Heart'. *Journal of the American College of Cardiology* 43 (9): 1698–1705. https://doi.org/10.1016/j.jacc.2003.11.058.

Corso, Giulia, Imre Mäger, Yi Lee, André Görgens, Jarred Bultema, Bernd Giebel, Matthew J. A. Wood, Joel Z. Nordin, and Samir EL Andaloussi. 2017. 'Reproducible and Scalable Purification of Extracellular Vesicles Using Combined Bind-Elute and Size Exclusion Chromatography'. *Scientific Reports* 7 (1): 11561. https://doi.org/10.1038/s41598-017-10646-x.

Coughlan, Christina, Kimberley D. Bruce, Olivier Burgy, Timothy D. Boyd, Cole R. Michel, Josselyn E. Garcia-Perez, Vanesa Adame, et al. 2020. 'Exosome Isolation by Ultracentrifugation and Precipitation and Techniques for Downstream Analyses'. *Current Protocols in Cell Biology* 88 (1). https://doi.org/10.1002/cpcb.110.

Coumans, Frank A.W., Alain R. Brisson, Edit I. Buzas, Françoise Dignat-George, Esther E.E. Drees, Samir El-Andaloussi, Costanza Emanueli, et al. 2017. 'Methodological Guidelines to Study Extracellular Vesicles'. *Circulation Research* 120 (10): 1632–48. https://doi.org/10.1161/CIRCRESAHA.117.309417.

Crawford, Wendy. n.d. ‘Microarray Analysis of Chromosome 14 Congenic Strains in the SHRSP’.

Creemers, Esther E., Anke J. Tijsen, and Yigal M. Pinto. 2012. ‘Circulating MicroRNAs: Novel Biomarkers and Extracellular Communicators in Cardiovascular Disease?’ Edited by Eva van Rooij. *Circulation Research* 110 (3): 483–95. https://doi.org/10.1161/CIRCRESAHA.111.247452.

Crescitelli, Rossella, Cecilia Lässer, Su Chul Jang, Aleksander Cvjetkovic, Carina Malmhäll, Nasibeh Karimi, Johanna L. Höög, et al. 2020. ‘Subpopulations of Extracellular Vesicles from Human Metastatic Melanoma Tissue Identified by Quantitative Proteomics after Optimized Isolation’. *Journal of Extracellular Vesicles* 9 (1): 1722433. https://doi.org/10.1080/20013078.2020.1722433.

Cvjetkovic, Aleksander, Jan Lötvall, and Cecilia Lässer. 2014. ‘The Influence of Rotor Type and Centrifugation Time on the Yield and Purity of Extracellular Vesicles’. *Journal of Extracellular Vesicles* 3 (1): 23111. https://doi.org/10.3402/jev.v3.23111.

Dai, Dao-Fu, Simon C. Johnson, Jason J. Villarin, Michael T. Chin, Madeline Nieves-Cintrón, Tony Chen, David J. Marcinek, et al. 2011. ‘Mitochondrial Oxidative Stress Mediates Angiotensin II–Induced Cardiac Hypertrophy and Gαq Overexpression–Induced Heart Failure’. *Circulation Research* 108 (7): 837–46. https://doi.org/10.1161/CIRCRESAHA.110.232306.

Dai, Qiuxia, Jing Lin, Teresa Craig, Youn-Min Chou, Carmen Hinojosa-Laborde, and Merry L. Lindsey. 2008. ‘Estrogen Effects on MMP-13 and MMP-14 Regulation of Left Ventricular Mass in Dahl Salt-Induced Hypertension’. *Gender Medicine* 5 (1): 74–85. https://doi.org/10.1016/S1550-8579(08)80010-1.

Dai, W, Q Dong, M Chen, L Zhao, A Chen, Z Li, and S Liu. 2016. ‘Changes in Cardiac Structure and Function in a Modified Rat Model of Myocardial Hypertrophy’. *Cardiovascular Journal of Africa* 27 (3): 134–42. https://doi.org/10.5830/CVJA-2015-053.

Dalal, Suman, Qinqin Zha, Christopher R. Daniels, Rebecca J. Steagall, William L. Joyner, Alain-Pierre Gadeau, Mahipal Singh, and Krishna Singh. 2014. ‘Osteopontin Stimulates Apoptosis in Adult Cardiac Myocytes via the Involvement of CD44 Receptors, Mitochondrial Death Pathway, and Endoplasmic Reticulum Stress’. *American Journal of Physiology-Heart and Circulatory Physiology* 306 (8): H1182–91. https://doi.org/10.1152/ajpheart.00954.2013.

Dang, Xuan T. T., Jayasinghe Migara Kavishka, Daniel Xin Zhang, Marco Pirisinu, and Minh T. N. Le. 2020. 'Extracellular Vesicles as an Efficient and Versatile System for Drug Delivery'. *Cells* 9 (10): 2191. https://doi.org/10.3390/cells9102191.

Danielson, Kirsty M., Jessica Estanislau, John Tigges, Vasilis Toxavidis, Virginia Camacho, Edward J. Felton, Joseph Khoory, et al. 2016. 'Diurnal Variations of Circulating Extracellular Vesicles Measured by Nano Flow Cytometry'. Edited by Francesco Bertolini. *PLOS ONE* 11 (1): e0144678. https://doi.org/10.1371/journal.pone.0144678.

De Bleser, Pieter, Bart Hooghe, Dominique Vlieghe, and Frans van Roy. 2007. 'A Distance Difference Matrix Approach to Identifying Transcription Factors That Regulate Differential Gene Expression'. *Genome Biology* 8 (5): R83. https://doi.org/10.1186/gb-2007-8-5-r83.

Delles, Christian, Martin W. McBride, Sandosh Padmanabhan, and Anna F. Dominiczak. 2008. 'The Genetics of Cardiovascular Disease'. *Trends in Endocrinology & Metabolism* 19 (9): 309–16. https://doi.org/10.1016/j.tem.2008.07.010.

Deng, Haiyan, Lei-Lei Ma, Fei-Juan Kong, and Zengyong Qiao. 2021. 'Distinct Phenotypes Induced by Different Degrees of Transverse Aortic Constriction in C57BL/6N Mice'. *Frontiers in Cardiovascular Medicine* 8 (April): 641272. https://doi.org/10.3389/fcvm.2021.641272.

Denhardt, David T., Masaki Noda, Anthony W. O'Regan, Dubravko Pavlin, and Jeffrey S. Berman. 2001. 'Osteopontin as a Means to Cope with Environmental Insults: Regulation of Inflammation, Tissue Remodeling, and Cell Survival'. *Journal of Clinical Investigation* 107 (9): 1055–61. https://doi.org/10.1172/JCI12980.

Deregibus, Maria Chiara, Vincenzo Cantaluppi, Raffaele Calogero, Marco Lo Iacono, Ciro Tetta, Luigi Biancone, Stefania Bruno, Benedetta Bussolati, and Giovanni Camussi. 2007. 'Endothelial Progenitor Cell–Derived Microvesicles Activate an Angiogenic Program in Endothelial Cells by a Horizontal Transfer of MRNA'. *Blood* 110 (7): 2440–48. https://doi.org/10.1182/blood-2007-03-078709.

Dickhout, Annemiek, and Rory R. Koenen. 2018. 'Extracellular Vesicles as Biomarkers in Cardiovascular Disease; Chances and Risks'. *Frontiers in Cardiovascular Medicine* 5 (August): 113. https://doi.org/10.3389/fcvm.2018.00113.

Dickhout, Jeffrey G., and Robert M. K. W. Lee. 1998. 'Blood Pressure and Heart Rate Development in Young Spontaneously Hypertensive Rats'. *American Journal of*

Physiology-Heart and Circulatory Physiology 274 (3): H794–800. https://doi.org/10.1152/ajpheart.1998.274.3.H794.

Dillmann, W.H. 2008. 'The Rat as a Model for Cardiovascular Disease'. *Drug Discovery Today: Disease Models* 5 (3): 173–78. https://doi.org/10.1016/j.ddmod.2009.03.006.

Ding, Yuejia, Yuan Wang, Qiujin Jia, Xiaoling Wang, Yanmin Lu, Ao Zhang, Shichao Lv, and Junping Zhang. 2020. 'Morphological and Functional Characteristics of Animal Models of Myocardial Fibrosis Induced by Pressure Overload'. *International Journal of Hypertension* 2020 (January): 1–14. https://doi.org/10.1155/2020/3014693.

Doenst, T., G. Pytel, A. Schrepper, P. Amorim, G. Farber, Y. Shingu, F. W. Mohr, and M. Schwarzer. 2010. 'Decreased Rates of Substrate Oxidation Ex Vivo Predict the Onset of Heart Failure and Contractile Dysfunction in Rats with Pressure Overload'. *Cardiovascular Research* 86 (3): 461–70. https://doi.org/10.1093/cvr/cvp414.

Doggrell, S. 1998. 'Rat Models of Hypertension, Cardiac Hypertrophy and Failure'. *Cardiovascular Research* 39 (1): 89–105. https://doi.org/10.1016/S0008-6363(98)00076-5.

Dominiczak, Anna F., Delyth Graham, Martin W. McBride, Nick J.R. Brain, Wai Kwong Lee, Fadi J. Charchar, Maciej Tomaszewski, Christian Delles, and Carlene A. Hamilton. 2005. 'Cardiovascular Genomics and Oxidative Stress'. *Hypertension* 45 (4): 636–42. https://doi.org/10.1161/01.HYP.0000154253.53134.09.

Dorn, Gerald W., and Thomas Force. 2005. 'Protein Kinase Cascades in the Regulation of Cardiac Hypertrophy'. *Journal of Clinical Investigation* 115 (3): 527–37. https://doi.org/10.1172/JCI24178.

Douglas, K, D Graham, D Crawford, M W McBride, and A F Dominiczak. 2010. 'Left Ventricular Function in a Model of Left Ventricular Hypertrophy' 28 (June): 213.

Doyle, Laura, and Michael Wang. 2019. 'Overview of Extracellular Vesicles, Their Origin, Composition, Purpose, and Methods for Exosome Isolation and Analysis'. *Cells* 8 (7): 727. https://doi.org/10.3390/cells8070727.

Dragomir, Mihnea, Baoqing Chen, and George A. Calin. 2018. 'Exosomal LncRNAs as New Players in Cell-to-Cell Communication'. *Translational Cancer Research* 7 (S2): S243–52. https://doi.org/10.21037/tcr.2017.10.46.

Dragovic, Rebecca A., Christopher Gardiner, Alexandra S. Brooks, Dionne S. Tannetta, David J.P. Ferguson, Patrick Hole, Bob Carr, et al. 2011. 'Sizing and Phenotyping of Cellular Vesicles Using Nanoparticle Tracking Analysis'. *Nanomedicine:*

Nanotechnology, Biology and Medicine 7 (6): 780–88. https://doi.org/10.1016/j.nano.2011.04.003.

Drüeke, Tilman B., and Olivier Devuyst. 2019. 'Blood Pressure Measurement in Mice: Tail-Cuff or Telemetry?' *Kidney International* 96 (1): 36. https://doi.org/10.1016/j.kint.2019.01.018.

Duncan, E. L., L. M. Thornton, A. Hinney, M. J. Daly, P. F. Sullivan, E. Zeggini, G. Breen, and C. M. Bulik. 2016. 'Genome-Wide Association Study Reveals First Locus for Anorexia Nervosa and Metabolic Correlations'. Preprint. Genomics. https://doi.org/10.1101/088815.

Dutil, Julie, and Alan Y. Deng. 2001. 'Further Chromosomal Mapping of a Blood Pressure QTL in Dahl Rats on Chromosome 2 Using Congenic Strains'. *Physiological Genomics* 6 (1): 3–9. https://doi.org/10.1152/physiolgenomics.2001.6.1.3.

Ekström, Karin, Hadi Valadi, Margareta Sjöstrand, Carina Malmhäll, Apostolos Bossios, Maria Eldh, and Jan Lötvall. 2012. 'Characterization of MRNA and MicroRNA in Human Mast Cell-Derived Exosomes and Their Transfer to Other Mast Cells and Blood CD34 Progenitor Cells'. *Journal of Extracellular Vesicles* 1 (1): 18389. https://doi.org/10.3402/jev.v1i0.18389.

Ellison, Georgina M, Cheryl D Waring, Carla Vicinanza, and Daniele Torella. 2012. 'Physiological Cardiac Remodelling in Response to Endurance Exercise Training: Cellular and Molecular Mechanisms'. *Heart* 98 (1): 5–10. https://doi.org/10.1136/heartjnl-2011-300639.

Elsemüller, Ann-Kathrin, Vanessa Tomalla, Ulrich Gärtner, Kerstin Troidl, Sylvia Jeratsch, Johannes Graumann, Nelli Baal, et al. 2019. 'Characterization of Mast Cell-derived RRNA-containing Microvesicles and Their Inflammatory Impact on Endothelial Cells'. *The FASEB Journal* 33 (4): 5457–67. https://doi.org/10.1096/fj.201801853RR.

Ely, D L, and M E Turner. 1990. 'Hypertension in the Spontaneously Hypertensive Rat Is Linked to the Y Chromosome.' *Hypertension* 16 (3): 277–81. https://doi.org/10.1161/01.HYP.16.3.277.

Erwig, L-P, and P M Henson. 2008. 'Clearance of Apoptotic Cells by Phagocytes'. *Cell Death & Differentiation* 15 (2): 243–50. https://doi.org/10.1038/sj.cdd.4402184.

Euler, Gerhild, Fabian Locquet, Joanna Kociszewska, Yvonne Osygus, Jacqueline Heger, Rolf Schreckenberg, Klaus-Dieter Schlüter, et al. 2021. 'Matrix Metalloproteinases Repress Hypertrophic Growth in Cardiac Myocytes'.

Cardiovascular Drugs and Therapy 35 (2): 353–65. https://doi.org/10.1007/s10557-020-07138-y.

EV-TRACK Consortium, Jan Van Deun, Pieter Mestdagh, Patrizia Agostinis, Özden Akay, Sushma Anand, Jasper Anckaert, et al. 2017. 'EV-TRACK: Transparent Reporting and Centralizing Knowledge in Extracellular Vesicle Research'. *Nature Methods* 14 (3): 228–32. https://doi.org/10.1038/nmeth.4185.

Fabbiano, Fabrizio, Jessica Corsi, Elena Gurrieri, Caterina Trevisan, Michela Notarangelo, and Vito G. D'Agostino. 2020. 'RNA Packaging into Extracellular Vesicles: An Orchestra of RNA-binding Proteins?' *Journal of Extracellular Vesicles* 10 (2). https://doi.org/10.1002/jev2.12043.

Fackler, Oliver T., and Robert Grosse. 2008. 'Cell Motility through Plasma Membrane Blebbing'. *Journal of Cell Biology* 181 (6): 879–84. https://doi.org/10.1083/jcb.200802081.

'Facts and Figures'. 2021. In . UK: British Heart Foundation. https://www.bhf.org.uk/what-we-do/news-from-the-bhf/contact-the-press-office/facts-and-figures.

Fader, Claudio Marcelo, Diego Germán Sánchez, María Belén Mestre, and María Isabel Colombo. 2009. 'TI-VAMP/VAMP7 and VAMP3/Cellubrevin: Two v-SNARE Proteins Involved in Specific Steps of the Autophagy/Multivesicular Body Pathways'. *Biochimica et Biophysica Acta (BBA) - Molecular Cell Research* 1793 (12): 1901–16. https://doi.org/10.1016/j.bbamcr.2009.09.011.

Feng, Du, Wen-Long Zhao, Yun-Ying Ye, Xiao-Chen Bai, Rui-Qin Liu, Lei-Fu Chang, Qiang Zhou, and Sen-Fang Sui. 2010. 'Cellular Internalization of Exosomes Occurs Through Phagocytosis'. *Traffic* 11 (5): 675–87. https://doi.org/10.1111/j.1600-0854.2010.01041.x.

Fischer, Silvia, and Elisabeth Deindl. 2021. 'Characterization of RNA in Extracellular Vesicles'. *Applied Sciences* 11 (16): 7520. https://doi.org/10.3390/app11167520.

Fischer, Silvia, Tibo Gerriets, Carina Wessels, Maureen Walberer, Sawa Kostin, Erwin Stolz, Kirila Zheleva, Andreas Hocke, Stefan Hippenstiel, and Klaus T. Preissner. 2007. 'Extracellular RNA Mediates Endothelial-Cell Permeability via Vascular Endothelial Growth Factor'. *Blood* 110 (7): 2457–65. https://doi.org/10.1182/blood-2006-08-040691.

Fleury, Audrey, Maria Carmen Martinez, and Soazig Le Lay. 2014. 'Extracellular Vesicles as Therapeutic Tools in Cardiovascular Diseases'. *Frontiers in Immunology* 5 (August). https://doi.org/10.3389/fimmu.2014.00370.

Founti, P, F Topouzis, L van Koolwijk, C E Traverso, N Pfeiffer, and A C Viswanathan. 2009. 'Biobanks and the Importance of Detailed Phenotyping: A Case Study--the European Glaucoma Society GlaucoGENE Project'. *British Journal of Ophthalmology* 93 (5): 577–81. https://doi.org/10.1136/bjo.2008.156273.

Fowler, Christie D. 2019. 'NeuroEVs: Characterizing Extracellular Vesicles Generated in the Neural Domain'. *The Journal of Neuroscience* 39 (47): 9262–68. https://doi.org/10.1523/JNEUROSCI.0146-18.2019.

Frantz, Simon A., Michael Kaiser, Sheila M. Gardiner, Dominique Gauguier, Madeleine Vincent, John R. Thompson, Terence Bennett, and Nilesh J. Samani. 1998. 'Successful Isolation of a Rat Chromosome 1 Blood Pressure Quantitative Trait Locus in Reciprocal Congenic Strains'. *Hypertension* 32 (4): 639–46. https://doi.org/10.1161/01.HYP.32.4.639.

Frerker, Nadine, Monika Kasprzycka, Bjrg Mikalsen, Pl Dag, Helge Scott, and Guttorm Haraldse. 2012. 'Role of Matricellular Proteins in Cardiac Allograft Fibrosis'. In *Cardiac Transplantation*, edited by Susan Moffatt-Bruce. InTech. https://doi.org/10.5772/28668.

Frey, N., and E.N. Olson. 2003. 'Cardiac Hypertrophy: The Good, the Bad, and the Ugly'. *Annual Review of Physiology* 65 (1): 45–79. https://doi.org/10.1146/annurev.physiol.65.092101.142243.

Frohlich, Edward D, Arantxa González, and Javier Díez. 2011. 'Hypertensive Left Ventricular Hypertrophy Risk: Beyond Adaptive Cardiomyocytic Hypertrophy'. *Journal of Hypertension* 29 (1): 17–26. https://doi.org/10.1097/HJH.0b013e328340d787.

Frühbeis, Carsten, Dominik Fröhlich, and Eva-Maria Krämer-Albers. 2012. 'Emerging Roles of Exosomes in Neuron–Glia Communication'. *Frontiers in Physiology* 3. https://doi.org/10.3389/fphys.2012.00119.

Fu, Shengyang, Yi Wang, Xiaohuan Xia, and Jialin C. Zheng. 2020. 'Exosome Engineering: Current Progress in Cargo Loading and Targeted Delivery'. *NanoImpact* 20 (October): 100261. https://doi.org/10.1016/j.impact.2020.100261.

Fu, Shihui, Yujie Zhang, Yulong Li, Leiming Luo, Yali Zhao, and Yao Yao. 2020. 'Extracellular Vesicles in Cardiovascular Diseases'. *Cell Death Discovery* 6 (1): 68. https://doi.org/10.1038/s41420-020-00305-y.

Furi, Istvan, Fatemeh Momen-Heravi, and Gyongyi Szabo. 2017. 'Extracellular Vesicle Isolation: Present and Future'. *Annals of Translational Medicine* 5 (12): 263–263. https://doi.org/10.21037/atm.2017.03.95.

Gandham, Srujan, Xianyi Su, Jacqueline Wood, Angela L. Nocera, Sarath Chandra Alli, Lara Milane, Alan Zimmerman, Mansoor Amiji, and Alexander R. Ivanov. 2020. 'Technologies and Standardization in Research on Extracellular Vesicles'. *Trends in Biotechnology* 38 (10): 1066–98. https://doi.org/10.1016/j.tibtech.2020.05.012.

Gao, Zhengfan, Bairen Pang, Jing Li, Na Gao, Tianli Fan, and Yong Li. 2021. 'Emerging Role of Exosomes in Liquid Biopsy for Monitoring Prostate Cancer Invasion and Metastasis'. *Frontiers in Cell and Developmental Biology* 9 (May): 679527. https://doi.org/10.3389/fcell.2021.679527.

Garaeva, Luiza, Roman Kamyshinsky, Yury Kil, Elena Varfolomeeva, Nikolai Verlov, Elena Komarova, Yuri Garmay, et al. 2021. 'Delivery of Functional Exogenous Proteins by Plant-Derived Vesicles to Human Cells in Vitro'. *Scientific Reports* 11 (1): 6489. https://doi.org/10.1038/s41598-021-85833-y.

Garcia-Menendez, Lorena, Georgios Karamanlidis, Stephen Kolwicz, and Rong Tian. 2013. 'Substrain Specific Response to Cardiac Pressure Overload in C57BL/6 Mice'. *American Journal of Physiology-Heart and Circulatory Physiology* 305 (3): H397–402. https://doi.org/10.1152/ajpheart.00088.2013.

Gennebäck, Nina, Urban Hellman, Linus Malm, Göran Larsson, Gunnar Ronquist, Anders Waldenström, and Stellan Mörner. 2013. 'Growth Factor Stimulation of Cardiomyocytes Induces Changes in the Transcriptional Contents of Secreted Exosomes'. *Journal of Extracellular Vesicles* 2 (1): 20167. https://doi.org/10.3402/jev.v2i0.20167.

Gheinani, Ali Hashemi, Mike Vögeli, Ulrich Baumgartner, Erik Vassella, Annette Draeger, Fiona C. Burkhard, and Katia Monastyrskaya. 2018. 'Improved Isolation Strategies to Increase the Yield and Purity of Human Urinary Exosomes for Biomarker Discovery'. *Scientific Reports* 8 (1): 3945. https://doi.org/10.1038/s41598-018-22142-x.

Giachelli, C M, N Bae, M Almeida, D T Denhardt, C E Alpers, and S M Schwartz. 1993. 'Osteopontin Is Elevated during Neointima Formation in Rat Arteries and Is a Novel Component of Human Atherosclerotic Plaques.' *Journal of Clinical Investigation* 92 (4): 1686–96. https://doi.org/10.1172/JCI116755.

Giachelli, Cecilia M, Donna Lombardi, Richard J Johnson, and Manuela Almeida. 1998. 'Evidence for a Role of Osteopontin in Macrophage Infiltration in Response to Pathological Stimuli in Vivo', February, 6.

Giacopelli, Francesca, Renato Marciano, Angela Pistorio, Paolo Catarsi, Silvana Canini, Gerard Karsenty, and Roberto Ravazzolo. 2004. 'Polymorphisms in the Osteopontin Promoter Affect Its Transcriptional Activity'. *Physiological Genomics* 20 (1): 87–96. https://doi.org/10.1152/physiolgenomics.00138.2004.

Gill, T., G. Smith, R. Wissler, and H. Kunz. 1989. 'The Rat as an Experimental Animal'. *Science* 245 (4915): 269–76. https://doi.org/10.1126/science.2665079.

Glennon, P E, P H Sugden, and P A Poole-Wilson. 1994. 'Cellular Mechanisms of Cardiac Hypertrophy', September, 4.

Gómez-Ambrosi, Javier, Victoria Catalán, Beatriz Ramírez, Amaia Rodríguez, Inmaculada Colina, Camilo Silva, Fernando Rotellar, et al. 2007. 'Plasma Osteopontin Levels and Expression in Adipose Tissue Are Increased in Obesity'. *The Journal of Clinical Endocrinology & Metabolism* 92 (9): 3719–27. https://doi.org/10.1210/jc.2007-0349.

Görgens, André, Michel Bremer, Rita Ferrer-Tur, Florian Murke, Tobias Tertel, Peter A. Horn, Sebastian Thalmann, et al. 2019. 'Optimisation of Imaging Flow Cytometry for the Analysis of Single Extracellular Vesicles by Using Fluorescence-Tagged Vesicles as Biological Reference Material'. *Journal of Extracellular Vesicles* 8 (1): 1587567. https://doi.org/10.1080/20013078.2019.1587567.

Görgens, André, Giulia Corso, Daniel W. Hagey, Rim Jawad Wiklander, Manuela O. Gustafsson, Ulrika Felldin, Yi Lee, et al. 2022. 'Identification of Storage Conditions Stabilizing Extracellular Vesicles Preparations'. *Journal of Extracellular Vesicles* 11 (6). https://doi.org/10.1002/jev2.12238.

Gottdiener, John S., James Bednarz, Richard Devereux, Julius Gardin, Allan Klein, Warren J. Manning, Annitta Morehead, et al. 2004. 'American Society of Echocardiography Recommendations for Use of Echocardiography in Clinical Trials'. *Journal of the American Society of Echocardiography* 17 (10): 1086–1119. https://doi.org/10.1016/j.echo.2004.07.013.

Graf, Kristof, Yung S. Do, Naoto Ashizawa, Woerner P. Meehan, Cecilia M. Giachelli, Charles C. Marboe, Eckart Fleck, and Willa A. Hsueh. 1997. 'Myocardial Osteopontin Expression Is Associated With Left Ventricular Hypertrophy'. *Circulation* 96 (9): 3063–71. https://doi.org/10.1161/01.CIR.96.9.3063.

Graf, Kristof, Yung S., Do, Ashizawa, Naoto, Meehan, Woerner P., Giachelli, Cecilia M., Marboe, Charles C., Fleck, Eckart, and Hsueh, Willa A. 1997. 'Myocardial Osteopontin Expression Is Associated With Left Ventricular Hypertrophy'. *Circulation* 96 (9): 3063–71. https://doi.org/10.1161/01.CIR.96.9.3063.

Grant, Barth D., and Julie G. Donaldson. 2009. 'Pathways and Mechanisms of Endocytic Recycling'. *Nature Reviews Molecular Cell Biology* 10 (9): 597–608. https://doi.org/10.1038/nrm2755.

Grothues, Frank, Gillian C Smith, James Moon, Nicholas Bellenger, Peter Collins, Helmut U Klein, and Dudley J Pennell. 2002. 'Comparison of Interstudy Reproducibility of Cardiovascular Magnetic Resonance with Two-Dimensional Echocardiography in Normal Subjects and in Patients with Heart Failure or Left Ventricular Hypertrophy'. *The American Journal of Cardiology* 90 (1): 29–34. https://doi.org/10.1016/s0002-9149(02)02381-0.

Grove, Megan L., Bing Yu, Barbara J. Cochran, Talin Haritunians, Joshua C. Bis, Kent D. Taylor, Mark Hansen, et al. 2013. 'Best Practices and Joint Calling of the HumanExome BeadChip: The CHARGE Consortium'. Edited by Yurii S. Aulchenko. *PLoS ONE* 8 (7): e68095. https://doi.org/10.1371/journal.pone.0068095.

Gs, Ajith Kumar, Binil Raj, Santhosh Kumar S, Sanjay G, and Chandrasekharan Cheranellore Kartha. 2014. 'Ascending Aortic Constriction in Rats for Creation of Pressure Overload Cardiac Hypertrophy Model'. *Journal of Visualized Experiments*, no. 88 (June): 50983. https://doi.org/10.3791/50983.

Gupta, Sanjiv, and A. A. Knowlton. 2007. 'HSP60 Trafficking in Adult Cardiac Myocytes: Role of the Exosomal Pathway'. *American Journal of Physiology-Heart and Circulatory Physiology* 292 (6): H3052–56. https://doi.org/10.1152/ajpheart.01355.2006.

Hafiane, Anouar, and Stella S. Daskalopoulou. 2018. 'Extracellular Vesicles Characteristics and Emerging Roles in Atherosclerotic Cardiovascular Disease'. *Metabolism* 85 (August): 213–22. https://doi.org/10.1016/j.metabol.2018.04.008.

Hanson, Phyllis I., and Anil Cashikar. 2012. 'Multivesicular Body Morphogenesis'. *Annual Review of Cell and Developmental Biology* 28 (1): 337–62. https://doi.org/10.1146/annurev-cellbio-092910-154152.

Hao Chen, Hyosook Hwang, Laurel A. K. McKee, Jessica N. Perez, Jessica A. Regan, Eleni Constantopoulos, Bonnie LaFleur, and John P. Konhilas. 2013. 'Temporal and

Morphological Impact of Pressure Overload in Transgenic FHC Mice'. *Frontiers in Physiology*, August, 12.

Hartjes, Thomas, Serhii Mytnyk, Guido Jenster, Volkert van Steijn, and Martin van Royen. 2019. 'Extracellular Vesicle Quantification and Characterization: Common Methods and Emerging Approaches'. *Bioengineering* 6 (1): 7. https://doi.org/10.3390/bioengineering6010007.

Hasenfuss, G. 1998. 'Animal Models of Human Cardiovascular Disease, Heart Failure and Hypertrophy'. *Cardiovascular Research* 39 (1): 60–76. https://doi.org/10.1016/S0008-6363(98)00110-2.

Hashem, M-Sherif, Hayrapet Kalashyan, Jonathan Choy, Soon K. Chiew, Abdel-Hakim Shawki, Ahmed H. Dawood, and Harald Becher. 2015. 'Left Ventricular Relative Wall Thickness Versus Left Ventricular Mass Index in Non-Cardioembolic Stroke Patients'. *Medicine* 94 (20): e872. https://doi.org/10.1097/MD.0000000000000872.

Hasilik, A., and E.F. Neufeld. 1980. 'Biosynthesis of Lysosomal Enzymes in Fibroblasts. Phosphorylation of Mannose Residues.' *Journal of Biological Chemistry* 255 (10): 4946–50. https://doi.org/10.1016/S0021-9258(19)85586-2.

Heineke, Joerg, and Jeffery D. Molkentin. 2006. 'Regulation of Cardiac Hypertrophy by Intracellular Signalling Pathways'. *Nature Reviews Molecular Cell Biology* 7 (8): 589–600. https://doi.org/10.1038/nrm1983.

Henne, William M., Nicholas J. Buchkovich, and Scott D. Emr. 2011. 'The ESCRT Pathway'. *Developmental Cell* 21 (1): 77–91. https://doi.org/10.1016/j.devcel.2011.05.015.

Hessvik, Nina Pettersen, and Alicia Llorente. 2018. 'Current Knowledge on Exosome Biogenesis and Release'. *Cellular and Molecular Life Sciences* 75 (2): 193–208. https://doi.org/10.1007/s00018-017-2595-9.

Heyen, Jonathan R. R., Eileen R. Blasi, Kristen Nikula, Ricardo Rocha, Heather A. Daust, Gregory Frierdich, John F. Van Vleet, Pam De Ciechi, Ellen G. McMahon, and Amy E. Rudolph. 2002. 'Structural, Functional, and Molecular Characterization of the SHHF Model of Heart Failure'. *American Journal of Physiology-Heart and Circulatory Physiology* 283 (5): H1775–84. https://doi.org/10.1152/ajpheart.00305.2002.

Hill, Andrew F, ed. 2017. *Exosomes and Microvesicles: Methods and Protocols*. Vol. 1545. Methods in Molecular Biology. New York, NY: Springer New York. https://doi.org/10.1007/978-1-4939-6728-5.

Hindorff, Lucia A., Elizabeth M. Gillanders, and Teri A. Manolio. 2011. 'Genetic Architecture of Cancer and Other Complex Diseases: Lessons Learned and Future Directions'. *Carcinogenesis* 32 (7): 945–54. https://doi.org/10.1093/carcin/bgr056.

Hou, Xuwei, Zhaohui Hu, Xiaohua Huang, Yan Chen, Xiuying He, Haiying Xu, and Ningfu Wang. 2014. 'Serum Osteopontin, but Not OPN Gene Polymorphism, Is Associated with LVH in Essential Hypertensive Patients'. *Journal of Molecular Medicine* 92 (5): 487–95. https://doi.org/10.1007/s00109-013-1099-9.

Hoy, Anna M., and Amy H. Buck. 2012. 'Extracellular Small RNAs: What, Where, Why?' *Biochemical Society Transactions* 40 (4): 886–90. https://doi.org/10.1042/BST20120019.

Hsu, Chieh, Yuichi Morohashi, Shin-ichiro Yoshimura, Natalia Manrique-Hoyos, SangYong Jung, Marcel A. Lauterbach, Mostafa Bakhti, et al. 2010. 'Regulation of Exosome Secretion by Rab35 and Its GTPase-Activating Proteins TBC1D10A–C'. *Journal of Cell Biology* 189 (2): 223–32. https://doi.org/10.1083/jcb.200911018.

Hudkins, Kelly L., Cecilia M. Giachelli, Yan Cui, William G. Couser, Richard J. Johnson, and Charles E. Alpers. 1999. 'Osteopontin Expression in Fetal and Mature Human Kidney'. *Journal of the American Society of Nephrology* 10 (3): 444–57. https://doi.org/10.1681/ASN.V103444.

Hunter, G K, C L Kyle, and H A Goldberg. 1994. 'Modulation of Crystal Formation by Bone Phosphoproteins: Structural Specificity of the Osteopontin-Mediated Inhibition of Hydroxyapatite Formation'. *Biochemical Journal* 300 (3): 723–28. https://doi.org/10.1042/bj3000723.

Hunter, Melissa Piper, Noura Ismail, Xiaoli Zhang, Baltazar D. Aguda, Eun Joo Lee, Lianbo Yu, Tao Xiao, et al. 2008. 'Detection of MicroRNA Expression in Human Peripheral Blood Microvesicles'. Edited by Yuk Ming Dennis Lo. *PLoS ONE* 3 (11): e3694. https://doi.org/10.1371/journal.pone.0003694.

Hyde, Craig L, Michael W Nagle, Chao Tian, Xing Chen, Sara A Paciga, Jens R Wendland, Joyce Y Tung, David A Hinds, Roy H Perlis, and Ashley R Winslow. 2016. 'Identification of 15 Genetic Loci Associated with Risk of Major Depression in Individuals of European Descent'. *Nature Genetics* 48 (9): 1031–36. https://doi.org/10.1038/ng.3623.

Icer, Mehmet Arif, and Makbule Gezmen-Karadag. 2018. 'The Multiple Functions and Mechanisms of Osteopontin'. *Clinical Biochemistry* 59 (September): 17–24. https://doi.org/10.1016/j.clinbiochem.2018.07.003.

Ihara, Hideyo, David T. Denhardt, Koichi Furuya, Teruhito Yamashita, Yukari Muguruma, Kunikazu Tsuji, Keith A. Hruska, et al. 2001. 'Parathyroid Hormone-Induced Bone Resorption Does Not Occur in the Absence of Osteopontin'. *Journal of Biological Chemistry* 276 (16): 13065–71. https://doi.org/10.1074/jbc.M010938200.

Ikeda, T, T Shirasawa, Y Esaki, S Yoshiki, and K Hirokawa. 1993. 'Osteopontin MRNA Is Expressed by Smooth Muscle-Derived Foam Cells in Human Atherosclerotic Lesions of the Aorta.' *Journal of Clinical Investigation* 92 (6): 2814–20. https://doi.org/10.1172/JCI116901.

Ingham, Kenneth C. 1984. *Enzyme Purification and Related Techniques. C*. Methods in Enzymology 104. New York: Academic Press.

Innes, Brendan A., Michael G. McLaughlin, Miroslav K. Kapuscinski, Howard J. Jacob, and Stephen B. Harrap. 1998. 'Independent Genetic Susceptibility to Cardiac Hypertrophy in Inherited Hypertension'. *Hypertension* 31 (3): 741–46. https://doi.org/10.1161/01.HYP.31.3.741.

Inomata, Hyoe, Takehiro Watanabe, Yoko Iizuka, Yi-Qiang Liang, Tomoji Mashimo, Toru Nabika, Katsumi Ikeda, et al. 2005. 'Identification of Quantitative Trait Loci for Cardiac Hypertrophy in Two Different Strains of the Spontaneously Hypertensive Rat'. *Hypertension Research* 28 (3): 273–81. https://doi.org/10.1291/hypres.28.273.

Irion, Camila Iansen, Kiera Parrish, Krista John-Williams, Sakir H. Gultekin, and Lina A. Shehadeh. 2018. 'Osteopontin Expression in Cardiomyocytes Is Increased in Pediatric Patients With Sepsis or Pneumonia'. *Frontiers in Physiology* 9 (December): 1779. https://doi.org/10.3389/fphys.2018.01779.

Ito, Hiroshi, Yukio Hirata, Susumu Adachi, Masato Tanaka, Motoyoshi Tsujino, Akira Koike, Akihiko Nogami, Fumiaki Marumo, and Michiaki Hiroe. n.d. 'Endothelin-1 Is an Autocrine/Paracrine Factor in the Mechanism', 6.

J. Simpson, Richard, and Suresh Mathivanan. 2012. 'Extracellular Microvesicles: The Need for Internationally Recognised Nomenclature and Stringent Purification Criteria'. *Journal of Proteomics & Bioinformatics* 05 (02). https://doi.org/10.4172/jpb.10000e10.

Jacob, H. J. 1999. 'Functional Genomics and Rat Models'. *Genome Research* 9 (11): 1013–16. https://doi.org/10.1101/gr.9.11.1013.

Jadli, Anshul S., Ananya Parasor, Karina P. Gomes, Ruchita Shandilya, and Vaibhav B. Patel. 2021. 'Exosomes in Cardiovascular Diseases: Pathological Potential of Nano-

Messenger'. *Frontiers in Cardiovascular Medicine* 8 (November): 767488. https://doi.org/10.3389/fcvm.2021.767488.

Jalaludin, Iqbal, David M. Lubman, and Jeongkwon Kim. 2021. 'A Guide to Mass Spectrometric Analysis of Extracellular Vesicle Proteins for Biomarker Discovery'. *Mass Spectrometry Reviews*, November. https://doi.org/10.1002/mas.21749.

Jankovičová, Jana, Petra Sečová, Katarína Michalková, and Jana Antalíková. 2020. 'Tetraspanins, More than Markers of Extracellular Vesicles in Reproduction'. *International Journal of Molecular Sciences* 21 (20): 7568. https://doi.org/10.3390/ijms21207568.

Jeffs, Baxter, Cervantes D. Negrin, Delyth Graham, James S. Clark, Niall H. Anderson, Dominique Gauguier, and Anna F. Dominiczak. 2000. 'Applicability of a "Speed" Congenic Strategy to Dissect Blood Pressure Quantitative Trait Loci on Rat Chromosome 2'. *Hypertension* 35 (1): 179–87. https://doi.org/10.1161/01.HYP.35.1.179.

Jenjaroenpun, Piroon, Yuliya Kremenska, Vrundha M. Nair, Maksym Kremenskoy, Baby Joseph, and Igor V. Kurochkin. 2013. 'Characterization of RNA in Exosomes Secreted by Human Breast Cancer Cell Lines Using Next-Generation Sequencing'. *PeerJ* 1 (November): e201. https://doi.org/10.7717/peerj.201.

Jeppesen, Dennis K., Aidan M. Fenix, Jeffrey L. Franklin, James N. Higginbotham, Qin Zhang, Lisa J. Zimmerman, Daniel C. Liebler, et al. 2019. 'Reassessment of Exosome Composition'. *Cell* 177 (2): 428-445.e18. https://doi.org/10.1016/j.cell.2019.02.029.

Jiang, Xiaoliang, Meiyu Shao, Xue Liu, Xing Liu, Xu Zhang, Yuming Wang, Kunlun Yin, et al. 2021. 'Reversible Treatment of Pressure Overload-Induced Left Ventricular Hypertrophy through *Drd5* Nucleic Acid Delivery Mediated by Functional Polyaminoglycoside'. *Advanced Science* 8 (5): 2003706. https://doi.org/10.1002/advs.202003706.

Johnson, Greg A., Robert C. Burghardt, Fuller W. Bazer, and Thomas E. Spencer. 2003. 'Osteopontin: Roles in Implantation and Placentation1'. *Biology of Reproduction* 69 (5): 1458–71. https://doi.org/10.1095/biolreprod.103.020651.

Johnson, Toby, Tom R. Gaunt, Stephen J. Newhouse, Sandosh Padmanabhan, Maciej Tomaszewski, Meena Kumari, Richard W. Morris, et al. 2011. 'Blood Pressure Loci Identified with a Gene-Centric Array'. *The American Journal of Human Genetics* 89 (6): 688–700. https://doi.org/10.1016/j.ajhg.2011.10.013.

Jong, Olivier G. de, Sander A. A. Kooijmans, Daniel E. Murphy, Linglei Jiang, Martijn J. W. Evers, Joost P. G. Sluijter, Pieter Vader, and Raymond M. Schiffelers. 2019. 'Drug Delivery with Extracellular Vesicles: From Imagination to Innovation'. *Accounts of Chemical Research* 52 (7): 1761–70. https://doi.org/10.1021/acs.accounts.9b00109.

Jong, Tristan V. de, Hao Chen, Wesley A. Brashear, Kelli J. Kochan, Andrew E. Hillhouse, Yaming Zhu, Isha S. Dhande, et al. 2022. 'MRatBN7.2: Familiar and Unfamiliar Features of a New Rat Genome Reference Assembly'. *Physiological Genomics* 54 (7): 251–60. https://doi.org/10.1152/physiolgenomics.00017.2022.

Juncker, David, Sébastien Bergeron, Veronique Laforte, and Huiyan Li. 2014. 'Cross-Reactivity in Antibody Microarrays and Multiplexed Sandwich Assays: Shedding Light on the Dark Side of Multiplexing'. *Current Opinion in Chemical Biology* 18 (February): 29–37. https://doi.org/10.1016/j.cbpa.2013.11.012.

Kahan, T. 2005. 'Left Ventricular Hypertrophy in Hypertension: Its Arrhythmogenic Potential'. *Heart* 91 (2): 250–56. https://doi.org/10.1136/hrt.2004.042473.

Kannemeier, C., A. Shibamiya, F. Nakazawa, H. Trusheim, C. Ruppert, P. Markart, Y. Song, et al. 2007. 'Extracellular RNA Constitutes a Natural Procoagulant Cofactor in Blood Coagulation'. *Proceedings of the National Academy of Sciences* 104 (15): 6388–93. https://doi.org/10.1073/pnas.0608647104.

Kato, Norihiro, Gina Hyne, Marie-Therese Bihoreau, Dominique Gauguier, G. Mark Lathrop, and John P. Rapp. 1999. 'Complete Genome Searches for Quantitative Trait Loci Controlling Blood Pressure and Related Traits in Four Segregating Populations Derived from Dahl Hypertensive Rats'. *Mammalian Genome* 10 (3): 259–65. https://doi.org/10.1007/s003359900983.

Katz, Michael G., Anthony S. Fargnoli, Sarah M. Gubara, Elena Chepurko, Charles R. Bridges, and Roger J. Hajjar. 2019. 'Surgical and Physiological Challenges in the Development of Left and Right Heart Failure in Rat Models'. *Heart Failure Reviews* 24 (5): 759–77. https://doi.org/10.1007/s10741-019-09783-4.

Kazanecki, Christian C., Dana J. Uzwiak, and David T. Denhardt. 2007. 'Control of Osteopontin Signaling and Function by Post-Translational Phosphorylation and Protein Folding'. *Journal of Cellular Biochemistry* 102 (4): 912–24. https://doi.org/10.1002/jcb.21558.

Keating, Brendan J., Sam Tischfield, Sarah S. Murray, Tushar Bhangale, Thomas S. Price, Joseph T. Glessner, Luana Galver, et al. 2008. 'Concept, Design and

Implementation of a Cardiovascular Gene-Centric 50 K SNP Array for Large-Scale Genomic Association Studies'. Edited by Pieter H. Reitsma. *PLoS ONE* 3 (10): e3583. https://doi.org/10.1371/journal.pone.0003583.

Kehat, Izhak, and Jeffery D. Molkentin. 2010. 'Molecular Pathways Underlying Cardiac Remodeling During Pathophysiological Stimulation'. *Circulation* 122 (25): 2727–35. https://doi.org/10.1161/CIRCULATIONAHA.110.942268.

Kerr, J F R, A H Wyllie, and A R Currie. 1972. 'Apoptosis: A Basic Biological Phenomenon with Wideranging Implications in Tissue Kinetics'. *British Journal of Cancer* 26 (4): 239–57. https://doi.org/10.1038/bjc.1972.33.

Khan, Shanzana I., Karen L. Andrews, Garry L. Jennings, Amanda K. Sampson, and Jaye P. F. Chin-Dusting. 2019. 'Y Chromosome, Hypertension and Cardiovascular Disease: Is Inflammation the Answer?' *International Journal of Molecular Sciences* 20 (12): 2892. https://doi.org/10.3390/ijms20122892.

Kim, Jongmin, Hyunwoo Shin, Jiyoon Kim, Junho Kim, and Jaesung Park. 2015. 'Isolation of High-Purity Extracellular Vesicles by Extracting Proteins Using Aqueous Two-Phase System'. Edited by Vladimir N. Uversky. *PLOS ONE* 10 (6): e0129760. https://doi.org/10.1371/journal.pone.0129760.

Kimes, B, and B Brandt. 1976. 'Properties of a Clonal Muscle Cell Line from Rat Heart'. *Experimental Cell Research* 98 (2): 367–81. https://doi.org/10.1016/0014-4827(76)90447-X.

Kirchner, Benedikt, Dominik Buschmann, Vijay Paul, and Michael W. Pfaffl. 2020. 'Postprandial Transfer of Colostral Extracellular Vesicles and Their Protein and MiRNA Cargo in Neonatal Calves'. Edited by Pierre Busson. *PLOS ONE* 15 (2): e0229606. https://doi.org/10.1371/journal.pone.0229606.

Kleiner, Jan Lukas, Odilia Köpke, Anton Faron, Yunyang Zhang, Jan Cornelssen, Mark Coburn, Stilla Frede, Lars Eichhorn, and Christina Katharina Weisheit. 2021. 'Characterization of Transverse Aortic Constriction in Mice Based on the Specific Recruitment of Leukocytes to the Hypertrophic Myocardium and the Aorta Ascendens'. Edited by Simon Kennedy. *Mediators of Inflammation* 2021 (November): 1–11. https://doi.org/10.1155/2021/1376859.

Koekemoer, Andrea L., Nelson W. Chong, Alison H. Goodall, and Nilesh J. Samani. 2009. 'Myocyte Stress 1 Plays an Important Role in Cellular Hypertrophy and Protection against Apoptosis'. *FEBS Letters* 583 (17): 2964–67. https://doi.org/10.1016/j.febslet.2009.08.011.

Kohri, K., S. Nomura, Y. Kitamura, T. Nagata, K. Yoshioka, M. Iguchi, T. Yamate, T. Umekawa, Y. Suzuki, and H. Sinohara. 1993. 'Structure and Expression of the MRNA Encoding Urinary Stone Protein (Osteopontin)'. *Journal of Biological Chemistry* 268 (20): 15180–84. https://doi.org/10.1016/S0021-9258(18)82453-X.

Kohri, Kenjiro, Yasuyuki Suzuki, Koji Yoshida, Kazuhiko Yamamoto, Naoya Amasaki, Takanori Yamate, Tohru Umekawa, Masanori Iguchi, Hyogo Sinohara, and Takashi Kurita. 1992. 'Molecular Cloning and Sequencing of CDNA Encoding Urinary Stone Protein, Which Is Identical to Osteopontin'. *Biochemical and Biophysical Research Communications* 184 (2): 859–64. https://doi.org/10.1016/0006-291X(92)90669-C.

Konoshenko, Maria Yu., Evgeniy A. Lekchnov, Alexander V. Vlassov, and Pavel P. Laktionov. 2018. 'Isolation of Extracellular Vesicles: General Methodologies and Latest Trends'. *BioMed Research International* 2018: 1–27. https://doi.org/10.1155/2018/8545347.

Korkmaz-Icöz, Sevil, Deniz Akca, Shiliang Li, Sivakkanan Loganathan, Paige Brlecic, Mihály Ruppert, Alex Ali Sayour, et al. 2021a. 'Left-Ventricular Hypertrophy in 18-Month-Old Donor Rat Hearts Was Not Associated with Graft Dysfunction in the Early Phase of Reperfusion after Cardiac Transplantation–Gene Expression Profiling'. *GeroScience*, April. https://doi.org/10.1007/s11357-021-00348-8.

———. 2021b. 'Left-Ventricular Hypertrophy in 18-Month-Old Donor Rat Hearts Was Not Associated with Graft Dysfunction in the Early Phase of Reperfusion after Cardiac Transplantation–Gene Expression Profiling'. *GeroScience* 43 (4): 1995–2013. https://doi.org/10.1007/s11357-021-00348-8.

Kostareva, Anna, Artem Kiselev, Alexandra Gudkova, Goar Frishman, Andreas Ruepp, Dmitrij Frishman, Natalia Smolina, et al. 2016. 'Genetic Spectrum of Idiopathic Restrictive Cardiomyopathy Uncovered by Next-Generation Sequencing'. Edited by Tomohiko Ai. *PLOS ONE* 11 (9): e0163362. https://doi.org/10.1371/journal.pone.0163362.

Kowal, Joanna, Guillaume Arras, Marina Colombo, Mabel Jouve, Jakob Paul Morath, Bjarke Primdal-Bengtson, Florent Dingli, Damarys Loew, Mercedes Tkach, and Clotilde Théry. 2016. 'Proteomic Comparison Defines Novel Markers to Characterize Heterogeneous Populations of Extracellular Vesicle Subtypes'. *Proceedings of the National Academy of Sciences* 113 (8): E968–77. https://doi.org/10.1073/pnas.1521230113.

Koziris, L. P., R. C. Hickson, R. T. Chatterton, R. T. Groseth, J. M. Christie, D. G. Goldflies, and T. G. Unterman. 1999. 'Serum Levels of Total and Free IGF-I and IGFBP-3 Are Increased and Maintained in Long-Term Training'. *Journal of Applied Physiology* 86 (4): 1436–42. https://doi.org/10.1152/jappl.1999.86.4.1436.

Kreimer, Simion, Arseniy M. Belov, Ionita Ghiran, Shashi K. Murthy, David A. Frank, and Alexander R. Ivanov. 2015. 'Mass-Spectrometry-Based Molecular Characterization of Extracellular Vesicles: Lipidomics and Proteomics'. *Journal of Proteome Research* 14 (6): 2367–84. https://doi.org/10.1021/pr501279t.

Krishnamurthy, Prasanna, J. Thomas Peterson, Venkateswaran Subramanian, Mahipal Singh, and Krishna Singh. 2009. 'Inhibition of Matrix Metalloproteinases Improves Left Ventricular Function in Mice Lacking Osteopontin after Myocardial Infarction'. *Molecular and Cellular Biochemistry* 322 (1–2): 53–62. https://doi.org/10.1007/s11010-008-9939-6.

Lai, Ruenn Chai, Fatih Arslan, May May Lee, Newman Siu Kwan Sze, Andre Choo, Tian Sheng Chen, Manuel Salto-Tellez, et al. 2010. 'Exosome Secreted by MSC Reduces Myocardial Ischemia/Reperfusion Injury'. *Stem Cell Research* 4 (3): 214–22. https://doi.org/10.1016/j.scr.2009.12.003.

Lang, Roberto M., Luigi P. Badano, Victor Mor-Avi, Jonathan Afilalo, Anderson Armstrong, Laura Ernande, Frank A. Flachskampf, et al. 2015. 'Recommendations for Cardiac Chamber Quantification by Echocardiography in Adults: An Update from the American Society of Echocardiography and the European Association of Cardiovascular Imaging'. *European Heart Journal – Cardiovascular Imaging* 16 (3): 233–71. https://doi.org/10.1093/ehjci/jev014.

Lannigan, Joanne, and Uta Erdbruegger. 2017. 'Imaging Flow Cytometry for the Characterization of Extracellular Vesicles'. *Methods* 112 (January): 55–67. https://doi.org/10.1016/j.ymeth.2016.09.018.

Lazzeroni, Davide, Ornella Rimoldi, and Paolo G Camici. 2016. 'From Left Ventricular Hypertrophy to Dysfunction and Failure'. *Circulation Journal* 80 (3): 555–64. https://doi.org/10.1253/circj.CJ-16-0062.

Le, Tyl, and Jjh Chong. 2016. 'Cardiac Progenitor Cells for Heart Repair'. *Cell Death Discovery* 2 (1): 16052. https://doi.org/10.1038/cddiscovery.2016.52.

Lee, Sang-Soo, Jong-Hoon Won, Gippeum J. Lim, Jeongran Han, Ji Youn Lee, Kyung-Ok Cho, and Young-Kyung Bae. 2019. 'A Novel Population of Extracellular Vesicles

Smaller than Exosomes Promotes Cell Proliferation'. *Cell Communication and Signaling* 17 (1): 95. https://doi.org/10.1186/s12964-019-0401-z.

Lee, Y., S. EL Andaloussi, and M. J. A. Wood. 2012. 'Exosomes and Microvesicles: Extracellular Vesicles for Genetic Information Transfer and Gene Therapy'. *Human Molecular Genetics* 21 (R1): R125–34. https://doi.org/10.1093/hmg/dds317.

Lener, Thomas, Mario Gimona, Ludwig Aigner, Verena Börger, Edit Buzas, Giovanni Camussi, Nathalie Chaput, et al. 2015. 'Applying Extracellular Vesicles Based Therapeutics in Clinical Trials – an ISEV Position Paper'. *Journal of Extracellular Vesicles* 4 (1): 30087. https://doi.org/10.3402/jev.v4.30087.

Leong, Xin-Fang, Chun-Yi Ng, and Kamsiah Jaarin. 2015. 'Animal Models in Cardiovascular Research: Hypertension and Atherosclerosis'. *BioMed Research International* 2015: 1–11. https://doi.org/10.1155/2015/528757.

Li, Guohong, Yiu-Fai Chen, Stacey S. Kelpke, Suzanne Oparil, and John A. Thompson. 2000. 'Estrogen Attenuates Integrin-β $_3$ –Dependent Adventitial Fibroblast Migration After Inhibition of Osteopontin Production in Vascular Smooth Muscle Cells'. *Circulation* 101 (25): 2949–55. https://doi.org/10.1161/01.CIR.101.25.2949.

Li, Jihe, Keyvan Yousefi, Wen Ding, Jayanti Singh, and Lina A. Shehadeh. 2017. 'Osteopontin RNA Aptamer Can Prevent and Reverse Pressure Overload-Induced Heart Failure'. *Cardiovascular Research* 113 (6): 633–43. https://doi.org/10.1093/cvr/cvx016.

Li, Kang, Rodosthenis S. Rodosthenous, Fatah Kashanchi, Thomas Gingeras, Stephen J. Gould, Lillian S. Kuo, Peter Kurre, et al. 2018. 'Advances, Challenges, and Opportunities in Extracellular RNA Biology: Insights from the NIH ExRNA Strategic Workshop'. *JCI Insight* 3 (7): e98942. https://doi.org/10.1172/jci.insight.98942.

Li, Pin, Melisa Kaslan, Sze Han Lee, Justin Yao, and Zhiqiang Gao. 2017. 'Progress in Exosome Isolation Techniques'. *Theranostics* 7 (3): 789–804. https://doi.org/10.7150/thno.18133.

Li, Xia, Alexander L. Corbett, Erfan Taatizadeh, Nishat Tasnim, Jonathan P. Little, Cathie Garnis, Mads Daugaard, Emma Guns, Mina Hoorfar, and Isaac T. S. Li. 2019. 'Challenges and Opportunities in Exosome Research—Perspectives from Biology, Engineering, and Cancer Therapy'. *APL Bioengineering* 3 (1): 011503. https://doi.org/10.1063/1.5087122.

Liangsupree, Thanaporn, Evgen Multia, and Marja-Liisa Riekkola. 2021. 'Modern Isolation and Separation Techniques for Extracellular Vesicles'. *Journal of*

Chromatography A 1636 (January): 461773. https://doi.org/10.1016/j.chroma.2020.461773.

Lin, Wen, Deqiang Li, Lan Cheng, Li Li, Feiyan Liu, Nicholas J. Hand, Jonathan A. Epstein, and Daniel J. Rader. 2018. 'Zinc Transporter Slc39a8 Is Essential for Cardiac Ventricular Compaction'. *Journal of Clinical Investigation* 128 (2): 826–33. https://doi.org/10.1172/JCI96993.

Linares, Romain, Sisareuth Tan, Céline Gounou, Nicolas Arraud, and Alain R. Brisson. 2015. 'High-Speed Centrifugation Induces Aggregation of Extracellular Vesicles'. *Journal of Extracellular Vesicles* 4 (1): 29509. https://doi.org/10.3402/jev.v4.29509.

Lindenmayer, George E., Louis A. Sordahl, Shoichi Harigaya, Julius C. Allen, Henry R. Besch, and Arnold Schwartz. 1971. 'Some Biochemical Studies on Subcellular Systems Isolated from Fresh Recipient Human Cardiac Tissue Obtained during Transplantation'. *The American Journal of Cardiology* 27 (3): 277–83. https://doi.org/10.1016/0002-9149(71)90303-1.

Lips, Daniel J, and Pieter A Doevendans. n.d. 'Molecular Determinants of Myocardial Hypertrophy and Failure: Alternative Pathways for Beneficial and Maladaptive Hypertrophy', 14.

Liu, Shang-Long, Pin Sun, Ying Li, Shi-Song Liu, and Yun Lu. 2019. 'Exosomes as Critical Mediators of Cell-to-Cell Communication in Cancer Pathogenesis and Their Potential Clinical Application'. *Translational Cancer Research* 8 (1): 298–311. https://doi.org/10.21037/tcr.2019.01.03.

López, Begoña, Arantxa González, Diana Lindner, Dirk Westermann, Susana Ravassa, Javier Beaumont, Idoia Gallego, et al. 2013. 'Osteopontin-Mediated Myocardial Fibrosis in Heart Failure: A Role for Lysyl Oxidase?' *Cardiovascular Research* 99 (1): 111–20. https://doi.org/10.1093/cvr/cvt100.

Lorell, Beverly H., and Blase A. Carabello. 2000. 'Left Ventricular Hypertrophy: Pathogenesis, Detection, and Prognosis'. *Circulation* 102 (4): 470–79. https://doi.org/10.1161/01.CIR.102.4.470.

Lötvall, Jan, Andrew F. Hill, Fred Hochberg, Edit I. Buzás, Dolores Di Vizio, Christopher Gardiner, Yong Song Gho, et al. 2014. 'Minimal Experimental Requirements for Definition of Extracellular Vesicles and Their Functions: A Position Statement from the International Society for Extracellular Vesicles'. *Journal of Extracellular Vesicles* 3 (1): 26913. https://doi.org/10.3402/jev.v3.26913.

Lotvall, Jan, and Hadi Valadi. 2007. 'Cell to Cell Signalling via Exosomes Through EsRNA'. *Cell Adhesion & Migration* 1 (3): 156–58. https://doi.org/10.4161/cam.1.3.5114.

Low, Joel Z. B., Tsung Fei Khang, and Martti T. Tammi. 2017. 'CORNAS: Coverage-Dependent RNA-Seq Analysis of Gene Expression Data without Biological Replicates'. *BMC Bioinformatics* 18 (S16): 575. https://doi.org/10.1186/s12859-017-1974-4.

Lund, Susan Amanda, Cecilia M. Giachelli, and Marta Scatena. 2009. 'The Role of Osteopontin in Inflammatory Processes'. *Journal of Cell Communication and Signaling* 3 (3–4): 311–22. https://doi.org/10.1007/s12079-009-0068-0.

Lyu, Linmao, Hui Wang, Bin Li, Qingyun Qin, Lei Qi, Mitzi Nagarkatti, Prakash Nagarkatti, Joseph S. Janicki, Xing Li Wang, and Taixing Cui. 2015. 'A Critical Role of Cardiac Fibroblast-Derived Exosomes in Activating Renin Angiotensin System in Cardiomyocytes'. *Journal of Molecular and Cellular Cardiology* 89 (December): 268–79. https://doi.org/10.1016/j.yjmcc.2015.10.022.

Margolis, Leonid, and Yoel Sadovsky. 2019. 'The Biology of Extracellular Vesicles: The Known Unknowns'. *PLOS Biology* 17 (7): e3000363. https://doi.org/10.1371/journal.pbio.3000363.

Maris, M Elizabeth, Russell B Melchert, Jacob Joseph, and Richard H Kennedy. 2005. 'Gender Differences in Blood Pressure and Heart Rate in Spontaneously Hypertensive and Wistar-Kyoto Rats'. *Clinical and Experimental Pharmacology and Physiology* 32 (1–2): 35–39. https://doi.org/10.1111/j.1440-1681.2005.04156.x.

Marketou, Maria E., Fragiskos Parthenakis, and Panos E. Vardas. 2016. 'Pathological Left Ventricular Hypertrophy and Stem Cells: Current Evidence and New Perspectives'. *Stem Cells International* 2016: 1–10. https://doi.org/10.1155/2016/5720758.

Marston, Steven, Cecile Montgiraud, Alex B. Munster, O'Neal Copeland, Onjee Choi, Cristobal dos Remedios, Andrew E. Messer, Elisabeth Ehler, and Ralph Knöll. 2015. 'OBSCN Mutations Associated with Dilated Cardiomyopathy and Haploinsufficiency'. Edited by Kumarasamy Thangaraj. *PLOS ONE* 10 (9): e0138568. https://doi.org/10.1371/journal.pone.0138568.

Mashouri, Ladan, Hassan Yousefi, Amir Reza Aref, Ali mohammad Ahadi, Fatemeh Molaei, and Suresh K. Alahari. 2019. 'Exosomes: Composition, Biogenesis, and

Mechanisms in Cancer Metastasis and Drug Resistance'. *Molecular Cancer* 18 (1): 75. https://doi.org/10.1186/s12943-019-0991-5.

Mateescu, Bogdan, Emma J. K. Kowal, Bas W. M. van Balkom, Sabine Bartel, Suvendra N. Bhattacharyya, Edit I. Buzás, Amy H. Buck, et al. 2017. 'Obstacles and Opportunities in the Functional Analysis of Extracellular Vesicle RNA – an ISEV Position Paper'. *Journal of Extracellular Vesicles* 6 (1): 1286095. https://doi.org/10.1080/20013078.2017.1286095.

Mathieu, Mathilde, Lorena Martin-Jaular, Grégory Lavieu, and Clotilde Théry. 2019. 'Specificities of Secretion and Uptake of Exosomes and Other Extracellular Vesicles for Cell-to-Cell Communication'. *Nature Cell Biology* 21 (1): 9–17. https://doi.org/10.1038/s41556-018-0250-9.

Matsui, Yutaka, Nan Jia, Hiroshi Okamoto, Shigeyuki Kon, Hisao Onozuka, Masatoshi Akino, Lizhi Liu, et al. 2004. 'Role of Osteopontin in Cardiac Fibrosis and Remodeling in Angiotensin II-Induced Cardiac Hypertrophy'. *Hypertension* 43 (6): 1195–1201. https://doi.org/10.1161/01.HYP.0000128621.68160.dd.

Mazzali, M., T. Kipari, V. Ophascharoensuk, J.A. Wesson, R. Johnson, and J. Hughes. 2002. 'Osteopontin—a Molecule for All Seasons'. *QJM: An International Journal of Medicine* 95 (1): 3–13. https://doi.org/10.1093/qjmed/95.1.3.

McAdams, Ryan M, Ronald J McPherson, Nazila M Dabestani, Christine A Gleason, and Sandra E Juul. 2010. 'Left Ventricular Hypertrophy Is Prevalent in Sprague–Dawley Rats'. *Comparative Medicine* 60 (5): 7.

McBride, Martin W., Fiona J. Carr, Delyth Graham, Niall H. Anderson, James S. Clark, Wai K. Lee, Fadi J. Charchar, M. Julia Brosnan, and Anna F. Dominiczak. 2003. 'Microarray Analysis of Rat Chromosome 2 Congenic Strains'. *Hypertension* 41 (3): 847–53. https://doi.org/10.1161/01.HYP.0000047103.07205.03.

McMullen, J. R., T. Shioi, L. Zhang, O. Tarnavski, M. C. Sherwood, P. M. Kang, and S. Izumo. 2003. 'Phosphoinositide 3-Kinase(P110) Plays a Critical Role for the Induction of Physiological, but Not Pathological, Cardiac Hypertrophy'. *Proceedings of the National Academy of Sciences* 100 (21): 12355–60. https://doi.org/10.1073/pnas.1934654100.

McMullen, Julie R, and Garry L. Jennings. 2007. 'DIFFERENCES BETWEEN PATHOLOGICAL AND PHYSIOLOGICAL CARDIAC HYPERTROPHY: NOVEL THERAPEUTIC STRATEGIES TO TREAT HEART FAILURE'. *Clinical and Experimental Pharmacology and Physiology* 34: 255–62.

McVey, Mark J., Christopher M. Spring, and Wolfgang M. Kuebler. 2018. 'Improved Resolution in Extracellular Vesicle Populations Using 405 Instead of 488 Nm Side Scatter'. *Journal of Extracellular Vesicles* 7 (1): 1454776. https://doi.org/10.1080/20013078.2018.1454776.

Melleby, Arne O, Andreas Romaine, Jan Magnus Aronsen, Ioanni Veras, Lili Zhang, Ivar Sjaastad, Ida G Lunde, and Geir Christensen. 2018. 'A Novel Method for High Precision Aortic Constriction That Allows for Generation of Specific Cardiac Phenotypes in Mice'. *Cardiovascular Research* 114 (12): 1680–90. https://doi.org/10.1093/cvr/cvy141.

Members of the Complex Trait Consortium. 2003. 'The Nature and Identification of Quantitative Trait Loci: A Community's View'. *Nature Reviews Genetics* 4 (11): 911–16. https://doi.org/10.1038/nrg1206.

Minciacchi, Valentina R., Michael R. Freeman, and Dolores Di Vizio. 2015. 'Extracellular Vesicles in Cancer: Exosomes, Microvesicles and the Emerging Role of Large Oncosomes'. *Seminars in Cell & Developmental Biology* 40 (April): 41–51. https://doi.org/10.1016/j.semcdb.2015.02.010.

Mittelbrunn, María, Cristina Gutiérrez-Vázquez, Carolina Villarroya-Beltri, Susana González, Fátima Sánchez-Cabo, Manuel Ángel González, Antonio Bernad, and Francisco Sánchez-Madrid. 2011. 'Unidirectional Transfer of MicroRNA-Loaded Exosomes from T Cells to Antigen-Presenting Cells'. *Nature Communications* 2 (1): 282. https://doi.org/10.1038/ncomms1285.

Mittmann, C, T Eschenhagen, and H Scholz. 1998. 'Cellular and Molecular Aspects of Contractile Dysfunction in Heart Failure'. *Cardiovascular Research*, 9.

Moreno, Carol, Mathew Hoffman, Timothy J. Stodola, Daniela N. Didier, Jozef Lazar, Aron M. Geurts, Paula E. North, Howard J. Jacob, and Andrew S. Greene. 2011. 'Creation and Characterization of a Renin Knockout Rat'. *Hypertension* 57 (3): 614–19. https://doi.org/10.1161/HYPERTENSIONAHA.110.163840.

Müller, Patrick, Andrey Kazakov, Philippe Jagoda, Alexander Semenov, Michael Böhm, and Ulrich Laufs. 2009. 'ACE Inhibition Promotes Upregulation of Endothelial Progenitor Cells and Neoangiogenesis in Cardiac Pressure Overload'. *Cardiovascular Research* 83 (1): 106–14. https://doi.org/10.1093/cvr/cvp123.

Müller, Patrick, Andrey Kazakov, Alexander Semenov, Michael Böhm, and Ulrich Laufs. 2008. 'Pressure-Induced Cardiac Overload Induces Upregulation of Endothelial and

Myocardial Progenitor Cells'. *Cardiovascular Research* 77 (1): 151–59. https://doi.org/10.1093/cvr/cvm037.

Munroe, Patricia B., Michael R. Barnes, and Mark J. Caulfield. 2013. 'Advances in Blood Pressure Genomics'. *Circulation Research* 112 (10): 1365–79. https://doi.org/10.1161/CIRCRESAHA.112.300387.

Muralidharan-Chari, Vandhana, James Clancy, Carolyn Plou, Maryse Romao, Philippe Chavrier, Graca Raposo, and Crislyn D'Souza-Schorey. 2009. 'ARF6-Regulated Shedding of Tumor Cell-Derived Plasma Membrane Microvesicles'. *Current Biology* 19 (22): 1875–85. https://doi.org/10.1016/j.cub.2009.09.059.

Murry, Charles E, Cecilia M Giachelli, Stephen M Schwartz, and Rudolf Vrackot. 1994. 'Macrophages Express Osteopontin during Repair of Myocardial Necrosis' 145 (6): 13.

Nabhan, J. F., R. Hu, R. S. Oh, S. N. Cohen, and Q. Lu. 2012. 'Formation and Release of Arrestin Domain-Containing Protein 1-Mediated Microvesicles (ARMMs) at Plasma Membrane by Recruitment of TSG101 Protein'. *Proceedings of the National Academy of Sciences* 109 (11): 4146–51. https://doi.org/10.1073/pnas.1200448109.

Nabika, Toru, Hiroki Ohara, Norihiro Kato, and Minoru Isomura. 2012. 'The Stroke-Prone Spontaneously Hypertensive Rat: Still a Useful Model for Post-GWAS Genetic Studies?' *Hypertension Research* 35 (5): 477–84. https://doi.org/10.1038/hr.2012.30.

Nadruz, W. 2015. 'Myocardial Remodeling in Hypertension'. *Journal of Human Hypertension* 29 (1): 1–6. https://doi.org/10.1038/jhh.2014.36.

Nair, Sreejayan, and Jun Ren, eds. 2007. *Vascular Biology Protocols*. Methods in Molecular Medicine 139. Totowa, N.J: Humana Press.

Nakamura, Michinari, and Junichi Sadoshima. 2018. 'Mechanisms of Physiological and Pathological Cardiac Hypertrophy'. *Nature Reviews Cardiology* 15 (7): 387–407. https://doi.org/10.1038/s41569-018-0007-y.

Nakao, Yasuhisa, Jun Aono, Mika Hamaguchi, Kayo Takahashi, Tomohisa Sakaue, Katsuji Inoue, Shuntaro Ikeda, and Osamu Yamaguchi. 2022. 'O-Ring-Induced Transverse Aortic Constriction (OTAC) Is a New Simple Method to Develop Cardiac Hypertrophy and Heart Failure in Mice'. *Scientific Reports* 12 (1): 85. https://doi.org/10.1038/s41598-021-04096-9.

Nakayama, Hiroyuki, Hiromi Nagai, Kyotaka Matsumoto, Ryosuke Oguro, Ken Sugimoto, Kei Kamide, Mitsuru Ohishi, et al. 2011. 'Association between Osteopontin Promoter Variants and Diastolic Dysfunction in Hypertensive Heart in the Japanese

Population'. *Hypertension Research* 34 (10): 1141–46. https://doi.org/10.1038/hr.2011.102.

Nauta, Jan F., Yoran M. Hummel, Jasper Tromp, Wouter Ouwerkerk, Peter van der Meer, Xuanyi Jin, Carolyn S.P. Lam, et al. 2020. 'Concentric vs. Eccentric Remodelling in Heart Failure with Reduced Ejection Fraction: Clinical Characteristics, Pathophysiology and Response to Treatment'. *European Journal of Heart Failure* 22 (7): 1147–55. https://doi.org/10.1002/ejhf.1632.

Neri Serneri, Gian Gastone, Maria Boddi, Pietro Amedeo Modesti, Ilaria Cecioni, Mirella Coppo, Luigi Padeletti, Antonio Michelucci, Andrea Colella, and Giorgio Galanti. 2001. 'Increased Cardiac Sympathetic Activity and Insulin-Like Growth Factor-I Formation Are Associated With Physiological Hypertrophy in Athletes'. *Circulation Research* 89 (11): 977–82. https://doi.org/10.1161/hh2301.100982.

Nica, Alexandra C., and Emmanouil T. Dermitzakis. 2013. 'Expression Quantitative Trait Loci: Present and Future'. *Philosophical Transactions of the Royal Society B: Biological Sciences* 368 (1620): 20120362. https://doi.org/10.1098/rstb.2012.0362.

Nie, Xiang, Jiahui Fan, Huaping Li, Zhongwei Yin, Yanru Zhao, Beibei Dai, Nianguo Dong, Chen Chen, and Dao Wen Wang. 2018. 'MiR-217 Promotes Cardiac Hypertrophy and Dysfunction by Targeting PTEN'. *Molecular Therapy - Nucleic Acids* 12 (September): 254–66. https://doi.org/10.1016/j.omtn.2018.05.013.

Niimura, Hideshi, Albert E Chudley, and Michael Sole. 1998. 'Mutations in the Gene for Cardiac Myosin-Binding Protein C and Late-Onset Familial Hypertrophic Cardiomyopathy'. *The New England Journal of Medicine*, 10.

Nolte-'t Hoen, Esther N. M., Henk P. J. Buermans, Maaike Waasdorp, Willem Stoorvogel, Marca H. M. Wauben, and Peter A. C. 't Hoen. 2012. 'Deep Sequencing of RNA from Immune Cell-Derived Vesicles Uncovers the Selective Incorporation of Small Non-Coding RNA Biotypes with Potential Regulatory Functions'. *Nucleic Acids Research* 40 (18): 9272–85. https://doi.org/10.1093/nar/gks658.

Nordin, Joel Z., Yi Lee, Pieter Vader, Imre Mäger, Henrik J. Johansson, Wolf Heusermann, Oscar P.B. Wiklander, et al. 2015. 'Ultrafiltration with Size-Exclusion Liquid Chromatography for High Yield Isolation of Extracellular Vesicles Preserving Intact Biophysical and Functional Properties'. *Nanomedicine: Nanotechnology, Biology and Medicine* 11 (4): 879–83. https://doi.org/10.1016/j.nano.2015.01.003.

O'Brien, E R, M R Garvin, D K Stewart, T Hinohara, J B Simpson, S M Schwartz, and C M Giachelli. 1994. 'Osteopontin Is Synthesized by Macrophage, Smooth Muscle, and

Endothelial Cells in Primary and Restenotic Human Coronary Atherosclerotic Plaques.' *Arteriosclerosis and Thrombosis: A Journal of Vascular Biology* 14 (10): 1648–56. https://doi.org/10.1161/01.ATV.14.10.1648.

O'Brien, Killian, Koen Breyne, Stefano Ughetto, Louise C. Laurent, and Xandra O. Breakefield. 2020. 'RNA Delivery by Extracellular Vesicles in Mammalian Cells and Its Applications'. *Nature Reviews Molecular Cell Biology* 21 (10): 585–606. https://doi.org/10.1038/s41580-020-0251-y.

Ohlendieck, Kay, and Stephen E. Harding. 2018. 'Centrifugation and Ultracentrifugation'. In *Wilson and Walker's Principles and Techniques of Biochemistry and Molecular Biology*, edited by Andreas Hofmann and Samuel Clokie, 8th ed., 424–53. Cambridge University Press. https://doi.org/10.1017/9781316677056.014.

Oláh, Attila, Balázs Tamás Németh, Csaba Mátyás, László Hidi, Árpád Lux, Mihály Ruppert, Dalma Kellermayer, et al. 2016. 'Physiological and Pathological Left Ventricular Hypertrophy of Comparable Degree Is Associated with Characteristic Differences of in Vivo Hemodynamics'. *American Journal of Physiology-Heart and Circulatory Physiology* 310 (5): H587–97. https://doi.org/10.1152/ajpheart.00588.2015.

Ophascharoensuk, Vuddhidej, Cecilia M. Giachelli, Katherine Gordon, Jeremy Hughes, Raimund Pichler, Paul Brown, Lucy Liaw, et al. 1999. 'Obstructive Uropathy in the Mouse: Role of Osteopontin in Interstitial Fibrosis and Apoptosis'. *Kidney International* 56 (2): 571–80. https://doi.org/10.1046/j.1523-1755.1999.00580.x.

O'Regan, Anthony, and Jeffrey S. Berman. 2001. 'Osteopontin: A Key Cytokine in Cell-Mediated and Granulomatous Inflammation: Osteopontin in Cell-Mediated and Granulomatous Inflammation'. *International Journal of Experimental Pathology* 81 (6): 373–90. https://doi.org/10.1046/j.1365-2613.2000.00163.x.

Ostrowski, Matias, Nuno B. Carmo, Sophie Krumeich, Isabelle Fanget, Graça Raposo, Ariel Savina, Catarina F. Moita, et al. 2010. 'Rab27a and Rab27b Control Different Steps of the Exosome Secretion Pathway'. *Nature Cell Biology* 12 (1): 19–30. https://doi.org/10.1038/ncb2000.

Palmieri, Valentina, Donatella Lucchetti, Ilaria Gatto, Alessandro Maiorana, Margherita Marcantoni, Giuseppe Maulucci, Massimiliano Papi, Roberto Pola, Marco De Spirito, and Alessandro Sgambato. 2014. 'Dynamic Light Scattering for the Characterization and Counting of Extracellular Vesicles: A Powerful Noninvasive Tool'. *Journal of Nanoparticle Research* 16 (9): 2583. https://doi.org/10.1007/s11051-014-2583-z.

Pandya, Kumar, and Oliver Smithies. 2011. ‘β-MyHC and Cardiac Hypertrophy: Size Does Matter’. *Circulation Research* 109 (6): 609–10. https://doi.org/10.1161/CIRCRESAHA.111.252619.

Panidis, Ioannis P., Morris N. Kotler, Jian-Fang Ren, Gary S. Mintz, John Ross, and Peter Kalman. 1984. ‘Development and Regression of Left Ventricular Hypertrophy’. *Journal of the American College of Cardiology* 3 (5): 1309–20. https://doi.org/10.1016/S0735-1097(84)80192-8.

Passier, Robert, Hong Zeng, Norbert Frey, Francisco J Naya, Rebekka L Nicol, Timothy A McKinsey, Paul Overbeek, James A Richardson, Stephen R Grant, and Eric N Olson. 2000. ‘CaM Kinase Signaling Induces Cardiac Hypertrophy and Activates the MEF2 Transcription Factor in Vivo’. *The Journal of Clinical Investigation* 105 (10): 12.

Patten, Richard D., and Monica R. Hall-Porter. 2009. ‘Small Animal Models of Heart Failure: Development of Novel Therapies, Past and Present’. *Circulation: Heart Failure* 2 (2): 138–44. https://doi.org/10.1161/CIRCHEARTFAILURE.108.839761.

Paylor, Ben, Justin Fernandes, Bruce McManus, and Fabio Rossi. 2013. ‘Tissue-Resident Sca1+ PDGFRα+ Mesenchymal Progenitors Are the Cellular Source of Fibrofatty Infiltration in Arrhythmogenic Cardiomyopathy’. *F1000Research* 2 (June): 141. https://doi.org/10.12688/f1000research.2-141.v1.

Pehlivan, Davut, Yavuz Bayram, Nilay Gunes, Zeynep Coban Akdemir, Anju Shukla, Tatjana Bierhals, Burcu Tabakci, et al. 2019. ‘The Genomics of Arthrogryposis, a Complex Trait: Candidate Genes and Further Evidence for Oligogenic Inheritance’. *The American Journal of Human Genetics* 105 (1): 132–50. https://doi.org/10.1016/j.ajhg.2019.05.015.

Pelliccia, Antonio, Barry J. Maron, Rosanna De Luca, Fernando M. Di Paolo, Antonio Spataro, and Franco Culasso. 2002. ‘Remodeling of Left Ventricular Hypertrophy in Elite Athletes After Long-Term Deconditioning’. *Circulation* 105 (8): 944–49. https://doi.org/10.1161/hc0802.104534.

Petretto, Enrico, Jonathan Mangion, Nicholas J Dickens, Stuart A Cook, Mande K Kumaran, Han Lu, Judith Fischer, et al. 2006. ‘Heritability and Tissue Specificity of Expression Quantitative Trait Loci’. Edited by Jonathan Flint. *PLoS Genetics* 2 (10): e172. https://doi.org/10.1371/journal.pgen.0020172.

Petrovčíková, Eva, Kristína Vičíková, and Vladimír Leksa. 2018. 'Extracellular Vesicles – Biogenesis, Composition, Function, Uptake and Therapeutic Applications'. *Biologia* 73 (4): 437–48. https://doi.org/10.2478/s11756-018-0047-0.

Pfeffer, M A, J M Pfeffer, M C Fishbein, P J Fletcher, J Spadaro, R A Kloner, and E Braunwald. 1979. 'Myocardial Infarct Size and Ventricular Function in Rats.' *Circulation Research* 44 (4): 503–12. https://doi.org/10.1161/01.RES.44.4.503.

Pocsfalvi, Gabriella, Christopher Stanly, Annalisa Vilasi, Immacolata Fiume, Giovambattista Capasso, Lilla Turiák, Edit I Buzas, and Károly Vékey. 2016. 'Mass Spectrometry of Extracellular Vesicles: MASS SPECTROMETRY OF EXTRACELLULAR VESICLES'. *Mass Spectrometry Reviews* 35 (1): 3–21. https://doi.org/10.1002/mas.21457.

Polyakova, Victoria, Stefan Hein, Sawa Kostin, Tibor Ziegelhoeffer, and Jutta Schaper. 2004. 'Matrix Metalloproteinases and Their Tissue Inhibitors in Pressure-Overloaded Human Myocardium during Heart Failure Progression'. *Journal of the American College of Cardiology* 44 (8): 1609–18. https://doi.org/10.1016/j.jacc.2004.07.023.

Prendergast, Emily N., Marcos Abraão de Souza Fonseca, Felipe Segato Dezem, Jenny Lester, Beth Y. Karlan, Houtan Noushmehr, Xianzhi Lin, and Kate Lawrenson. 2018. 'Optimizing Exosomal RNA Isolation for RNA-Seq Analyses of Archival Sera Specimens'. Edited by Dawit Tesfaye. *PLOS ONE* 13 (5): e0196913. https://doi.org/10.1371/journal.pone.0196913.

Pulliero, Alessandra, Laura Pergoli, Sebastiano La Maestra, Rosanna Tindara Micale, Anna Camoirano, Valentina Bollati, Alberto Izzotti, and Silvio De Flora. 2019. 'Extracellular Vesicles in Biological Fluids. A Biomarker of Exposure to Cigarette Smoke and Treatment with Chemopreventive Drugs'. *Journal of Preventive Medicine and Hygiene*, November, E327 Pages. https://doi.org/10.15167/2421-4248/JPMH2019.60.4.1284.

Rao, Xiayu, Xuelin Huang, Zhicheng Zhou, and Xin Lin. 2014. 'An Improvement of the 2ˆ(–Delta Delta CT) Method for Quantitative Real-Time Polymerase Chain Reaction Data Analysis', 13.

Rapacciuolo, Antonio, Giovanni Esposito, Kathleen Caron, Lan Mao, Steven A Thomas, and Howard A Rockman. 2001. 'Important Role of Endogenous Norepinephrine and Epinephrine in the Development of in Vivo Pressure-Overload Cardiac Hypertrophy'. *Journal of the American College of Cardiology* 38 (3): 876–82. https://doi.org/10.1016/S0735-1097(01)01433-4.

Raposo, Graça, and Willem Stoorvogel. 2013. ‘Extracellular Vesicles: Exosomes, Microvesicles, and Friends’. *Journal of Cell Biology* 200 (4): 373–83. https://doi.org/10.1083/jcb.201211138.

Rapp, J P. 1982. ‘Dahl Salt-Susceptible and Salt-Resistant Rats. A Review.’ *Hypertension* 4 (6): 753–63. https://doi.org/10.1161/01.HYP.4.6.753.

Rapp, John P. 2000. ‘Genetic Analysis of Inherited Hypertension in the Rat’. *Physiological Reviews* 80 (1): 135–72. https://doi.org/10.1152/physrev.2000.80.1.135.

Rat Genome Sequencing Project Consortium. 2004. ‘Genome Sequence of the Brown Norway Rat Yields Insights into Mammalian Evolution’. *Nature* 428 (6982): 493–521. https://doi.org/10.1038/nature02426.

Reckelhoff, Jane F., Huimin Zhang, and Kumud Srivastava. 2000. ‘Gender Differences in Development of Hypertension in Spontaneously Hypertensive Rats: Role of the Renin-Angiotensin System’. *Hypertension* 35 (1): 480–83. https://doi.org/10.1161/01.HYP.35.1.480.

Renault, Marie-Ange, Fanny Robbesyn, Patricia Réant, Victorine Douin, Danièle Daret, Cécile Allières, Isabelle Belloc, et al. 2010. ‘Osteopontin Expression in Cardiomyocytes Induces Dilated Cardiomyopathy’. *Circulation: Heart Failure* 3 (3): 431–39. https://doi.org/10.1161/CIRCHEARTFAILURE.109.898114.

Richards, Daniel A., Mark J. Aronovitz, Timothy D. Calamaras, Kelly Tam, Gregory L. Martin, Peiwen Liu, Heather K. Bowditch, Phyllis Zhang, Gordon S. Huggins, and Robert M. Blanton. 2019. ‘Distinct Phenotypes Induced by Three Degrees of Transverse Aortic Constriction in Mice’. *Scientific Reports* 9 (1): 5844. https://doi.org/10.1038/s41598-019-42209-7.

Riehle, Christian, and Johann Bauersachs. 2019. ‘Small Animal Models of Heart Failure’. *Cardiovascular Research* 115 (13): 1838–49. https://doi.org/10.1093/cvr/cvz161.

Rikkert, L. G., R. Nieuwland, L. W. M. M. Terstappen, and F. A. W. Coumans. 2019. ‘Quality of Extracellular Vesicle Images by Transmission Electron Microscopy Is Operator and Protocol Dependent’. *Journal of Extracellular Vesicles* 8 (1): 1555419. https://doi.org/10.1080/20013078.2018.1555419.

Rinott, R., A. Jaimovich, and N. Friedman. 2011. ‘Exploring Transcription Regulation through Cell-to-Cell Variability’. *Proceedings of the National Academy of Sciences* 108 (15): 6329–34. https://doi.org/10.1073/pnas.1013148108.

Rittling, Susan R., Hiroko N. Matsumoto, Marc D. Mckee, Antonio Nanci, Xiao-Rong An, Kristine E. Novick, Aaron J. Kowalski, Masaki Noda, and David T. Denhardt. 1998. 'Mice Lacking Osteopontin Show Normal Development and Bone Structure but Display Altered Osteoclast Formation In Vitro'. *Journal of Bone and Mineral Research* 13 (7): 1101–11. https://doi.org/10.1359/jbmr.1998.13.7.1101.

Roberts, Robert, and Ulrich Sigwart. 2001. 'New Concepts in Hypertrophic Cardiomyopathies, Part I', 4.

Robinson, Paul, Peter J. Griffiths, Hugh Watkins, and Charles S. Redwood. 2007. 'Dilated and Hypertrophic Cardiomyopathy Mutations in Troponin and α-Tropomyosin Have Opposing Effects on the Calcium Affinity of Cardiac Thin Filaments'. *Circulation Research* 101 (12): 1266–73. https://doi.org/10.1161/CIRCRESAHA.107.156380.

Rockman, Howard A, ROBERT S Ross, Adrienne N Harris, Kirk U Knowlton, MARK E STEINHELPERt, LOREN J FIELDt, JOHN Ross, and Kenneth R Chien. 1991. 'Segregation of Atrial-Specific and Inducible Expression of an Atrial Natriuretic Factor Transgene in an in Vivo Murine Model of Cardiac Hypertrophy.' *Proc. Natl. Acad. Sci. USA*, 5.

Romano, Francesca, Claudia Chiarenza, Fioretta Palombi, Antonio Filippini, Fabrizio Padula, Elio Ziparo, and Paola De Cesaris. 2006. 'Platelet-Derived Growth Factor-BB-Induced Hypertrophy of Peritubular Smooth Muscle Cells Is Mediated by Activation of P38 MAP-Kinase and of Rho-Kinase'. *Journal of Cellular Physiology* 207 (1): 123–31. https://doi.org/10.1002/jcp.20554.

Rosa-Fernandes, Livia, Victória Bombarda Rocha, Victor Corasolla Carregari, Andrea Urbani, and Giuseppe Palmisano. 2017. 'A Perspective on Extracellular Vesicles Proteomics'. *Frontiers in Chemistry* 5 (November): 102. https://doi.org/10.3389/fchem.2017.00102.

Rosca, Mariana G., Bernard Tandler, and Charles L. Hoppel. 2013. 'Mitochondria in Cardiac Hypertrophy and Heart Failure'. *Journal of Molecular and Cellular Cardiology* 55 (February): 31–41. https://doi.org/10.1016/j.yjmcc.2012.09.002.

Rosca, Mariana G., Edwin J. Vazquez, Janos Kerner, William Parland, Margaret P. Chandler, William Stanley, Hani N. Sabbah, and Charles L. Hoppel. 2008. 'Cardiac Mitochondria in Heart Failure: Decrease in Respirasomes and Oxidative Phosphorylation'. *Cardiovascular Research* 80 (1): 30–39. https://doi.org/10.1093/cvr/cvn184.

Rosen, Boaz D., Thor Edvardsen, Shenghan Lai, Ernesto Castillo, Li Pan, Michael Jerosch-Herold, Shantanu Sinha, et al. 2005. 'Left Ventricular Concentric Remodeling Is Associated With Decreased Global and Regional Systolic Function: The Multi-Ethnic Study of Atherosclerosis'. *Circulation* 112 (7): 984–91. https://doi.org/10.1161/CIRCULATIONAHA.104.500488.

Rossi, Marcos A. 1998. 'Pathologic Fibrosis and Connective Tissue Matrix in Left Ventricular Hypertrophy Due to Chronic Arterial Hypertension in Humans': *Journal of Hypertension* 16 (7): 1031–41. https://doi.org/10.1097/00004872-199816070-00018.

Rücker-Martin, C. 2002. 'Dedifferentiation of Atrial Myocytes during Atrial Fibrillation: Role of Fibroblast Proliferation in Vitro'. *Cardiovascular Research* 55 (1): 38–52. https://doi.org/10.1016/S0008-6363(02)00338-3.

Rucker-Martin, Catherine, Francoise Pecker, David Godreau, and Stephane N Hatem. 2002. 'Dedifferentiation of Atrial Myocytes during Atrial FIbrillation: Role of FIbroblast Proliferation in Vitro'. *Cardiovascular Research*, 15.

Ruppert, Mihály, Sevil Korkmaz-Icöz, Shiliang Li, Béla Merkely, Matthias Karck, Tamás Radovits, and Gábor Szabó. 2017. 'Reverse Electrical Remodeling Following Pressure Unloading in a Rat Model of Hypertension-Induced Left Ventricular Myocardial Hypertrophy'. *Hypertension Research* 40 (7): 637–45. https://doi.org/10.1038/hr.2017.1.

Ruppert, Mihály, Bálint Károly Lakatos, Szilveszter Braun, Márton Tokodi, Christian Karime, Attila Oláh, Alex Ali Sayour, et al. 2020. 'Longitudinal Strain Reflects Ventriculoarterial Coupling Rather Than Mere Contractility in Rat Models of Hemodynamic Overload–Induced Heart Failure'. *Journal of the American Society of Echocardiography* 33 (10): 1264-1275.e4. https://doi.org/10.1016/j.echo.2020.05.017.

Sakai, Satoshi, Takashi Miyauchi, Takeshi Sakurai, Yoshitoshi Kasuya, Masaki Ihara, Iwao Yamaguchi, Katsutoshi Goto, and Yasuro Sugishita. 1996. 'Endogenous Endothelin-1 Participates in the Maintenance of Cardiac Function in Rats With Congestive Heart Failure: Marked Increase in Endothelin-1 Production in the Failing Heart'. *Circulation* 93 (6): 1214–22. https://doi.org/10.1161/01.CIR.93.6.1214.

Sam, Flora, Douglas B. Sawyer, Donny L.-F. Chang, Franz R. Eberli, Soeun Ngoy, Mohit Jain, Jay Amin, Carl S. Apstein, and Wilson S. Colucci. 2000. 'Progressive Left Ventricular Remodeling and Apoptosis Late after Myocardial Infarction in Mouse

Heart'. *American Journal of Physiology-Heart and Circulatory Physiology* 279 (1): H422–28. https://doi.org/10.1152/ajpheart.2000.279.1.H422.

Sampson, Amanda K., Karen L. Andrews, Delyth Graham, Martin W. McBride, Geoffrey A. Head, Merlin C. Thomas, Jaye P.F. Chin-Dusting, Anna F. Dominiczak, and Garry L. Jennings. 2014. 'Origin of the Y Chromosome Influences Intrarenal Vascular Responsiveness to Angiotensin I and Angiotensin (1-7) in Stroke-Prone Spontaneously Hypertensive Rats'. *Hypertension* 64 (6): 1376–83. https://doi.org/10.1161/HYPERTENSIONAHA.114.03756.

Scatena, Marta, Manuela Almeida, Michelle L Chaisson, Nelson Fausto, Roberto F Nicosia, and Cecilia M Giachelli. 1998. 'NF-□B Mediates ⎵v␋3 Integrin-Induced Endothelial Cell Survival'. *The Journal of Cell Biology* 141: 11.

Scatena, Marta, Lucy Liaw, and Cecilia M. Giachelli. 2007. 'Osteopontin: A Multifunctional Molecule Regulating Chronic Inflammation and Vascular Disease'. *Arteriosclerosis, Thrombosis, and Vascular Biology* 27 (11): 2302–9. https://doi.org/10.1161/ATVBAHA.107.144824.

Schröder, Rolf, and Benedikt Schoser. 2009. 'Myofibrillar Myopathies: A Clinical and Myopathological Guide'. *Brain Pathology* 19 (3): 483–92. https://doi.org/10.1111/j.1750-3639.2009.00289.x.

'Scientific Program 2012 ISEV Meeting Wednesday 18th April'. 2012. *Journal of Extracellular Vesicles* 1 (1): 18182. https://doi.org/10.3402/jev.v1i0.18182.

Seok, Hee Young, Jinghai Chen, Masaharu Kataoka, Zhan-Peng Huang, Jian Ding, Jinglu Yan, Xiaoyun Hu, and Da-Zhi Wang. 2014. 'Loss of MicroRNA-155 Protects the Heart From Pathological Cardiac Hypertrophy'. *Circulation Research* 114 (10): 1585–95. https://doi.org/10.1161/CIRCRESAHA.114.303784.

Serneri, Gian Gastone Neri, Maria Boddi, Ilaria Cecioni, Simone Vanni, Mirella Coppo, Maria Letizia Papa, Brunella Bandinelli, et al. 2001. 'Cardiac Angiotensin II Formation in the Clinical Course of Heart Failure and Its Relationship With Left Ventricular Function'. *Circulation Research* 88 (9): 961–68. https://doi.org/10.1161/hh0901.089882.

Shah, Ravi, Tushar Patel, and Jane E. Freedman. 2018. 'Circulating Extracellular Vesicles in Human Disease'. *New England Journal of Medicine* 379 (10): 958–66. https://doi.org/10.1056/NEJMra1704286.

Shah, Sonia, Christopher P. Nelson, Tom R. Gaunt, Pim van der Harst, Timothy Barnes, Peter S. Braund, Debbie A. Lawlor, et al. 2011. 'Four Genetic Loci Influencing Electrocardiographic Indices of Left Ventricular Hypertrophy'. *Circulation: Cardiovascular Genetics* 4 (6): 626–35. https://doi.org/10.1161/CIRCGENETICS.111.960203.

Shanks, Garrett W., David J. Tester, Sneha Nishtala, Jared M. Evans, and Michael J. Ackerman. 2017. 'Genomic Triangulation and Coverage Analysis in Whole-Exome Sequencing–Based Molecular Autopsies'. *Circulation: Cardiovascular Genetics* 10 (5): e001828. https://doi.org/10.1161/CIRCGENETICS.117.001828.

Shao, Haifeng, David S. Sinasac, Lindsay C. Burrage, Craig A. Hodges, Pamela J. Supelak, Mark R. Palmert, Carol Moreno, Allen W. Cowley, Howard J. Jacob, and Joseph H. Nadeau. 2010. 'Analyzing Complex Traits with Congenic Strains'. *Mammalian Genome* 21 (5–6): 276–86. https://doi.org/10.1007/s00335-010-9267-5.

Shenasa, Mohammad, and Hossein Shenasa. 2017. 'Hypertension, Left Ventricular Hypertrophy, and Sudden Cardiac Death'. *International Journal of Cardiology* 237 (June): 60–63. https://doi.org/10.1016/j.ijcard.2017.03.002.

Shephard, Roy J, and Gary J Balady. 1999. 'Exercise as Cardiovascular Therapy', 10.

Shimizu, Ippei, and Tohru Minamino. 2016. 'Physiological and Pathological Cardiac Hypertrophy'. *Journal of Molecular and Cellular Cardiology* 97 (August): 245–62. https://doi.org/10.1016/j.yjmcc.2016.06.001.

Shiraga, H., W. Min, W. J. VanDusen, M. D. Clayman, D. Miner, C. H. Terrell, J. R. Sherbotie, J. W. Foreman, C. Przysiecki, and E. G. Neilson. 1992. 'Inhibition of Calcium Oxalate Crystal Growth in Vitro by Uropontin: Another Member of the Aspartic Acid-Rich Protein Superfamily.' *Proceedings of the National Academy of Sciences* 89 (1): 426–30. https://doi.org/10.1073/pnas.89.1.426.

Shirakawa, Kohsuke, and Motoaki Sano. 2021. 'Osteopontin in Cardiovascular Diseases'. *Biomolecules* 11 (7): 1047. https://doi.org/10.3390/biom11071047.

Shrivastava, Surya, and Kevin V. Morris. 2021. 'The Multifunctionality of Exosomes; from the Garbage Bin of the Cell to a Next Generation Gene and Cellular Therapy'. *Genes* 12 (2): 173. https://doi.org/10.3390/genes12020173.

Simone, Giovanni de, Stephen R. Daniels, Thomas R. Kimball, Mary J. Roman, Carmela Romano, Marcello Chinali, Maurizio Galderisi, and Richard B. Devereux. 2005. 'Evaluation of Concentric Left Ventricular Geometry in Humans: Evidence for Age-

Related Systematic Underestimation'. *Hypertension* 45 (1): 64–68. https://doi.org/10.1161/01.HYP.0000150108.37527.57.

Simpson, P. 1983. 'Norepinephrine-Stimulated Hypertrophy of Cultured Rat Myocardial Cells Is an Alpha 1 Adrenergic Response.' *Journal of Clinical Investigation* 72 (2): 732–38. https://doi.org/10.1172/JCI111023.

Simpson, P, A McGrath, and S Savion. 1982. 'Myocyte Hypertrophy in Neonatal Rat Heart Cultures and Its Regulation by Serum and by Catecholamines.' *Circulation Research* 51 (6): 787–801. https://doi.org/10.1161/01.RES.51.6.787.

Singh, Krishna, Geza Sirokman, Catherine Communal, Kathleen G. Robinson, Chester H. Conrad, Wesley W. Brooks, Oscar H. L. Bing, and Wilson S. Colucci. 1999. 'Myocardial Osteopontin Expression Coincides With the Development of Heart Failure'. *Hypertension* 33 (2): 663–70. https://doi.org/10.1161/01.HYP.33.2.663.

Singh, Mahipal, Suman Dalal, and Krishna Singh. 2014. 'Osteopontin: At the Cross-Roads of Myocyte Survival and Myocardial Function'. *Life Sciences* 118 (1): 1–6. https://doi.org/10.1016/j.lfs.2014.09.014.

Singh, Mahipal, Cerrone R. Foster, Suman Dalal, and Krishna Singh. 2010. 'Osteopontin: Role in Extracellular Matrix Deposition and Myocardial Remodeling Post-MI'. *Journal of Molecular and Cellular Cardiology* 48 (3): 538–43. https://doi.org/10.1016/j.yjmcc.2009.06.015.

Singh, Shalini, Isabella W.Y. Mak, Robert W. Cowan, Robert Turcotte, Gurmit Singh, and Michelle Ghert. 2011. 'The Role of TWIST as a Regulator in Giant Cell Tumor of Bone'. *Journal of Cellular Biochemistry* 112 (9): 2287–95. https://doi.org/10.1002/jcb.23149.

Skog, Johan, Tom Würdinger, Sjoerd van Rijn, Dimphna H. Meijer, Laura Gainche, William T. Curry, Bob S. Carter, Anna M. Krichevsky, and Xandra O. Breakefield. 2008. 'Glioblastoma Microvesicles Transport RNA and Proteins That Promote Tumour Growth and Provide Diagnostic Biomarkers'. *Nature Cell Biology* 10 (12): 1470–76. https://doi.org/10.1038/ncb1800.

Skoog, Douglas A., F. James Holler, and Stanley R. Crouch. 2007. *Principles of Instrumental Analysis*. 6th ed. Belmont, CA: Thomson Brooks/Cole.

Sluijter, Joost P., Pieter A. Doevendans, and Marie-José Goumans. 2011. 'Letter by Sluijter et al Regarding Article, "Human Cardiac Stem Cell Differentiation Is Regulated by a Mircrine Mechanism"'. *Circulation* 124 (17). https://doi.org/10.1161/CIRCULATIONAHA.111.037655.

Sluijter, Joost Petrus Gerardus, Sean Michael Davidson, Chantal M Boulanger, Edit Iren Buzás, Dominique Paschalis Victor de Kleijn, Felix Benedikt Engel, Zoltán Giricz, et al. 2018. 'Extracellular Vesicles in Diagnostics and Therapy of the Ischaemic Heart: Position Paper from the Working Group on Cellular Biology of the Heart of the European Society of Cardiology'. *Cardiovascular Research* 114 (1): 19–34. https://doi.org/10.1093/cvr/cvx211.

Smith, George Davey, Shah Ebrahim, Sarah Lewis, Anna L. Hansell, Lyle J. Palmer, and Paul R. Burton. 2005. 'Genetic Epidemiology and Public Health: Hope, Hype, and Future Prospects'. *The Lancet* 366 (9495): 1484–98. https://doi.org/10.1016/S0140-6736(05)67601-5.

Smith, Jennifer R, G Thomas Hayman, Shur-Jen Wang, Stanley J F Laulederkind, Matthew J Hoffman, Mary L Kaldunski, Monika Tutaj, et al. 2019. 'The Year of the Rat: The Rat Genome Database at 20: A Multi-Species Knowledgebase and Analysis Platform'. *Nucleic Acids Research*, November, gkz1041. https://doi.org/10.1093/nar/gkz1041.

Smith, Laura L, and Cecilia M Giachelli. 1998. 'Structural Requirements for ␣9␣1-Mediated Adhesion and Migration to Thrombin-Cleaved Osteopontin', 10.

Smith, Vivienne-Elizabeth, Peter Schulman, Mozafareddin K. Karimeddini, William B. White, Moideen K. Meeran, and Arnold M. Katz. 1985. 'Rapid Ventricular Filling in Left Ventricular Hypertrophy: II. Pathologic Hypertrophy'. *Journal of the American College of Cardiology* 5 (4): 869–74. https://doi.org/10.1016/S0735-1097(85)80425-3.

Smith, Zachary J., Changwon Lee, Tatu Rojalin, Randy P. Carney, Sidhartha Hazari, Alisha Knudson, Kit Lam, et al. 2015. 'Single Exosome Study Reveals Subpopulations Distributed among Cell Lines with Variability Related to Membrane Content'. *Journal of Extracellular Vesicles* 4 (1): 28533. https://doi.org/10.3402/jev.v4.28533.

Sodek, J., A. Paes Batista Da Silva, and R. Zohar. 2006. 'Osteopontin and Mucosal Protection'. *Journal of Dental Research* 85 (5): 404–15. https://doi.org/10.1177/154405910608500503.

Sokolova, Viktoriya, Anna-Kristin Ludwig, Sandra Hornung, Olga Rotan, Peter A. Horn, Matthias Epple, and Bernd Giebel. 2011. 'Characterisation of Exosomes Derived from Human Cells by Nanoparticle Tracking Analysis and Scanning Electron

Microscopy'. *Colloids and Surfaces B: Biointerfaces* 87 (1): 146–50. https://doi.org/10.1016/j.colsurfb.2011.05.013.

Songstad, Nils Thomas, David Johansen, Ole-Jacob How, Per Ivar Kaaresen, Kirsti Ytrehus, and Ganesh Acharya. 2014. 'Effect of Transverse Aortic Constriction on Cardiac Structure, Function and Gene Expression in Pregnant Rats'. Edited by Rajesh Gopalrao Katare. *PLoS ONE* 9 (2): e89559. https://doi.org/10.1371/journal.pone.0089559.

Spinale, Francis G. 2007. 'Myocardial Matrix Remodeling and the Matrix Metalloproteinases: Influence on Cardiac Form and Function'. *Physiological Reviews* 87 (4): 1285–1342. https://doi.org/10.1152/physrev.00012.2007.

Stenmark, Harald. 2009. 'Rab GTPases as Coordinators of Vesicle Traffic'. *Nature Reviews Molecular Cell Biology* 10 (8): 513–25. https://doi.org/10.1038/nrm2728.

Stewart, Alexandre F.R., Joseph Suzow, Toru Kubota, Takahisa Ueyama, and Hsiao-Huei Chen. 1998. 'Transcription Factor RTEF-1 Mediates α $_1$ -Adrenergic Reactivation of the Fetal Gene Program in Cardiac Myocytes'. *Circulation Research* 83 (1): 43–49. https://doi.org/10.1161/01.RES.83.1.43.

Stoner, Samuel A., Erika Duggan, Danilo Condello, Abraham Guerrero, James R. Turk, Padma K. Narayanan, and John P. Nolan. 2016. 'High Sensitivity Flow Cytometry of Membrane Vesicles: Vesicle Flow Cytometry'. *Cytometry Part A* 89 (2): 196–206. https://doi.org/10.1002/cyto.a.22787.

Stranska, Ruzena, Laurens Gysbrechts, Jens Wouters, Pieter Vermeersch, Katarzyna Bloch, Daan Dierickx, Graciela Andrei, and Robert Snoeck. 2018. 'Comparison of Membrane Affinity-Based Method with Size-Exclusion Chromatography for Isolation of Exosome-like Vesicles from Human Plasma'. *Journal of Translational Medicine* 16 (1): 1. https://doi.org/10.1186/s12967-017-1374-6.

Struhl, Kevin. 2007. 'Transcriptional Noise and the Fidelity of Initiation by RNA Polymerase II'. *Nature Structural & Molecular Biology* 14 (2): 103–5. https://doi.org/10.1038/nsmb0207-103.

Subramanian, Venkateswaran, Prasanna Krishnamurthy, Krishna Singh, and Mahipal Singh. 2007. 'Lack of Osteopontin Improves Cardiac Function in Streptozotocin-Induced Diabetic Mice'. *American Journal of Physiology-Heart and Circulatory Physiology* 292 (1): H673–83. https://doi.org/10.1152/ajpheart.00569.2006.

Sud, Amit, Ben Kinnersley, and Richard S. Houlston. 2017. 'Genome-Wide Association Studies of Cancer: Current Insights and Future Perspectives'. *Nature Reviews Cancer* 17 (11): 692–704. https://doi.org/10.1038/nrc.2017.82.

Sunkara, Vijaya, Hyun-Kyung Woo, and Yoon-Kyoung Cho. 2016. 'Emerging Techniques in the Isolation and Characterization of Extracellular Vesicles and Their Roles in Cancer Diagnostics and Prognostics'. *The Analyst* 141 (2): 371–81. https://doi.org/10.1039/C5AN01775K.

Swynghedauw, B. 1997. 'Cardiac Hypertrophy, Arrhythmogenicity and the New Myocardial Phenotype. II. The Cellular Adaptational Process'. *Cardiovascular Research* 35 (1): 6–12. https://doi.org/10.1016/S0008-6363(97)00076-X.

Szalay, Gudrun, Martina Sauter, Michael Haberland, Ulrich Zuegel, Andreas Steinmeyer, Reinhard Kandolf, and Karin Klingel. 2009. 'Osteopontin: A Fibrosis-Related Marker Molecule in Cardiac Remodeling of Enterovirus Myocarditis in the Susceptible Host'. *Circulation Research* 104 (7): 851–59. https://doi.org/10.1161/CIRCRESAHA.109.193805.

Tam, Vivian, Nikunj Patel, Michelle Turcotte, Yohan Bossé, Guillaume Paré, and David Meyre. 2019. 'Benefits and Limitations of Genome-Wide Association Studies'. *Nature Reviews Genetics* 20 (8): 467–84. https://doi.org/10.1038/s41576-019-0127-1.

Tan, Aaron, Jayakumar Rajadas, and Alexander M. Seifalian. 2013. 'Exosomes as Nano-Theranostic Delivery Platforms for Gene Therapy'. *Advanced Drug Delivery Reviews* 65 (3): 357–67. https://doi.org/10.1016/j.addr.2012.06.014.

Tan, Kiat T., Adam A. Dempsey, and Choong-Chin Liew. 1999. 'Cardiac Genes and Gene Databases for Cardiovascular Disease Genetics'. *Current Hypertension Reports* 1 (1): 51–58. https://doi.org/10.1007/s11906-999-0073-y.

Tanase, H, Y Yamori, C T Hansen, and W Lovenberg. 1982. 'Heart Size in Inbred Strains of Rats. Part 1. Genetic Determination of the Development of Cardiovascular Enlargement in Rats.' *Hypertension* 4 (6): 864–72. https://doi.org/10.1161/01.HYP.4.6.864.

Tauro, Bow J., David W. Greening, Rommel A. Mathias, Hong Ji, Suresh Mathivanan, Andrew M. Scott, and Richard J. Simpson. 2012. 'Comparison of Ultracentrifugation, Density Gradient Separation, and Immunoaffinity Capture Methods for Isolating Human Colon Cancer Cell Line LIM1863-Derived Exosomes'. *Methods* 56 (2): 293–304. https://doi.org/10.1016/j.ymeth.2012.01.002.

Tavakoli, Reza, Simona Nemska, Peiman Jamshidi, Max Gassmann, and Nelly Frossard. 2017. 'Technique of Minimally Invasive Transverse Aortic Constriction in Mice for Induction of Left Ventricular Hypertrophy'. *Journal of Visualized Experiments*, no. 127 (September): 56231. https://doi.org/10.3791/56231.

Thakur, Basant Kumar, Haiying Zhang, Annette Becker, Irina Matei, Yujie Huang, Bruno Costa-Silva, Yan Zheng, et al. 2014. 'Double-Stranded DNA in Exosomes: A Novel Biomarker in Cancer Detection'. *Cell Research* 24 (6): 766–69. https://doi.org/10.1038/cr.2014.44.

Thane, Kristen E., Airiel M. Davis, and Andrew M. Hoffman. 2019. 'Improved Methods for Fluorescent Labeling and Detection of Single Extracellular Vesicles Using Nanoparticle Tracking Analysis'. *Scientific Reports* 9 (1): 12295. https://doi.org/10.1038/s41598-019-48181-6.

The STAR Consortium. 2008. 'SNP and Haplotype Mapping for Genetic Analysis in the Rat'. *Nature Genetics* 40 (5): 560–66. https://doi.org/10.1038/ng.124.

Théry, Clotilde, Sebastian Amigorena, Graça Raposo, and Aled Clayton. 2006. 'Isolation and Characterization of Exosomes from Cell Culture Supernatants and Biological Fluids'. *Current Protocols in Cell Biology* 30 (1). https://doi.org/10.1002/0471143030.cb0322s30.

Théry, Clotilde, Kenneth W Witwer, Elena Aikawa, Maria Jose Alcaraz, Johnathon D Anderson, Ramaroson Andriantsitohaina, Anna Antoniou, et al. 2018. 'Minimal Information for Studies of Extracellular Vesicles 2018 (MISEV2018): A Position Statement of the International Society for Extracellular Vesicles and Update of the MISEV2014 Guidelines'. *Journal of Extracellular Vesicles* 7 (1): 1535750. https://doi.org/10.1080/20013078.2018.1535750.

Tielking, Katharina, Silvia Fischer, Klaus T. Preissner, Peter Vajkoczy, and Ran Xu. 2019. 'Extracellular RNA in Central Nervous System Pathologies'. *Frontiers in Molecular Neuroscience* 12 (October): 254. https://doi.org/10.3389/fnmol.2019.00254.

Tomaszewski, Maciej, Radoslaw Debiec, Peter S. Braund, Christopher P. Nelson, Robert Hardwick, Paraskevi Christofidou, Matthew Denniff, et al. 2010. 'Genetic Architecture of Ambulatory Blood Pressure in the General Population: Insights From Cardiovascular Gene-Centric Array'. *Hypertension* 56 (6): 1069–76. https://doi.org/10.1161/HYPERTENSIONAHA.110.155721.

Torella, D., G. M. Ellison, I. Karakikes, and B. Nadal-Ginard. 2007. 'Cardiovascular Development: Towards Biomedical Applicability: Resident Cardiac Stem Cells'. *Cellular and Molecular Life Sciences* 64 (6): 661–73. https://doi.org/10.1007/s00018-007-6519-y.

Tosar, Juan Pablo, Alfonso Cayota, Erez Eitan, Marc K. Halushka, and Kenneth W. Witwer. 2017. 'Ribonucleic Artefacts: Are Some Extracellular RNA Discoveries Driven by Cell Culture Medium Components?' *Journal of Extracellular Vesicles* 6 (1): 1272832. https://doi.org/10.1080/20013078.2016.1272832.

Trueblood, Nathan A., Zhonglin Xie, Catherine Communal, Flora Sam, Soeun Ngoy, Lucy Liaw, Alan W. Jenkins, et al. 2001. 'Exaggerated Left Ventricular Dilation and Reduced Collagen Deposition After Myocardial Infarction in Mice Lacking Osteopontin'. *Circulation Research* 88 (10): 1080–87. https://doi.org/10.1161/hh1001.090842.

Turchinovich, Andrey, Oxana Drapkina, and Alexander Tonevitsky. 2019. 'Transcriptome of Extracellular Vesicles: State-of-the-Art'. *Frontiers in Immunology* 10 (February): 202. https://doi.org/10.3389/fimmu.2019.00202.

Turchinovich, Andrey, Ludmila Weiz, Anne Langheinz, and Barbara Burwinkel. 2011. 'Characterization of Extracellular Circulating MicroRNA'. *Nucleic Acids Research* 39 (16): 7223–33. https://doi.org/10.1093/nar/gkr254.

Turner, Monte E., Joel Farkas, Jeff Dunmire, Daniel Ely, and Amy Milsted. 2009. 'Which Sry Locus Is the Hypertensive Y Chromosome Locus?' *Hypertension* 53 (2): 430–35. https://doi.org/10.1161/HYPERTENSIONAHA.108.124131.

Turner, Monte E, Carey Martin, Almir S Martins, Jeffrey Dunmire, Joel Farkas, Daniel L Ely, and Amy Milsted. 2007. 'Genomic and Expression Analysis of Multiple Sry Loci from a Single Rattus Norvegicus Y Chromosome'. *BMC Genetics* 8 (1): 11. https://doi.org/10.1186/1471-2156-8-11.

Urabe, Fumihiko, Nobuyoshi Kosaka, Kagenori Ito, Takahiro Kimura, Shin Egawa, and Takahiro Ochiya. 2020. 'Extracellular Vesicles as Biomarkers and Therapeutic Targets for Cancer'. *American Journal of Physiology-Cell Physiology* 318 (1): C29–39. https://doi.org/10.1152/ajpcell.00280.2019.

Usman, Waqas Muhammad, Tin Chanh Pham, Yuk Yan Kwok, Luyen Tien Vu, Victor Ma, Boya Peng, Yuen San Chan, et al. 2018. 'Efficient RNA Drug Delivery Using Red Blood Cell Extracellular Vesicles'. *Nature Communications* 9 (1): 2359. https://doi.org/10.1038/s41467-018-04791-8.

Valadi, Hadi, Karin Ekström, Apostolos Bossios, Margareta Sjöstrand, James J Lee, and Jan O Lötvall. 2007. 'Exosome-Mediated Transfer of MRNAs and MicroRNAs Is a Novel Mechanism of Genetic Exchange between Cells'. *Nature Cell Biology* 9 (6): 654–59. https://doi.org/10.1038/ncb1596.

Vestad, Beate, Alicia Llorente, Axl Neurauter, Santosh Phuyal, Bente Kierulf, Peter Kierulf, Tore Skotland, Kirsten Sandvig, Kari Bente F. Haug, and Reidun Øvstebø. 2017. 'Size and Concentration Analyses of Extracellular Vesicles by Nanoparticle Tracking Analysis: A Variation Study'. *Journal of Extracellular Vesicles* 6 (1): 1344087. https://doi.org/10.1080/20013078.2017.1344087.

Veziroglu, Eren M., and George I. Mias. 2020. 'Characterizing Extracellular Vesicles and Their Diverse RNA Contents'. *Frontiers in Genetics* 11 (July): 700. https://doi.org/10.3389/fgene.2020.00700.

Villarroya-Beltri, Carolina, Cristina Gutiérrez-Vázquez, Fátima Sánchez-Cabo, Daniel Pérez-Hernández, Jesús Vázquez, Noa Martin-Cofreces, Dannys Jorge Martinez-Herrera, Alberto Pascual-Montano, María Mittelbrunn, and Francisco Sánchez-Madrid. 2013. 'Sumoylated HnRNPA2B1 Controls the Sorting of MiRNAs into Exosomes through Binding to Specific Motifs'. *Nature Communications* 4 (1): 2980. https://doi.org/10.1038/ncomms3980.

Vindis, Cécile, Romina D'Angelo, Elodie Mucher, Anne Nègre-Salvayre, Angelo Parini, and Jeanne Mialet-Perez. 2010. 'Essential Role of TRPC1 Channels in Cardiomyoblasts Hypertrophy Mediated by 5-HT2A Serotonin Receptors'. *Biochemical and Biophysical Research Communications* 391 (1): 979–83. https://doi.org/10.1016/j.bbrc.2009.12.001.

Visscher, Peter M, and Michael E Goddard. 2019. 'From R.A. Fisher's 1918 Paper to GWAS a Century Later'. *Genetics* 211 (4): 1125–30. https://doi.org/10.1534/genetics.118.301594.

Vogel, Robert, Frank A. W. Coumans, Raluca G. Maltesen, Anita N. Böing, Katherine E. Bonnington, Marike L. Broekman, Murray F. Broom, et al. 2016. 'A Standardized Method to Determine the Concentration of Extracellular Vesicles Using Tunable Resistive Pulse Sensing'. *Journal of Extracellular Vesicles* 5 (1): 31242. https://doi.org/10.3402/jev.v5.31242.

Wada, Takeo, Marc D. McKee, Susie Steitz, and Cecilia M. Giachelli. 1999. 'Calcification of Vascular Smooth Muscle Cell Cultures: Inhibition by Osteopontin'. *Circulation Research* 84 (2): 166–78. https://doi.org/10.1161/01.RES.84.2.166.

Wakker, S.I. van de, J. van Oudheusden, E.A. Mol, M.T. Roefs, W. Zheng, A. Görgens, S. El Andaloussi, J.P.G. Sluijter, and P. Vader. 2022. 'Influence of Short Term Storage Conditions, Concentration Methods and Excipients on Extracellular Vesicle Recovery and Function'. *European Journal of Pharmaceutics and Biopharmaceutics* 170 (January): 59–69. https://doi.org/10.1016/j.ejpb.2021.11.012.

Waldenström, Anders, Nina Gennebäck, Urban Hellman, and Gunnar Ronquist. 2012. 'Cardiomyocyte Microvesicles Contain DNA/RNA and Convey Biological Messages to Target Cells'. Edited by Gangjian Qin. *PLoS ONE* 7 (4): e34653. https://doi.org/10.1371/journal.pone.0034653.

Waldenström, Anders, and Gunnar Ronquist. 2014. 'Role of Exosomes in Myocardial Remodeling'. *Circulation Research* 114 (2): 315–24. https://doi.org/10.1161/CIRCRESAHA.114.300584.

Walsh-Wilkinson, Elisabeth, Marie-Claude Drolet, Marie Arsenault, and Jacques Couet. 2020. 'Sex Differences in the Evolution of Left Ventricle Remodeling in Rats with Severe Volume Overload'. *BMC Cardiovascular Disorders* 20 (1): 51. https://doi.org/10.1186/s12872-020-01360-0.

Wang, Jian, Yao Song, Yan Zhang, Han Xiao, Qiang Sun, Ning Hou, Shuilong Guo, et al. 2012. 'Cardiomyocyte Overexpression of MiR-27b Induces Cardiac Hypertrophy and Dysfunction in Mice'. *Cell Research* 22 (3): 516–27. https://doi.org/10.1038/cr.2011.132.

Wang, Kai, Shile Zhang, Jessica Weber, David Baxter, and David J. Galas. 2010. 'Export of MicroRNAs and MicroRNA-Protective Protein by Mammalian Cells'. *Nucleic Acids Research* 38 (20): 7248–59. https://doi.org/10.1093/nar/gkq601.

Wang, Kathryn X., and David T. Denhardt. 2008. 'Osteopontin: Role in Immune Regulation and Stress Responses'. *Cytokine & Growth Factor Reviews* 19 (5–6): 333–45. https://doi.org/10.1016/j.cytogfr.2008.08.001.

Watkins, Sarah J., Gillian M. Borthwick, and Helen M. Arthur. 2011. 'The H9C2 Cell Line and Primary Neonatal Cardiomyocyte Cells Show Similar Hypertrophic Responses in Vitro'. *In Vitro Cellular & Developmental Biology - Animal* 47 (2): 125–31. https://doi.org/10.1007/s11626-010-9368-1.

Webber, Jason, and Aled Clayton. 2013. 'How Pure Are Your Vesicles?' *Journal of Extracellular Vesicles* 2 (1): 19861. https://doi.org/10.3402/jev.v2i0.19861.

Weber, Andreas, Annalena L Büttner, Philipp Rellecke, Georgi Petrov, Alexander Albert, Stephan U Sixt, Artur Lichtenberg, and Payam Akhyari. 2020. 'Osteopontin as Novel

Biomarker for Reversibility of Pressure Overload Induced Left Ventricular Hypertrophy'. *Biomarkers in Medicine* 14 (7): 513–23. https://doi.org/10.2217/bmm-2019-0410.

Weeks, Kate L., and Julie R. McMullen. 2011. 'The Athlete's Heart vs. the Failing Heart: Can Signaling Explain the Two Distinct Outcomes?' *Physiology* 26 (2): 97–105. https://doi.org/10.1152/physiol.00043.2010.

Weinheimer, Carla J, Ling Lai, Daniel P Kelly, and Attila Kovacs. 2015. 'Novel Mouse Model of Left Ventricular Pressure Overload and Infarction Causing Predictable Ventricular Remodelling and Progression to Heart Failure'. *Clinical and Experimental Pharmacology and Physiology* 42 (1): 33–40. https://doi.org/10.1111/1440-1681.12318.

Weintraub, Andrea S, Lynn M Schnapp, Xinjie Lin, and Mark B Taubman. 2000. 'Osteopontin Deficiency in Rat Vascular Smooth Muscle Cells Is Associated with an Inability to Adhere to Collagen and Increased Apoptosis'. *Laboratory Investigation* 80 (11): 1603–15. https://doi.org/10.1038/labinvest.3780171.

Weisman, H F, D E Bush, J A Mannisi, M L Weisfeldt, and B Healy. 1988. 'Cellular Mechanisms of Myocardial Infarct Expansion.' *Circulation* 78 (1): 186–201. https://doi.org/10.1161/01.CIR.78.1.186.

Welsh, Joshua A., Judith A. Holloway, James S. Wilkinson, and Nicola A. Englyst. 2017. 'Extracellular Vesicle Flow Cytometry Analysis and Standardization'. *Frontiers in Cell and Developmental Biology* 5 (August): 78. https://doi.org/10.3389/fcell.2017.00078.

Welton, Joanne Louise, Jason Paul Webber, Laur-Alexandru Botos, Michael Jones, and Aled Clayton. 2015. 'Ready-Made Chromatography Columns for Extracellular Vesicle Isolation from Plasma'. *Journal of Extracellular Vesicles* 4 (1): 27269. https://doi.org/10.3402/jev.v4.27269.

Wesson, Jeffrey A., Elaine M. Worcester, John H. Wiessner, Neil S. Mandel, and Jack G. Kleinman. 1998. 'Control of Calcium Oxalate Crystal Structure and Cell Adherence by Urinary Macromolecules'. *Kidney International* 53 (4): 952–57. https://doi.org/10.1111/j.1523-1755.1998.00839.x.

Wiklander, Oscar P. B., R. Beklem Bostancioglu, Joshua A. Welsh, Antje M. Zickler, Florian Murke, Giulia Corso, Ulrika Felldin, et al. 2018. 'Systematic Methodological Evaluation of a Multiplex Bead-Based Flow Cytometry Assay for Detection of Extracellular Vesicle Surface Signatures'. *Frontiers in Immunology* 9 (June): 1326. https://doi.org/10.3389/fimmu.2018.01326.

Wilde, Elena, Aisah A. Aubdool, Pratish Thakore, Lineu Baldissera, Khadija M. Alawi, Julie Keeble, Manasi Nandi, and Susan D. Brain. 2017. 'Tail-Cuff Technique and Its Influence on Central Blood Pressure in the Mouse'. *Journal of the American Heart Association* 6 (6): e005204. https://doi.org/10.1161/JAHA.116.005204.

Willms, Eduard, Henrik J. Johansson, Imre Mäger, Yi Lee, K. Emelie M. Blomberg, Mariam Sadik, Amr Alaarg, et al. 2016. 'Cells Release Subpopulations of Exosomes with Distinct Molecular and Biological Properties'. *Scientific Reports* 6 (1): 22519. https://doi.org/10.1038/srep22519.

Wu, Jian, Daxiang Li, Lingling Du, Mustafa Baldawi, Marjorie E. Gable, Amir Askari, and Lijun Liu. 2015. 'Ouabain Prevents Pathological Cardiac Hypertrophy and Heart Failure through Activation of Phosphoinositide 3-Kinase α in Mouse', 15.

Wu, Penglong, Xun Yuan, Faqian Li, Jianhua Zhang, Wei Zhu, Meng Wei, Jingbo Li, and Xuejun Wang. 2017. 'Myocardial Upregulation of Cathepsin D by Ischemic Heart Disease Promotes Autophagic Flux and Protects Against Cardiac Remodeling and Heart Failure'. *Circulation: Heart Failure* 10 (7): e004044. https://doi.org/10.1161/CIRCHEARTFAILURE.117.004044.

Wu, Yueting, Wentao Deng, and David J. Klinke II. 2015. 'Exosomes: Improved Methods to Characterize Their Morphology, RNA Content, and Surface Protein Biomarkers'. *The Analyst* 140 (19): 6631–42. https://doi.org/10.1039/C5AN00688K.

Xia, Ying, Keunsang Lee, Na Li, Daniel Corbett, Leonardo Mendoza, and Nikolaos G. Frangogiannis. 2009. 'Characterization of the Inflammatory and Fibrotic Response in a Mouse Model of Cardiac Pressure Overload'. *Histochemistry and Cell Biology* 131 (4): 471–81. https://doi.org/10.1007/s00418-008-0541-5.

Xie, Zhonglin, Mahipal Singh, and Krishna Singh. 2004. 'Osteopontin Modulates Myocardial Hypertrophy in Response to Chronic Pressure Overload in Mice'. *Hypertension* 44 (6): 826–31. https://doi.org/10.1161/01.HYP.0000148458.03202.48.

Xie, Zhonglin, Mahipal Singh, Deborah A. Siwik, William L. Joyner, and Krishna Singh. 2003. 'Osteopontin Inhibits Interleukin-1β-Stimulated Increases in Matrix Metalloproteinase Activity in Adult Rat Cardiac Fibroblasts'. *Journal of Biological Chemistry* 278 (49): 48546–52. https://doi.org/10.1074/jbc.M302727200.

Xu, Ming-yue, Zhi-shuai Ye, Xian-tao Song, and Rong-chong Huang. 2019. 'Differences in the Cargos and Functions of Exosomes Derived from Six Cardiac Cell Types: A Systematic Review'. *Stem Cell Research & Therapy* 10 (1): 194. https://doi.org/10.1186/s13287-019-1297-7.

Xu, Rong, David W. Greening, Hong-Jian Zhu, Nobuhiro Takahashi, and Richard J. Simpson. 2016. 'Extracellular Vesicle Isolation and Characterization: Toward Clinical Application'. *Journal of Clinical Investigation* 126 (4): 1152–62. https://doi.org/10.1172/JCI81129.

Xu, Yan, Nobu Nakane, and Elisabeth Maurer-Spurej. 2011. 'Novel Test for Microparticles in Platelet-Rich Plasma and Platelet Concentrates Using Dynamic Light Scattering: NOVEL TEST FOR MICROPARTICLES'. *Transfusion* 51 (2): 363–70. https://doi.org/10.1111/j.1537-2995.2010.02819.x.

Yalçin, Fatih, Nagehan Kucukler, Oscar Cingolani, Blaid Mbiyangandu, Lars Sorensen, Aurelio Pinherio, M Roselle Abraham, and Theodore P Abraham. 2019. 'Evolution of Ventricular Hypertrophy and Myocardial Mechanics in Physiological and Pathological Hypertrophy'. *J Appl Physiol*, 9.

Yang, Yan, Yan Wang, and Ping-jin Gao. 2020. 'Osteopontin Associated with Left Ventricular Hypertrophy and Diastolic Dysfunction in Essential Hypertension'. *Journal of Human Hypertension* 34 (5): 388–96. https://doi.org/10.1038/s41371-019-0246-3.

Yokosaki, Yasuyuki, Nariaki Matsuura, Tomohiro Sasaki, Isao Murakami, Holm Schneider, Shigeki Higashiyama, Yoshiki Saitoh, Michio Yamakido, Yasuyuki Taooka, and Dean Sheppard. 1999. 'The Integrin A9β1 Binds to a Novel Recognition Sequence (SVVYGLR) in the Thrombin-Cleaved Amino-Terminal Fragment of Osteopontin'. *Journal of Biological Chemistry* 274 (51): 36328–34. https://doi.org/10.1074/jbc.274.51.36328.

Yokosaki, Yasuyuki, Kumi Tanaka, Fumiko Higashikawa, Keisuke Yamashita, and Akira Eboshida. 2005. 'Distinct Structural Requirements for Binding of the Integrins Avβ6, Avβ3, Avβ5, A5β1 and A9β1 to Osteopontin'. *Matrix Biology* 24 (6): 418–27. https://doi.org/10.1016/j.matbio.2005.05.005.

Yu, Hui, and Zhanli Wang. 2019. 'Cardiomyocyte-Derived Exosomes: Biological Functions and Potential Therapeutic Implications'. *Frontiers in Physiology* 10 (August): 1049. https://doi.org/10.3389/fphys.2019.01049.

Yu, Jun, Xiaosong Gu, and Sheng Yi. 2016. 'Ingenuity Pathway Analysis of Gene Expression Profiles in Distal Nerve Stump Following Nerve Injury: Insights into Wallerian Degeneration'. *Frontiers in Cellular Neuroscience* 10 (December). https://doi.org/10.3389/fncel.2016.00274.

Yu, Qianli, Randy Vazquez, Elham Vali Khojeini, Chirag Patel, Raj Venkataramani, and Douglas F. Larson. 2009. 'IL-18 Induction of Osteopontin Mediates Cardiac Fibrosis and Diastolic Dysfunction in Mice'. *American Journal of Physiology-Heart and Circulatory Physiology* 297 (1): H76–85. https://doi.org/10.1152/ajpheart.01285.2008.

Yu, Xian, Lingyan Deng, Dan Wang, Na Li, Xiao Chen, Xiang Cheng, Jin Yuan, et al. 2012. 'Mechanism of TNF-α Autocrine Effects in Hypoxic Cardiomyocytes: Initiated by Hypoxia Inducible Factor 1α, Presented by Exosomes'. *Journal of Molecular and Cellular Cardiology* 53 (6): 848–57. https://doi.org/10.1016/j.yjmcc.2012.10.002.

Yuan, Zhong-Yu, Li-Ting Cheng, Ze-Feng Wang, and Yong-Quan Wu. 2021. 'Desmoplakin and Clinical Manifestations of Desmoplakin Cardiomyopathy'. *Chinese Medical Journal* 134 (15): 1771–79. https://doi.org/10.1097/CM9.0000000000001581.

Zaborowski, MikoŁaj P., Leonora Balaj, Xandra O. Breakefield, and Charles P. Lai. 2015. 'Extracellular Vesicles: Composition, Biological Relevance, and Methods of Study'. *BioScience* 65 (8): 783–97. https://doi.org/10.1093/biosci/biv084.

Zaragoza, Carlos, Carmen Gomez-Guerrero, Jose Luis Martin-Ventura, Luis Blanco-Colio, Begoña Lavin, Beñat Mallavia, Carlos Tarin, Sebastian Mas, Alberto Ortiz, and Jesus Egido. 2011. 'Animal Models of Cardiovascular Diseases'. *Journal of Biomedicine and Biotechnology* 2011: 1–13. https://doi.org/10.1155/2011/497841.

Zeller, Tanja, Stefan Blankenberg, and Patrick Diemert. 2012. 'Genomewide Association Studies in Cardiovascular Disease—An Update 2011'. *Clinical Chemistry* 58 (1): 92–103. https://doi.org/10.1373/clinchem.2011.170431.

Zhang, Mengdi, Ke Jin, Liang Gao, Zhengkui Zhang, Fang Li, Fangfang Zhou, and Long Zhang. 2018. 'Methods and Technologies for Exosome Isolation and Characterization'. *Small Methods* 2 (9): 1800021. https://doi.org/10.1002/smtd.201800021.